HZDR-017

JOINT PROJECT: INTERACTION AND TRANSPORT OF ACTINIDES IN NATURAL CLAY ROCK WITH CONSIDERATION OF HUMIC SUBSTANCES AND CLAY ORGANICS

Characterization and quantification of the influence of clay organics on the interaction and diffusion of uranium and americium in the clay

Katja Schmeide, Claudia Joseph, Susanne Sachs, Robin Steudtner, Bianca Raditzky, Alix Günther, Gert Bernhard

Wissenschaftlich-Technische Berichte
HZDR-017 · ISSN 2191-8708

WISSENSCHAFTLICH-
TECHNISCHE BERICHTE

HZDR
HELMHOLTZ
ZENTRUM DRESDEN
ROSSENDORF

Wissenschaftlich-Technische Berichte
HZDR-017

Katja Schmeide, Claudia Joseph, Susanne Sachs,
Robin Steudtner, Bianca Raditzky, Alix Günther,
Gert Bernhard

Joint Project: Interaction and transport of actinides in natural clay rock with consideration of humic substances and clay organics

Characterization and quantification of the influence of clay organics on the interaction and diffusion of uranium and americium in the clay

HZDR
HELMHOLTZ
ZENTRUM DRESDEN
ROSSENDORF

Das diesem Bericht zugrunde liegende Vorhaben wurde mit Mitteln des Bundesministeriums für Wirtschaft und Technologie unter dem Förderkennzeichen 02 E 10156 gefördert. Die Verantwortung für den Inhalt dieser Veröffentlichung liegt bei den Autoren.

Vorhaben:

VERBUNDPROJEKT: Wechselwirkung und Transport von Actiniden im natürlichen Tongestein unter Berücksichtigung von Huminstoffen und Tonorganika

Charakterisierung und Quantifizierung des Einflusses von Tonorganika auf die Wechselwirkung und die Diffusion von Uran und Americium im Ton

Laufzeit des Vorhabens: 01.07.2006 bis 30.06.2011

Projektleiter: Prof. Dr. G. Bernhard

Institut für Radiochemie, Helmholtz-Zentrum Dresden-Rossendorf

Abstract

The objective of this project was the study of basic interaction processes in the systems actinide - clay organics - aquifer and actinide - natural clay - clay organics - aquifer. Thus, complexation, redox, sorption and diffusion studies were performed.

To evaluate the influence of nitrogen, phosphorus and sulfur containing functional groups of humic acid (HA) on the complexation of actinides in comparison to carboxylic groups, the Am(III) and U(VI) complexation by model ligands was studied by UV-Vis spectroscopy and TRLFS. The results show that Am(III) is mainly coordinated via carboxylic groups, however, probably stabilized by nitrogen groups. The U(VI) complexation is dominated by carboxylic groups, whereas nitrogen and sulfur containing groups play a minor role. Phosphorus containing groups may contribute to the U(VI) complexation by HA, however, due to their low concentration in HA they play only a subordinate role compared to carboxylic groups. Applying synthetic HA with varying sulfur contents (0 to 6.9 wt.%), the role of sulfur functionalities of HA for the U(VI) complexation and Np(V) reduction was studied. The results have shown that sulfur functionalities can be involved in U(VI) humate complexation and act as redox-active sites in HA for the Np(V) reduction. However, due to the low content of sulfur in natural HA, its influence is less pronounced.

In the presence of carbonate, the U(VI) complexation by HA was studied in the alkaline pH range by means of cryo-TRLFS (-120°C) and ATR FT-IR spectroscopy. The formation of the ternary $UO_2(CO_3)_2HA(II)^{4-}$ complex was detected. The complex formation constant was determined with $\log \beta_{0.1\ M} = 24.57 \pm 0.17$.

For aqueous U(VI) citrate and oxalate species, luminescence emission properties were determined by cryo-TRLFS and used to determine stability constants. The existing data base could be validated.

The U(VI) complexation by lactate, studied in the temperature range 7 to 65°C, was found to be endothermic and entropy-driven. In contrast, the complex stability constants determined for U(VI) humate complexation at 20 and 40°C are comparable, however, decrease at 60°C.

For aqueous U(IV) citrate, succinate, mandelate and glycolate species stability constants were determined. These ligands, especially citrate, increase solubility and mobility of U(IV) in solution due to complexation.

The U(VI) sorption onto crushed Opalinus Clay (OPA, Mont Terri, Switzerland) was studied in the absence and presence of HA or low molecular weight organic acids, in dependence on temperature and CO_2 presence using OPA pore water as background electrolyte. Distribution coefficients (K_d) were determined for the sorption of U(VI) and HA onto OPA with $(0.0222 \pm 0.0004)\ m^3/kg$ and $(0.129 \pm 0.006)\ m^3/kg$, respectively. The U(VI) sorption is not influenced by HA (≤ 50 mg/L), however, decreased by low molecular weight organic acids ($\geq 1\times10^{-5}$ M), especially by citrate and tartrate. With increasing temperature, the U(VI) sorption increases both in the absence and in the presence of clay organics.

The U(VI) diffusion in compacted OPA is not influenced by HA at 25 and 60°C. Predictions of the U(VI) diffusion show that an increase of the temperature to 60°C does not accelerate the migration of U(VI). With regard to uranium-containing waste, it is concluded that OPA is suitable as host rock for a future nuclear waste repository since OPA has a good retardation potential for U(VI).

Zusammenfassung

Ziel des Projektes war die Untersuchung grundlegender Wechselwirkungsprozesse in den Systemen Actinid - Tonorganika - Aquifer und Actinid - Tongestein - Tonorganika - Aquifer. Dazu wurden Komplexierungs-, Redox-, Sorptions- und Diffusionsstudien durchgeführt.

Um den Einfluss stickstoff-, phosphor- und schwefelhaltiger funktioneller Gruppen von Huminsäuren (HA) auf die Komplexierung von Actiniden im Vergleich zu Carboxylgruppen einzuschätzen, wurde die Am(III)- und U(VI)-Komplexierung mit Modellliganden mittels UV-Vis-Spektroskopie und TRLFS untersucht. Die Ergebnisse zeigen, dass Am(III) hauptsächlich über Carboxylgruppen koordiniert wird, wobei stickstoffhaltige Gruppen wahrscheinlich stabilisierend wirken. Die U(VI)-Komplexierung wird von Carboxylgruppen dominiert, stickstoff- und schwefelhaltige Gruppen spielen eine untergeordnete Rolle. Phosphorhaltige Gruppen können zur U(VI)-Komplexierung durch HA beitragen. Aufgrund ihrer niedrigen Konzentration in HA spielen sie gegenüber Carboxylgruppen jedoch nur eine untergeordnete Rolle. Weiterhin wurde unter Anwendung von synthetischen HA mit variierenden Schwefelgehalten (0 bis 6.9 Gew.%) die Rolle von Schwefelfunktionalitäten der HA für die U(VI)-Komplexierung und Np(V)-Reduktion untersucht. Die Ergebnisse zeigen, dass die HA-Schwefelfunktionalitäten sowohl zur U(VI)-Humat-Komplexierung als auch zur Np(V)-Reduktion durch HA beitragen können. Aufgrund des relativ niedrigen Schwefelgehaltes in natürlichen HA ist dieser Beitrag unter umweltrelevanten Bedingungen jedoch niedrig.

In Gegenwart von Carbonat wurde die U(VI)-Humat-Komplexierung unter alkalischen Bedingungen mittels cryo-TRLFS (-120°C) und ATR FT-IR untersucht. Die Bildung des ternären $UO_2(CO_3)_2HA(II)^{4-}$ Komplexes wurde nachgewiesen. Die Komplexbildungskonstante wurde mit $\log \beta_{0.1\ M} = 24.57 \pm 0.17$ bestimmt.

Für U(VI)-Citrat- und Oxalatspezies wurden die Lumineszenzemissionseigenschaften mittels cryo-TRLFS ermittelt und für die Bestimmung von Stabilitätskonstanten genutzt. Literaturwerte konnten so validiert werden.

Die U(VI)-Komplexierung mit Lactat im Temperaturbereich 7 bis 65°C erfolgt endotherm und entropiegetrieben. Dagegen sind die für die U(VI)-Humat-Komplexierung bestimmten Stabilitätskonstanten bei 20 und 40°C vergleichbar, sinken jedoch bei weiterer Temperaturerhöhung auf 60°C.

Die für U(IV)-Citrat-, Succinat-, Mandelat- und Glykolatspezies bestimmten Stabilitätskonstanten zeigen, dass diese Liganden, insbesondere Citrat, die Löslichkeit und somit die Mobilität von U(IV) erhöhen.

Die U(VI)-Sorption an homogenisiertem Opalinustonpulver (OPA, Mont Terri, Schweiz) wurde in Ab- und Anwesenheit von HA oder niedermolekularen organischen Säuren als Funktion der Temperatur und Atmosphäre unter Anwendung von OPA-Porenwasser als Hintergrundelektrolyt untersucht. Verteilungskoeffizienten (K_d) wurden für die U(VI)- und HA-Sorption an OPA mit $(0.0222 \pm 0.0004)\ m^3/kg$ bzw. $(0.129 \pm 0.006)\ m^3/kg$ bestimmt. Die U(VI)-Sorption wird durch HA (≤ 50 mg/L) nicht beeinflusst, jedoch durch niedermolekulare organische Säuren ($\geq 1\times10^{-5}$ M), insbesondere durch Citrat und Tartrat, verringert. Mit steigender Temperatur nimmt die U(VI)-Sorption sowohl in Ab- als auch in Anwesenheit von Tonorganika zu.

Die U(VI)-Diffusion in intakten OPA-Bohrkernen wird durch HA bei 25 und 60°C nicht beeinflusst. Abschätzungen zur U(VI)-Diffusion zeigen, dass eine Temperaturerhöhung auf 60°C die U(VI)-Migration durch OPA nicht beschleunigt. Bezüglich uranhaltiger Abfälle ist OPA als Wirtsgestein für ein nukleares Endlager geeignet, da es ein gutes Rückhaltevermögen gegenüber U(VI) aufweist.

Contents

1 Introduction

A reliable long-term risk assessment for future nuclear waste repository sites requires the identification, characterization and quantification of all migration processes, relevant for potentially released radionuclides, and their underlying chemical and physical processes.

In addition to salt and crystalline rock, argillaceous rock is considered as potential host rock and backfill material for nuclear waste repositories in deep geological formations. The swelling properties of clay minerals, their large surface areas and their high retention efficiency towards safety relevant radionuclides are advantageous and make them ideal barriers against radionuclide migration. In natural clay, organic matter is strongly associated with mineral constituents. Low molecular weight organic acids such as acetic, lactic, propionic and formic acid as well as fulvic and humic acids can be released from the clay under certain conditions. This was shown by extraction experiments (Claret et al., 2003; Glaus et al., 2005; Courdouan et al., 2007, 2008). These clay organics are able to influence the transport of actinides in the environment by forming soluble complexes or stable colloids.

Thus, to study basic interaction processes in the systems actinide - clay organics - aquifer as well as actinide - natural clay - clay organics - aquifer, complexation, redox, sorption and diffusion studies have to be performed. Since elevated temperatures of up to 100°C are expected for the disposal of high-level nuclear waste in clay formations (Brasser et al., 2008), these studies should also be performed at elevated temperatures.

The objective of the complexation studies is to determine complex formation constants not known so far or the validation of known complex formation constants by complementary spectroscopic methods to improve the thermodynamic database. Thus, the complexation of Am(III), U(IV) and U(VI) with low molecular weight organic ligands as well as with humic substances will be studied in the present project, partly under variation of the temperature (7 to 65°C), to determine thermodynamic constants. Furthermore, in continuation of the actinide humate complexation studies performed previously, the objective of the present study is to evaluate the influence of nitrogen, phosphorus and sulfur containing functional groups of humic acid on the complexation of actinides in comparison to carboxylic groups. For this, the Am(III) and U(VI) complexation with various model ligands as well as with synthetic humic acids, enriched with sulfur functional groups, will be studied. The sulfur containing synthetic humic acids will also be applied to clarify the role of sulfur functional groups for the Np(V) reduction by humic acid. The specification of those individual processes contributing to the

total complexation and redox activity of humic substances improves the understanding of thermodynamic and kinetic aspects of environmental processes involving humic substances.

The U(VI) humate complexation studies, mainly performed in the acidic pH range or at pH 7 and with exclusion of carbonate so far, should be extended to the alkaline pH range and should be performed in the presence of carbonate. This is to verify or exclude the formation of ternary U(VI) carbonato humate complexes. The information on such a complex is necessary for a reliable geochemical modeling of the mobility of U(VI) under environmentally relevant conditions.

The sorption and diffusion studies within this project will focus on the natural clay 'Opalinus Clay' from the Mont Terri underground laboratory, Switzerland. The U(VI) sorption onto crushed Opalinus Clay will be studied in the absence and presence of humic acid or low molecular weight organic acids and in dependence on temperature (10 to 60°C) using Opalinus Clay pore water as background electrolyte. Furthermore, pH-dependent studies of the U(VI) sorption onto Opalinus Clay will be performed in the absence and presence of humic acid using $NaClO_4$ as background solution. The U(VI) sorption onto kaolinite will be studied in dependence on ionic strength and composition of the background electrolyte. These sorption studies will lead to a better process understanding. To determine U(VI) migration in Opalinus Clay as well as the influence of humic acid and temperature on the U(VI) migration, the U(VI) diffusion in compacted Opalinus Clay will be studied in the absence and presence of humic acid at 25 and 60°C using synthetic Opalinus Clay pore water. Diffusion and distribution coefficients (D_e and K_d) will be determined for U(VI) and humic acid.

The U(VI) sorption and especially the U(VI) diffusion experiments will contribute to a more realistic description of the migration behavior of U(VI) in the natural clay rock Opalinus Clay since the resulting parameters will be used for modeling the actinide migration through argillaceous rocks in the absence and presence of clay organics in the temperature range up to 60°C. This will lead to an improved risk assessment for potential nuclear waste repositories.

This research project is performed in collaboration with the R&D projects of the Karlsruher Institut für Technologie (Institut für Nukleare Entsorgung), Johannes Gutenberg-Universität Mainz (Institut für Kernchemie), Institut für Interdisziplinäre Isotopenforschung Leipzig (now HZDR, Institut für Radiochemie), Universität des Saarlandes (Institut für Anorganische und Analytische Chemie und Radiochemie), Technische Universität Dresden (Sachgebiet Strahlenschutz), Technische Universität München (Fachgebiet Theoretische Chemie) and Universität Potsdam (Institut für Chemie-Physikalische Chemie) that were funded by Bundesministerium für Wirtschaft und Technologie (BMWi).

2 Complexation of actinides in different oxidation states with humic substance model ligands and clay organics

The complexation of metal ions by humic substances is mainly attributed to carboxylic groups (Kim, 1986; Choppin, 1992; Denecke et al., 1997; Sachs et al., 2005; Schmeide et al., 2003, 2005, 2006) and phenolic OH groups (Pompe et al., 2000b; Sachs and Bernhard, 2005) as their dominant functionalities. In addition to these oxygen containing functional groups, humic substances also contain nitrogen, phosphorus and sulfur containing functionalities.

The objective of this work was to determine the influence of various nitrogen, phosphorus and sulfur containing functional groups on the complexation of actinides in different oxidation states (U(VI) and Am(III)) and to evaluate their contribution in comparison to oxygen containing functional groups. For this, simple organic model ligands that can occur as building blocks for humic substances were used, for instance, anthranilic acid, nicotinic acid, picolinic acid, phenylphosphonic acid, benzenesulfonic acid and 4-hydroxybenzenesulfonic acid (cf. sections 2.1, 2.5, 2.6, 2.7).

A further objective of this work was the determination or validation of complex formation constants to improve the thermodynamic database. Thus, the U(IV) complexation with citric acid, succinic acid, mandelic acid and glycolic acid was studied (cf. section 2.2). The U(VI) complexation with lactic acid was studied in the temperature range 7 to 65°C (cf. section 2.4). Moreover, the up to now unknown luminescence emission properties of U(VI) citrate and oxalate species were determined and applied for the determination of complex formation constants (cf. section 2.3).

2.1 Am(III) complexation by anthranilic acid, picolinic acid, nicotinic acid and phthalic acid – Determination of complex formation constants by UV-Vis spectroscopy and TRLFS

During decomposition of organic matter and the following humification process nitrogen becomes incorporated into HA. The nitrogen content of HA varies between 0.8 and 4.3 wt.% (Stevenson, 1994). The nitrogen functionalities formed are derived from proteinaceous materials (like amino acids or peptides as fragments of proteins), amino sugars and heterocyclic compounds (like pyridines or pyrroles), respectively (Schulten and Schnitzer, 1998; Vairavamurthy and Wang, 2002). Whereas oxygen functionalities are acknowledged as the most important binding partners for actinides, the contribution of these nitrogen

functionalities to the interaction behavior of HA is widely unknown. Only few studies concerning the interaction of HA with certain trace metals such as Co, Ni or Cu (Xia et al., 1997; Croué et al., 2003) have been published, revealing the involvement of amine functionalities in complex formation. Furthermore, in the literature there are references to the complexation of actinides with multidentate N-donor ligands, which play a crucial role for the separation of trivalent actinides from trivalent lanthanides (Guillaumont, 2006; Denecke et al., 2007; Heitzmann et al., 2009). However, concerning the influence of nitrogen containing functionalities on the HA complexation with trivalent actinides, especially Am(III), no results are available so far. To address this lack of knowledge, we studied the complexation of Am(III) with anthranilic acid (AA), nicotinic acid (Nic) and picolinic acid (Pic). For comparison, the complex formation was also studied with phthalic acid (PA) as an example for the interaction of Am(III) with oxygen functionalities. The structures of the ligands are given in Fig. 2.1.

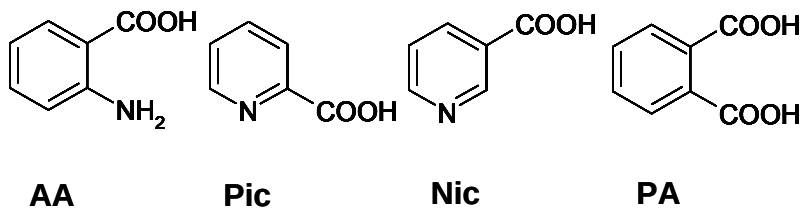

Fig. 2.1. Structures of the model ligands studied.

2.1.1 Experimental

Sample preparation

All experiments were carried out at room temperature (23 ± 2°C). Solutions were prepared using Milli-Q water (mod. Milli-RO/Milli-Q-System, Millipore, Schwalbach, Germany). The ionic strength was adjusted to 0.1 M by adding 3 M $NaClO_4$ (p.a., Merck). The measurements were performed at pH 3.8 ± 0.1 or 6.0 ± 0.1. The pH adjustments were done with diluted NaOH (high grade, Merck) and $HClO_4$ (p.a., Merck) solutions. Stock solutions (1×10^{-2} M, pH 3.8 or 6.0) of AA (p.a., Merck), Nic (p.a., Sigma-Aldrich), Pic (99%, Acros Organics) and PA (99%, Sigma-Aldrich) were prepared freshly for each experiment. An Am(III) stock solution was prepared by dissolving AmO_2 in 30% nitric acid with further dilution to a final concentration of 2.2×10^{-4} M. All samples containing Am(III) were prepared in a glove box under nitrogen atmosphere. For spectrophotometric TRLFS titrations, 2.7 mL of a 5×10^{-6} M Am^{3+} solution (pH 3.8 or 6.0, 0.1 M $NaClO_4$) were titrated with aliquots (38 µL) of the ligand stock solution. Thus, the ligand concentration was varied between 0 and 1×10^{-3} M in 8

titration steps. Static fluorescence measurements were performed at every titration step. The absorption measurements were carried out at a constant metal-to-ligand ratio of 1:200 (Am^{3+}: 5×10^{-6} M, ligand: 1×10^{-3} M) at both pH values. The pH was checked after each titration experiment.

Methods

Absorption spectra were recorded in the wavelength range from 400 to 700 nm using a CARY-5G UV-Vis-NIR spectrometer (Varian). For determination of the Am(III) absorption, the spectra were background corrected and analyzed in the wavelength range from 490 to 530 nm.

The Am(III) luminescence was measured using a pulsed flash-lamp-pumped Nd:YAG-MOPO laser system (Spectra Physics). The excitation wavelength varied from 503 to 508 nm depending on the absorption maxima determined for Am(III) and its complexes with the respective ligands. The luminescence emission was focused into a spectrograph (model 2300i, Acton Research) via fiber optics and recorded using a digital delay generator and an ICCD camera system (Roper Scientific). The gate width of the camera was set to be 500 ns. Am(III) single and time-resolved emission spectra were recorded between 631 and 768 nm, averaging three spectra with 100 laser pulses each. For time-resolved measurements, 60 spectra were recorded at delay times ranging from 30 to 150 ns with a step size of 2 ns.

2.1.2 Results and discussion

Spectroscopic characteristics of Am(III) in aqueous solution

At the pH values studied, Am(III) exhibits a very sensitive absorption band at 503.3 nm in aqueous solution (cf. Fig. 2.2), which is based on the electronic transition from the $^7F_0$ ground state to the first excited state $^5L_6$. This band is strongly influenced by any alteration of the first coordination sphere and therefore, its spectroscopic characteristics provide information on the chemical speciation of the metal ion. Complexation of Am(III) by organic ligands often results in a bathochromic shift of the absorption maximum, as it was described by several authors (Moulin et al., 1987; Morgenstern et al., 2000; Müller et al., 2010).

Excitation of Am(III) solutions at 503 nm yields one unique emission band at about 691 nm (cf. Fig. 2.3), which corresponds to the $^5D_1 \rightarrow {}^7F_1$ transition. The position of the emission maximum does not differ at the studied pH values, which indicates that only the Am^{3+} aquo ion is predominant up to pH 6. For determination of the luminescence lifetimes, the sum of

the luminescence intensities over the measured wavelength range was fitted by an exponential decay function:

$$I(t) = \sum I \cdot \exp(- t / \tau) \quad (2.1)$$

I(t) is the total luminescence intensity at the time *t*, *I* the intensity of the luminescent species at $t = 0$ and τ the corresponding luminescence lifetime. The luminescence decay was mono-exponential and the lifetime for the Am^{3+} aquo ion was determined to be 23.9 ± 0.8 ns, which is in very good agreement with literature data (e.g., Beitz, 1994; Barkleit et al., 2011). The number of associated water molecules in the first coordination sphere of the Am^{3+} aquo ion can be calculated using the following linear relationship given by Kimura and Kato (1998):

$$n\ H_2O \pm 0.5 = 2.56 \cdot 10^{-7} \cdot \frac{1}{\tau} - 1.43 \quad (2.2)$$

Applying this equation, *n* H_2O could be calculated to be 9.3 ± 0.5, which fits other experimental results very well (e.g., 9.6 ± 0.5 published by Barkleit et al. (2011)). The hydration shell water molecules are known to quench fluorescence lifetimes due to the coupling of the fluorophore excited states to the vibrations of the coordinated O-H oscillators (Runde et al., 2000). Hence, with the displacement of inner sphere water molecules against ligand molecules due to complexation, the lifetime of Am(III) should increase, as it was shown by various authors (e.g., Beitz et al., 1994; Kimura and Kato, 1998; Runde et al., 2000; Barkleit et al., 2011).

Interaction of Am(III) with nitrogen containing ligands

The investigated nitrogen containing ligands AA, Pic and Nic generally show similar behavior in aqueous solution. All have comparable dissociation constants (e.g., AA: $pK_{a1} = 2.01$ and $pK_{a2} = 4.78$ at $I = 0.1$ M and room temperature (Martell et al., 1998)) and occur in three different species in aqueous solution: The fully protonated acid predominates the speciation under very acidic conditions. The zwitterionic species is formed due to dissociation of the carboxylic acid and dominates the speciation at pH 2 - 5. Further increasing pH results in completely deprotonation of the ligand. To investigate the interaction of Am(III) with the zwitterionic and the negatively charged ligand species, the measurements were carried out at pH 3.8 and 6.0.

Fig. 2.2 depicts a summary of the measured absorption spectra of various Am(III) ligand solutions in comparison with an aqueous Am(III) standard solution (5×10^{-6} M) at both studied pH values. Neither with addition of AA nor with addition of Nic to the Am(III) solution a shift of the Am^{3+} (aq.) absorption band was observed at pH 3.8. It seems that Am(III) does not

form a complex with these ligands under the given experimental conditions. At pH 6.0, with addition of AA and Nic the absorption maximum is shifted to higher wavelengths from 503.3 nm to 504.1 nm and 505.4 nm, respectively, indicating a complex formation between Am(III) and the completely dissociated ligands. In contrast to that, with addition of 1×10^{-3} M Pic a bathochromic shift of the absorption maximum to 504.0 nm and a slight decrease of the absorbance is already observable at pH 3.8, indicating a complex formation of Am(III) with the zwitterionic species. This shift is even more pronounced at pH 6.0. A new absorption maximum evolves at 508.1 nm, suggesting the formation of a third Am(III) species with the fully deprotonated Pic.

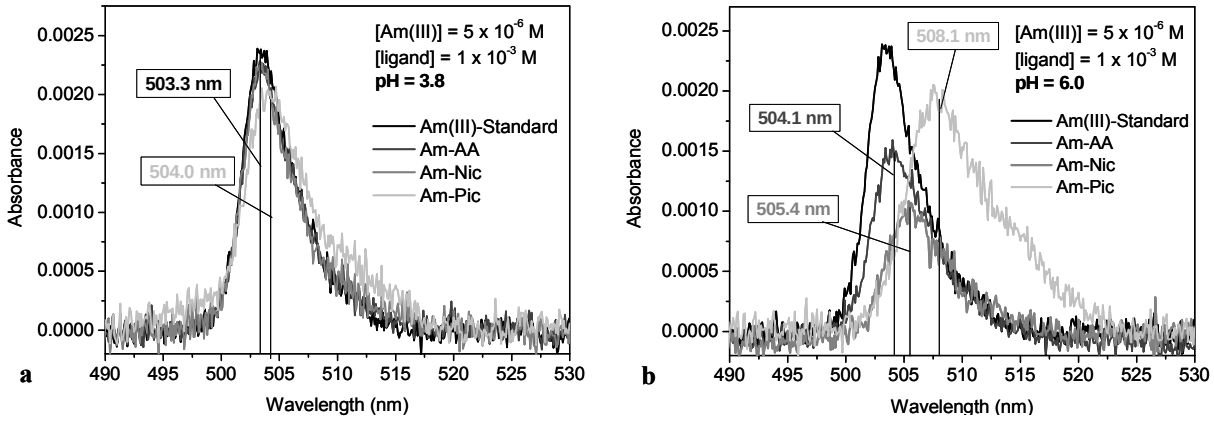

Fig. 2.2. Absorption spectra of Am(III) solutions with nitrogen containing ligands in comparison with an aqueous Am(III) standard solution (5×10^{-6} M) at pH 3.8 (a) and pH 6.0 (b).

The wavelengths of the absorption maxima determined for the Am(III) ligand solutions were used as excitation wavelengths for the TRLFS measurements. Studying the interaction of Am(III) with AA and Nic at pH 3.8, no significant changes of the luminescence intensities as well as of the determined lifetimes were observed with increasing ligand concentration (not shown). Thus, as implied by the UV-Vis measurements, there is no evidence for a complex formation between Am(III) and the zwitterionic species of AA and Nic.

Figure 2.3 depicts the development of the Am(III) emission spectra as a function of Pic concentration. Contrary to the measurements with AA and Nic, in the presence of Pic the spectrum of Am(III) shows an increase in the luminescence intensity with increasing ligand concentration even at pH 3.8, where the ligand should still occur predominantly in its zwitterionic form. The analysis of the time-resolved luminescence spectra results in prolonging lifetimes from 23.9 ± 0.8 ns for the free Am^{3+} aquo ion to an approximately constant value of 27.2 ± 0.1 ns with increasing ligand concentration. Both observations point to a complexation of Am(III) with Pic. According to Eq. (2.2), the lifetime of the determined complex species corresponds to 8.0 ± 0.5 water molecules in the first coordination sphere of

Am(III), implying the replacement of one water molecule by the ligand. This can be interpreted as formation of a 1:1 complex where one Pic molecule displaces one water molecule.

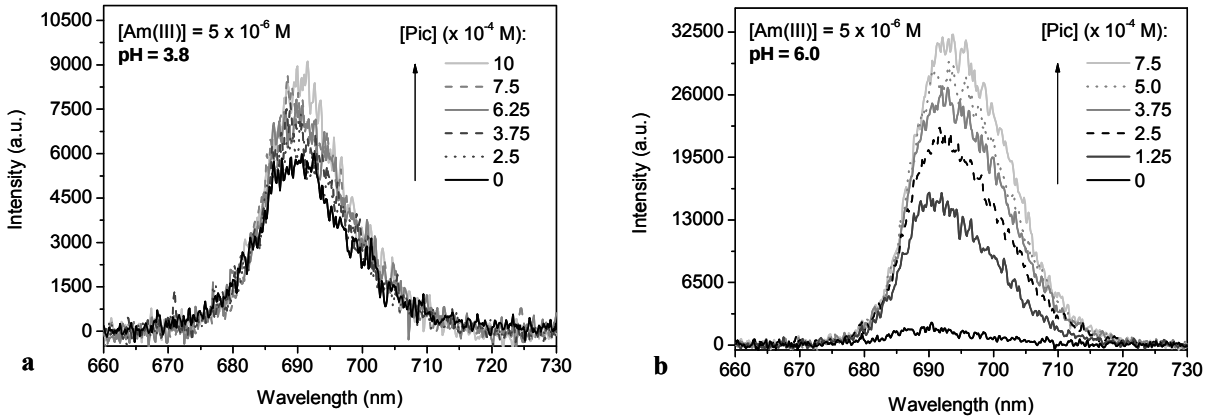

Fig. 2.3. Luminescence emission spectra of 5×10^{-6} M Am(III) at pH 3.8 (a) and pH 6.0 (b) as a function of Pic concentration.

The complex stability constants were calculated via SPECFIT (Binstead et al., 2005), using the following equation for the direct reaction of Am(III) with the zwitterionic Pic species:

$$x\ Am^{3+} + y\ {}^{+}HNC_5H_4COO^{-} \rightleftarrows [Am_x(HNC_5H_4COO)_y]^{(3x)+} \qquad (2.3)$$

The complex formation constant was calculated with $\log \beta_{11} = 3.81 \pm 0.44$ (cf. Table 2.1).
As shown in Fig. 2.3b, the luminescence intensity of Am(III) further increases at pH 6.0. With increasing Pic concentration also a slight shift of the emission maximum from about 691 nm to 694 nm could be observed. In all samples, mono-exponential luminescence decay was determined. The luminescence lifetime increases due to complex formation to 42.0 ± 1.8 ns.

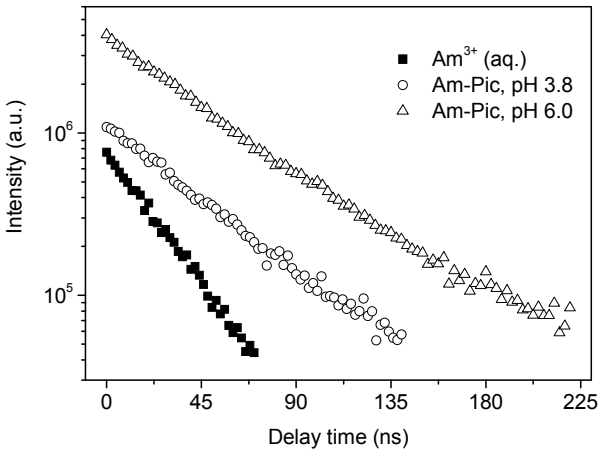

Fig. 2.4. Luminescence decay of Am^{3+} (aq.) in comparison with those measured in the Am(III) picolinate system at pH 3.8 and 6.0.

The change of the luminescence decay in dependence on pH is depicted in Fig. 2.4. The lifetime of the determined complex species corresponds to 4.7 ± 0.5 water molecules in the inner coordination sphere of the metal ion, implying the replacement of about 4 water molecules by the ligand, which can be interpreted as formation of 1:1 and 1:2 complexes. The complexation reactions can be expressed as follows:

$$x\ Am^{3+} + y\ NC_5H_4COO^- \rightleftarrows [Am_x(NC_5H_4COO)_y]^{(3x-y)+} \quad (2.4)$$

The averaged formation constants for this reaction were calculated to be $\log \beta_{11} = 3.83 \pm 0.22$ and $\log \beta_{12} = 7.34 \pm 0.04$ (cf. Table 2.1).

As implied by the UV-Vis measurements, a complexation of Am(III) with AA and Nic could also be determined at pH 6.0. Both systems are characterized by an increase in luminescence intensities and lifetimes. Interestingly, in the Am(III) nicotinate system an additional increase of pH up to 7.6 as well as a decrease of the Am(III) concentration in solution during the spectroscopic titration could be determined. The UV-Vis as well as the emission spectra show an increase in the background, indicating the formation of insoluble complex species or colloids. Therefore, the calculation of the complex stability constant was not possible.

For the Am(III) anthranilate complex a luminescence lifetime of 28.6 ± 0.5 ns was determined, corresponding to 7.8 ± 0.5 water molecules in the first coordination sphere. According to that, one water molecule is replaced through ligand exchange, indicating the formation of a 1:1 complex of Am(III) with the fully deprotonated AA:

$$x\ Am^{3+} + y\ H_2NC_6H_4COO^- \rightleftarrows [Am_x(H_2NC_6H_4COO)_y]^{(3x-y)+} \quad (2.5)$$

The complex formation constant was calculated to be $\log \beta_{11} = 3.70 \pm 0.11$ (cf. Table 2.1). Since stability constants for this reaction or for the complexation of Am(III) with other nitrogen containing ligands were not reported in the literature so far, a comparison with other data is not possible.

Interaction of Am(III) with phthalic acid

The aromatic ligand PA offers two carboxylic groups, which are considered to be one of the most dominant functionalities in HA. The dissociation constants of PA reported for an ionic strength of 0.1 M and room temperature are $pK_{a1} = 2.66$ and $pK_{a2} = 4.72$ (Martell et al., 2003). Figure 2.5a depicts the absorption spectra of Am(III) phthalate complexes at both investigated pH values. Upon addition of PA the absorption maximum of Am(III) shows a decrease in the absorbance as well as a small bathochromic shift from 503.3 to 503.7 nm and 504.2 nm at pH 3.8 and 6.0, respectively, both indications for complex formation. The small differences in the

spectroscopic characteristics are hints for the formation of only one phthalate complex with Am(III) at both pH values. This assumption is also supported by the TRLFS measurements. At both pH values the analysis of the spectra results in a similar increase of the luminescence intensities with increasing ligand concentration.

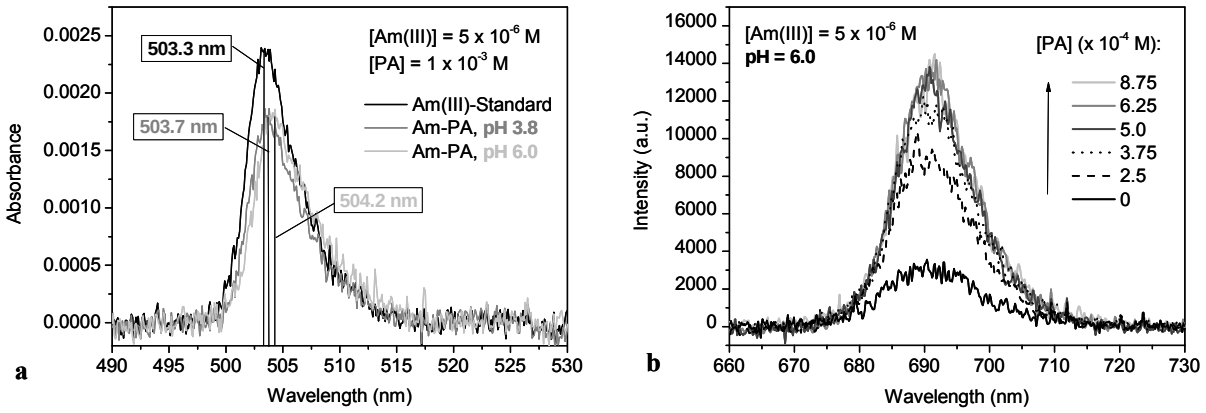

Fig. 2.5. Absorption spectra of Am(III) phthalate solutions (a) and luminescence emission spectra of 5×10^{-6} M Am(III) as a function of PA concentration at pH 6.0 (b).

Figure 2.5b shows the representative emission spectra of Am(III) as a function of the PA concentration at pH 6.0. The position of the peak maxima as well as the luminescence lifetimes determined at pH 3.8 are comparable to those obtained at pH 6.0, indicating the formation of an Am(III) complex with the fully deprotonated ligand. For all measured samples, a mono-exponential luminescence decay was observed. The lifetime of the complex was calculated to be 27.6 ± 1.1 ns, corresponding to 7.8 ± 0.5 water molecules in the inner coordination sphere of the metal ion. According to that, one water molecule is replaced through ligand exchange, indicating the formation of a 1:1 complex of Am(III) with PA. The spectroscopic properties of the Am(III) phthalate complex are listed in Table 2.1.

In analogy to the experiments with the nitrogen containing ligands the complex stability constants were calculated using SPECFIT. The complexation reaction can be expressed as follows:

$$x\,Am^{3+} + y\,C_6H_4(COO)_2^{2-} \rightleftarrows [Am_x(C_6H_4(COO)_2)_y]^{(3x-2y)+} \qquad (2.6)$$

The averaged formation constant for this reaction was calculated to be $\log \beta_{11} = 3.99 \pm 0.16$. Since the complexation of Am(III) with PA was also studied for the first time, no data are available for comparison. Nevertheless, this value is in agreement with that determined for Eu(III), the analog lanthanide ion ($\log \beta_1 = 3.7 \pm 0.3$ (Jain et al., 2009)). However, in case of Eu(III) also the formation of a 1:2 complex with PA was reported, which was not observed

under the studied experimental conditions in the present work. In comparison with the data of Panak et al. (1995), our complexation constant is slightly higher than the constant determined for the Cm(III) complexation with PA. The authors reported the formation of a 1:1 complex with a stability constant of $\log \beta_{11} = 3.62 \pm 0.02$.

Table 2.1. Summary of the spectroscopic data and determined stability constants $\log \beta$ for the various Am(III) species identified in this study.

Species	pH	M_xL_y	Absorption (nm)	Lifetime (ns)	n H_2O	$\log \beta_{0.1\ M}$
Am^{3+}	3.8 / 6.0	10	503.3	23.9 ± 0.8	9.3	-
$AmAA^{2+}$	6.0	11	504.1	28.55 ± 0.5	7.5	3.70 ± 0.11
$AmPicH^{3+}$	3.8	11	504.0	27.2 ± 0.1	8.0	3.81 ± 0.44
$AmPic^{2+}$	6.0	11	508.1	42.0 ± 1.8	4.7	3.83 ± 0.22
$Am(Pic)_2^+$		12				7.34 ± 0.04
$AmNic^{2+}$	6.0 – 7.6	11	505.4	27.8 ± 1.2	7.8	-
$AmPA^+$	3.8 / 6.0	11	503.7 / 504.2	27.6 ± 1.1	7.8	3.99 ± 0.16

Conclusion

For the first time, the complexation of Am(III) with the nitrogen containing ligands AA, Nic and Pic as well as with PA was studied in aqueous solution at pH 3.8 and 6.0. All complexes determined for nitrogen containing ligands show comparable complex stabilities (cf. Table 2.1). Only Pic was found to interact with Am(III) at pH 3.8, although it should occur predominantly in its zwitterionic form. It seems very likely that a complexation with zwitterionic ligands is hindered, due to electrostatic repulsion between the protonated nitrogen functionalities and Am^{3+}. Based on the present results, it could not be clarified whether the nitrogen is involved in the complexation or not. For example, a chelation of Eu(III) with Pic at pH 6.0 was reported by Park et al. (1999). Barkleit et al. (2011) mentioned that a chelation would cause bi-exponential decay due to the hindrance of the fast ligand-water exchange between the first coordination sphere and the solution. According to that, the mono-exponential decay of all studied complexes supports the assumption that Am(III) is only coordinated via the carboxylic groups. In comparison with the Am(III) complexation by other aromatic ligands containing carboxylic groups, the complex stabilities of the nitrogen containing ligands are somewhat higher than that determined for the Am(III) salicylate ($\log \beta_{11}$ = 2.56 ± 0.08 (Müller et al., 2011)) which has only one carboxylic group. The stability constant determined for Am(III) complexation by pyromellitic acid ($\log \beta_{110}$ = 5.42 ± 0.16 (Barkleit et al., 2011)), which offers three carboxylic groups, is somewhat higher than

those determined for Am(III) complexation by nitrogen containing ligands. Although each of the investigated nitrogen containing ligands offers only one carboxylic group, the stabilities of their determined complexes are comparable to that of the Am(III) phthalate complex, which offers two carboxylic groups. This indicates a stabilization of the Am(III) complexes with nitrogen containing ligands.

Transferring these results to the HA system, the Am(III) complexation by HA should be more influenced by nitrogen containing functional groups than U(VI), due to the softer character of Am(III) according to Pearson`s theory (Pearson, 1963). However, the obtained results allow the conclusion that these functionalities play only a subordinate role compared to oxygen functionalities in HA.

2.2 U(IV) complexation by citric acid, succinic acid, mandelic acid and glycolic acid – Determination of complex formation constants by UV-Vis spectroscopy

Both the speciation and the mobility of actinides in aquatic systems strongly depend on their oxidation state due to the different precipitation, complexation, sorption and colloid formation behavior of the various oxidation states (e.g., Choppin, 2006). Under reducing conditions as prevalent in deep underground nuclear waste repositories as well as in the depth of flooded uranium mines, actinide species occur in lower oxidation states. For instance, in contrast to U(VI) which is mobile, U(IV) is much less mobile due to the low solubility of U(IV) hydrous oxide ($UO_2{\cdot}xH_2O$(am)) (Neck and Kim, 2001; Opel et al., 2007). However, in the presence of inorganic or organic ligands U(IV) may become mobile due to formation of soluble complexes. Thus, the speciation of U(IV) in aqueous solution has to be studied to predict its migration behavior in natural environments. In this work, citric acid, succinic acid as well as mandelic acid and glycolic acid were chosen as model ligands to study the U(IV) complexation. These ligands stand for a variety of organic ligands in aqueous systems. This study is described in more detail in (Schmeide and Bernhard, 2008).

2.2.1 Experimental

Sample preparation

Sample solutions were prepared in an inert gas glove box (N_2 atmosphere) using CO_2-free solutions. The U(IV) concentration was kept constant at 1×10^{-3} M or 5×10^{-4} M, the ligand concentration was varied between 0 and 0.2 M. The concentration of hydrogen ions (1.0, 0.5,

0.1 M) was adjusted by adding aliquots of 5 M $HClO_4$ simultaneously taking into consideration the $[H^+]$ stemming from the U(IV) stock solution. The ionic strength was 1.0 M (H,Na)ClO_4. The amount of U(VI) in the samples was ≤ 1.5% of the total U as determined by fluorescence spectroscopy.

Spectroscopic measurements

The UV-Vis absorption spectra were recorded with a high-resolution dual beam UV-Vis-NIR spectrophotometer (CARY-5G, Varian). The measurements were performed using a 1-cm quartz glass cuvette (Hellma) in the spectral range from 800 to 300 nm with a speed of 60 nm/min at room temperature (22 ± 1°C). The cuvette was always filled and sealed in the inert gas box. Each spectrum was analyzed in two regions of wavelength: 446 to 524 nm and 570 to 727 nm.

Calculations

Stability constants were determined using the factor analysis program SPECFIT (Binstead et al., 2005). For this, the acidity constants of citric acid (pK_{a1} = 5.31, pK_{a2} = 4.17, pK_{a3} = 2.84 at I = 0.5 M $NaClO_4$) (Hummel et al., 2005), succinic acid (pK_{a1} = 5.12, pK_{a2} = 3.93 at I = 0.5 M), mandelic acid (pK_a = 3.18 at I = 1.0 M) and glycolic acid (pK_a = 3.61 at I = 1.0 M) (Martell et al., 1998) as well as the formation constants of U(IV) hydrolysis species (Guillaumont et al., 2003) were applied. Ionic strength corrections were conducted applying the Specific Ion Interaction Theory (SIT) (Guillaumont et al., 2003).

2.2.2 Results and discussion

U(IV) complexation with citric acid

The complexation of U(IV) with citric acid has been investigated in dependence on hydrogen ion concentration (0.1, 0.5, 1.0 M). From the pK_a values reported for citric acid (cf. paragraph Calculations) follows, that the citric acid is completely protonated in the pH range applied in this work. That means, citric acid does not contribute to the ionic strength under these pH conditions. Thus, the ionic strength of the sample solutions is mainly determined by $[H^+]$.
Exemplary, Fig. 2.6 shows the evolution of the U(IV) spectrum in the two wavelength ranges analyzed for increasing citric acid concentrations (0 to 0.2 M) at an acidity of $[H^+]$ = 0.5 M. In the wavelength range 570 to 727 nm, the solvated U^{4+} shows absorption maxima at 649.1 nm and 671.7 nm in the absence of citric acid. With increasing citric acid concentration the intensity of the peak at 649 nm decreases and simultaneously, the peak is shifted to longer

wavelengths. At U(IV):citric acid ratios higher than 1:20 the intensity of this peak increases again. In the wavelength range 446 to 524 nm, the intensity of the peak at 495 nm decreases with increasing citric acid concentration. The intensity of the shoulder at 486 nm increases when the U(IV):citric acid ratio is higher than 1:20. These changes of the U(IV) spectrum can be attributed to the complexation of U(IV) by citric acid.

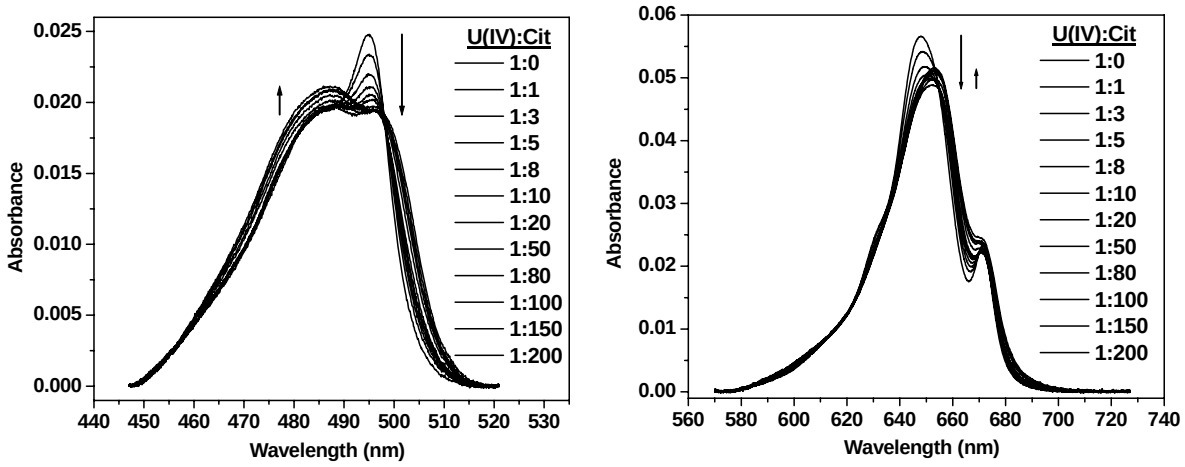

Fig. 2.6. Two wavelength ranges of the UV-Vis spectra for 1×10^{-3} M U(IV) as a function of the citric acid (Cit) concentration at $[H^+] = 0.5$ M and $I = 0.5$ M.

The experimental data were analyzed considering the most basic form of the citrate anion Cit^{3-}. The U(IV) citrate complexation reaction can be expressed as:

$$x\ U^{4+} + y\ H^+ + z\ Cit^{3-} \rightleftarrows U_xH_yCit_z^{(4x+y-3z)} \qquad (2.7)$$

For the calculation of the stability constants, 8 datasets were analyzed (4 series of experiments ($[H^+]$ = 1 M, 0.5 M, 0.1 M (2x)) with 2 wavelength ranges each). Thereby, the formation of 1:1 and 1:2 complexes was detected in the citrate media. Within the experimental uncertainty, no significant effect of the acidity and ionic strength of the sample solutions on the stability constants has been observed. The mean values of the stability constants were determined with $\log \beta_{101} = 13.5 \pm 0.2$ und $\log \beta_{102} = 25.1 \pm 0.2$. Due to the strong complexation of U(IV) by citric acid, the U(IV) hydrolysis is prevented. The stability of An(IV) citrate complexes against hydrolysis is already described in the literature (e.g., Durbin et al., 1998; Suzuki et al., 2006). Furthermore, U(IV) is stabilized against oxidation due to complexation. The stability of U(IV) against oxidation can further be explained by the reducing properties of citric acid (Bonin et al., 2007; Sevostyanova, 1982).

The $\log \beta$ values determined for 1:1 and 1:2 complexes in this work are higher than the values reported by Nebel and Urban (1966) with 11.5 and 19.5 and also slightly higher than the values reported by Bonin et al. (2008) with 12.8 and 24.1.

From Table 2.2 follows that the log β values obtained for U(IV) complexation by citric acid fit well in the series of log β values determined for the complexation of further tetravalent actinides (Th(IV), Np(IV), Pu(IV)) by citric acid.

Table 2.2. Stability constants for the system An(IV) citrate.

	Th(IV)	**U(IV)**	**Np(IV)**	**Pu(IV)**
log β_{101}	11.6 (I = 0.1 M) [a]	11.5 (I = 0.5 M) [b]	13.6 (I = 0.6 M) [d]	15.3 (I = 0.5 M) [e]
	13.0 (I = 0.5 M) [b]	12.8 (I = 0.8 M) [c]		17.6 (I = 0.15 M) [f]
	12.5 (I = 0.3 M) [c]	13.5 ± 0.2 [g]		13.8 (I = 1.0 M) [c]
log β_{102}	21.1 (I = 0.1 M) [a]	19.5 (I = 0.5 M) [b]	25.3 (I = 0.4 M) [d]	30.2 (I = 0.5 M) [e]
	21.0 (I = 0.5 M) [b]	24.1 (I = 0.8 M) [c]		25.0 (I = 0.15 M) [f]
	22.9 (I = 0.3 M) [c]	25.1 ± 0.2 [g]		26.6 (I = 1.0 M) [c]

[a] (Raymond et al., 1987), [b] (Nebel and Urban, 1966), [c] (Bonin et al., 2008), [d] (Bonin et al., 2007), [e] (Nebel, 1966), [f] (Yule, 1991), [g] (this work: I = 0.11 to 1.0 M).

In the literature, most of the studies assume that An(IV) is complexed by the most basic form of the citrate anion (Cit^{3-}) (Nebel, 1966; Nebel and Urban, 1966; Raymond et al., 1987; Bonin et al., 2007; Bonin et al., 2008). However, recent structural studies on uranyl complexes with citric and citramalic acid (Felmy et al., 2006; Thuéry, 2007; Thuéry, 2008) suggest that citrate is bound to the cation both by its carboxylate site to the central carbon atom and by its hydroxyl group in alpha position (chelate formation), i.e. with the acid-base form H_2Cit^-. This option also has to be taken into account.

U(IV) complexation with succinic acid, mandelic acid and glycolic acid

The complexation of U(IV) with succinic and mandelic acid has been investigated at an acidity of $[H^+]$ = 0.1 and 0.5 M and an ionic strength of 0.5 and 1.0 M, respectively. From the pK_a values reported for these ligands (cf. paragraph Calculations) follows, that the ligands are completely protonated under the experimental conditions applied in this work.

Figures 2.7 to 2.9 show the evolution of the U(IV) spectrum in the two wavelength ranges analyzed for increasing ligand concentrations (0 to 0.2 M). The U(IV) complexation reaction can be expressed as:

$$x\ U^{4+} + y\ H^+ + z\ \text{ligand}^- \rightleftarrows U_xH_y\text{ligand}_z^{(4x+y-z)} \qquad (2.8)$$

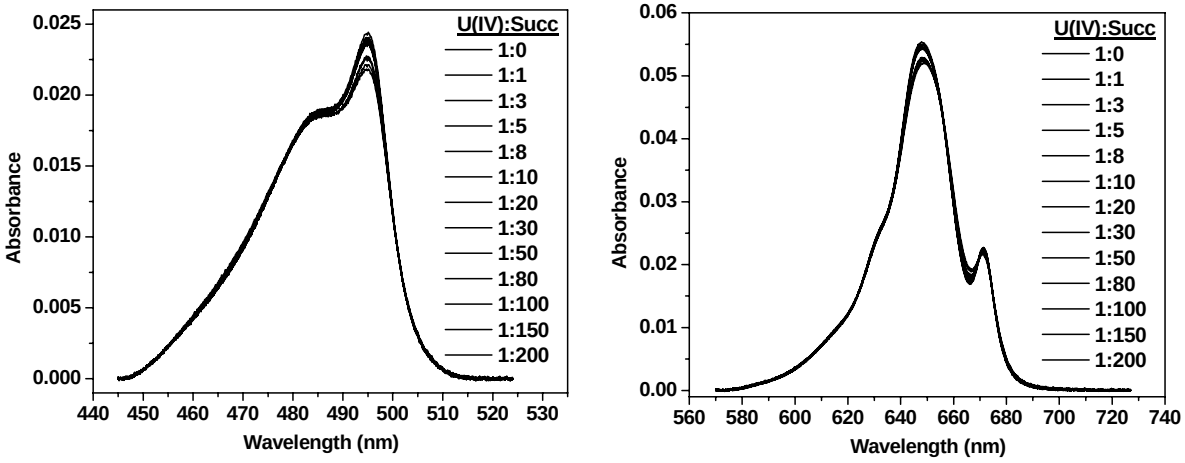

Fig. 2.7. Two wavelength ranges of the UV-Vis spectra for 1×10^{-3} M U(IV) as a function of the succinic acid (Succ) concentration at $[H^+] = 0.5$ M and $I = 0.5$ M.

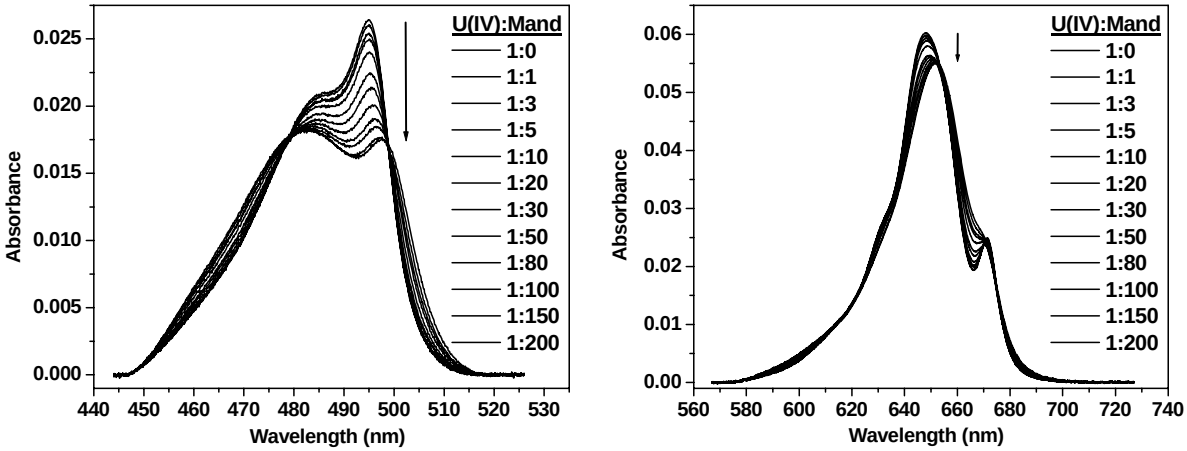

Fig. 2.8. Two wavelength ranges of the UV-Vis spectra for 1×10^{-3} M U(IV) as a function of the mandelic acid (Mand) concentration at $[H^+] = 0.5$ M and $I = 1.0$ M.

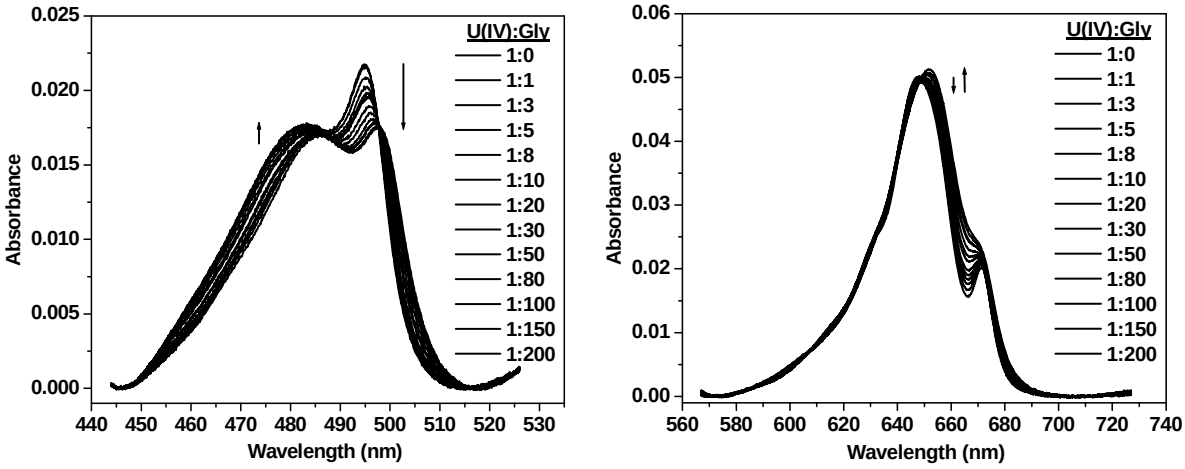

Fig. 2.9. Two wavelength ranges of the UV-Vis spectra for 1×10^{-3} M U(IV) as a function of the glycolic acid (Gly) concentration at $[H^+] = 0.1$ M and $I = 1.0$ M.

Especially, the spectra obtained for the U(IV) succinate system (cf. Fig. 2.7) show that the changes of the peak intensity and position are much weaker pronounced than in case of the U(IV) citrate system. For the U(IV) complexation by succinic acid, the formation of 1:1 complexes of the type $M_xH_yL_z$ was detected with $\log \beta_{101} = 9.0 \pm 0.2$ ($I = 0.5$ M). This value is lower than the stability constant determined with $\log K = 9.78$ ($I = 0.5$ M) by means of solubility experiments by (Merkusheva et al., 1970).

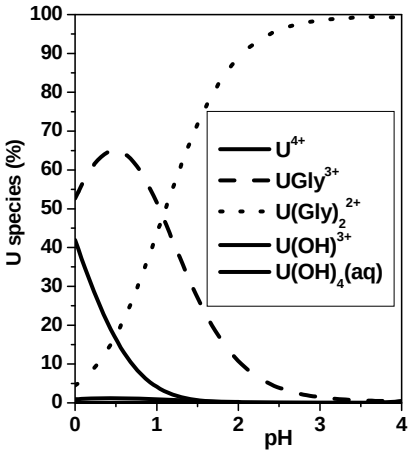

Fig. 2.10. U(IV) speciation in the presence of glycolic acid ([U(IV)] = 5×10^{-4} M, [Gly] = 0.1 M, $I = 1.0$ M).

In contrast to succinic acid, the formation of 1:1 and 1:2 complexes in solution was detected in the mandelate and glycolate media. The stability constants for 1:1 and 1:2 U(IV) ligand complexes of the type $M_xH_yL_z$ were determined with $\log \beta_{101} = 4.53 \pm 0.09$ and $\log \beta_{102} = 8.02 \pm 0.13$ for mandelate and with $\log \beta_{101} = 4.71 \pm 0.08$ and $\log \beta_{102} = 8.25 \pm 0.15$ for glycolate. The U(IV) speciation, calculated for the glycolic acid system (Fig. 2.10), exemplifies that the U(IV) hydrolysis is impeded due to the strong complexation of U(IV) by the ligand.

Conclusion

The stability constants for 1:1 and 1:2 U(IV) citrate complexes were determined with $\log \beta_{101} = 13.5 \pm 0.2$ and $\log \beta_{102} = 25.1 \pm 0.2$. This shows a strong interaction between U(IV) and citric acid. That means, the uranium speciation in citrate containing waters is strongly influenced by the U(IV) citrate complex. The comparison of the stability constants determined for the U(IV) complexation with various ligands shows that the interaction of U(IV) with succinate, mandelate and glycolate is much weaker than the interaction of U(IV) with citrate. Due to complexation with organic ligands the solubility and the mobility of U(IV) in aquatic systems is increased.

2.3 U(VI) complexation by citric acid and oxalic acid – Determination of luminescence properties at -120°C by cryo-TRLFS

Citric acid and oxalic acid are known to form strong complexes with U(VI) in aqueous solution in the acidic to alkaline pH range. The objective of the present study was to determine the up to now unknown luminescence emission properties of the U(VI) citrate and U(VI) oxalate species formed in the pH range from 2 to 4 and to apply these luminescence properties for the determination of complex formation constants. For this, time-resolved laser-induced fluorescence spectroscopy (TRLFS) at room temperature and TRLFS coupled with a cryogenic temperature technique (-120°C, cryo-TRLFS) were applied. The results of this study are published in-depth by Günther et al. (2011).

2.3.1 Experimental

The preparation of the sample solutions for the TRLFS measurements at 25°C ([U(VI)] = 5×10^{-5} M, [ligand] = 0 to 5×10^{-4} M, I = 0.1 or 0.5 M, pH 2 to 4) and at -120°C ([U(VI)] = 5×10^{-5} M, [ligand] = 0 to 5×10^{-3} M, I = 0.1, pH 3.5) as well as the TRLFS measurements are described in detail in (Günther et al., 2011).

2.3.2 Results and discussion

TRLFS measurements at room temperature (25°C)

Figure 2.11a shows the luminescence emission spectra of U(VI) as a function of the total citric acid concentration at pH 3.5 as an example. It was found that the luminescence intensity decreases with increasing ligand concentration. The U(VI) luminescence signals of the complex solutions do not shift in comparison to the luminescence emission bands of the reference solution without citric acid. Each time-resolved spectrum shows a mono-exponential luminescence decay (not shown). That means, that the formed U(VI) citrate species do not show luminescence at room temperature and only the luminescence properties of the uncomplexed U(VI) cation are visible in the spectra. The averaged luminescence lifetimes of the U(VI) cation are τ = 1561 ± 163 ns (I = 0.1 M) and τ = 1712 ± 190 ns (I = 0.5 M). Dynamic quenching due to citric acid or due to complex species at a $[U]_0$:$[cit]_0$ ratio higher than 1:1 can not be excluded.

Similar results were obtained for TRLFS measurements of U(VI) oxalate at pH 2 to 4. Exemplary, the luminescence spectra of this system obtained at pH 3 are shown in Fig. 2.11b.

With increasing ligand concentration the luminescence intensity decreases without shift of the emission bands. Generally, the exponential luminescence decay is of first order. We observed only a decrease of the luminescence of the uncomplexed U(VI) ion. The averaged lifetimes of the UO_2^{2+} cation up to $[U]_0$:$[ox]_0$ ratios of 1:3 (I = 0.1 M) and 1:2 (I = 0.5 M) are determined with τ = 1343 ± 66 ns (I = 0.1 M) and τ = 1299 ± 46 ns (I = 0.5 M), respectively. The lifetimes seem to be quite short for UO_2^{2+}, however, reference solutions without ligand measured under the same experimental conditions showed data in the same range. At $[U]_0$:$[ox]_0$ ratios in the solution higher than 1:3 (I = 0.1 M) or higher than 1:2 (I = 0.5 M) we did not observe an exponential luminescence decay with a continuous decrease of the luminescence intensity during measuring time of 20 µs. A small increase of the luminescence intensity was detected in the first 400 ns of the time-resolved measurements. Then, the luminescence intensity decreased mono-exponentially. Here, it seems that the system is not photo stable. A decomplexation of U(VI) oxalates might be possible.

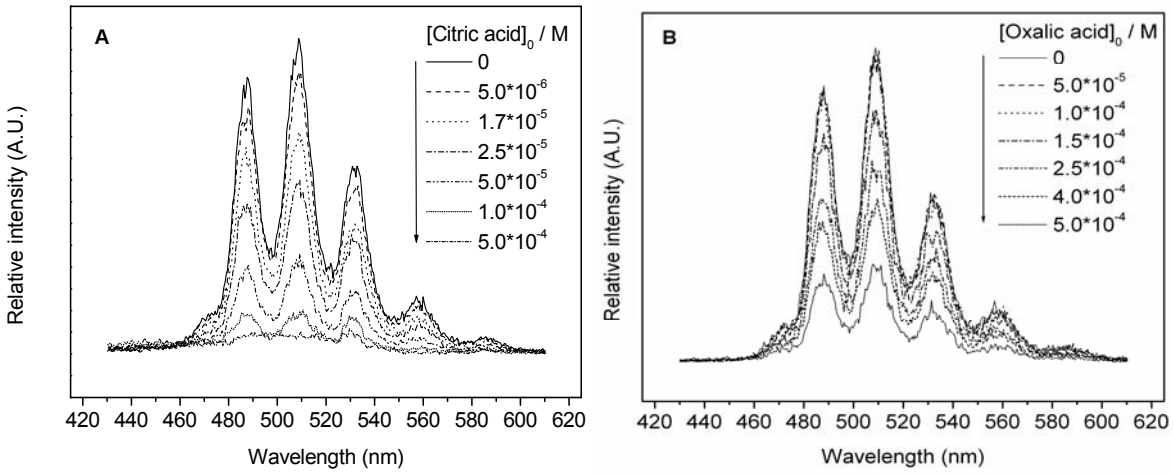

Fig 2.11. Luminescence emission spectra of U(VI) as a function of the ligand concentration measured at room temperature (25°C), $[U(VI)]_0 = 5\times10^{-5}$ M, I = 0.1 M: (a) – citric acid at pH 3.5, (b) – oxalic acid at pH 3.

TRLFS measurements at cryogenic temperature (-120°C)

The aim of the TRLFS measurements of the U(VI) ligand complex solutions at cryogenic temperature conditions was to study whether U(VI) complex species can be detected directly at low temperature. Measurements at -120°C are expected to improve significantly the intensity and resolution of luminescence spectra in consequence of lower quenching effects due to ligands and/or water.

The measurements at cryogenic temperature of a series of complex solutions containing constant U(VI) concentration and increasing ligand concentrations at constant pH showed at

first a small decrease and after that, a significant increase of the luminescence intensity (not shown here).

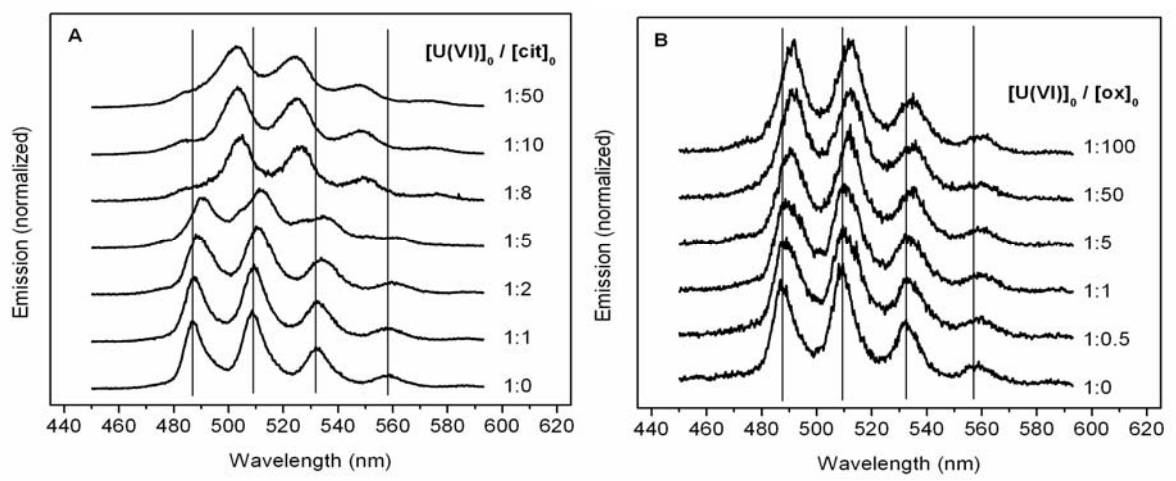

Fig. 2.12. Luminescence emission spectra of U(VI) as a function of the ligand concentration measured at cryogenic temperature (-120°C), $[U(VI)]_0 = 5\times10^{-5}$ M, I = 0.1 M, pH 3.5: (a) – citric acid, (b) – oxalic acid.

In contrast to the TRLFS measurements at room temperature, it can be seen that the U(VI) luminescence signals shift significantly to higher wavelengths at a $[U]_0$:$[cit]_0$ ratio of 1:2 and higher. This is shown in Fig. 2.12a, where the normalized luminescence emission spectra of U(VI) as a function of the total citric acid concentration measured at -120°C are compiled. For the U(VI) oxalic acid system we found comparable results with the exception, that the shift of the luminescence signals with increasing ligand concentration is less pronounced compared to the shifts due to the complexation of U(VI) by citric acid under the given experimental conditions (Fig. 2.12b). These results clearly show, that at cryogenic temperature (-120°C) the determination of emission properties of U(VI) citrate and U(VI) oxalate species is possible.

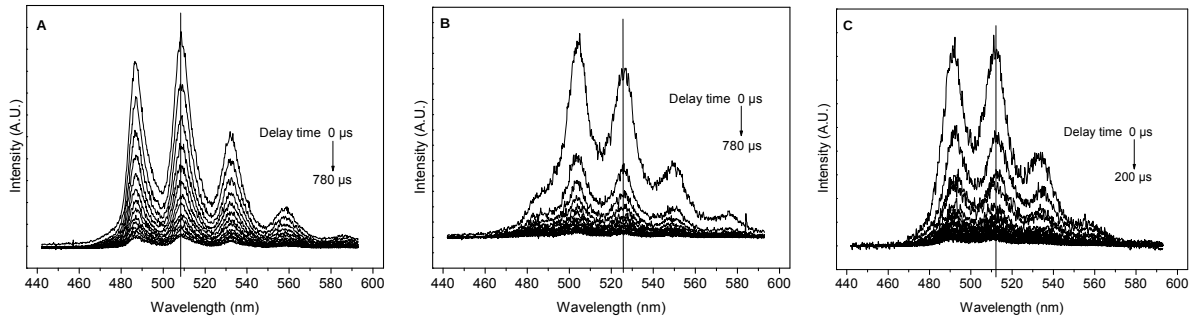

Fig. 2.13. Time-resolved luminescence emission spectra measured at cryogenic temperature (-120°C), $[U(VI)]_0 = 5\times10^{-5}$ M, I = 0.1 M, pH 3.5: (a) – without ligand, (b) – with 4×10^{-4} M citric acid, (c) – with 5×10^{-3} M oxalic acid (not all spectra of the measurements are shown here).

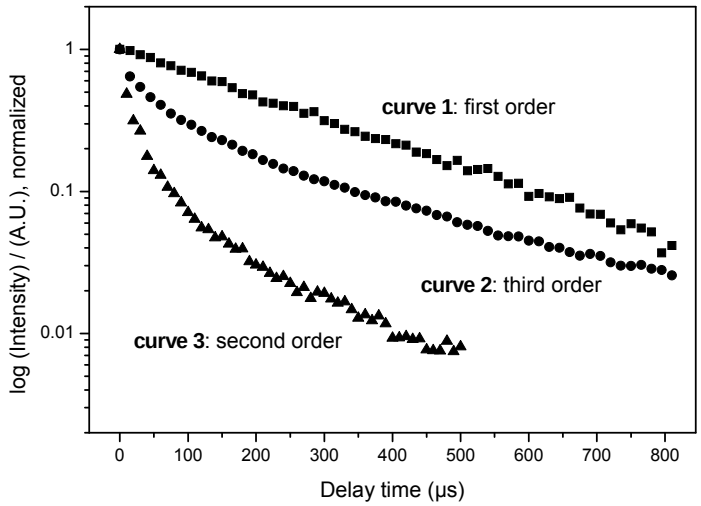

Fig. 2.14. Exponential luminescence decay of U(VI) measured at cryogenic temperature (-120°C), $[U(VI)]_0 = 5\times10^{-5}$ M, $I = 0.1$ M, pH 3.5, curve 1 – without ligand, curve 2 – with 4×10^{-4} M citric acid and curve 3 – with 5×10^{-3} M oxalic acid.

Figures 2.13a-c show three examples for time-resolved measurements at -120°C: spectra of U(VI) solution in absence of ligands (Fig. 2.13a) in comparison to spectra of U(VI) solutions in the presence of citric acid (Fig. 2.13b) or oxalic acid (Fig. 2.13c). Their corresponding luminescence decay curves are shown in Fig. 2.14. Time-resolved spectra of the U(VI) citric acid system show a three-exponential luminescence decay at a $[U]_0$:$[cit]_0$ ratio of 1:2 and higher (example: curve 2 in Fig. 2.14). Thus, three U(VI) species are the main components in these complex solutions. The averaged luminescence lifetimes are $\tau_1 = 286 \pm 29$ µs for the uncomplexed U(VI) cation, $\tau_2 = 79 \pm 15$ µs and $\tau_3 = 10 \pm 3$ µs for two different complex species. The luminescence lifetime of the uncomplexed U(VI) cation at cryogenic temperature is much higher than that at room temperature. The reason for this is the decrease of the dynamic quenching effect by water because the water molecules take stable grid places in the ice crystal after shook freezing of the samples. Comparable results were obtained by Wang et al., 2004. By analysis of the exponential luminescence decay obtained for U(VI) oxalic acid samples maximal three different lifetimes were obtained, too. For the uncomplexed U(VI) cation $\tau_1 = 261 \pm 13$ µs was determined. The lifetimes $\tau_2 = 9 \pm 3$ µs and $\tau_3 = 102 \pm 7$ µs were assigned to the U(VI) oxalate species. Exemplary, curve 3 in Fig. 2.14 shows a bi-exponential decay of the U(VI) luminescence in oxalate solution at the high $[U]_0$:$[ox]_0$ ratio of 1:100. That means, at this concentration ratio only the two U(VI) oxalate species but no uncomplexed U(VI) occur.

Complex formation constants and luminescence properties of the single species

The complex formation constants for the different U(VI) citrate and U(VI) oxalate species, formed according to Eq. (2.9) or Eq. (2.10), determined with SPECFIT are summarized in Table 2.3.

$$xUO_2^{2+} + yH^+ + zcit^{3-} \rightleftarrows ((UO_2)_xH_ycit_z)^{(2x+y-3z)} \quad (2.9)$$

$$xUO_2^{2+} + yH^+ + zox^{2-} \rightleftarrows ((UO_2)_xH_yox_z)^{(2x+y-2z)} \quad (2.10)$$

Table 2.3. Complex formation constants of U(VI) citrate and U(VI) oxalate species calculated with SPECFIT and selected literature data.

Species	**xyz**	**log β_{xyz}**	**Ionic medium**	**Method / references**
UO_2cit^-	101	7.67 ± 0.12	0.1 M $NaClO_4$	TRLFS [a] / this work
		7.24 ± 0.16	0.1 M $NaClO_4$	TRLFS [b] / this work
		7.51 ± 0.11	0.5 M $NaClO_4$	TRLFS [a] / this work
		7.40 ± 0.21	0.1 M KNO_3	Potentiometry [c]
$(UO_2)_2(cit)_2^{2-}$	202	18.85 ± 0.42	0.1 M $NaClO_4$	TRLFS [a] / this work
		18.90 ± 0.26	0.1 M $NaClO_4$	TRLFS [b] / this work
		18.75 ± 0.34	0.5 M $NaClO_4$	TRLFS [a] / this work
		18.87 ± 0.06	0.1 M KNO_3	Potentiometry [c]
UO_2ox	101	5.92 ± 0.03	0.1 M $NaClO_4$	TRLFS [a] / this work
		5.88 ± 0.29	0.1 M $NaClO_4$	TRLFS [b] / this work
		5.63 ± 0.06	0.5 M $NaClO_4$	TRLFS [a] / this work
		6.36 ± 0.07	0.1 M $NaClO_4$ / 20°C	Spectrophotometry [c]
$UO_2(ox)_2^{2-}$	102	10.30 ± 0.38	0.1 M $NaClO_4$	TRLFS [a] / this work
		10.26 ± 0.13	0.1 M $NaClO_4$	TRLFS [b] / this work
		10.79 ± 0.37	0.5 M $NaClO_4$	TRLFS [a] / this work
		10.59 ± 0.07	0.1 M $NaClO_4$ / 20°C	Spectrophotometry [c]

[a] Spectra measured at room temperature (25°C)

[b] Spectra measured at cryogenic temperature (-120°C)

[c] Rajan and Martell, 1965

The results show that the first U(VI) citrate species formed in the low pH range is of type ML. The second U(VI) citrate complex is binuclear of type M_2L_2. The carboxylic groups of citric acid in these complexes are completely deprotonated. These stoichiometric compositions of the U(VI) citrate species were obtained by analysis of all TRLF spectra measured at room temperature (analyzing the decrease of the luminescence intensity of the uncomplexed U(VI) ion) as well as measured at cryogenic temperature (analyzing the emissions of the complex species in addition) using factor analysis program SPECFIT.

The results obtained for the U(VI) oxalate system after the same fit procedure of the corresponding TRLFS data show that in addition to the 1:1 U(VI) oxalate species of type ML, a 1:2 species of type ML_2 is formed. The complex formation constants determined for the citrate and oxalate system by means of TRLFS at room temperature and cryogenic temperature are in good agreement with complex formation constants determined at $I = 0.5$ M $NaClO_4$ by concurrently performed UV-Vis spectroscopic measurements at room temperature: $\log \beta(UO_2cit^-) = 7.51 \pm 0.05$, $\log \beta((UO_2)_2(cit)_2^{2-}) = 18.89 \pm 0.04$, $\log \beta(UO_2ox) = 6.34 \pm 0.35$, $\log \beta(UO_2(ox)_2^{2-}) = 10.40 \pm 0.13$. Accepted formation constants for U(VI) citrate species in $NaClO_4$ solution as background electrolyte and at $I = 0.1$ M or $I = 0.5$ M were not found in the literature and corresponding data bases. Thus, the formation constants obtained by evaluating luminescence emission data are comparable with data obtained by potentiometry for the corresponding complex species formed in KNO_3 (Table 2.3). In the case of the U(VI) oxalate system the complex formation constants are in good agreement with literature data, which were determined applying spectrophotometry under almost identical experimental conditions (Table 2.3).

In addition to the determination of the stoichiometry (x,y,z) of the U(VI) complexes and the corresponding stability constants we divided the mixed emission spectra into single component spectra with the data analysis program SPECFIT. The results of the mathematical deconvolution of the mixed TRLF spectra (measured at -120°C) for the U(VI) citrate and oxalate system are shown in Figs. 2.15a,b. The spectroscopic data are given in Table 2.4.

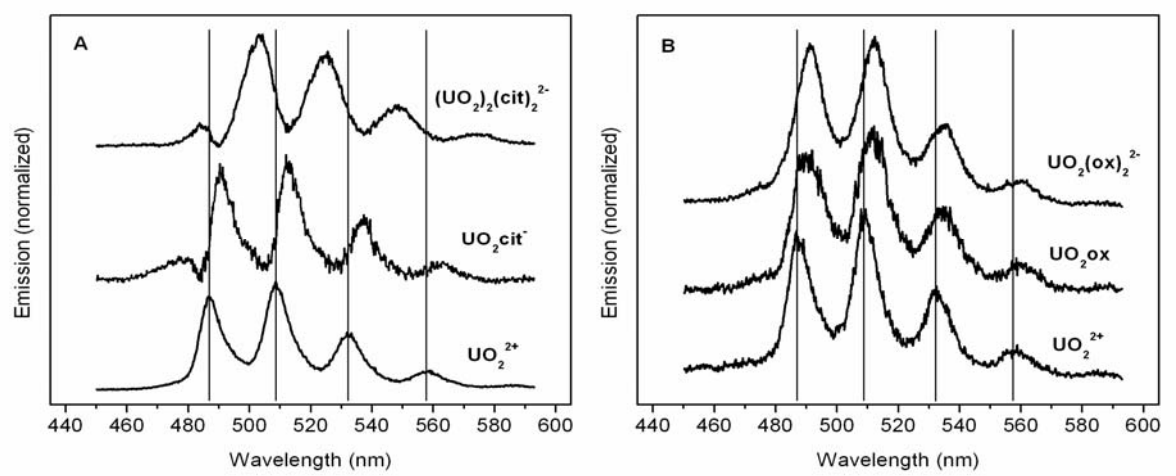

Fig. 2.15. TRLF - single component spectra of the different U(VI) citrate species (a) and U(VI) oxalate species (b) in comparison to the spectrum of UO_2^{2+} as result of the peak deconvolution by SPECFIT.

Table 2.4. Luminescence properties of U(VI) citrate and U(VI) oxalate species in comparison to the U(VI) cation at -120°C.

System	Species	Luminescence emission bands (nm)					
U(VI)/cit	UO_2^{2+}	472.8	487.9	509.1	532.1	557.6	585.1
	UO_2cit^-	475.3	491.8	513.5	537.0	561.9	
	$(UO_2)_2(cit)_2^{2-}$	483.6	502.7	524.5	548.1	574.0	
U(VI)/ox	UO_2^{2+}	473.3	488.1	509.4	532.6	557.7	585.1
	UO_2ox	472.9	490.8	511.6	534.1	559.5	587.1
	$UO_2(ox)_2^{2-}$	472.6	491.0	512.2	534.8	559.9	

The main emission bands of the 1:1 and 2:2 U(VI) citrate complexes show a bathochromic shift of up to 14-16 nm compared to the emission bands of the uncomplexed U(VI) ion. In contrast, the shift of the emission bands of both U(VI) oxalate species to the emission bands of the uncomplexed U(VI) ion is less pronounced (about 3 nm). The pronounced shift in the spectra at $[U]_0$:$[cit]_0$ ratios from 1:5 to 1:8 can not be explained, since the calculated U(VI) species distributions (17.8% UO_2^{2+}; 40.0% 1:1 complex; 42.2% 2:2 complex for the first case and 11.0% UO_2^{2+}; 42.2% 1:1 complex, 46.8% 2:2 complex for the second case) are not so different.

The calculated U(VI) citrate species distribution applying complex formation constants determined in this work shows that both U(VI) citrate species are formed concurrently at pH 3.5 in the same ratio. Therefore, it is very difficult to assign surely the luminescence lifetimes obtained at -120° C (cf. section TRLFS measurements at cryogenic temperature (-120°C)) to the individual U(VI) citrate complex species, because the absolute intensities of the species are not known. According to the calculated species distribution at different U(VI) to oxalic acid concentration ratios in the samples using obtained complex formation constants by SPECFIT (at first the formation of the 1:1 complex at low oxalic acid concentrations and later additionally the formation of the 1:2 U(VI) oxalate species at higher oxalic acid concentrations) the short lifetime τ_2 is assigned to the 1:1 complex species and the longer lifetime τ_3 to the 1:2 U(VI) oxalate complex.

Conclusion

For the first time, luminescence properties and stability constants were determined for aqueous U(VI) citrate and oxalate species in the acidic pH range by laser-induced fluorescence spectroscopy at -120°C. This is a great improvement toward TRLFS

measurements at room temperature, where emission signals of the complex species are not detectable.

2.4 U(VI) complexation by lactic acid – Determination of complex formation constants in dependence on temperature (7 to 65°C) by UV-Vis spectroscopy and TRLFS

After disposal in nuclear waste repositories the chemical and migration behavior of actinides depends on many factors, e.g., pH value and redox potential of the solution, concentration of complex partners and temperature. It is estimated that maximum temperatures in the near field of a repository could reach 100°C (Brasser et al., 2008) in dependence on the waste forms (Rao et al., 2002) and the host rock (Warwick et al., 1997). Thus, for long-term safety assessment, knowledge of the interaction of actinides such as uranium with inorganic and organic ligands at elevated temperatures is required. The majority of the complexation studies are conducted at ambient conditions (18 - 25°C) and data are published in (Guillaumont et al., 2003; Hummel et al., 2005). Thermodynamic data on the hydrolysis of U(VI) and the complexation of U(VI) by some carboxylates at elevated temperatures are summarized by Rao (2007). In the present work, the U(VI) complexation by lactic acid (pH 3.0) was studied in the temperature range from 7 to 65°C. For this, UV-Vis absorption spectroscopy and TRLFS were applied. The results of this study will be published in (Steudtner et al., 2012, in preparation).

2.4.1 Experimental

The complexation experiments were performed at a fixed U(VI) concentration of 5×10^{-4} M (UV-Vis) or 5×10^{-5} M (TRLFS). The lactate concentration was varied between 0 and 0.1 M (UV-Vis) or 0 and 0.01 M (TRLFS). These measurements were carried out at an ionic strength of 0.1 M ($NaClO_4$) at pH 3 and at variable temperatures (7, 25, 45, 65°C). The pH value was adjusted with $HClO_4$ or NaOH. The UV-Vis measurements were performed using a CARY-5G UV-Vis-NIR Spectrometer (Varian). The spectra were recorded between 375 and 500 nm. The luminescence of U(VI) was measured after excitation with laser pulses at 266 nm (Minilite laser system, Continuum) and an averaged pulse energy of 250 µJ. The emitted fluorescence light was detected using a spectrograph (iHR 550, HORIBA Jobin Yvon) and an ICCD camera (HORIBA Jobin Yvon). The TRLFS spectra were recorded from 450.0 to 649.9 nm by accumulating 50 laser pulses using a gate time of 20 µs.

2.4.2 Results and discussion

UV-Vis measurements

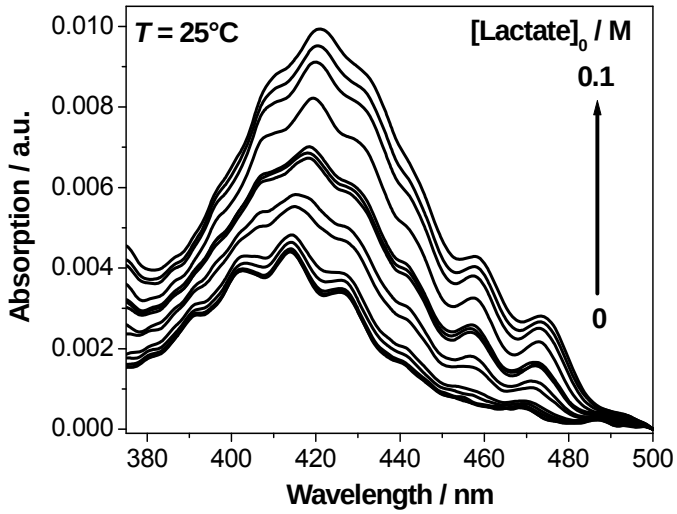

Fig. 2.16. Absorption spectra of U(VI) solutions as a function of the lactate concentration ([U(VI)] = 5×10^{-4} M, I = 0.1 M, pH 3, 25°C).

Exemplary for the UV-Vis spectrophotometric titrations of U(VI) solutions as a function of the lactate concentration in the temperature range from 7 to 65°C, the absorption spectra obtained at 25°C are shown in Fig. 2.16. At each temperature, an increase of the absorbance and a red shift of 10 nm of the absorption maxima, in comparison to the bands of the free U(VI) ion, indicate the formation of U(VI) lactate species. The absorption spectra were evaluated using the factor analysis program SPECFIT (Binstead et al., 2005). Single component spectra of three species (free UO_2^{2+} and two complex species) could be extracted and complex formation constants for the 1:1 and the 1:2 complex were determined. The U(VI) band positions of the various U(VI) lactate species are compiled in Table 2.5.

Table 2.5. Main absorption bands of the U(VI) species in the U(VI) lactate system.

U(VI) species	Band positions / nm						
$\mathbf{UO_2^{2+}}$	391.3	402.4	414.4	426.6	439.4	453.6	468.6
$\mathbf{UO_2Lac^{+}}$	396.1	408.2	419.4	431.4	443.4	457.4	472.9
$\mathbf{UO_2(Lac)_2}$	400.0	412.5	423.3	435.3	447.6	461.7	476.6

For the free UO_2^{2+} ion, an absorption maximum at 414.4 nm was detected. The 1:1 and the 1:2 complex exhibit an absorption maximum at 419.4 and 423.3 nm, respectively. No significant changes of the molar absorption coefficient of the U(VI) species were observed

when the temperature of U(VI) lactate solutions was increased from 7 to 65°C. The complex formation reaction of U(VI) with lactate can be written as follows:

$$UO_2^{2+} + Lac^- \rightleftarrows UO_2Lac^+ \quad (2.11)$$

$$UO_2^{2+} + 2\ Lac^- \rightleftarrows UO_2(Lac)_2 \quad (2.12)$$

The complex formation constants, determined for the 1:1 and 1:2 complexes, increase by 3.9 and 17.4 times, respectively, when the temperature is increased from 7 to 65°C (cf. Table 2.6). The complex formation constants, determined by Starý and Balek (1962) in 0.1 M $NaClO_4$ solution at 20°C by extraction can be included very good in the temperature-dependent study. This verifies the determined complex formation constants.

Table 2.6. Summary of complex stability constants ($\log \beta$) of the U(VI) lactate complexes (I = 0.1 M ($NaClO_4$)) in comparison to literature data.

Complex	T / °C	UV-Vis	TRLFS	Extraction
		$\log \beta_{11}$	$\log \beta_{11}$	$\log \beta_{11}$
UO_2Lac^+	7	2.75 ± 0.09	2.71 ± 0.08	---
	20	---	---	2.81 ± 0.06
	25	2.94 ± 0.08	3.18 ± 0.08	---
	45	3.19 ± 0.15	3.29 ± 0.21	---
	65	3.34 ± 0.07	3.70 ± 0.13	---
		$\log \beta_{12}$	$\log \beta_{12}$	$\log \beta_{12}$
$UO_2(Lac)_2$	7	4.40 ± 0.27	---	---
	20	---	---	4.56 ± 0.10
	25	4.85 ± 0.19	---	---
	45	5.55 ± 0.20	---	---
	65	5.64 ± 0.20	---	---
Reference		this work	this work	(Starý and Balek, 1962)

TRLFS measurements

Exemplary for all temperatures, Fig. 2.17 shows the luminescence spectra of U(VI) as a function of the lactate concentration measured at 25°C. The U(VI) luminescence spectra are characterized by six emission bands (at 470.7, 488.0, 509.3, 532.6, 557.9 and 585.1 nm) that were consistent with the typical band positions of the free UO_2^{2+} ion observed by Billard et al. (2003). At all temperatures studied, we observed a decrease of the U(VI) luminescence intensity with increasing ligand concentration but no shift of the U(VI) emission bands. This

is characteristic for static luminescence quenching due to complex formation by forming a non-fluorescent U(VI) lactate species. The fluorescence decay of the free UO_2^{2+} ion can be described by a mono-exponential decay function and the calculated lifetimes are summarized in Table 2.7.

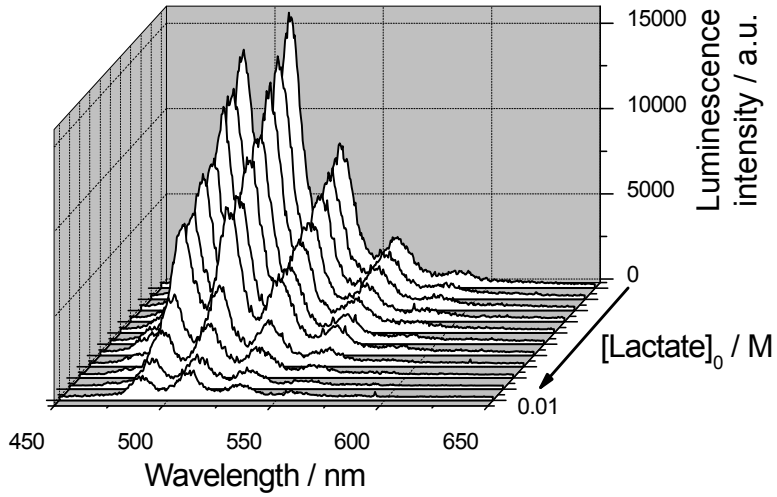

Fig. 2.17. Luminescence spectra of U(VI) solutions as a function of the lactate concentration ([U(VI)] = 5×10^{-5} M, I = 0.1 M, pH 3, 25°C).

Table 2.7. Temperature-dependence of fluorescence lifetimes (τ) of the free UO_2^{2+} ion as function of the lactate concentration ([U(VI)] = 5×10^{-5} M, I = 0.1 M, pH 3).

T / °C	**7**	**25**	**45**	**65**
Lactate / M	**τ / µs**	**τ / µs**	**τ / µs**	**τ / µs**
0	5.27	1.32	0.36	0.12
1×10^{-5}	5.08	1.26	0.36	0.13
1×10^{-4}	5.00	1.28	0.36	0.14
5×10^{-4}	4.67	1.23	0.34	0.09
1×10^{-3}	4.30	1.13	0.35	0.12
5×10^{-3}	1.99	0.77	0.28	0.08
1×10^{-2}	1.53	0.57	0.22	0.06

The lifetime of the free UO_2^{2+} ion decreases with increasing ligand concentration caused by an additional dynamic quenching process. The determined lifetimes can be used to calculate the luminescence intensities if no dynamic quenching occurs (Stern and Volmer, 1919; Glorius et al., 2008). The corrected luminescence intensities were then used to calculate the concentration of the non-complexed U(VI) in every sample. In contrast to the UV-Vis

measurements, only the complex formation constant for the complex reaction given in Eq. (2.11) could be calculated from the luminescence spectra.

The results of the UV-Vis and TRLFS measurements show an increase of the complex formation constants with increasing temperature from 7 to 65°C (cf. Table 2.6). Similar effects of the temperature were previously observed for a few reactions of U(VI) with other carboxylates (Rao, 2007).

The enthalpy (ΔH) and entropy (ΔS) of the complexation were determined graphically from the temperature-dependent stability constants by using the van't Hoff equation in a modified linear form. The plot of the natural logarithm of the equilibrium constant versus the reciprocal temperature gives a straight line.

$$\ln \beta = -\frac{\Delta H}{RT} + \frac{\Delta S}{R} \tag{2.13}$$

The slope is equal to minus the enthalpy divided by the universal gas constant ($R = 8.314$ J·K^{-1}·mol^{-1}) and the intercept is equal to the entropy divided by R. When the complex stability constants (Table 2.6) are introduced into the van't Hoff plot, the slope is negative (cf. Fig. 2.18). A negative slope represents an endothermic reaction. Energy is used for formation of the U(VI) lactate complexes from the reactants. ΔH and ΔS values of 18.7 ± 1.8 kJ·mol^{-1} and 119.2 ± 6.1 J·mol^{-1}·K^{-1} for the UO_2Lac^+ complex and of 40.8 ± 7.0 kJ·mol^{-1} and 230.4 ± 22.5 J·mol^{-1}·K^{-1} for the $UO_2(Lac)_2$ complex are calculated. A positive entropy change indicates a spontaneous reaction between U(VI) and lactate. It can be concluded that the complexation of U(VI) with lactate is endothermic (ΔH pos.) and entropy-driven (ΔS pos.). Similar thermodynamics has been observed for the complexation of U(VI) with other carboxylates such as acetate and malonate (Rao, 2007).

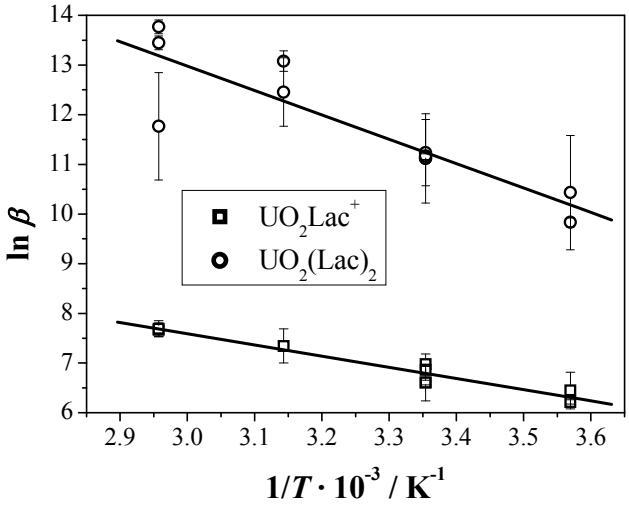

Fig. 2.18. van't Hoff plot of the obtained U(VI) lactate complex stability constants.

Conclusion

Thermodynamic parameters were determined for the U(VI) lactate system by absorption and fluorescence spectroscopy. The complex stability constants of the U(VI) lactate complexes (UO_2Lac^+, $UO_2(Lac)_2$) increase with increasing temperature (7 – 65°C). The complexation of U(VI) with lactate is endothermic (ΔH pos.) and entropy-driven (ΔS pos.). Since the U(VI) lactate complexes are weaker than the U(VI) citrate and oxalate complexes (cf. section 2.3), the influence of lactate on the speciation of U(VI) and thus, on the migration behavior of U(VI) in a nuclear waste repository is lower compared to the influence of citric or oxalic acid.

2.5 U(VI) complexation by anthranilic acid and nicotinic acid – Determination of complex formation constants by fs-TRLFS and TRLFS

Analog to the Am(III) complexation study (cf. section 2.1), the complexation of U(VI) with nitrogen containing organic model ligands was investigated in order to simulate humic substance functionalities. Representing simple aromatic structural units of HA molecules, anthranilic acid (AA) and nicotinic acid (Nic) were selected (cf. Fig. 2.19). Since AA exhibits unique fluorescence emission after excitation, the U(VI) complexation by AA was studied using a femtosecond-pulsed laser system (fs-TRLFS). Since Nic shows no distinct fluorescence emission or analyzable spectra under the studied conditions, the U(VI) complexation by Nic was studied applying a conventional TRLFS system. The results of this study are published in-depth by Raditzky et al. (2010).

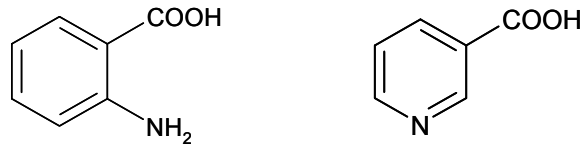

Anthranilic acid (AA) | Nicotinic acid (Nic)

Fig. 2.19. Structures of the nitrogen containing model ligands AA and Nic.

2.5.1 Experimental

Sample preparation

Anthranilic acid (p.a., Merck) and nicotinic acid (p.a., Sigma-Aldrich) stock solutions were prepared freshly for each experiment. The complex solutions were prepared from stock

solutions of the ligand (1×10^{-3} M) and $UO_2(ClO_4)_2$ (5×10^{-3} M in 0.02 M $HClO_4$). The ionic strength was kept constant in all measurements at 0.1 M by adding aliquots of an $NaClO_4$ stock solution. All experiments were carried out at 23 ± 2°C. Solutions were prepared using Milli-Q water (mod. Milli-RO/Milli-Q-System, Millipore, Schwalbach, Germany) and necessary pH adjustments were done with diluted NaOH and $HClO_4$ solutions. Table 2.8 summarizes the composition of all solutions studied.

Table 2.8. Composition of the studied solutions.

Ligand	Used system	c_{metal} (M)	c_{ligand} (M)	pH
AA	fs-TRLFS	$0 - 3\times10^{-4}$	1×10^{-5}	1.5 – 4.5
Nic	Minilite	5×10^{-5}	$0 - 8\times10^{-4}$	2.5 – 4.5

TRLFS measurements

fs-TRLFS system

A Nd:YVO_4 laser (Spectra Physics) was used as pump source for the Ti:Sapphire oscillator. After amplification, third harmonic generation was used to provide femtosecond pulses with an excitation wavelength of 266 nm. The emitted fluorescence was focused into a spectrograph (Acton Research) and collected by an intensified CCD camera (Picostar HR, La Vision Inc.). The delay generator allows time delays between 0 and 100 ns in various steps from ps up to ns. The time-resolved spectra were recorded from 348 to 551 nm at delay times ranging from 0 to 30 ns in 0.1 ns increments. The gate width for the fluorescence detection was set to 2 ns.

TRLFS system

The U(VI) luminescence in solution was measured using a Nd:YAG laser system (Continuum Minilite II, Continuum Electro Optics Inc.) with an excitation wavelength of 266 nm. The trigger input of the detection system was coupled directly to the trigger output of the laser. The luminescence emission was focused into a spectrograph (iHR 550, HORIBA Jobin Yvon) via fiber optics and detected using an ICCD camera system and a built-in delay generator (HORIBA Jobin Yvon). The TRLFS spectra were measured from 371 to 674 nm at a gate time of 2 µs by averaging 100 laser pulses. For the time-resolved measurements 101 spectra were recorded during a delay time of 10000 ns with a step size of 100 ns. The first time step started between 40 and 80 ns after the excitation pulse.

2.5.2 Results and discussion

Interaction of U(VI) with anthranilic acid

Like other amino acids, AA is an amphoteric compound. It occurs in three different species in aqueous solution: the completely protonated acid (AAH_2), the zwitterionic species ($AAH^{+/-}$) and the completely deprotonated anthranilate (AA^-). The pK_a values of AA at an ionic strength of 0.1 M and room temperature are pK_{a1} = 2.01 and pK_{a2} = 4.78 (Martell et al., 1998). Figure 2.20a shows the fluorescence emission spectra of AA as a function of the U(VI) concentration at pH 3.5.

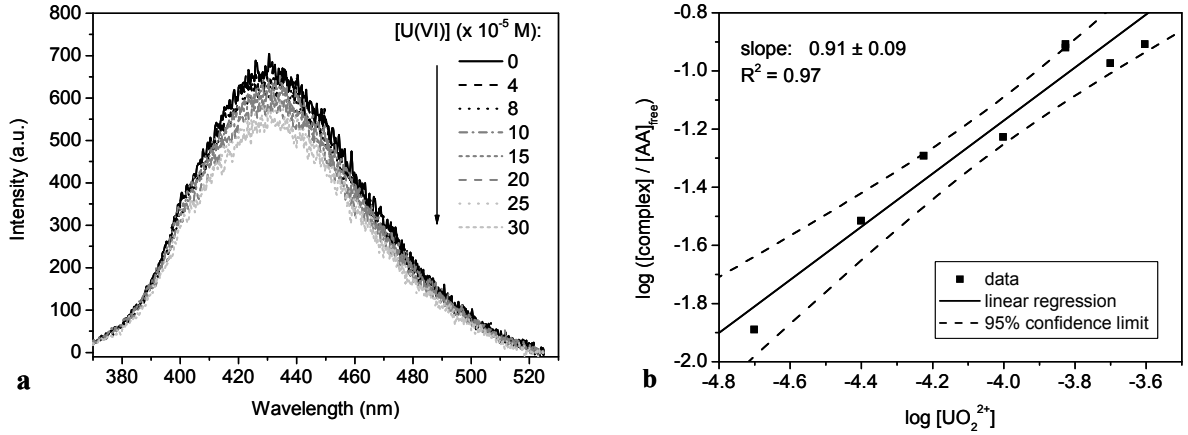

Fig. 2.20. (a) Fluorescence emission spectra of 1×10^{-5} M AA as a function of the U(VI) concentration and (b) slope analysis of the complex formation of U(VI) with AA at pH 3.5.

With addition of the metal ion the fluorescence intensity of AA decreases with increasing U(VI) concentration. The observed decrease is typical for static fluorescence quenching processes due to complex formation, thereby reducing the concentration of non-complexed AA. No shift of the main emission band was observed, implying that the formed complex does not show any fluorescence in the considered wavelength range. The obtained fluorescence lifetimes are in good agreement with those determined for the ligand species without U(VI) (Raditzky et al., 2010). For all experiments no changes in the lifetimes were observed, which verifies the assumption of static quenching and exclude the occurrence of dynamic quenching effects. For all measurements at pH < 2, a complexation of AA with U(VI) could not be detected.

For the experiments at pH values above 2, the following equation for the direct reaction of U(VI) with the zwitterionic $AAH^{+/-}$ species was obtained:

$$x\,UO_2^{2+} + y\,{}^{+}H_3NC_6H_4COO^- \rightleftarrows (UO_2)_x(H_3NC_6H_4COO)_y^{(2x)+} \qquad (2.14)$$

Assuming that the measured luminescence intensity is proportional to the concentration of the free prevailing AA species in equilibrium, the stoichiometry can be graphically determined via validation plot, using a modified logarithmic form of the mass action law:

$$\log \frac{[(UO_2)_x(H_3NC_6H_4COO)_y^{(2x)+}]}{[^+H_3NC_6H_4COO^-]^y} = x \log [UO_2^{2+}] + \log \beta_{xy} \qquad (2.15)$$

An example for the slope analysis at pH 3.5 is given in Fig. 2.20b. A slope near 1 was determined, suggesting the formation of a predominant 1:1 complex. The spectra analysis program SPECFIT (Binstead et al., 2005) was used to validate the determined stoichiometry and to calculate the stability constant of the complex. The averaged formation constant for this reaction was calculated to be $\log \beta_{11} = 3.14 \pm 0.17$ (cf. Table 2.9). This is comparable to literature data ($\log \beta_{11} = 2.95 \pm 0.01$), although this value was determined in a 20% mixture of ethanol and water (Mahmoud et al., 1996). The formation of a 1:2 complex or a chelate was not detectable under the given experimental conditions (low concentrations, fixed ligand concentration). To estimate whether or not the $-NH_3^+$ functionality dissociates during the complex formation, the stability constants derived from the slope analysis were plotted as a function of $\log [H^+]$, as described in (Geipel et al., 2004). From the slope of this plot the number of protons released due to complex formation can be obtained. Taking into account that AA is not completely deprotonated in the pH range from 2.5 to 4.5, only one proton can possibly be released. A slope of about -0.1 was derived, leading to the conclusion that the proton of the protonated amino group is not released during the complexation. Therefore, it is very probable that the amino group does not participate in complex formation at the investigated pH range and that the U(VI) ion is only coordinated via the carboxylic group. This is in agreement with literature data. Alcock et al. (1996a) examined the AA complex with U(VI) using crystal structure analysis discovering that the amino group does not participate in chelating U(VI).

Interaction of U(VI) with nicotinic acid

Like AA, Nic exists as zwitterionic species ($^+HNC_5H_4COO^-$) in aqueous solution. The dissociation constants as well as the species distribution of Nic are comparable to those of AA. The luminescence spectra of U(VI) as a function of the Nic concentration at pH 2.5 are given in Fig. 2.21a. In all samples a mono-exponential luminescence decay was observed indicating the presence of the free U(VI) ion with a lifetime of about 1.29 ± 0.10 µs. With increasing Nic concentration a strong decrease of the U(VI) luminescence intensity was observed. No shifts of the main emission bands were detected. Therefore, it is concluded that

the formed complex does not show any luminescence in the considered wavelength range and time scale.

The complex formation of Nic with U(VI) was determined in the whole examined pH range from 2.5 to 4.5. In analogy to the experiments with AA a slope analysis was performed. The validation plot for the complexation of U(VI) with Nic at pH 2.5 is shown in Fig. 2.21b. Unlike AA, the slope was calculated to be 1.32 ± 0.10, suggesting the additional formation of 1:2 complexes at higher ligand concentrations.

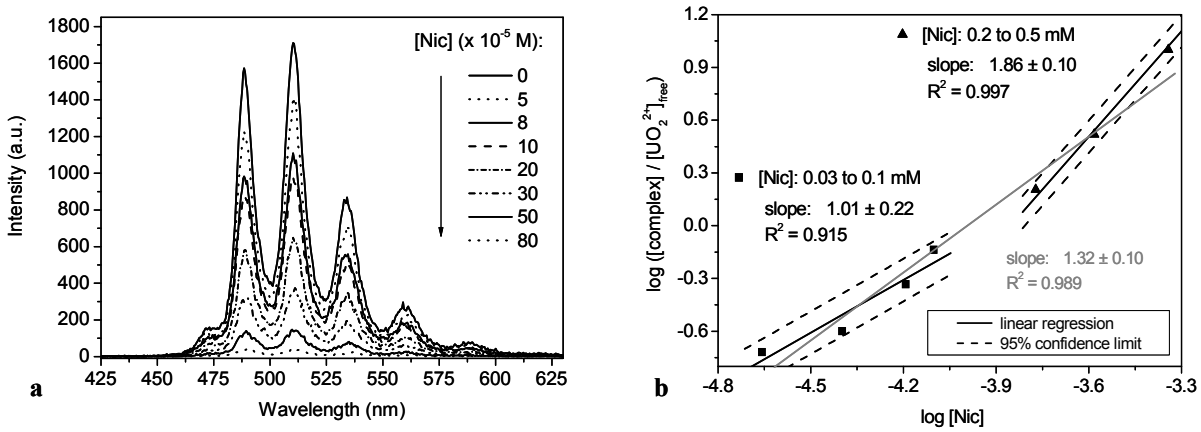

Fig. 2.21. (a) Luminescence spectra of 5×10^{-5} M U(VI) as a function of Nic concentration and (b) slope analysis of the complex formation of U(VI) with Nic at pH 2.5.

To verify this, the plotted data points were split into two sections with different ligand concentration ranges (section 1: [Nic]: 3×10^{-5} M to 1×10^{-4} M, section 2: [Nic]: 2×10^{-4} M to 5×10^{-4} M) and the slope of each section was calculated separately. The results show that a 1:2 complex is formed at ligand concentrations above 1×10^{-4} M. According to the measurements with AA, we suggest that the $-NH^{+}$ functionality of Nic does not dissociate during the complex formation, resulting in the following equation for the direct reaction of U(VI) with the zwitterionic Nic species:

$$x\,UO_2^{2+} + y\,{}^{+}HNC_5H_4COO^{-} \rightleftarrows (UO_2)_x(HNC_5H_4COO)_y^{(2x)+} \qquad (2.16)$$

The averaged formation constants for this reaction were calculated to be $\log \beta_{11} = 3.73 \pm 0.30$ and $\log \beta_{12} = 7.46 \pm 0.17$ (cf. Table 2.9). These values are in good agreement with constants determined for the complexation of U(VI) with picolinic acid, which is an isomer of Nic. The formation constants for $[(UO_2)_x(Pic)_y]^{2x-y}$ were found to be $\log \beta_{11} = 3.75$ and $\log \beta_{12} = 7.48$ (Budantseva et al., 2006). It was concluded that the binding of U(VI) takes place via the carboxylic group of the ligand. The formation of a chelate is not possible at the considered pH and concentration range. This is in agreement with literature data. For the U(VI) nicotinate

complex Alcock et al. (1996b) described a structure where U(VI) is located in an inversion centre of two ligand molecules and is only coordinated by oxygen atoms. It is interesting that the formation constant of the U(VI) anthranilate complex is slightly lower than that of the nicotinate system. It seems that the amino group causes an electrostatic repulsion between $-NH_3^+$ and UO_2^{2+}, while this repulsion is understated in the Nic molecule in consequence of the *meta* position of $-NH^+$. In addition to that, the pyridine nitrogen seems to stabilize the U(VI) complexation due to electronic and mesomeric effects.

Table 2.9. Summary of complex stability constants for the U(VI) ligand species (I = 0.1 M).

Ligand	pH	log β_{11}	log β_{12}
Anthranilic acid	1.5	-	
	2.5	3.20 ± 0.20	
	3.5	3.03 ± 0.20	
	4.5	3.21 ± 0.20	
averaged log β		**3.14 ± 0.17**	
Nicotinic acid	2.5	3.75 ± 0.12	7.35 ± 0.34
	3.5	3.90 ± 0.15	7.48 ± 0.24
	4.5	3.54 ± 0.18	7.54 ± 0.11
averaged log β		**3.73 ± 0.30**	**7.46 ± 0.17**

Transferring these results to the HA system, the present investigation has shown that oxygen containing functional groups dominate the U(VI) complexation in the investigated pH range. It is known from literature that deprotonation reactions of organic ligands can be forced in the presence of metal ions. The possibility of dissociation and chelate formation even at low pH is reported, e.g., it was shown that phenolic OH groups contribute to the interaction between U(VI) and HA already at pH 4 (Pompe et al., 2000b). Accordingly in the case of Nic and AA, it is also possible that the acidity of the nitrogen functional groups could be influenced when coordinated to U(VI). This study showed that this is not the case for both investigated ligands. However, it can not be excluded that deprotonated amino groups may contribute to the U(VI) complexation at pH values above 4.5, e.g. due to hydrogen bonding. In future, this has to be studied in more detail to answer this question.

2.6 U(VI) complexation by phenylphosphonic acid – Determination of complex formation constants by TRLFS

Phosphorus has been known to be present in the humic fractions of natural organic matter (Stevenson, 1994), although in small and widely varying amounts (e.g., 0.12 - 1.42 wt.% in soil HA (Makarov, 1997)). The identity and stability of phosphorus associated with humic substances is not fully understood. However, from ^{31}P-NMR spectroscopy it was concluded that the organic phosphorus detected in HA is probably derived from phosphonic acids, phospholipids or phosphoric mono- and diesters (Makarov, 2005; He et al., 2006). The aim of the work was to investigate the potential influence of phosphorus containing functionalities on the U(VI) complexation in comparison to oxygen functionalities, using phenylphosphonic acid (cf. Fig. 2.22) as a simple organic model ligand for aromatic phosphonate functionalities in HA. The U(VI) complexation was examined using time-resolved laser-induced fluorescence spectroscopy (TRLFS).

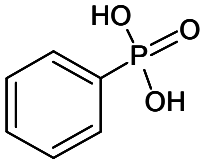

Phenylphosphonic acid
(PPA)

Fig. 2.22. Structure of the phosphorus containing model ligand PPA.

2.6.1 Experimental

Sample preparation

Phenylphosphonic acid (99%) was purchased from Acros Organics. The complex solutions were made from stock solutions of the ligand (1×10^{-3} M), which were prepared freshly for each experiment, and $UO_2(ClO_4)_2$ (5×10^{-3} M in 0.02 M $HClO_4$). The TRLFS experiments were performed at a total U(VI) concentration of 5×10^{-5} M by varying the ligand concentration from 0 to 5×10^{-4} M. To minimize the formation of hydrolytic species of U(VI), the complex formation experiments were performed in the pH range 1.5 to 4.0. Solutions were prepared using Milli-Q water (mod. Milli-RO/Milli-Q-System, Millipore, Schwalbach, Germany). The ionic strength was adjusted to 0.1 M by adding 0.5 M $NaClO_4$ (p.a., Merck). The pH was adjusted using diluted NaOH (high grade, Merck) and $HClO_4$ (p.a., Merck) solutions.

TRLFS measurements

The spectra were recorded at room temperature using a Nd:YAG laser system (Continuum Minilite II, Continuum Electro Optics Inc.). The excitation wavelength was 266 nm with pulse energies between 0.2 and 0.5 mJ. The U(VI) luminescence emission was focused into a spectrograph (iHR 550, HORIBA Jobin Yvon GmbH) via fiber optics and detected using an ICCD camera system and a built-in delay generator (HORIBA Jobin Yvon). All settings of the camera and spectrograph as well as the collection and storage of the measured data were controlled by the software LabSpec 5.21.12 (HORIBA Jobin Yvon). The TRLFS spectra were measured from 371 to 674 nm at a gate time of 2 µs by averaging 100 laser pulses. For the time-resolved measurements 101 spectra were recorded during a delay time of 10000 ns with a step size of 100 ns.

2.6.2 Results and discussion

Figure 2.23a shows the luminescence emission spectra of U(VI) as a function of the PPA concentration at pH 2.

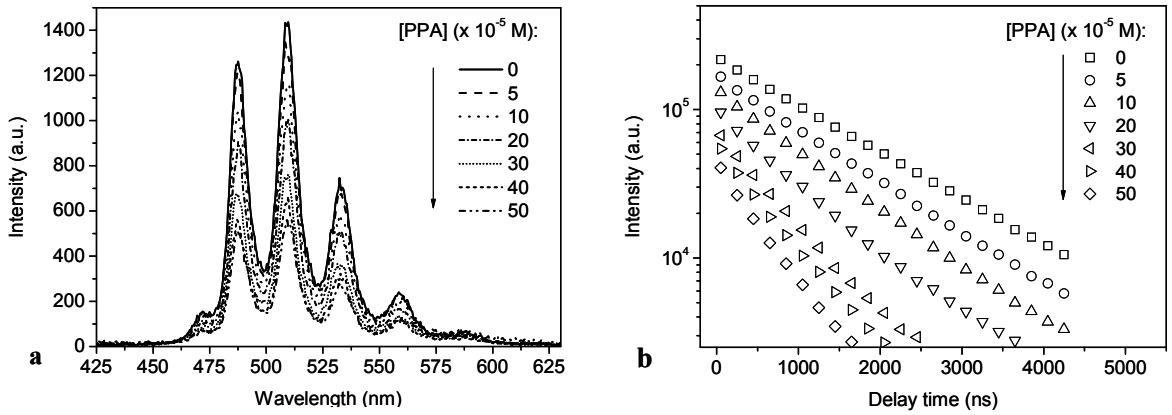

Fig. 2.23. (a) Emission spectra of 5×10^{-5} M U(VI) as a function of PPA concentration and (b) luminescence decay of U(VI) as a function of the ligand concentration at pH 2.

The spectra show a strong decrease of the U(VI) luminescence intensity with increasing ligand concentration at all pH values studied. No shift of the main emission bands was observed, implying that the formed complex does not show any luminescence emission in the considered wavelength range. The observed decrease is typical for static fluorescence quenching processes due to complex formation, thereby reducing the concentration of non-complexed metal ion. A mono-exponential luminescence decay was observed in all samples between pH 1.5 and 3.0. In the absence of the ligand, a luminescence lifetime of about 1.39 ± 0.11 µs was determined, which can be attributed to the free UO_2^{2+} ion. Only for the samples at

pH 4.0 it was possible to determine a bi-exponential luminescence decay, due to the formation of U(VI) hydroxo species. However, with increasing ligand concentration the lifetime of the free UO_2^{2+} ion decreases to 0.55 ± 0.05 µs (cf. Fig. 2.23b), indicating additional dynamic quenching processes caused by the free ligand.

The determined lifetimes were used to correct the measured U(VI) intensities for the dynamic quenching part, using the $I_0/I = \tau_0/\tau$ relation deduced from the Stern-Volmer equation:

$$\frac{I_0}{I} = \frac{\tau_0}{\tau} = 1 + K_{SV} \cdot [Q] \tag{2.17}$$

where I_0 and τ_0 represent the U(VI) intensity and lifetime, respectively, without dynamic quench, whereas I and τ are the measured intensity and lifetime, respectively, when the quenching substance Q (in this case the free PPA) is added. The corrected luminescence intensities were then used to calculate all necessary concentrations (e.g., the concentration of the uncomplexed UO_2^{2+}). To estimate the complexation constant, the intensity ratio ((I_0/I)-1) was plotted against the concentration of the uncomplexed ligand. The slope represents the stability constant K_{SV}. Figure 2.24a shows the Stern-Volmer plot for the complex formation of U(VI) with PPA at pH 2.0.

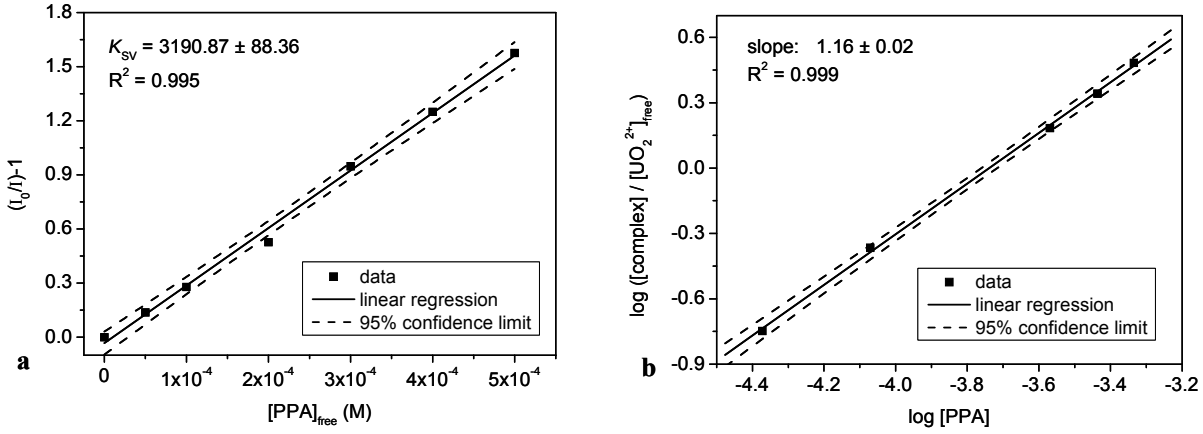

Fig. 2.24. (a) Stern-Volmer plot and (b) slope analysis of the complex formation of U(VI) with PPA at pH 2.

The pK_a values of PPA at an ionic strength of 0.1 M and room temperature are pK_{a1} = 1.7 and pK_{a2} = 7.0 (Martell et al., 1998). Thus, the complex formation between pH 1.5 and 4.0 can be written as:

$$x\ UO_2^{2+} + y\ C_6H_5PO_3H^- \rightleftarrows (UO_2)_x(C_6H_5PO_3H)_y^{(2x-y)+} \tag{2.18}$$

The averaged formation constant for this reaction was calculated to be $\log K_{11} = 3.49 \pm 0.08$ (Stern-Volmer plot) (cf. Table 2.10).

Assuming that the corrected luminescence intensity is proportional to the concentration of the free UO_2^{2+} ion in equilibrium, the stoichiometry of the complex can be graphically determined via slope analysis, using a modified logarithmic form of the mass action law:

$$\log \frac{[(UO_2)_x(C_6H_5PO_3H)_y^{(2x-y)+}]}{[UO_2^{2+}]^x} = y \log [C_6H_5PO_3H^-] + \log K_{xy} \quad (2.19)$$

An example for the slope analysis at pH 2 is given in Fig. 2.24b. A slope > 1 was calculated, suggesting the formation of 1:1 and 1:2 complexes. The spectra analysis program SPECFIT (Binstead et al., 2005) was used to validate the graphically determined stoichiometry and to calculate the stability constants of the complexes. The averaged formation constants are listed in Table 2.10. In comparison with aliphatic phosphorus containing ligands, the stability constants for the U(VI) phenylphosphonate system are somewhat smaller than those determined for the complexation of U(VI) with e.g., phosphoethanolamine $\log \beta_{11} = 4.5 \pm 0.1$ (Koban and Bernhard, 2007). This suggests a destabilization of the U(VI) phenylphosphonate system due to structural or steric reasons.

Table 2.10. Summary of the complex stability constants of the U(VI) ligand species (I = 0.1 M).

Complex	M_xL_y [a]	$\log K_{xy}$ [b] (SV-plot)	$\log K_{xy}$ [b,c] (slope analysis)	$\log \beta_{xy}$ [b] (SPECFIT)
$UO_2C_6H_5PO_3H^+$	11	3.49 ± 0.08	3.50 ± 0.12	3.61 ± 0.14
$UO_2(C_6H_5PO_3H)_2$	12			6.95 ± 0.22

[a] M... metal; L...ligand

[b] ± t-distribution for 95% confidence interval

[c] fixed slope (n = 1)

The present investigation has shown that the complexation strength of aromatic phosphonate groups toward U(VI) is comparable or even higher than that of oxygen functionalities such as carboxylic groups. The obtained formation constants are for example higher than those determined for the U(VI) complex formation with benzoic acid (e.g., $\log \beta_{11} = 3.37 \pm 0.14$ (Glorius et al., 2007)). Transferring these results to the HA system, the phosphorus containing functional groups may contribute to the U(VI) complexation by HA, however, due to the low concentrations of phosphorus in HA these functionalities play only a subordinate role compared to oxygen functionalities, especially carboxylic groups.

2.7 U(VI) complexation by benzenesulfonic acid and 4-hydroxybenzene sulfonic acid – Determination of complex formation constants by TRLFS

The sulfur content of HA varies between 0 and 2 wt.% (Stevenson, 1982). Regarding to their oxidation states, reduced sulfur (e.g. thiols, sulfides) or oxidized sulfur groups (e.g. sulfonates, sulfates) could be found (Solomon et al., 2003). Complexation studies of HA with zinc (Xia et al., 1997) and mercury (Skyllberg et al., 2006) showed that reduced sulfur groups (probable thiols) are favored to coordinate the metal ions. See also literature compiled in section 3.2.

The aim of this work was to determine the influence of sulfur containing functional groups on the U(VI) complexation and to evaluate their contribution in comparison to oxygen containing functional groups. For this, simple organic model ligands that can occur as building blocks for HA are used in the first instance with the objective to transfer the results to HA. As model ligands benzenesulfonic acid (BSA) and 4-hydroxybenzenesulfonic acid (HBSA) were applied. Their structures are given in Fig. 2.25. These model ligands represent an intermediate state since the oxidation state of sulfur is between the most reduced form (thiol) and the most oxidized form (ester-SO_4-S). However, also sulfonate groups are present in HA. The U(VI) complexation was examined using time-resolved laser-induced fluorescence spectroscopy (TRLFS).

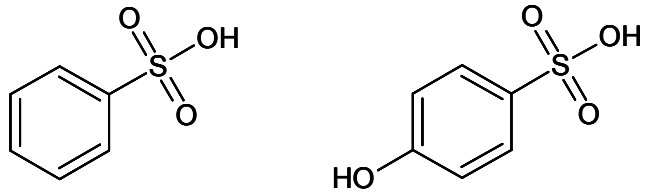

Benzenesulfonic acid (BSA) 4-Hydroxybenzenesulfonic acid (HBSA)

Fig. 2.25. Structures of the sulfur containing model ligands BSA and HBSA.

2.7.1 Experimental

Sample preparation

A U(VI) stock solution (5×10^{-3} M $UO_2(ClO_4)_2$ in 0.05 M $HClO_4$) was used for all experiments. Aqueous ligand stock solutions (0.2 M) of BSA (sodium salt, 97%, Sigma-Aldrich, St. Louis, Missouri, USA) and HBSA (sodium salt, dihydrate, 99%, Acros Organics, Geel, Belgium) were prepared freshly for the experiments. The TRLFS measurements were

performed at a constant U(VI) concentration of 1.08×10^{-4} M. The ligand concentration was varied between 0 and 5×10^{-3} M. The ionic strength was kept constant at 0.1 M by adding aliquots of a 0.2 M $NaClO_4$ stock solution ($NaClO_4 \cdot H_2O$, *p.a.*, Merck, Darmstadt, Germany). All solutions were prepared with distilled water. The pH was adjusted to pH 2.4 ± 0.05 with $HClO_4$ (*p.a.*, Merck) to minimize the formation of hydrolytic U(VI) species.

TRLFS measurements

All experiments were performed at room temperature (21 ± 2°C) under ambient atmosphere ($pCO_2 = 10^{-3.5}$ atm). TRLFS laser pulses at 410 nm with an average pulse energy of 0.6 mJ (Nd:YAG-MOPO laser system, mod. GCR 230 (20 Hz), Spectra Physics, Mountain View, USA) were used for excitation of the U(VI) luminescence. The sample solution was rinsed through a flow-through cuvette (Hellma, Müllheim, Germany) with a speed of 1 ml/min using a peristaltic pump (mod. Reglo Digital, Ismatec, IDEX Health & Science GmbH, Wertheim, Germany) to remove possibly formed photodegradation products. The emitted luminescence light was detected in a right angle setup by an Acton Research 300i spectrograph (Acton Research corporation, Acton MA, USA). The spectra were recorded in time-resolved mode using an ICCD camera (1024 pixels; mod. PI-MAX 3, Roper Scientific GmbH, Ottobrunn, Germany). The time difference between the trigger of the laser system and the start of the camera was adjusted by a delay generator DG 540 (Stanford Research Instruments, Sunnyvale, USA). The spectra were recorded in the wavelength range from 467 to 601 nm by accumulating 100 laser pulses using a camera gate time of 5 µs. For the time-resolved measurements the delay times were varied from 30 to 10,030 ns after application of the laser pulse using a step size of 100 ns. All settings of the camera and the spectrograph were computer controlled with the program WinSpec/32, version 2.5.19.6, Roper Scientific 2003. The measured time-resolved spectra were analyzed using the program OriginPro 7.5G (OriginLab Corporation, USA) in order to determine the fluorescence lifetimes. The time dependency of the luminescence signal was analyzed by fitting the sum of the luminescence intensities over the measured wavelength range by an exponential decay function:

$$I(t) = \sum I \cdot \mathrm{e}^{-\frac{t}{\tau}} \tag{2.20}$$

where $I(t)$ is the total luminescence intensity at the time t, I the luminescence intensity of the luminescent compound (in this case U(VI)) at $t = 0$ and τ the corresponding lifetime.

2.7.2 Results and discussion

Figure 2.26 shows the luminescence spectra of the U(VI) sample solutions as a function of the ligand concentration for BSA (a) and HBSA (b) at pH 2.4. Both ligands cause a strong decrease of the U(VI) luminescence intensity with increasing ligand concentration. No shift of the luminescence peaks is observed. Both observations are typical for this so-called static luminescence quenching. With this effect, all processes of luminescence decrease caused by the formation of non-luminescent complexes, thereby reducing the concentration of the non-complexed luminescent compound, are described.

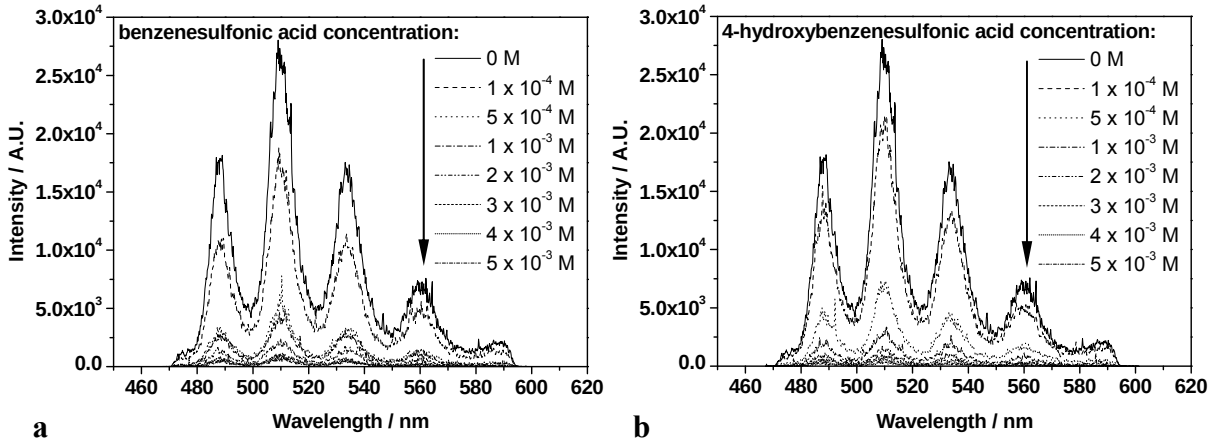

Fig. 2.26. Luminescence spectra of U(VI) (1.08×10^{-4} M) with benzenesulfonic acid (a) and 4-hydroxybenzenesulfonic acid (b) at pH 2.4 as a function of the ligand concentration.

The luminescence decay is mono-exponential in all samples. In the absence of the ligand, the luminescence lifetime, which can be attributed to the non-complexed U(VI) ion, amounts to 1830 ± 20 ns, which is in agreement with literature values (Moll et al., 2003; Günther et al., 2007). However, the lifetime decreases with increasing ligand concentration (Fig. 2.27) for BSA from 1450 ± 20 ns to 110 ± 3 ns and for HBSA from 1320 ± 10 ns to 70 ± 2 ns. This indicates an additional dynamic luminescence quenching, caused by the free ligand. For determination of the stability constant the U(VI) luminescence signal has to be corrected for the dynamic quenching part. For this, the Stern-Volmer equation (2.21) is used.

$$\frac{I_0}{I} = \frac{\tau_0}{\tau} = 1 + K_{SV} \cdot [Q] \qquad (2.21)$$

I_0/I is the ratio of the U(VI) luminescence intensity without dynamic quench (I_0) to the measured intensity (I). For determination of I_0 the ratio of the respective luminescence lifetimes of U(VI) without quencher (τ_0) and with quencher (τ) is used. K_{SV} presents the Stern-Volmer constant, Q is the quenching substance (in this case the free organic ligand). This correction method is well established and described in more detail in the literature (e.g., Geipel et al., 2004).

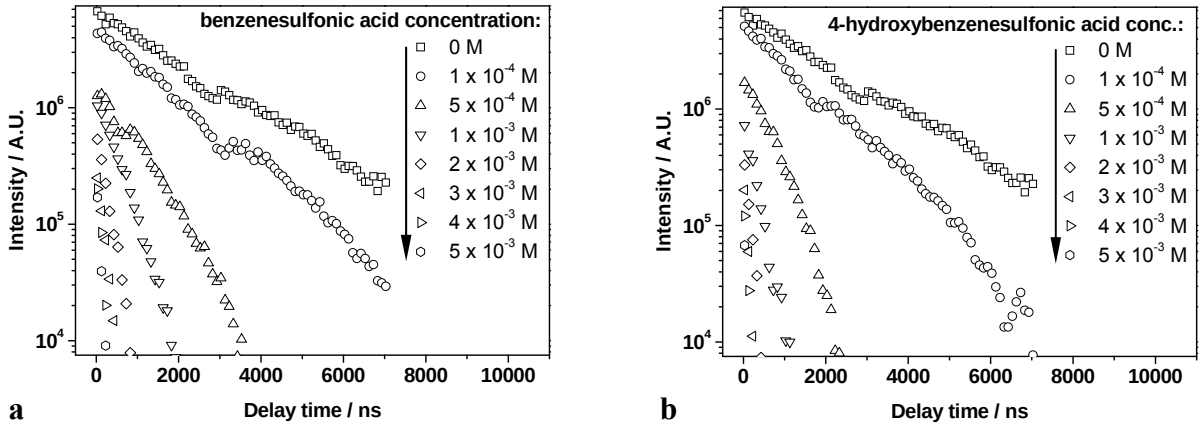

Fig. 2.27. Luminescence decay of U(VI) as a function of the ligand concentration (dynamic quenching).

In order to determine the complex stability constants, knowledge of the ligands pK_a values is necessary. In the case of BSA, the pK_a values reported in the literature for the sulfonate group vary in a wide range from -6.56 ± 0.06 (Cerfontain et al., 1975) to 2.554 (Dean, 1999). As shown by Joseph et al. (2008) using potentiometric titration the pK_a has to be significantly smaller than 0. Dong et al. (2009) assumed pK_a values for the sulfonate group of BSA and HBSA with -2.7 and -2, respectively. Thus, under the experimental conditions applied in this study, the sulfonate group at both ligands can be regarded as deprotonated. The pK_a of the hydroxyl group in HBSA is 8.56 ± 0.05 (Joseph et al., 2008), and therefore, it occurs in its protonated form. Thus, only the deprotonated sulfonate group has to be considered in a complex formation reaction (2.22).

$$UO_2^{2+} + n\,L^- \rightleftarrows UO_2L_n^{(2-n)+} \tag{2.22}$$

Based on this reaction the following logarithmic form of the mass action law was obtained:

$$\log \frac{\left[UO_2L_n^{(2-n)+}\right]}{\left[UO_2^{2+}\right]} = n \cdot \log\left[L^-\right] + \log K \tag{2.23}$$

With the assumption that the corrected luminescence intensity I_0 is proportional to the concentration of the free U(VI) ion in equilibrium, the complex stoichiometry and the complex stability constant can be graphically determined via validation plot (Fig. 2.28). The slope (n) of this plot represents the stoichiometry of the formed complex, the intersection with the y-axis at log [L^-] = 0 is equal to the equilibrium constant log *K*.

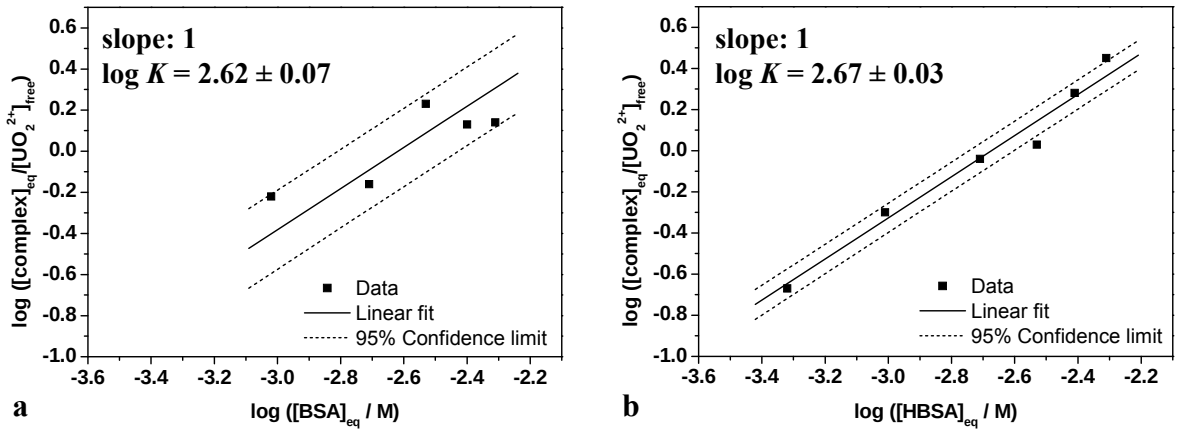

Fig. 2.28. Validation plot of the complexation of U(VI) with benzenesulfonic acid (a) and 4-hydroxybenzenesulfonic acid (b) at pH 2.4.

For both complex systems a slope close to 1 was calculated indicating the formation of a predominant 1:1 complex.

For low BSA concentrations (1×10^{-4} and 5×10^{-4} M), stability constants out of the confidence limit (95%) were calculated. Thus, they were not considered in the validation plot ([BSA] = 1×10^{-3} to 5×10^{-3} M). For the complexation of U(VI) by BSA, a 1:1 complex with a stability constant of log *K* = 2.62 ± 0.07 was determined. Joseph et al. (2008) did not observe a static quench in their TRLFS measurements, because the BSA concentrations used for their experiments were too low ([BSA] = 1×10^{-4} to 8×10^{-4} M). Thus, they concluded that there was no complexation of U(VI) by BSA.

For HBSA, the lowest ligand concentration of 1×10^{-4} M showed no static quench after dynamic quench correction. Thus, it was not considered in the validation plot (Fig. 2.28b). The stability constant for the formation of a 1:1 complex was determined to be log *K* = 2.67 ± 0.03. This value corroborates the stability constant of log K_{110} = 2.76 ± 0.15 determined by Joseph et al. (2008) using TRLFS with ultrafast pulses (fs-TRLFS).

The experimental results show that the sulfonate group of both ligands interacts with U(VI) with the same strength independent of the presence of an additional p-hydroxyl group at the aromatic compound.

However, compared to the interaction of U(VI) with oxygen functionalities of HA (Pompe et al., 2000b) the constants determined for the interaction of U(VI) with sulfonate groups are three orders of magnitude lower. Thus, complexation of U(VI) by oxygen functionalities will be preferred compared to sulfonate groups. This is in agreement with the results of Sachs and Bernhard (2010), discussed in section 3.2.2.

3 Complexation and redox reactions of actinides with humic substances

3.1 Spectroscopic characterization of the ternary U(VI) carbonato humate complex by cryo-TRLFS and ATR FT-IR

Knowledge of the actinide speciation in natural systems is of great importance for understanding of their transport behavior. The migration of actinides such as uranium in the environment is affected by complexation, sorption and redox processes, their solubility, as well as their ability to form colloids (Silva and Nitsche, 1995; Kim, 2006). The complexation of U(VI) with various inorganic and organic ligands and the consequences for the chemical speciation of U(VI) under environmentally relevant conditions has been studied thoroughly and data are summarized e.g. in (Guillaumont et al., 2003; Hummel et al., 2005). Besides low molecular weight organic ligands, humic substances (fulvic acids (FA) and humic acids (HA)), polyelectrolytic organic macromolecules, which occur in soils, sediments and waters, can influence the interaction behavior of actinides in the environment due to their complexing, sorption and redox properties and their ability for colloid formation (Kim, 1986; Choppin, 1992; Silva and Nitsche, 1995).

Under environmentally relevant conditions, actinide ions, such as UO_2^{2+}, can be complexed by HA. In previous studies, the formation of a binary (UO_2HA(II) (Czerwinski et al., 1994; Pompe et al., 1998; Montavon et al., 2000)) and a ternary (UO_2(OH)HA(I) (Zeh et al., 1997; Sachs et al., 2007a; Pashalidis and Buckau, 2007)) complex of U(VI) with HA was described based on the metal ion charge neutralization model (CNM, (Kim and Czerwinski, 1996)). Complex stability constants determined for the UO_2HA(II) complex range from $\log \beta = 5.83 \pm 0.09$ (Montavon et al., 2000) to 6.33 ± 0.15 (Czerwinski et al., 1994) ($I = 0.1$ M). For the ternary UO_2(OH)HA(I) complex, complex stability constants were determined with 14.7 ± 0.5 (Zeh et al., 1997), 14.89 ± 0.54 (Sachs et al., 2007a) and 15.3 (Pashalidis and Buckau, 2007). Beside the binary humate complex, the ternary humate

complex can dominate the U(VI) speciation under weak acidic and near-neutral pH conditions in the presence of HA under carbonate-free conditions (Sachs et al., 2007a). However, in the presence of carbonate, the formation of ternary U(VI) carbonato humate complexes is assumed in the literature (Glaus et al., 1995) comparable to ternary Eu(III), Am(III) and Cm(III) carbonato humate (Dierckx et al., 1994; Panak et al., 1996) as also discussed in (McCarthy et al., 1998) and (Reiller, 2005). Furthermore, the potential formation of ternary actinide carbonato humate complexes was already discussed in sorption studies (Křepelová et al., 2006; Schmeide and Bernhard, 2010). Information on such complexes is necessary for a reliable description of the mobility of actinides under environmentally relevant conditions.
Hence, the objective of this study was the direct spectroscopic identification and characterization of aqueous U(VI) humate complexes as function of pH and carbonate concentration by time-resolved laser-induced fluorescence spectroscopy at low temperature (cryo-TRLFS) and by attenuated total reflection Fourier-transform infrared (ATR FT-IR) spectroscopy. The results of the study are published in-depth by Steudtner et al. (2011a, 2011b).

3.1.1 Ternary U(VI) carbonato humate complex studied by cryo-TRLFS

3.1.1.1 Experimental

Complexation experiments were performed at a fixed U(VI) concentration of 1×10^{-5} M. The HA concentration was varied between 0 and 100 mg/L. The measurements were carried out at an ionic strength of 0.1 M. The pH values of the solutions were adjusted to pH 8.5 using diluted $HClO_4$ and NaOH solutions. For further experimental details see Steudtner et al. (2011a).

3.1.1.2 Results and discussion

Binary UO_2^{2+}-CO_3^{2-} system

The binary UO_2^{2+}-CO_3^{2-} system is used for evaluation of the measurement system at low temperature. The measured emission spectra of the HA-free samples in both series are characterized by five emission bands and the fluorescence decay can be described by a mono-exponential decay function (Table 3.1). The obtained fluorescence lifetimes and the positions of the emission bands are in very good agreement with literature data (Wang et al., 2004; Steudtner et al., 2010) for $UO_2(CO_3)_3^{4-}$ (Table 3.1), since the $UO_2(CO_3)_3^{4-}$ complex dominates the U(VI) speciation at pH 8.5 in the absence of HA.

Table 3.1. Band positions and fluorescence lifetime of the HA-free samples in comparison to literature data of $UO_2(CO_3)_3^{4-}$.

	Fluorescence emission (nm)					τ (µs)	T (K)	Reference
Series 1	480.7	499.9	520.3	542.5	566.6	834.1 ± 8.9	153	this work
Series 2	480.2	499.3	519.9	543.4	565.4	820.4 ± 11.8	153	this work
$UO_2(CO_3)_3^{4-}$	480.8	500.1	520.9	543.1	566.8	829.3 ± 13.5	153	(Steudtner et al., 2010)
$UO_2(CO_3)_3^{4-}$	479.6	499.2	519.9	542.4	565.5	883.6	6	(Wang et al., 2004)

Series 1: Ternary UO_2^{2+}-HA-CO_3^{2-} system – constant [U]

Figure 3.1 shows the luminescence spectra of U(VI) as a function of the HA concentration. A decrease of the U(VI) luminescence intensity is observed with increasing HA concentration. No shift in the peak maxima of the fluorescence emission bands is detected. At low temperature (T = 153 K) fluorescence quenching effects are suppressed (Wang et al., 2008; Wimmer et al., 2009). Thus, the decrease in the U(VI) luminescence intensity points to a complexation between $UO_2(CO_3)_3^{4-}$ and HA forming a non-fluorescent U(VI) carbonato humate species. Also the binary UO_2HA(II) complex (Pompe et al., 2000b) and the ternary UO_2(OH)HA(I) complex (Sachs et al., 2007a) do not show individual fluorescence signals.

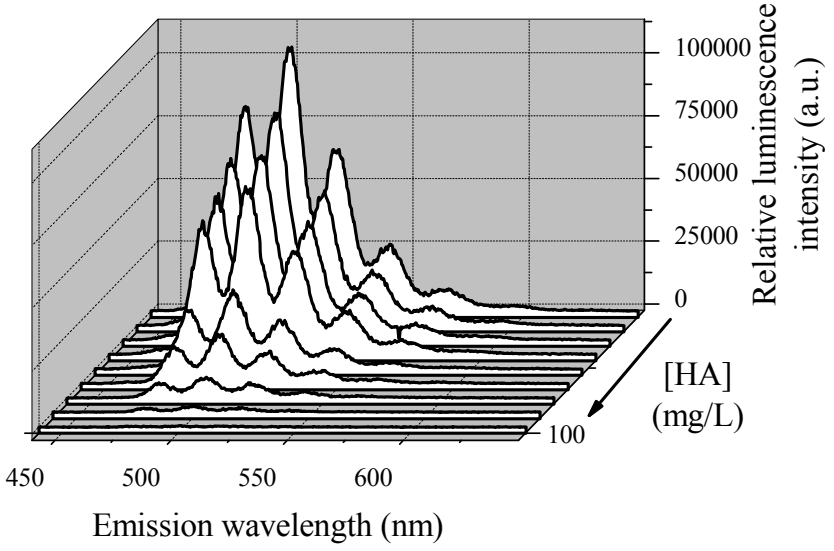

Fig. 3.1. U(VI) luminescence spectra (t = t_0) as a function of the HA concentration at pH 8.5 ($[U(VI)]_{tot} = 1\times10^{-5}$ M, $[HA]_{tot}$ = 0 − 100 mg/L, I = 0.1 M ($NaClO_4$), T = 153 K, $pCO_2 = 10^{-3.5}$ atm).

Based on the measured fluorescence spectra, the complex stability constant of the U(VI) carbonato humate complex is calculated applying the complexation models mentioned above. The obtained complex stability constants are summarized in Table 3.2. Within the experimental uncertainties, the log *K* values agree very well. By slope analysis (Fig. 3.2) a slope of 1.12 ± 0.11 is obtained. This value verifies the assumed ligand exchange reaction for the complex formation.

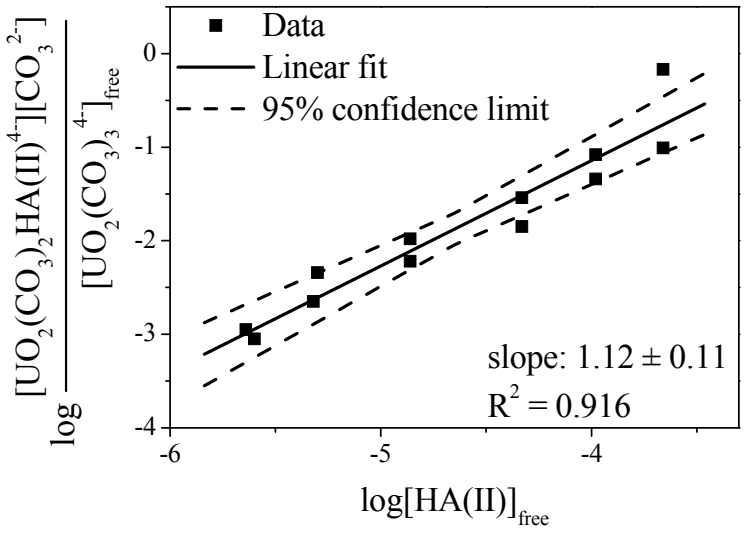

Fig. 3.2. Slope analysis for the complexation of U(VI) with HA at pH 8.5 ($[U(VI)]_{tot} = 1\times10^{-5}$ M, $[HA]_{tot}$ = 0 − 100 mg/L, I = 0.1 M ($NaClO_4$), T = 153 K, $pCO_2 = 10^{-3.5}$ atm).

Series 2: Ternary UO_2^{2+}-HA-CO_3^{2-} system – constant [HA]

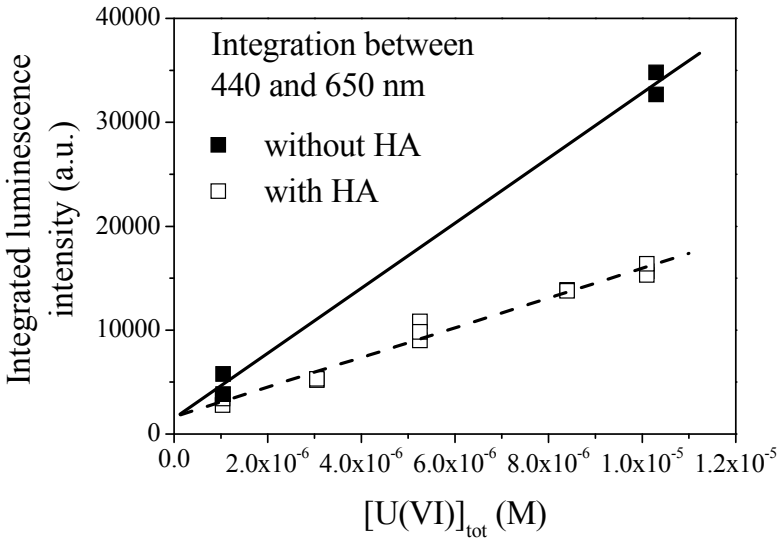

Fig. 3.3. Integrated luminescence intensity of U(VI) as a function of the U(VI) concentration in the absence and presence of HA at pH 8.5. ($[U(VI)]_{tot} = 1\times10^{-6} - 1\times10^{-5}$ M, $[HA]_{tot}$ = 2 mg/L, I = 0.1 M ($NaClO_4$), T = 153 K, $pCO_2 = 10^{-3.5}$ atm).

In agreement to series 1, the U(VI) luminescence spectra of series 2 obtained in the absence and presence of HA exhibit the luminescence characteristics of the $UO_2(CO_3)_3^{4-}$ complex. The fluorescence lifetime and the position of the emission bands are in very good agreement with series 1 and literature data, cf. Table 3.1.

The integrated luminescence intensity of U(VI) as a function of the U(VI) concentration in the absence and presence of HA is depicted in Fig. 3.3. With increasing U(VI) concentration the U(VI) luminescence intensity increases linearly in the absence and presence of HA. The U(VI) luminescence intensity determined for the U(VI)-HA system is lower than that determined for the HA-free system. This can be attributed to a static fluorescence quenching process due to the complex formation. For all experiments no shift of the main emission bands and no changes in the fluorescence lifetimes are observed, which verifies the assumption of static fluorescence quenching and excludes the occurrence of dynamic quenching effects. The formed U(VI) carbonato humate complex does not show any fluorescence in the considered wavelength range, which corresponds to the results of series 1. The complex stability constants determined for the $UO_2(CO_3)_2HA(II)^{4-}$ complex by mathematical analysis and by the multivariate data analysis program SPECFIT amount to $\log K = 2.97 \pm 0.26$ and $\log K = 2.56 \pm 0.41$ ($\log \beta_{SPECFIT} = 24.30 \pm 0.41$), respectively. The results agree very well with the data obtained from series 1 (Table 3.2).

Table 3.2. Complex stability constants obtained for the formation of $UO_2(CO_3)_2HA(II)^{4-}$ (I = 0.1 M ($NaClO_4$)).

$UO_2(CO_3)_3^{4-} + HA(II) \rightleftarrows UO_2(CO_3)_2HA(II)^{4-} + CO_3^{2-}$		**log *K***
Series 1 – constant [U]	mathematical analysis	2.98 ± 0.17
	SPECFIT	2.82 ± 0.09
Series 2 – constant [HA]	mathematical analysis	2.97 ± 0.26
	SPECFIT	2.56 ± 0.41
Mean		2.83 ± 0.17

The complex stability constants for the $UO_2(CO_3)_2HA(II)^{4-}$ complex, compiled in Table 3.2, range from $\log K = 2.56 \pm 0.41$ to $\log K = 2.98 \pm 0.17$. The average formation constant is calculated with $\log K = 2.83 \pm 0.17$ for an ionic strength of 0.1 M. The brutto stability

constant for the reaction of the single components determined by SPECFIT amounts to $\log \beta_{SPECFIT} = 24.57 \pm 0.17$ ($UO_2^{2+} + 2CO_3^{2-} + HA(II) \rightleftarrows UO_2(CO_3)_2HA(II)^{4-}$).

3.1.2 Binary and ternary U(VI) humate complexes studied by ATR FT-IR

3.1.2.1 Experimental

Complexation experiments were performed at a fixed U(VI) concentration of 1×10^{-3} M. The HA concentration was kept constant at 1 g/L. The measurements were carried out at an ionic strength of 0.1 M. The pH values of the solutions were titrated between pH 10 and 2 using diluted $HClO_4$ and NaOH solutions. For further experimental details see Steudtner et al. (2011b).

3.1.2.2 Results and discussion

U(VI) speciation in the presence of humic acid

For U(VI) speciation calculations in the presence of HA, the geochemical speciation code EQ3/6 (Wolery, 1992) modified for HA calculation (Sachs et al., 2004) was used applying the currently accepted thermodynamic data for U(VI) compiled in (Guillaumont et al., 2003), as well as complex stability constants and loading capacities (LC) for $UO_2HA(II)$ (Montavon et al., 2000; Pompe et al., 2000a, 2000b) and $UO_2(OH)HA(I)$ (Sachs et al., 2007a). The LC represents the mole fraction of complexing sites of a HA accessible for metal ion complexation under the given experimental conditions (Kim and Czerwinski, 1996). The pH-dependency of the LC was calculated from the literature data by linear regression resulting in Eq. (3.1).

$$LC = -0.555 + 0.186 \cdot pH \qquad (3.1)$$

The pH-dependent U(VI) speciation in the presence of HA is shown in Fig. 3.4 for experimental conditions applied in this study. The speciation pattern shows the free UO_2^{2+} ion as the predominant species below pH 3.0. Upon increasing pH from 3.0 to 4.0, the fraction of UO_2^{2+} decreases with the start of complexation of U(VI) by HA. Under the considered conditions, the binary $UO_2HA(II)$ complex and the ternary $UO_2(OH)HA(I)$ complex dominate the U(VI) speciation in the pH range between 3.5 and 7.5 with maxima at pH 4.2 and 6.5, respectively. Above pH 7.5, the U(VI) speciation is dominated by the U(VI) carbonato species $(UO_2)_2CO_3(OH)_3^-$ and $UO_2(CO_3)_3^{4-}$. UO_2Cl^+ and $UO_2(CO_3)_2^{2-}$ contribute less than 5% to the U(VI) speciation under the chosen conditions (Fig. 3.4). It should be noted that the

OECD/NEA Chemical Thermodynamics Database (Guillaumont et al., 2003) predicts further U(VI) species, e.g. chloro, oligomeric hydroxo and carbonate complexes, which are not shown in Fig. 3.4 for clarity since their contribution is less than 1%.

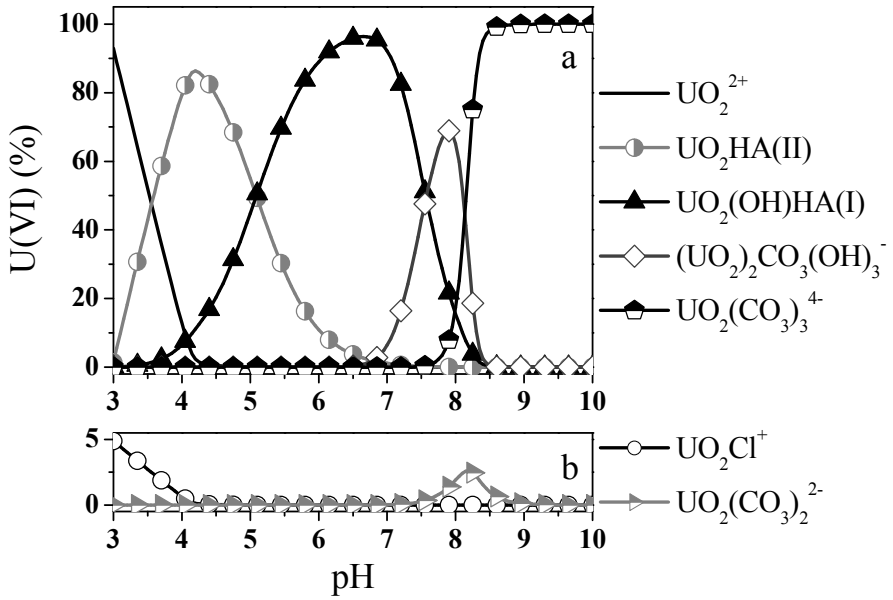

Fig. 3.4. Speciation of U(VI) in the presence of HA ([U(VI)] = 1 mM, $[HA]_{tot}$ = 1 g/L, I = 0.1 M (NaCl), $pCO_2 = 10^{-3.5}$ atm). U(VI) species below 1% are not plotted.

FT-IR spectroscopy of U(VI) humate solutions as a function of pH value

ATR FT-IR spectroscopy can be applied for the identification of molecular species in aqueous solution. Previous investigations have shown the sensitivity of the UO_2 asymmetric stretching mode (υ_3) to changes in the coordination environment (Lefevre et al., 2008; Müller et al., 2008; Müller et al., 2009). Complexation of UO_2^{2+} weakens the O=U=O bonds, increases bond lengths and causes shifts to lower frequencies of $\upsilon_3(UO_2)$. The extent of these shifts is related to the stability of the U(VI) ligand interaction. This sensitivity allows the use of this mode as a marker for specific molecular information on coordination of UO_2^{2+} in aqueous solution. Further molecular information on complexation reactions can also be obtained from the vibrational modes of the inorganic or organic ligand. For instance, the carbonate ion can be coordinated in a mono or a bidentate configuration with metal ions, resulting in a reduction of the symmetry of the free carbonate ion with D_{3h} to C_{2v}. Then, the band of the IR active $\upsilon_3(CO_3^{2-})$ is split into an asymmetric and a symmetric band. From the magnitude of splitting, coordination can be elucidated, e.g. for a bidentate coordination a higher splitting is observed than for monodentate coordination (Jolivet et al., 1980).

The results of the spectrophotometric titrations of aqueous solutions of 1 mM U(VI) and 1 g/L HA at two different carbonate concentrations are depicted in Fig. 3.5. The titrations were

performed starting from pH 10 down to an acidic pH level. The spectra shown in Fig. 3.5 were obtained from solutions prepared under ambient atmosphere ($pCO_2 = 10^{-3.5}$ atm). In comparison, Fig. 3.5 represents the data derived from solutions prepared under N_2 atmosphere. Since the ATR FT-IR measurements were performed at ambient atmosphere, carbonate could not be completely excluded. These solutions contain a significantly reduced amount of carbonate ($pCO_2 = 10^{-5.5}$ atm). The IR data exhibit different spectral features as a function of pH. The band in the range from 970 to 870 cm^{-1} is assigned to the antisymmetric stretching vibrational mode (υ_3) of the UO_2^{2+} unit (Quiles and Burneau, 2000). A comparison of both series shows very similar results at acidic pH values (< 6). In contrast, the U(VI) complexation behavior strongly differs at higher pH values (> 6), where carbonate influences the speciation.

At ambient atmosphere, the IR spectra obtained in the pH range from 9.2 to 7.4 show absorption of $\upsilon_3(UO_2)$ at 895 cm^{-1} and two strong bands at 1503 and 1386 cm^{-1} (Fig. 3.5). These bands are assigned to the asymmetric and symmetric stretching vibrations of bidentate complexed carbonate, respectively (Bargar et al., 2000). The spectra obtained in the pH range from 9.2 to 7.4 are contradictory to the recently accepted thermodynamic data shown in Fig. 3.4. The U(VI) speciation show the predominance of the $UO_2(CO_3)_3^{4-}$ complex only at pH > 8.5. However, the spectra are dominated by carbonate complexed U(VI) up to pH 7.4. In addition, a smaller blue shift of $\upsilon_3(UO_2)$ compared to the $UO_2(CO_3)_3^{4-}$ model spectrum (Müller et al., 2008) is detected. The spectral data at high pH (Fig. 3.5) provide an indication for a change of the U(VI) carbonate speciation in the presence of HA possibly due to the formation of a ternary U(VI) carbonato humate complex and can not clearly be resolved at this state of knowledge.

Upon decreasing pH to 6.8, the U(VI) speciation changes which becomes obvious from the hypsochromic shift of $\upsilon_3(UO_2)$ to 914 cm^{-1} and from the decreasing intensity of the carbonate modes. In addition, further bands at 1523 and 1460 cm^{-1} are observed in the spectrum at pH 6.8, which are in agreement with bands previously reported as intrinsic optical absorption properties of aqueous U(VI) species containing hydroxyl groups (Müller et al., 2009). From comparison of the spectrum at pH 6.8 with the spectrum obtained at pH 7.2 in the titration series with the strongly reduced carbonate concentration (cf. Fig. 3.5) it might be conceivable that very similar complexes with absorption of $\upsilon_3(UO_2)$ at about 912 cm^{-1} are formed. The thermodynamic data predict a formation of the $UO_2(OH)HA(I)$ complex for those near neutral pH conditions (cf. Fig. 3.4).

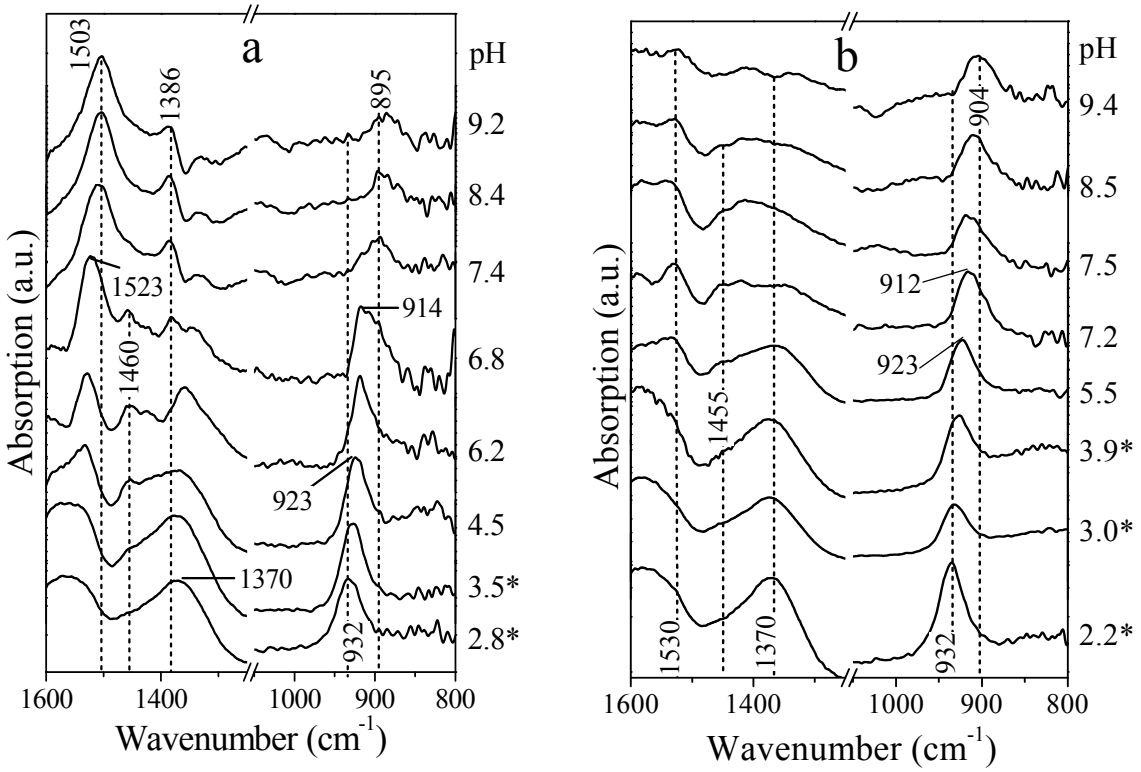

Fig. 3.5. Infrared spectra of U(VI) humate solutions as function of carbonate content and pH value ([U(VI)] = 1 mM, $[HA]_{tot}$ = 1 g/L, I = 0.1 M (NaCl)): at ambient atmosphere ($pCO_2 = 10^{-3.5}$ atm) (a) and at reduced carbonate concentration ($pCO_2 = 10^{-5.5}$ atm) (b). *Between pH 2.2 and 3.9 suspended precipitates were measured.

Since no differences between both titration systems could be detected upon further decreasing the pH level below 6.0, a combined discussion of the results can be provided. An increasing acidity of the solutions results in further changes in the U(VI) speciation. The $\upsilon_3(UO_2)$ band indicates the transfer from one U(VI) species with absorption at about 914 cm^{-1} to another with absorption maximum at about 923 cm^{-1} between pH 4.5 and 5.5. This species can be attributed to the binary humate complex $UO_2HA(II)$ which is supported by the thermodynamic data (cf. Fig. 3.4).

A brown precipitate was formed in the solution at a very acidic pH level (pH < 4.0). At pH 1.1 the solid species was separated from the solution by centrifugation. The spectrum of the supernatant exhibited one band with absorption maximum of $\upsilon_3(UO_2)$ at 961 cm^{-1} which is assigned to the fully hydrated UO_2^{2+} cation (Müller et al., 2008; Quiles and Burneau, 2000). In the spectra of the suspended precipitate obtained between pH 2.2 and 3.9, one single peak with a maximum at 932 cm^{-1} was observed. This absorption band is in very good agreement with data published by Schmeide et al. (2003). In this work a solid U(VI) humate species was precipitated at pH 2. Its characterization by infrared spectroscopy showed one band centered

at 934 cm^{-1}. In the present work the presence of precipitates in the U(VI) humate solutions at pH higher than 4.0 was ruled out by application of PCS and ultracentrifugation.

$$[HA(II)] = LC \times \frac{PEC \times HA}{z} \qquad \text{(Kim and Czerwinski, 1996)} \qquad (3.2)$$

[HA(II)] …concentration of HA in mol/L
LC ...loading capacity calculated based on Eq. (3.1)
PEC …proton exchange capacity ($(4.60\times10^{-3}$ eq/g) (Pompe et al., 2000a))
HA …concentration of HA in g/L
z ...charge of complexing metal ion

Determination of complex formation constants for the U(VI) humate system

For the first time, multiwavenumber infrared spectroscopic data are applied for the calculation of complex stability constants. The quantitative analysis was carried out applying the data analysis program SPECFIT (Gampp et al., 1985; Binstead et al., 2005). The signal of the antisymmetric (υ_3) stretching vibration of the UO_2^{2+} unit between 870 and 1000 cm^{-1} was used for analysis. As initial data the U(VI) concentration (ICP-MS), total inorganic carbon content (TIC), the HA concentration (based on Eq. (3.2) (Kim and Czerwinski, 1996)), the p*K* values of carbonate and the stability constants ($\log \beta_{0.1\ M}$) of the relevant U(VI) hydroxide complexes (UO_2OH^+, $(UO_2)_2(OH)_2^{2+}$, $(UO_2)_3(OH)_5^+$, $(UO_2)_4(OH)_7^+$), carbonate complexes ($UO_2CO_{3(aq)}$, $UO_2(CO_3)_2^{2-}$, $UO_2(CO_3)_3^{4-}$) and of the mixed hydroxo carbonate complex ($(UO_2)_2CO_3(OH)_3^-$), taken from Guillaumont et al. (2003), were imported into the program. From the variations in the infrared spectra as a function of pH, stability constants for the U(VI) humate complexation were calculated using the following procedure.

Based on relevant complexation studies of HA with actinides and lanthanides, possible U(VI) humate species of the type M_xHA_y or $M_xL_zHA_y$ with L representing OH^- or CO_3^{2-} were introduced in the data analysis program. SPECFIT performs a global analysis of the equilibrium system with singular value decomposition and non-linear regression modeling by the Levenberg–Marquardt method. The analysis of the present data was conducted for different species compositions of the formed complexes. The best modulation represents a minimum of the residual spectra of the imported data in combination with a realistic model for the complexation reaction. Four different species could be detected in the U(VI) humate systems under the experimental conditions applied in this study. For each aqueous complex the stability constant and the single component spectrum were successfully extracted. The results of the SPECFIT analyses are summarized in Table 3.3.

Table 3.3. Calculated complex formation constants and band maxima of the antisymmetric stretching vibration of U(VI) humate complexes in comparison to literature data.

#	U(VI) humate species	[U(VI)]	log $\beta_{0.1\ M}$	$\nu_3(UO_2)$ (cm^{-1})	Reference
(1)	$UO_2HA(II)$*	1 mM	---	932	(Steudtner et al., 2011b)
		0.1 M	---	934	(Schmeide et al., 2003)
(2)	$UO_2^{2+} + HA(II) \rightleftharpoons UO_2HA(II)$	1 mM	6.70 ± 0.25	925	(Steudtner et al., 2011b)
		0.5 mM	6.20 ± 0.56	---	(Pompe et al., 2000b)
(3)	$UO_2^{2+} + OH^- + HA(I) \rightleftharpoons UO_2(OH)HA(I)$	1 mM	15.14 ± 0.25	913	(Steudtner et al., 2011b)
		< 0.01 mM	14.89 ± 0.54	---	(Sachs et al., 2007a)
		solid	15.3	---	(Pashalidis and Buckau, 2007)
(4)	$UO_2^{2+} + 2\ CO_3^{2-} + HA(II) \rightleftharpoons UO_2(CO_3)_2HA(II)^{4-}$	1 mM	24.47 ± 0.70	895	(Steudtner et al., 2011b)
		< 0.01 mM	24.57 ± 0.17	---	(Steudtner et al., 2011a)
(5)	$UO_2FA + CO_3^{2-} \rightleftharpoons UO_2FACO_3$	n/a	5.0 (I=0.3 M)	---	(Glaus et al., 1995)

*solid

The formation constants log β for aqueous $UO_2HA(II)$ and $UO_2(OH)HA(I)$ at an ionic strength of 0.1 M were calculated to be 6.70 ± 0.25 and 15.14 ± 0.25, respectively. These values are in very good agreement with data determined by Pompe et al. (2000b) and Sachs et al. (2007a) by means of TRLFS and by Pashalidis and Buckau (2007) by solubility measurements. The complex formation constant determined for the aqueous complex $UO_2(CO_3)_2HA(II)^{4-}$ with log $\beta_{0.1\ M}$ = 24.47 ± 0.70 is in very good agreement with the value obtained from cryo-TRLFS measurements as reported by Steudtner et al. (2011a). Thus, the formation of a mixed U(VI) carbonato fulvate (UO_2FACO_3) complex which was only described by Glaus et al. (1995), can not be confirmed in our studies, neither by ATR FT-IR nor by cryo-TRLFS. In contrast, we identified a reaction between one UO_2^{2+} ion, two carbonate ions and one humate unit according to Eq. 4 in Table 3.3, thus, forming the ternary $UO_2(CO_3)_2HA(II)^{4-}$ complex. A comparable mixed complexation reaction with humate and carbonate as a second ligand was already described for Eu(III) by Dierckx et al. (1994), who detected the formation of a ternary $Eu(CO_3)_2HA(I)$ complex in solution.

The normalized single component spectra of the different complexes formed in the U(VI) humate carbonate system, derived by mathematical deconvolution of the mixed infrared spectra are presented in Fig. 3.6. It should be noted, that the bands of $\upsilon_3(UO_2)$ are rather broad and at this state of knowledge a contribution of further species to the FT-IR signal can not be

ruled out completely. Generally, a reduced absorption can be derived for the ternary complexes compared to the binary complexes from the obtained data.

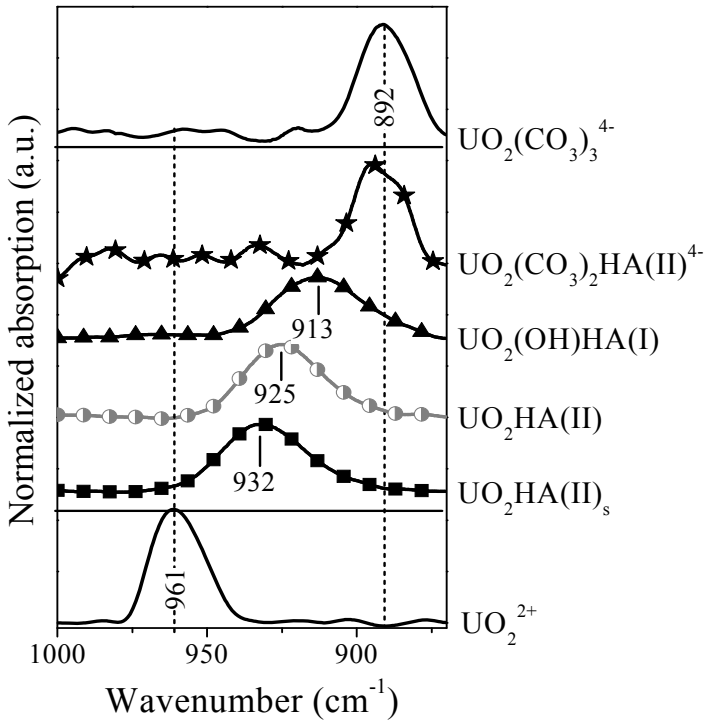

Fig. 3.6. Normalized single component IR spectra of different U(VI) species resulting from peak deconvolution with SPECFIT ([U(VI)] = 1 mM, $[HA]_{tot}$ = 1 g/L, I = 0.1 M (NaCl)). The model spectra of UO_2^{2+} and $UO_2(CO_3)_3^{4-}$ are taken from (Müller et al., 2008).

3.1.3 Conclusion

For the first time, the complexation between U(VI) and HA in the presence of carbonate was studied applying cryo-TRLFS and ATR FT-IR spectroscopy. In both studies, the formation of the ternary U(VI) carbonato humate complex $UO_2(CO_3)_2HA(II)^{4-}$ was observed and the complex formation reaction of U(VI) carbonato humate complex can be written in general as:

$$UO_2^{2+} + 2\ CO_3^{2-} + HA(II) \rightleftarrows UO_2(CO_3)_2HA(II)^{4-} \qquad (3.3)$$

The complex stability constant for the $UO_2(CO_3)_2HA(II)^{4-}$ complex is calculated with $\log \beta_{0.1\ M} = 24.57 \pm 0.17$. The result of the slope analysis with a slope of 1.12 ± 0.11 verifies the postulated ligand exchange reaction. In addition, IR spectroscopy was used to validate the complex formation constant of the ternary U(VI) carbonato humate complex. From the variations in the IR spectra as a function of pH, stability constants for the U(VI) humate complexation were calculated. The obtained complex stability constant of $\log \beta_{0.1\ M} = 24.47 \pm 0.70$ for the $UO_2(CO_3)_2HA(II)^{4-}$complex validated the constant measured

by cryo-TRLFS. In addition, the formation constants $\log \beta$ for aqueous $UO_2HA(II)$ and $UO_2(OH)HA(I)$ at an ionic strength of 0.1 M were calculated with 6.70 ± 0.25 and 15.14 ± 0.25, respectively. These values are in very good agreement with data determined by TRLFS (Pompe et al., 2000b; Sachs et al., 2007a) and by solubility measurements (Pashalidis and Buckau, 2007).

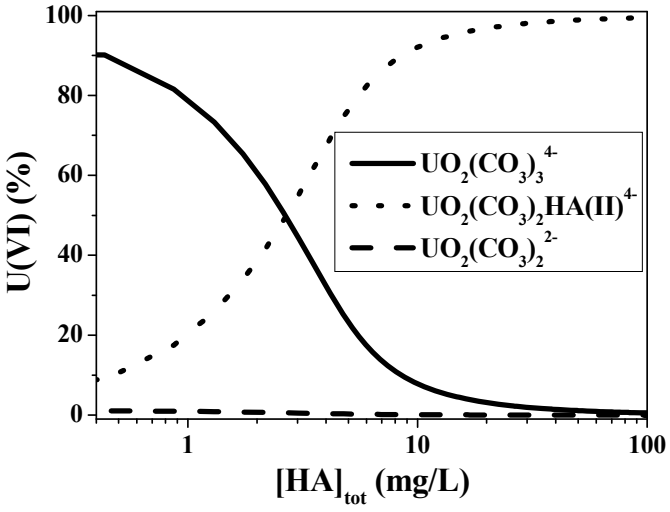

Fig. 3.7. Revised U(VI) species distribution at pH 8.5 in the presence of CO_2 and HA as a function of the HA concentration ($[U(VI)]_{tot} = 1\times10^{-5}$ M, $I = 0.1$ M ($NaClO_4$), $pCO_2 = 10^{-3.5}$ atm).

Using the complex formation constant determined for the ternary U(VI) carbonato humate complex, the species distribution of U(VI) was recalculated for the experimental conditions applied in this study. The revised U(VI) speciation in the presence of CO_2 and HA is shown in Fig. 3.7. Up to an environmentally relevant HA concentration of 2 mg/L (Gaffney et al., 1996) the U(VI) species distribution is dominated by the $UO_2(CO_3)_3^{4-}$ complex. Above 2 mg/L the $UO_2(CO_3)_2HA(II)^{4-}$ complex becomes increasingly important. It can be concluded that in the presence of HA the formation of the ternary U(VI) carbonato humate complex can significantly influence the U(VI) speciation under environmental conditions. This result is similar with previous studies with regard to the formation of ternary lanthanide or actinide carbonato humate complexes (Dierckx et al., 1994; Panak et al., 1996).

3.2 Influence of sulfur functionalities on the interaction behavior of humic acids with actinide ions

Humic substances (humic and fulvic acids) exhibit different amounts of sulfur depending on their origin. For instance, soil and aquatic humic substances are characterized by 0.1-3.6 and

0.5-1.43 wt.% sulfur, respectively (Xia et al., 1998). For humic acids (HA), sulfur contents ranging from, e.g., 0 to 2 wt.% were reported (Stevenson, 1982). Sulfur occurs in humic substances in multiple oxidation states in form of oxidized (sulfonates, ester-bonded sulfates, sulfonic acids, sulfones, sulfoxides) and reduced (thiols, sulfides, di- and polysulfides, thiophenes) organic sulfur functionalities (e.g., Vairavamurthy et al., 1997; Xia et al., 1998; Olivella et al., 2002). These functionalities occur in different proportions caused by the different sources of humic substances but also by the method used for isolation of the humic material (e.g., Xia et al., 1998; Hutchison et al., 2001).

Although the complexation behavior of HA is mainly attributed to carboxylic and phenolic OH groups, sulfur containing ligands which are less abundant in HA can complex metal ions. They play a role in complexing trace metals, e.g., Cd, Co, Ni, Pb, and Hg (Xia et al., 1998), which are classified as soft acids or borderline metals by Pearson's theory (Pearson, 1963). Extended X-ray absorption fine structure spectroscopic studies of the binding environment of Zn(II) (Xia et al., 1997) and Hg(II) (Xia et al., 1999; Hesterberg et al., 2001) complexed with humic substances reveal the involvement of reduced sulfur functionalities such as thiols, disulfides, polysulfides, and disulfanes in the complexation. Although actinide ions like UO_2^{2+} are classified as hard acids according to Pearson's theory, there is a possibility that their complexation behavior toward organic ligands is influenced by sulfur functionalities, such as thiols, classified as soft bases. There are references which document the role of thiol groups for the stabilization of U(VI) cysteine complexes (Raghavan and Santappa, 1970) and the involvement of thiol groups in the complexation of U(VI) with thiosalicylic acid (Raghavan and Santappa, 1970 and 1973). The stabilization of U(VI) cysteine complexes by thiol groups can further be deduced from Günther et al. (2007), who studied the complexation of U(VI) with L-cysteine in comparison to glycine.

In contrast, the redox activity of humic substances has been primarily ascribed to the reversible hydroquinone/quinone redox couple with semiquinone-type free radicals as significant electron donor/acceptor intermediate species (e.g., Lovley et al., 1996; Scott et al., 1998; Cory and McKnight, 2005; Aeschbacher et al., 2011). Furthermore, it is ascribed to the oxidation of phenolic OH groups to phenoxy radicals (e.g., Helburn and MacCarthy, 1994; Rocha et al., 2003; Schmeide and Bernhard, 2009; Sachs and Bernhard, 2011a) with their subsequent reactions, such as coupling reactions and tautomerizations (Musso, 1967), leading to a regeneration of phenolic OH groups. In addition, reduced forms of organically bound sulfur present in natural organic matter have been proposed as potential redox-active groups (Szulczewski et al., 2001; Fimmen et al., 2007; Ratasuk and Nanny, 2007). By means of

XANES spectroscopy, it could be shown that a thiol/disulfide redox couple is involved in the Cr(VI) reduction by humic substances in chromium-contaminated soils analog to the Cr(VI) reduction by simple thiol containing compounds such as cysteine and glutathione (Szulczewski et al., 2001). Thus, it is to check whether or not sulfur functional groups in humic substances act as redox-active functional units also toward actinides such as Np(V).
In the present project, the role of sulfur functionalities of HA for the U(VI) complexation and Np(V) reduction in aqueous solution was studied. For that synthetic HA model substances with varying sulfur contents were synthesized based on the melanoidin concept (e.g., Sachs and Bernhard, 2011b). The studies performed and their results, which are described in the following sections, are published in-depth by Sachs et al. (2010) and Schmeide et al. (2012a).

3.2.1 Synthesis and characterization of sulfur containing humic acid model substances

3.2.1.1 Synthesis

Sulfur containing HA model substances with varying amounts of sulfur (type M1-S) were synthesized according to HA type M1 (Pompe et al., 1996) using D(+)-xylose (>99%, Fluka, Taufkirchen, Germany), glycine (99%, Aldrich, Steinheim, Germany), L-phenylalanine (for biochemistry, Merck), and L-cysteine (for biochemistry, Merck) as precursors. In order to ensure constant molar amino acid concentrations in the reaction mixtures, the glycine concentration in the reaction mixtures was decreased for the same amount as the L-cysteine concentration was increased. Table 3.4 summarizes the composition of the reaction mixtures for the syntheses of HA type M1-S with varying amounts of sulfur. For comparison, sulfur free synthetic HA type M1 was synthesized under identical conditions in the absence of L-cysteine. The synthesis procedure is described in detail in (Sachs et al., 2010).

Table 3.4. Reaction mixtures for the synthesis of HA type M1 and M1-S (Sachs et al., 2010).

	M1 (He4/07-A1)	**M1-S-1 (He4/07-A2)**	**M1-S-2 (He3/08-A3)**	**M1-S-3 (He2/09-A4)**
D(+)-xylose (g)	3.4	3.4	3.4	3.4
L-phenylalanine (g)	1.0	1.0	1.0	1.0
Glycine (g)	0.500	0.340	0.156	0
L-cysteine (g)	0	0.250	0.550	0.807
H_2O (mL)	8	8	8	8

3.2.1.2 Characterization

Elemental composition and functional group contents

Table 3.5 summarizes the results of the elemental analysis as well as of the determination of functional groups (Sachs et al., 2010; Schmeide et al., 2012a). The synthetic products exhibit an elemental composition close to that of natural HA. Due to the use of increasing amounts of cysteine for the synthesis, the sulfur content of the HA is increased from 0 to 6.9 wt.%.

The synthetic products exhibit low proton exchange capacities (PEC) and carboxylic group contents. However, HA with low amounts of functional groups are also found in nature. With increasing initial cysteine concentration in the starting materials and thus, with increasing sulfur content of the HA, PEC and carboxylic group content are increased. The phenolic/acidic OH group content of all synthetic HA is nearly the same. HA type M1 shows an apparent dissociation constant (pK_{app}) comparable to natural HA. With increasing sulfur content of the HA from 0 to 3.9 wt.%, the pK_{app} values are decreased, indicating an increase in the acidic strength of the materials. Under consideration of the experimental error, a further increase of the sulfur content to 6.9 wt.% does not affect pK_{app}.

Table 3.5. Characterization of synthetic HA type M1 and M1-S (Sachs et al., 2010; Schmeide et al., 2012a).

HA	Elemental composition				
	C (wt.%)	**H (wt.%)**	**N (wt.%)**	**S (wt.%)**	**O (wt.%)**
M1	59.8 ± 0.1	5.4 ± 0.1	5.2 ± 0.1	0	29.5 ± 0.2
M1-S-1	61.3 ± 0.1	5.4 ± 0.1	4.9 ± 0.1	1.9 ± 0.1	26.6 ± 0.1
M1-S-2	59.2 ± 0.3	5.2 ± 0.1	4.6 ± 0.1	3.9 ± 0.1	27.1 ± 0.3
M1-S-3	60.1 ± 0.1	5.5 ± 0.1	4.7 ± 0.1	6.9 ± 0.1	22.7 ± 0.1
Natural HA [a]	50 - 60	4 - 6	2 - 6	0 - 2	30 - 35

HA	Functional groups			
	COOH (meq/g)	**Phenol./acidic OH (meq/g)**	**PEC (meq/g)**	**pK_{app}**
M1	1.18 ± 0.20	1.82 ± 0.01	1.56 ± 0.13	4.30 ± 0.23
M1-S-1	1.49 ± 0.02	2.35 ± 0.02	1.63 ± 0.16	4.12 ± 0.17
M1-S-2	1.64 ± 0.06	1.86 ± 0.02	1.90 ± 0.17	3.58 ± 0.28
M1-S-3	1.70 ± 0.14	1.88 ± 0.01	1.96 ± 0.23	3.76 ± 0.13
Natural HA	1.5 - 5.7 [b]	2.1 – 5.7 [b]		3.35 - 4.85 [c]

[a] Stevenson, 1982. [b] Stevenson, 1994. [c] Kurková, 2004.

Independent of the sulfur content, all synthetic products exhibit comparable FTIR spectra (not shown) indicating similar overall structures (Sachs et al., 2010). The HA show FTIR absorption bands that are comparable to those of natural HA (Stevenson, 1994).

Identification of sulfur species

The sulfur speciation in synthetic HA type M1-S was studied by X-ray photoelectron spectroscopy (XPS) at the Institut für Kernchemie, Johannes Gutenberg-Universität Mainz. XPS spectra of synthetic HA were measured in comparison to those of L-cysteine and purified natural HA from Aldrich (AHA; S = 3.8 ± 0.1 wt.%; Sachs et al., 2004) as described in detail in (Sachs et al., 2010). The dry sample powders were pressed into indium foil without further treatment. Spectra were recorded with the UNI-SPECS ESCA System (Specs GmbH, Berlin, Germany) with a PHOIBOS 100 energy analyzer. The spectra were excited by non-monochromatic Mg K_α radiation (1253.6 eV). The pass energy (E_p) of the analyzer was 13 or 50 eV, depending on the desired signal-to-noise ratio and spectral resolution. The resolution measured as the full width at half-maximum of the Ag $3d_{5/2}$ line was 1.0 eV (E_p = 13 eV) or 2.3 eV (E_p = 50 eV). The vacuum during the measurements was 2×10^{-8} mbar. The electrostatic charging of the sample surface was corrected by setting the C 1*s* binding energy of aliphatic carbon equal to 285.0 eV. The data evaluation is described in Sachs et al. (2010). Errors of the determined binding energies and relative line intensities were ±0.1 eV and ±5%, respectively.

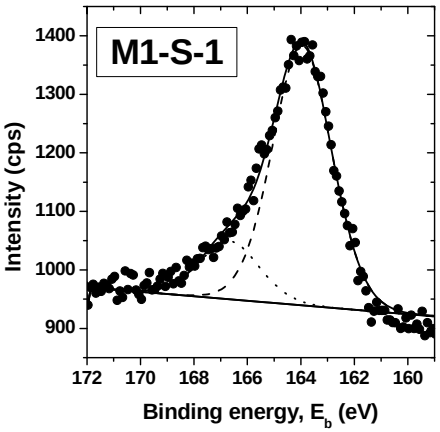

Fig. 3.8. XPS spectrum of the S 2*p* lines of HA model substance M1-S-1 measured with E_p = 50 eV (● Experiment, --- Fit; Sachs et al., 2010).

Figure 3.8 shows a XPS spectrum of the S 2*p* lines of HA M1-S-1. The XPS spectrum of HA M1-S-2 (not shown) is similar (Sachs et al., 2010). The theoretical fit of the spectra resulted in two peaks indicating the occurrence of at least two different types of sulfur species. In

contrast to that, HA M1-S-3 shows one S 2*p* line. The spectrum of AHA points also to the occurrence of two different sulfur species comparable to HA M1-S-1 and M1-S-2. Table 3.6 summarizes the binding energies (E_b) of the S 2*p* lines as well as the percentage of the individual sulfur components on the total sulfur content of the HA.

Table 3.6. Binding energies (E_b) of S 2*p* XPS lines and percentage of the individual sulfur species on the total sulfur content (Sachs et al., 2010).

Sample	E_b **(eV)**	**% of** S_{total}	E_b **(eV)**	**% of** S_{total}	E_b **(eV)**	**% of** S_{total}
L-cysteine	163.8	100				
AHA	164.5	70-80			168.3	20-30
M1-S-1	164.0	82	166.7	18		
M1-S-2	163.9	90-95	166.8	5-10		
M1-S-3	163.9	100				

All studied HA as well as cysteine show a S 2*p* line at about 164.0 eV. In addition to that, HA M1-S-1 and M1-S-2 show a signal at about 166.8 eV, whereas the second sulfur line of AHA is found at 168.3 eV. Based on literature data for sulfur containing organic model compounds (Lindberg et al., 1970), the signals can be attributed to reduced and oxidized sulfur species. The S 2*p* line at 164.0 eV corresponds to thiols, dialkylsulfides and/or disulfides, which can not easily be distinguished. The peak centered at about 166.8 eV is ascribed to sulfoxides. The signal at 168.3 eV in the spectrum of AHA results from contributions of higher oxidized sulfur species like sulfones and/or sulfonates. Comparable sulfur species were already found for natural humic substances by XPS (Urban et al., 1999) and XANES (e.g., Xia et al., 1998; Prietzel et al., 2007). Table 3.6 shows, the amount of reduced sulfur groups of the synthetic products increases from about 82% in M1-S-1 to 100% in M1-S-3. In HA M1-S-3 no oxidized sulfur species are detectable. From quantitative analysis of the XPS spectra it can be concluded that reduced sulfur functionalities dominate the sulfur speciation in all studied HA. Comparable high fractions of reduced sulfur functionalities were already described for natural HA extracted from soils (Hutchison et al., 2001).

3.2.2 Impact of sulfur functionalities on the U(VI) complexation by humic acids

The U(VI) complexation of sulfur containing HA model substances M1-S was studied in comparison to that of sulfur free HA M1 applying two independent spectroscopic methods, time-resolved laser-induced fluorescence spectroscopy (TRLFS) and TRLFS with femtosecond laser pulses (fs-TRLFS). The influence of sulfur containing functional groups of

HA on the U(VI) complexation was estimated and compared to that of oxygen containing functional groups (Sachs et al., 2010).

3.2.2.1 Experimental

Sample preparation

Complexation experiments were performed in air ($pCO_2 = 10^{-3.5}$ atm) at room temperature. U(VI) humate solutions were prepared from stock solutions of HA (0.2 g/L) and $UO_2(ClO_4)_2$ (1×10^{-4} M U(VI), 0.1 M $HClO_4$). The sample preparation is described in (Sachs et al., 2010). Table 3.7 summarizes the composition of the studied samples. For TRLFS measurements, HA-free U(VI) solutions were used for calibration of the U(VI) luminescence signal as a function of the U(VI) concentration.

Table 3.7. U(VI) humate solutions studied by TRLFS and fs-TRLFS (pH = 3.80 ± 0.02; I = 0.1 M $NaClO_4$; $pCO_2 = 10^{-3.5}$ atm; Sachs et al., 2010).

HA	Method	U (µmol/L)	HA (mg//L)
M1	TRLFS	0.63-5.50	10
	fs-TRLFS	0.78-10.9	10
M1-S-1	TRLFS	0.82-9.66	10
	fs-TRLFS	0.81-13.0	10
M1-S-2	TRLFS	0.93-10.4	10
	fs-TRLFS	0.78-15.2	10
M1-S-3	TRLFS	1.00-15.5	10
	fs-TRLFS	0.98-27.4	10

Spectroscopic measurements

The U(VI) luminescence as function of the U(VI) concentration was measured by TRLFS using a Nd:YAG laser system (Continuum Minilite II, Continuum Electro Optics Inc., Santa Clara, USA) pulsed with a repetition rate of 10 Hz. The excitation wavelength was 266 nm, the pulse energies about 300 µJ. The luminescence emission was focused into a spectrograph (iHR 550, HORIBA Jobin Yvon GmbH, Munich, Germany) and detected using an intensified camera system with 1024 useable pixels and a built-in delay generator (HORIBA Jobin Yvon). TRLFS spectra were measured by averaging 200 laser pulses in the wavelength range between 371 and 674 nm with a gate width of 2 µs at delay times of 150 or 175 ns.

The fs-TRLFS measurements for determination of the HA fluorescence as a function of the U(VI) concentration were performed with a femtosecond laser pulse based TRLFS system. The system is described in (Geipel et al., 2004). A Nd:YVO_4 laser (Spectra Physics, Mountain

View, USA) with a repetition rate of 1 kHz was used as pump source for a Ti:Sapphire oscillator. After amplification, third harmonic generation was applied to provide femtosecond pulses with an excitation wavelength of 266 nm and pulse energies between 0.09 and 0.11 µJ. The fluorescence signal was focused into a spectrograph (Acton Research, 300i, Acton, USA) and collected by an ICCD camera system with 1376 useable pixels (Picostar HR, LaVision Inc., Göttingen, Germany). Time-resolved fluorescence spectra were collected at delay times between 0 and 30 ns after application of the laser pulse, with time steps of 0.1 or 0.2 ns applying a delay generator. Spectra were measured with a gate width of 2 ns in the wavelength range between 327 and 533 nm (Sachs et al., 2010).

3.2.2.2 Results and discussion

Results of TRLFS measurements

Figure 3.9a shows selected U(VI) luminescence spectra as function of the U(VI) concentration at constant HA concentration.

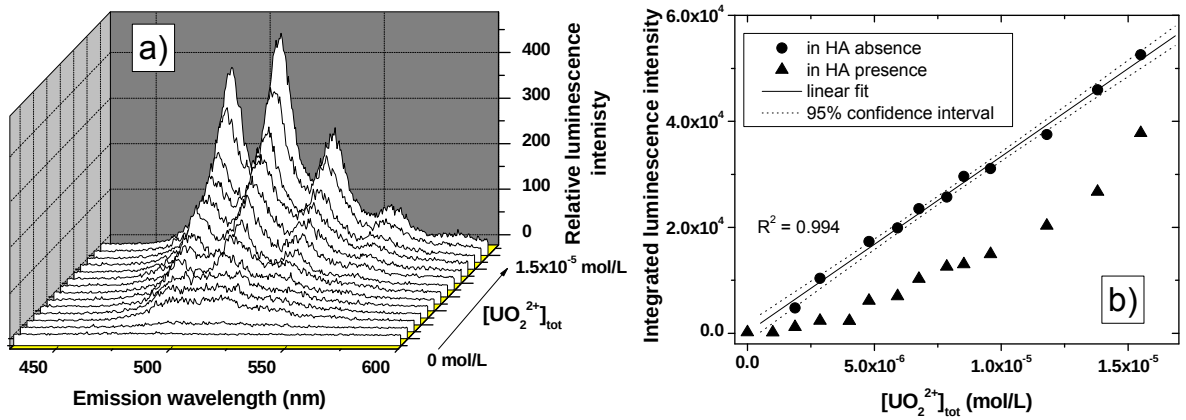

Fig. 3.9. (a) U(VI) luminescence in the presence of HA M1-S-3 as a function of the U(VI) concentration. (b) Integrated luminescence intensities of U(VI) (430-600 nm) in the absence and presence of HA M1-S-3 (delay time t = 175 ns; $[UO_2^{2+}]_{tot}$ = 0-15.5 µmol/L; [HA] = 0 or 10 mg/L; I = 0.1 M $NaClO_4$; pH = 3.80 ± 0.02; $pCO_2 = 10^{-3.5}$ atm; Sachs et al., 2010).

The U(VI) luminescence intensity is increased with increasing U(VI) concentration in the presence of constant HA concentrations. The obtained U(VI) luminescence spectra represent the sum of the luminescence of the free UO_2^{2+} ion and of the first hydrolytic uranyl species (UO_2OH^+). No emission signals of HA or U(VI) humate complexes were detected. The luminescence spectra were deconvoluted using single spectra of UO_2^{2+} and UO_2OH^+ to isolate the contribution of the free UO_2^{2+} ion to the overall luminescence signal. The spectrum of UO_2OH^+ was included in the peak deconvolution because of the strong fluorescence yield of

UO_2OH^+ in comparison to UO_2^{2+}. However, the concentration of UO_2OH^+ (<2%) present in the experiments was neglected in the further data evaluation. In the absence of HA, the U(VI) speciation in solution is dominated by the UO_2^{2+} ion which occurs to >98% under the applied experimental conditions.

A static quenching of the luminescence of the free UO_2^{2+} ion was observed for the complexation of UO_2^{2+} with HA. After peak deconvolution, the UO_2^{2+} luminescence intensities for each sample, with and without HA, were integrated between 430 and 600 nm (Fig. 3.9b). The results of the solutions without HA were used to determine the free UO_2^{2+} concentration when U(VI) humate is present.

The TRLFS data were evaluated based on the metal ion charge neutralization model (CNM; Kim and Czerwinski, 1996). According to this model, the UO_2^{2+} ion binds two proton exchanging sites of the HA molecule (Eq. (3.4)).

$$UO_2^{2+} + HA(II) \rightleftarrows UO_2HA(II) \tag{3.4}$$

HA(II) represents the HA ligand and $UO_2HA(II)$ is the U(VI) humate complex. The complex stability constant *K* is formulated by

$$K = \frac{[UO_2HA(II)]}{[UO_2^{2+}]_{free} \bullet [HA(II)]_{free}} . \tag{3.5}$$

$[UO_2HA(II)]$ is the U(VI) humate complex concentration, $[UO_2^{2+}]_{free}$ the free UO_2^{2+} concentration and $[HA(II)]_{free}$ the free HA ligand concentration. CNM introduces the loading capacity (LC; Eq. (3.6)) which corresponds to the maximal available mole fraction of HA binding sites under the applied experimental conditions.

$$LC = \frac{[UO_2HA(II)]_{max}}{[HA(II)]_{tot}} \tag{3.6}$$

$[UO_2HA(II)]_{max}$ is the maximal UO_2^{2+} concentration permissible for complexation with functional sites of a given HA and $[HA(II)]_{tot}$ the total molar HA concentration (Eq. (3.7)).

$$[HA(II)]_{tot} = \frac{[HA] \bullet PEC}{2} \tag{3.7}$$

In Eq. (3.7) [HA] stands for the weight concentration of HA in g/L, PEC for the proton exchange capacity of HA in eq/g, and 2 for the nominal charge of the complexing UO_2^{2+} ion. Applying this model, the metal ion complexation by HA is described independently of the experimental conditions and the origin of the HA. Comparable complexation constants are obtained for the complexation of a metal ion with different HA. Differences in the

complexation behavior of HA under the same experimental conditions are reflected in different LC values. If sulfur containing functional groups influence the U(VI) complexation by HA, various LC values should result for HA with different sulfur contents.

Complexation constants log *K* and LC values that were determined from the TRLFS measurements as described in (Sachs et al., 2010) are summarized in Table 3.8. Under consideration of the standard deviations, the complexation constants for all HA are similar. The LC values of HA M1 and M1-S-1 with 0 and 1.9 wt.% sulfur, respectively, are comparable. However, with further increasing sulfur content of the HA up to 6.9 wt.%, a significant increase of the LC values up to 44% was determined by TRLFS. This increase of the LC values points to an increase of the mole fraction of maximal available U(VI) binding sites of HA with sulfur contents >2 wt.%.

Table 3.8. Complexation data for the complexation of U(VI) with HA type M1-S in comparison to sulfur free HA M1 (pH = 3.80 ± 0.02; I = 0.1 M $NaClO_4$; $pCO_2 = 10^{-3.5}$ atm; Sachs et al., 2010).

	TRLFS		fs-TRLFS		
	LC (%) [a]	**log *K***	**C_L (µmol/L)** [b]	**$C_{L,norm.}$ (%)** [c]	**log *K***
M1	28.8 ± 4.8	5.98 ± 0.18	2.21 ± 1.29	28 ± 17	5.65 ± 0.11
M1-S-1	27.3 ± 1.4	6.15 ± 0.09	2.25 ± 1.59	28 ± 20	5.56 ± 0.11
M1-S-2	38.6 ± 3.0	6.19 ± 0.22	3.60 ± 0.68	38 ± 7	6.13 ± 0.11
M1-S-3	44.2 ± 2.1	6.38 ± 0.25	4.78 ± 1.47	49 ± 15	5.68 ± 0.09

[a] LC: Loading capacity of HA (Kim and Czerwinski, 1996).

[b] C_L: Total concentration of HA ligand sites (Ryan and Weber, 1982).

[c] $C_{L,\,norm.}$: Total concentration of HA ligand sites normalized to the total HA concentration $[HA(II)]_{tot}$ as defined by Kim and Czerwinski (1996).

Results of fs-TRLFS measurements

Time-resolved fluorescence spectra of the HA were measured with constant HA concentration as a function of the U(VI) concentration. The spectra at the fluorescence maximum at t = 0 ns relative to the laser pulse were used for data evaluation. Selected spectra for HA type M1-S-3 are shown in Fig. 3.10a. The spectra were integrated between 410 and 500 nm and the resulting fluorescence intensities were normalized to 100%. Figure 3.10b depicts the normalized fluorescence intensities of HA M1-S-3 as a function of the total U(VI) concentration. With increasing U(VI) concentration a decrease of the HA fluorescence is observed. This static fluorescence quenching process proceeds non-linear as already reported

by Acker (2003). After saturation of the HA binding sites with U(VI), the HA shows a residual fluorescence.

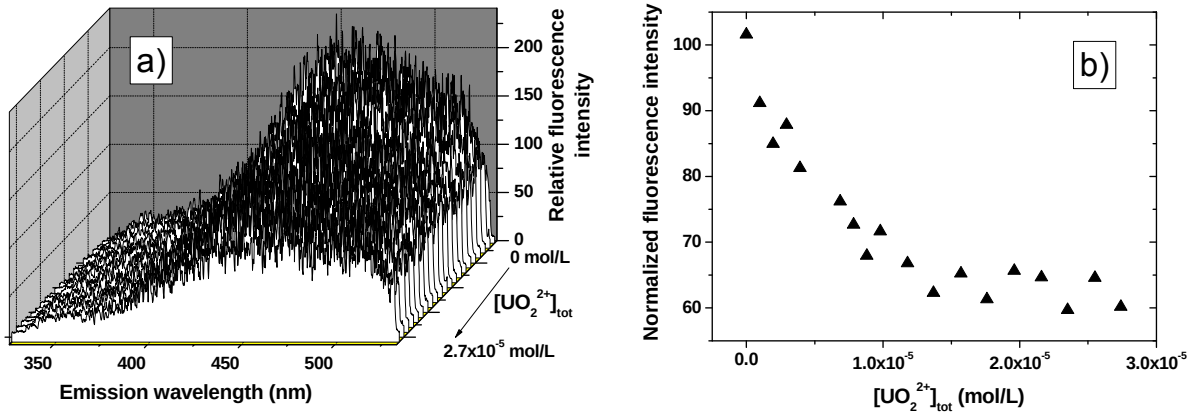

Fig. 3.10. (a) Fluorescence spectra of HA M1-S-3 as a function of the U(VI) concentration. (b) Integrated fluorescence intensities of HA M1-S-3 (410-500 nm; delay time t = 0 ns; $[UO_2^{2+}]_{tot}$ = 0-27.4 µmol/L; [HA] = 10 mg/L; *I* = 0.1 M $NaClO_4$; pH = 3.80 ± 0.02; $pCO_2 = 10^{-3.5}$ atm; Sachs et al., 2010).

An evaluation of the fs-TRLFS data based on CNM is not possible as already described in (Sachs et al., 2007a). Ryan and Weber (1982) developed a model for evaluation of non-linear fluorescence quenching data. Assuming the formation of a 1:1 complex between a humic substance as ligand and a metal ion, this model provides a correlation between the measured fluorescence intensities, the complex concentration ([ML]) and the total concentration of ligand (C_L) present in solution (Eq. (3.8)).

$$\frac{[ML]}{C_L} = \frac{I_L - I_M}{I_L - I_{ML}} \tag{3.8}$$

I_L represents the fluorescence of the free ligand at start of the fluorescence titration, I_M the measured fluorescence intensity at a certain metal ion concentration and I_{ML} the residual fluorescence intensity when the available ligand is completely bound. I_{ML} is a limiting value at the endpoint of the fluorescence titration below which the fluorescence intensity does not decrease due to further addition of metal ions.

Including mass balances for metal ion and ligand as well as the conditional stability constant of an assumed 1:1 complex, Eq. (3.9) is obtained according to (Ryan and Weber, 1982):

$$I_M = \frac{(I_{ML} - I_L)}{(2 \bullet K \bullet C_L)} \bullet [(K \bullet C_L + K \bullet C_M + 1) - \sqrt{(K \bullet C_L + K \bullet C_M + 1)^2 - 4 \bullet K^2 \bullet C_L \bullet C_M}] + I_L \tag{3.9}$$

Normalizing the fluorescence intensity data on a relative scale, I_L is equal to 100. Using the measured fluorescence intensities as a function of the added metal ion concentration (C_M), the total ligand concentration (C_L) available for complexation under the applied experimental conditions and the conditional stability constant (*K*) can be obtained solving Eq. (3.9) by non-linear regression (Ryan and Weber, 1982). The fitting procedure is described in (Sachs et al., 2010).

Considering the formation of a 1:1 complex between UO_2^{2+} and HA as given in Eq. (3.4), C_L represents the HA ligand concentration ([HA(II)]) available for complexation of UO_2^{2+} under the applied experimental conditions. Relating this value to the total HA concentration ($[HA(II)]_{tot}$; Eq. (3.7)), a value is obtained ($C_{L,norm.}$) which corresponds to LC.

Table 3.8 summarizes the complexation constants (log *K*) and the total ligand concentrations (C_L) for the complexation of U(VI) with HA M1(-S). Under consideration of the standard deviations, all HA show similar log *K* values. Although the total ligand concentrations (C_L) are characterized by high standard deviations, it becomes obvious that these are increased from 2.2 µmol/L (M1) to 4.8 µmol/L (M1-S-3). This might partly be caused by the increase of the PEC values and the carboxylic group contents of the HA (cf. Table 3.5) resulting in a higher number of potentially available binding sites. However, by normalizing C_L to $[HA(II)]_{tot}$, the increase in PEC is taken into account. Comparing the $C_{L,norm.}$ for all HA it becomes evident that the total ligand concentrations of HA M1-S-2 and M1-S-3 are significantly higher than those of HA M1 and M1-S-1. This points again to an increase of the available number of HA binding sites for U(VI) complexation with increasing sulfur content.

Comparison of the complexation data

The U(VI) complexation constants measured by TRLFS and fs-TRLFS, respectively, are comparable for the individual HA. The log *K* values deduced from fs-TRLFS are slightly lower than those from TRLFS. This can be attributed to technical measurement reasons of both laser systems as discussed by Acker (2003), causing experimental uncertainties in the determination of the luminescence of the free UO_2^{2+} ion and the fluorescence of the HA.

Despite of the high uncertainties of C_L, LC and $C_{L,norm.}$ values obtained from TRLFS and fs-TRLFS measurements, respectively, agree well. This allows the conclusion that under the applied conditions the number of HA binding sites available for complexation of U(VI) is increased with increasing HA sulfur content beginning from sulfur contents >2 wt.%. Taking the XPS data into account, it can be specified that the increase of the number of U(VI) binding sites can be ascribed to an increasing amount of reduced sulfur functionalities,

probably thiol groups. The increase of LC and $C_{L,norm.}$ correlates also with the increasing acidity of the HA reflected in decreasing pK_{app} values. The steady rise of the fraction of HA binding sites for U(VI) points to a contribution of reduced sulfur functionalities to the complexation in the acidic pH range. Thiol groups, which can be assumed as the dominating sulfur species in the studied HA, are normally protonated in the acidic pH range (e.g., -SH in cysteine: pK_a = 8.33; Bräse et al., 2007). In our former study (Pompe et al., 2000b), the influence of HA phenolic OH groups, which are characterized by similar acidities as thiol groups, on the U(VI) complexation at pH 4 was investigated. Already at pH 4, where phenolic OH groups are assumed to be protonated, U(VI) LC values of HA were found to be decreased after blocking of phenolic OH groups. This decrease was ascribed to a contribution of intermolecular hydrogen bonds between phenolic OH groups and axial oxygen atoms of the UO_2^{2+} ions to the complexation. A contribution of phenolic OH groups acting as ligands after proton release due to mesomeric substituent effects was also not excluded. Such effects could also impact the acidity of thiol groups resulting in their involvement in the U(VI) complexation. The formation of hydrogen bonds between thiol groups and axial oxygen atoms of the UO_2^{2+} unit and/or stabilizing electronic effects between free electrons of sulfur atoms and the UO_2^{2+} ion may contribute to the complexation or the stabilization between U(VI) and HA. Nevertheless, other processes that can influence the fraction of HA binding sites should also be taken into account. Steric hindrances within the HA, which might be overcome in the presence of increasing sulfur contents, could influence the complexation behavior of the sulfur free HA. Moreover, an inhibitory effect of L-cysteine on the melanoidin formation, that was discussed in (Kwak and Lim, 2004; Sachs et al. 2010), could influence the molecular size/mass of the HA with possible consequences for the complexation properties. The hypothesis that thiol groups are involved in the interaction between HA and U(VI) is supported by the literature (Raghavan and Santappa, 1970 and 1973; Günther et al., 2007).

Natural HA predominantly show sulfur contents between 0 and 2 wt.% (Stevenson, 1982). To estimate the role of sulfur functionalities for the U(VI) complexation by HA with environmentally relevant sulfur contents in comparison to oxygen functionalities, the complexation behavior of HA M1 and M1-S-1 with 0 and 1.9 wt.% sulfur, respectively, has to be considered (Table 3.8). For these HA no differences in the complexation constants (log K) and also in the fraction of ligand sites (LC, C_L) were observed. From that it can be concluded that for environmentally relevant sulfur concentrations in HA and under acidic conditions, reduced sulfur functionalities play only a subordinate role for the U(VI) complexation compared to oxygen containing functional groups, especially carboxylic groups. However,

with increasing sulfur content the complexation behavior toward U(VI) may change. Furthermore, the role of sulfur functionalities for the U(VI) complexation may change with increasing pH value (Sachs et al., 2010).

3.2.3 Impact of sulfur functionalities on the Np(V) reduction by humic acids

The role of sulfur functional groups of HA for their reduction capability toward Np(V) was studied for the first time. For this, the Np(V) reduction capability of HA model substances M1-S was studied as a function of pH (pH 5.0, 7.0 and 9.0) under anaerobic conditions and compared to that of the respective sulfur free synthetic HA type M1.

3.2.3.1 Experimental

Sample preparation

The samples were prepared in a glove box (N_2 atmosphere) according the procedure described by Schmeide et al. (2012a). The final Np and HA concentrations were 5×10^{-6} M and 100 mg/L, respectively. The ionic strength of the solutions was 0.1 M ($NaClO_4$). The pH values of the samples (pH 5.0, 7.0, 9.0) were adjusted with NaOH (p.a., Merck) or $HClO_4$ (p.a., Merck) solutions, no buffers were added. During the experiments, the pH of the solutions was checked and readjusted repeatedly. All samples were stored in 50 mL centrifuge tubes (Cellstar, Greiner Bio-One, Kremsmünsterand, Austria) at room temperature. The tubes were wrapped in aluminum foil to exclude light-induced degradation processes of the organic material. The experiments were conducted over an 11-month period. The Np concentration in solution was determined by liquid scintillation counting (LSC, Winspectral α/β, Wallac 1414, Perkin Elmer, Rodgau, Germany) using α-β discrimination. For this, 600 µL aliquots were mixed with 15 mL of a Ultima Gold scintillation cocktail (Perkin Elmer).

Methods for Np redox speciation

For monitoring the concentrations of Np(V) and Np(IV) in solution over time, samples were taken after different time intervals and characterized by solvent extraction, ultrafiltration, and E_h measurements as described by Schmeide et al. (2012a).

3.2.3.2 Results and discussion

Exemplary, the results of the Np(V) reduction experiments at pH 5.0 and 7.0 are shown in Fig. 3.11 as Np(V) fraction of total Np versus equilibration time.

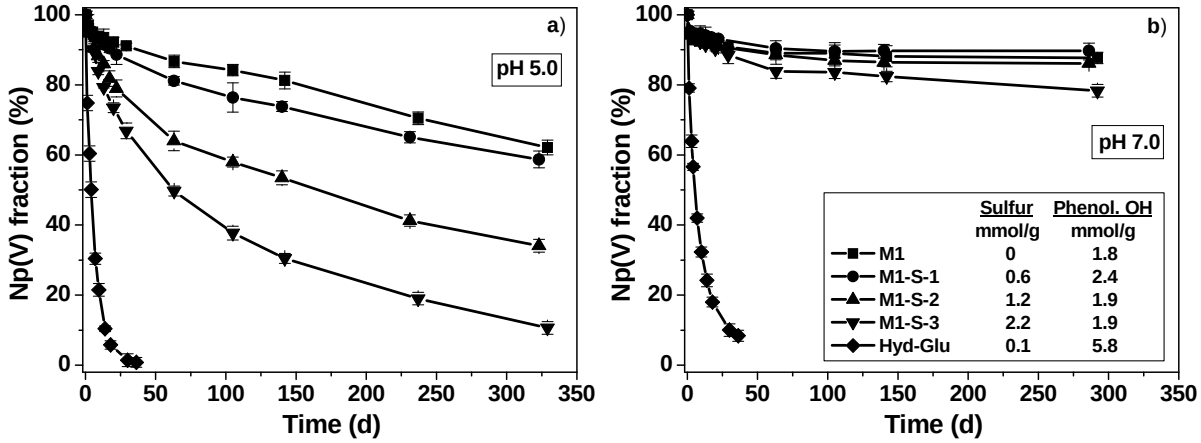

Fig. 3.11. Time-dependence of the Np(V) reduction by HA type M1(-S) at pH 5.0 (a) and pH 7.0 (b). For comparison, the Np(V) reduction by HA type Hyd-Glu (Schmeide and Bernhard, 2009) is shown. The legend holds for both figures. ($[Np]_{tot}$ = 5×10^{-6} M; [HA] = 100 mg/L; I = 0.1 M ($NaClO_4$), N_2; Schmeide et al., 2012a).

At pH 5.0, the ability to reduce Np(V) increases in the sequence M1 < M1-S-1 < M1-S-2 < M1-S-3 (Fig. 3.11a). Since the phenolic/acidic OH group content is nearly the same for these HA, the increasing Np(V) reduction can be correlated to the increasing sulfur contents of the HA (0 to 6.9 wt.% which correspond to molar sulfur concentrations of 0 to 2.2 mmol/g, cf. inset Fig. 3.11b). Reduced organic sulfur species, such as thiols, dialkylsulfides and/or disulfides, were determined as the dominating sulfur functionalities in these HA by XPS (Sachs et al., 2010). Their percentage of the total sulfur content is generally high and moreover, increases from M1-S-1 (82%) via M1-S-2 (90-95%) to M1-S-3 (100%). Szulczewski et al. (2001) showed by XANES spectroscopy that thiols are oxidized to disulfides during Cr(VI) reduction by HA. Ratasuk and Nanny (2007) identified thiols and disulfides as the main redox moieties of humic substances at pH 6.5 by means of cyclic oxidation and reduction reactions. Thus, for the Np(V) reduction by sulfur containing HA it is concluded that, in addition to hydroquinone-like moieties and non-quinoid phenols, the reduced sulfur functional groups contribute to the reduction capability of HA.

In contrast to the results obtained at pH 5.0, the differences in the reduction behavior of the HA type M1(-S) with different sulfur contents are much smaller at pH 7.0 (cf. Fig. 3.11b). Merely for M1-S-3, with the highest content of reduced sulfur species, a slightly stronger Np(V) reduction is observed. Generally, however, rate and extent of Np(V) reduction at pH 7.0 is low. The curves obtained at pH 9.0 (not shown) run parallel to those obtained at pH 7.0, however, the Np(V) fraction in solution is about 10% lower compared to pH 7.0. Again M1-S-3 induces a slightly stronger Np(V) reduction compared to the other humic acids, however, overall the effect of increasing sulfur contents is small.

The redox potentials, determined in the Np/HA sample solutions at pH 5.0, decrease from 294 ± 10 mV (Np/M1) via 279 ± 8 mV (Np/M1-S-1) and 205 ± 4 mV (Np/M1-S-2) to 188 ± 2 mV (Np/M1-S-3). The trend of decreasing redox potentials in Np/HA sample solution with increasing content of reduced sulfur functional groups of HA correlates with increasing Np(V) reduction from M1 to M1-S-3. In (Schmeide et al., 2012a) the redox potentials measured in the sample solutions are discussed in detail in the context of the E_h-pH diagram for neptunium and are compared to the pH-dependency of the redox potential generally observed for HA as well as to the redox potentials given in the literature for the tripeptide glutathione and for the macromolecular protein thioredoxin, which both can serve as model substances to illustrate redox potentials of thiols.

Furthermore, to illustrate the pH-dependency of the redox reactions and especially to explain the stronger effect of reduced sulfur functional groups of HA on Np(V) at pH 5.0 compared to that at pH 7.0 or 9.0, all potential electron-transfer reactions for the Np(V) reduction by sulfur functional groups of HA are given and discussed in (Schmeide et al., 2012a).

In the following the reduction behavior of the HA enriched with sulfur functional groups (M1-S) will be compared to that of a HA enriched with phenolic OH groups. For this, the Np(V) reduction by HA type Hyd-Glu, studied at pH 5.0 and 7.0 under identical experimental conditions (Schmeide and Bernhard, 2009), is shown in Fig. 3.11. Hyd-Glu is a synthetic HA model substance that was synthesized by oxidation of hydroquinone in the presence of glutamic acid in alkaline solution (Sachs and Bernhard, 2011a). Elemental composition and carboxylic group content of Hyd-Glu are comparable to those of natural HA. However, its phenolic/acidic OH group content (5.8 ± 0.2 meq/g) is in the range of the upper value given for natural HA (2.1-5.7 meq/g (Stevenson, 1994)) and higher than the phenolic/acidic OH group content of HA type M1-S (cf. Table 3.5).

As can be seen in Fig. 3.11, both rate and extent of Np(V) reduction was higher in the case of Hyd-Glu which can be attributed to its enhanced phenolic/acidic OH group content. At pH 5.0, quantitative reduction of Np(V) (≥99% Np(IV)) was achieved by Hyd-Glu within 36 d whereas only about 37% Np(V) were reduced by M1-S-3 within this time. For the Np(V) reduction by Hyd-Glu two kinetics are observed, whereby the fast one predominates. Also for the Np(V) reduction by sulfur containing HA type M1-S two kinetics can be observed. After a fast Np(V) reduction in the initial phase, further Np(V) reduction proceeded with a slow kinetics. Even after the long experimental period of about 11 months Np(V) was only partially reduced to Np(IV) and equilibrium has not been reached. If reduced-sulfur structures other than thiol groups in HA occur essentially as intra-molecular bridges as reported by

Vairavamurthy et al. (1997), then steric hindrances within the HA colloids may be responsible for this effect to some extent. The results show that phenolic OH groups contribute stronger and faster to the total Np(V) reducing capacity of HA than sulfur functional groups. This effect becomes stronger with increasing pH value.

Thus, in contrast to HA type Hyd-Glu which was shown to be suitable to stabilize the reduced states of redox-sensitive actinides such as Np in redox and sorption studies (Schmeide and Bernhard, 2009 and 2010) due to its high reducing capacity, HA type M1-S are suitable primarily for mechanistic studies of redox and complexation processes.

The ultrafiltration results verified the results of solvent extraction (cf. Schmeide et al., 2012a).

A fundamental parameter of humic substances is their reducing capacity (RC) which represents the electron equivalents per mass unit humic substance transferred by a humic substance to an added oxidant. The Np(V) reducing capacities at pH 5.0, calculated from the Np(IV) concentration in the sample solutions after 11 months, increase in the sequence M1 (0.019 meq/g HA) < M1-S-1 (0.022 meq/g HA) < M1-S-2 (0.034 meq/g HA) < M1-S-3 (0.045 meq/g HA). These Np(V) reducing capacities correlate linearly with the content of sulfur functional groups of the HA according to Eq. (3.10).

$$RC\ (meq/g\ HA) = 0.0175 + 0.0125 \cdot [S_{total}]\ (mmol/g\ HA);\ R^2 = 0.97 \qquad (3.10)$$

The results obtained in the present work have shown that in addition to quinone-like moieties and non-quinoid phenols (Schmeide and Bernhard, 2009) that dominate the redox behavior of humic substances, sulfur functional groups act as further redox-active sites in humic substances toward actinides. However, the impact of the individual reducing moieties is pH-dependent. While reduced sulfur functional groups contribute to the Np(V) reduction preferentially at slightly acidic pH, phenolic OH groups play a role preferentially in the alkaline pH range. In natural humic substances the content of sulfur functional groups is low compared to other redox-active functional units (quinoid moieties and phenolic OH groups). Moreover, the ratio of reduced to total (reduced and oxidized) sulfur functional groups is lower in most natural humic substances. Thus, in nature the extent of the contribution of sulfur functional groups to the overall redox and complexation capacity of humic substances is expected to be less pronounced.

For the interaction of metal ions with humic substances it can be concluded that, although certain functional groups dominate, there is an overlapping of different reduction and complexation paths.

3.3 U(VI) humate complexation in dependence on temperature (20-60°C)

The storage of heat producing radioactive waste will result in a significant temperature increase in the surrounding host rock. Temperature distributions for different conditions have been calculated, e.g., within the Opalinus Clay temperatures may reach a maximum of ~75°C in the vicinity of nuclear spent fuel canisters (Johnson et al., 2002). Thermal evolution is an important aspect in the long-term safety assessment of nuclear waste repositories since the temperature can affect many processes which influence the migration behavior of actinides.
The formation of metal humate complexes has been the focus of many studies, however, only few studies regarding temperature effects have been published so far. Marquardt et al. (1996) investigated the Np(V) complexation with HA at temperatures from 21 to 60°C. Samadfam et al. (1996) studied the complexation thermodynamics of Sr(II) with Aldrich HA in the temperature range between 10 and 40°C. The Ni(II) humate equilibrium reaction was investigated up to 80°C by Warwick et al. (1997). Interestingly, all groups noted a decrease in binding with increasing temperature.
The aim of this work was to determine the temperature-dependence of the U(VI) humate complexation in aqueous solution. To determine the HA proton exchange capacity (PEC) in dependence on temperature, potentiometric titrations of HA were performed between 20 and 80°C. The U(VI) complexation was studied at 20, 40 and 60°C using time-resolved laser-induced fluorescence spectroscopy (TRLFS).

3.3.1 Experimental

Purified commercially available natural HA from Aldrich (AHA, batch A2/98) was used for all measurements. The purification process is described in detail elsewhere (Sachs et al., 2004). Solutions were prepared using Milli-Q water (mod. Milli-RO/Milli-Q-System, Millipore, Schwalbach, Germany). The ionic strength was kept constant at 0.1 M ($NaClO_4$).

Potentiometric titration

All solutions were prepared with carbonate free deionized water under N_2 atmosphere in a glove box. A HA stock solution was prepared by dissolving 10 mg AHA in 1 mL 0.1 M NaOH (high grade, Merck). This solution was diluted with 0.1 M $NaClO_4$ obtaining a total volume of 50 mL. To determine the excess volume of NaOH, which was not used to deprotonate the HA, an aliquot of the AHA stock solution was titrated against 0.1 M $HClO_4$

(p.a., Merck). The titrations were carried out in a temperature-controlled glass vessel (T = 20-80 ± 0.1°C) under nitrogen atmosphere with the automatic titration system GP Titrino 736 (Methrom, software TiNet 2.50). The pH values were measured with a Schott Blue Line 11pH electrode, which was calibrated at the designated temperature for each experimental run with WTW DIN buffer solutions.

Preparation of U(VI) humate solutions

The samples were prepared from stock solutions of AHA (0.2 g/L), which were prepared freshly for each experiment and $UO_2(ClO_4)_2$ (5×10^{-4} M in 5×10^{-3} M $HClO_4$). The TRLFS studies were performed at constant HA (5 mg/L) and varying U(VI) (1.7×10^{-6} to 1.7×10^{-5} M) concentration. All samples were tempered in a water filled thermostat at 20, 40 or 60°C until the solutions reached the designated temperature (± 1°C). The pH values were then adjusted to 3.79 ± 0.02 with diluted NaOH and $HClO_4$ solutions. Reference samples of U(VI) without AHA were prepared under the same experimental conditions to determine the relative luminescence intensity as a function of the UO_2^{2+} concentration. The total U concentration in each sample was checked by ICP-MS analysis. To verify the AHA concentration, the amount of total organic carbon (TOC) was determined in the humate solutions.

TRLFS measurements

The U(VI) luminescence in solution was measured using a Nd:YAG laser system (Continuum Minilite II, Continuum Electro Optics Inc.). The fourth harmonic oscillation of the Nd:YAG (266 nm) with pulse energies between 0.2-0.5 mJ was used to excite U(VI). The emission signal was focused into a spectrograph (iHR 550, HORIBA Jobin Yvon) via fiber optics and detected using an ICCD camera system and a built-in delay generator (HORIBA Jobin Yvon). Aliquots of the tempered solutions were filled in a quartz cuvette and stored in a thermostatic cuvette holder (Quantum Northwest). To minimize temperature deviations, the samples were tempered at least 15 minutes prior to the measurements. The U(VI) luminescence spectra were recorded 175 ns after the excitation pulse to exclude the detection of occurring AHA fluorescence. The spectra were collected in the wavelength range between 371 and 674 nm at a gate time of 2 µs by averaging 100 laser pulses.

3.3.2 Results and discussion

As a precondition for the complexation studies, the proton exchange capacity (PEC) of AHA was determined in dependence on temperature applying potentiometric titration. As it is

depicted in Fig. 3.12, all PEC values between 20 and 60°C amount to about 4.45 ± 0.04 meq/g and do not show significant differences. Starting at 70°C, the PEC decreases with further increasing temperature to 3.77 ± 0.13 meq/g at 80°C. This indicates a change in the HA structure, presumably due to the irreversible loss of water, as it was described by Kolokassidou et al. (2007) for T > 70°C. Thus, a different complexation behavior of AHA toward U(VI) can be expected at higher temperatures.

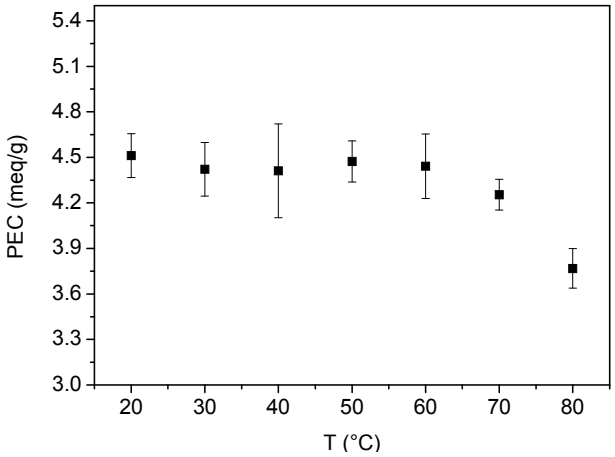

Fig. 3.12. Proton exchange capacity (PEC) of AHA in dependence on temperature.

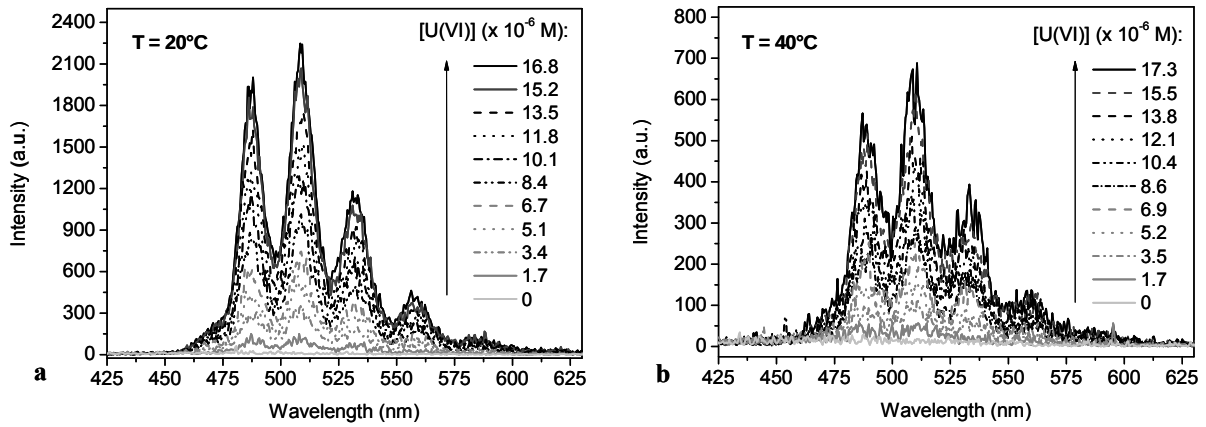

Fig. 3.13. Luminescence emission spectra of U(VI) humate solutions as a function of U(VI) concentration at 20°C (a) and 40°C (b).

Generally, the luminescence intensity of U(VI) as well as the lifetime decrease with increasing temperature. Simultaneously, the signal-to-noise ratio decreases. Therefore, it was not possible to measure the U(VI) luminescence adequately at temperatures above 60°C at the studied experimental conditions. Figure 3.13 shows the baseline-corrected emission spectra of the U(VI) humate solutions at 20 and 40°C. The measured luminescence is a sum of the spectra of the free UO_2^{2+} ion and the first hydrolytic species UO_2OH^+, which occurs in the

studied solutions (pH 3.8) with about 2%. Therefore, all spectra were deconvoluted by a non-linear least-square method according to Pompe et al. (1998) to calculate the luminescence contribution of the free uranyl ion to the sum spectra.

Figure 3.14a shows the emission spectra for the U(VI) humate solutions at 40°C after peak deconvolution. The determined UO_2^{2+} luminescence intensities of the U(VI) humate solutions as well as the reference solutions were integrated in the wavelength range between 430 and 600 nm. The results are shown in Fig. 3.14b. A strong decrease of the U(VI) luminescence intensities of the humate containing solutions compared to those without HA was observed, due to the complex formation between AHA and U(VI).

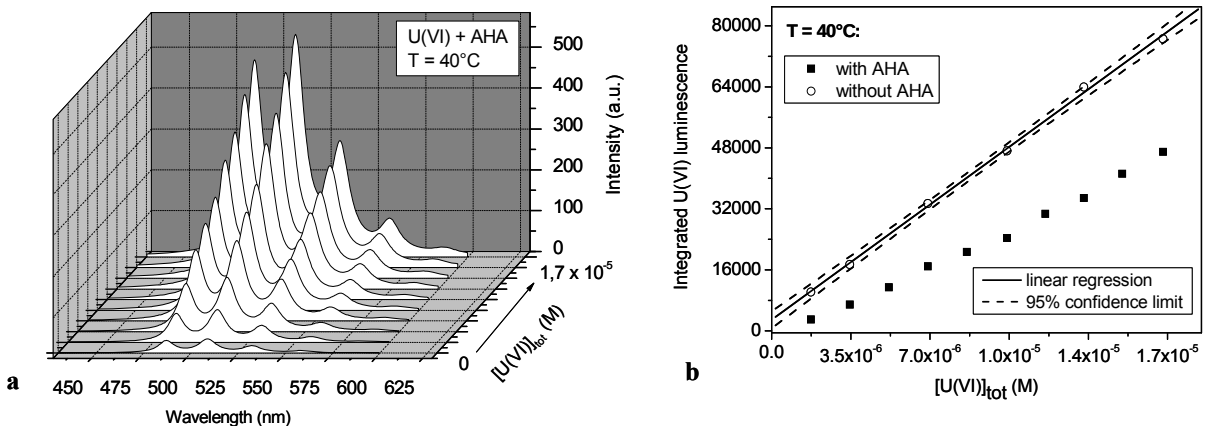

Fig. 3.14. Deconvoluted emission spectra of U(VI) humate solutions (a) and integrated luminescence intensities of the investigated solutions with and without AHA (b), plotted as a function of the U(VI) concentration at 40°C.

The experimental data were evaluated using the charge neutralization model by Kim and Czerwinski (1996). According to this model, the complexation reaction can be written as:

$$UO_2^{2+} + HA(II) \rightleftarrows UO_2HA(II) \tag{3.11}$$

It is assumed that UO_2^{2+} binds two complexing sites of the HA molecule. Because not all complexing sites of HA are available for the complexation, the loading capacity (LC) was introduced by this model:

$$\beta = \frac{[UO_2HA(II)]}{[UO_2^{2+}]_{free} \cdot ([HA(II)]_{tot} \cdot LC - [UO_2HA(II)])} \tag{3.12}$$

The LC was determined graphically by linear regression of the experimental data after rearranging Eq. (3.12):

$$[UO_2^{2+}]_{free} = LC \cdot \frac{[UO_2^{2+}]_{free} \cdot [HA(II)]_{tot}}{[UO_2HA(II)]} - \frac{1}{\beta} \quad (3.13)$$

$$[HA(II)]_{tot} = \frac{[HA] \cdot PEC}{z} \quad (3.14)$$

$[HA(II)]_{tot}$ was calculated according to Eq. (3.14) using the PEC values previously determined for each temperature. The graphic determination of LC is shown in Fig. 3.15 for the studies at 40°C. Applying LC, the complex stability constants were calculated for each experimental point, according to Eq. (3.12). The calculated stability constants as well as the LC values for 20, 40 and 60°C are summarized in Table 3.9.

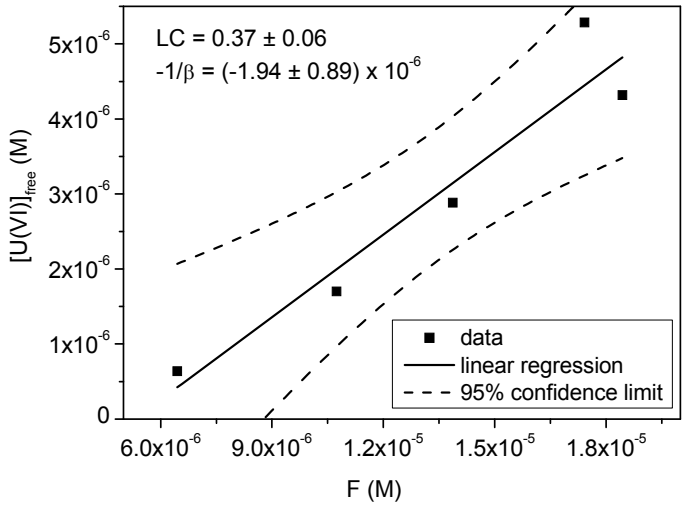

Fig. 3.15. Graphic determination of the loading capacity (LC) for the U(VI) complexation with AHA at 40°C.

Table 3.9. Summary of the determined complexation constants and loading capacities for the U(VI) complexation with AHA in dependence on temperature.

T (°C)	PEC (meq/g)	LC (%)	log $\beta_{0.1\ M}$
20	4.51 ± 0.15	34.9 ± 2.8	5.73 ± 0.07
40	4.41 ± 0.31	38.1 ± 2.0	5.75 ± 0.13
60	4.44 ± 0.21	16.9 ± 3.9	5.38 ± 0.21

As implied by the determined PEC values, the LC as well as the complex stability constants determined at 20 and 40°C are comparable. The log β of about 5.7 is in good agreement with literature data (e.g., log β = 5.88 ± 0.22 (Pompe et al., 1998) and log β = 6.20 ± 0.56 (Pompe et al., 2000b). At 60°C, the LC value decreases significantly to 17%, which is an indication that fewer AHA complexing sites are available for U(VI) at increased temperature. The

complexation constant is also decreased to log β = 5.38 ± 0.21, which seems to be a typical behavior for HA and was already reported for other systems in literature.

Marquardt et al. (1996) found a decrease in the relative contribution of Np(V) humate from 38 to 13% with increasing temperature. Also Samadfam et al. (1996) and Warwick et al. (1997) demonstrated that the humate binding decreases with increasing temperature. Furthermore, Warwick et al. (1997) mentioned the appearance of coagulation of HA at 60 and 80°C. Although we could not verify this for 60°C, it might be possible that coagulation or precipitation of the AHA is increased at higher temperatures.

Kolokassidou et al. (2007), who studied the thermal stability of HA from Gorleben groundwaters, observed a reversible water release due to thermal treatment of HA at 60°C. Above 70°C, this process becomes irreversible, maybe due to the release of chemisorbed water molecules and water molecules produced by condensation or decarboxylation. They also determined the formation of more condensed polyaromatic structures above 70°C, which could be an explanation for the decreasing complexation tendency of HA.

In conclusion, the U(VI) humate binding is reduced at elevated temperatures, as it was also found for several other metals. Therefore, the formation of potentially mobile metal humate species may be limited in the vicinity of heat generating nuclear waste.

4 Sorption of U(VI) onto Opalinus Clay

To determine the retardation ability of the clay host rock toward radionuclides, knowledge about the geochemical interaction processes between radionuclides and the host rock such as sorption or diffusion is necessary. In this chapter the results of the sorption studies for U(VI) and argillaceous rock are presented. In an argillaceous rock nuclear waste repository the radioactive decay of the actinides and their fission products will result in elevated temperatures of up to 100°C close to the waste containers (Brasser et al., 2008). Thus, in addition, temperature-dependent U(VI) sorption experiments were performed.

In the past, many clay sorption studies focused on the interaction of actinides with pure clay minerals such as kaolinite (Redden et al., 1998; Thompson et al., 1998; Kornilovich et al., 2000; Křepelová et al., 2006; Sachs and Bernhard, 2008; Schmeide and Bernhard, 2010). Since pure clay minerals have a definite composition, the possible interaction processes are easier to elucidate and to model. Inert background electrolytes such as sodium chloride (Redden et al., 1998; Kornilovich et al., 2000) or sodium perchlorate (Kowal-Fouchard et al., 2004; Bradbury and Baeyens, 2006; Křepelová et al., 2006; Sachs and Bernhard, 2008; Schmeide and Bernhard, 2010) were used for the experiments. Thus, an influence of competing complexing ions had not to be considered.

In this work, sorption studies were extended from pure clay minerals and inert background electrolytes to complex natural systems. In natural environments, complex salt solutions, the so-called pore waters of argillaceous rock, occur as background electrolytes of the clay. Pore water contains ions which can act as competing reactants in sorption studies. As a representative for natural clay, Opalinus Clay (OPA) from Mont Terri, Switzerland, which is discussed as possible host rock for nuclear waste disposal sites, was investigated.

In natural clay, organic matter is strongly associated with mineral constituents. Humic substances, such as fulvic and humic acids (HA) as well as low molecular weight organic acids, can be released from the clay under certain conditions. This was shown by extraction experiments (Claret et al., 2003; Glaus et al., 2005; Courdouan et al., 2007, 2008). Because of the variety of functional groups, humic substances show a pronounced ability for complex formation. Furthermore, they are known for their inherent redox properties (Schmeide and Bernhard, 2009) and for their ability to form stable colloids (Artinger et al., 2002). Due to this, they can influence the transport of actinides in the environment.

In the present study, the U(VI) sorption onto OPA was investigated in the absence and presence of HA or low molecular weight organic acids, in dependence on temperature and

CO_2 presence. In all experiments, OPA pore water (Pearson, 1998) was used as background electrolyte. In addition, the U(VI) sorption onto OPA was investigated in dependence on pH using 0.1 M $NaClO_4$ as background electrolyte. The results were compared to the experiments of Křepelová et al. (2006), who investigated the U(VI) sorption onto kaolinite.
The obtained sorption results provide a contribution to the thermodynamic sorption database used for modeling of geochemical interaction processes of actinide ions and possible host rocks of a nuclear waste repository.

4.1 Characterization of Opalinus Clay

For the studies OPA from the Mont Terri Rock Laboratory, Switzerland, was used. There, OPA occurs with a maximum overburden of about 300 m and a thickness of about 150 m (Pearson et al., 2003). Bore cores were taken by the Federal Institute for Geosciences and Natural Resources (BGR) using air as drilling medium (Bossart and Thury, 2008) in September 2003.

Table 4.1. Mineralogy of OPA shaly facies (average of nine samples) (Pearson et al., 2003).

Mineral	**wt.%**
Clay minerals	58-76
• Illite	16-40
• Illite/smectite ML	5-20
• Chlorite	4-20
• Kaolinite	15-33
Quartz	6-24
Calcite	5-28
Siderite	1-4
Albite	0.6-2.2
K-feldspar	1-3.1
Dolomite/ankerite	0.2-2
Pyrite	0.6-2
Organic carbon	< 0.1-1.5

Generally, the OPA formation is subdivided into five lithological sub-units with ‘sandy’, ‘shaly’, and ‘calcareous-sandy’ facies (Pearson et al., 2003). In the present study, sorption experiments with U(VI) were carried out with two OPA batches. Batch BHE-24/1 and batch BLT-11/01 were used for sorption experiments under aerobic and anaerobic conditions,

respectively. Both batches can be assigned to the shaly fraction of OPA. Table 4.1 presents the mineralogy of OPA for shaly facies as average of nine samples (Pearson et al., 2003).
Both OPA batches were characterized before starting the sorption experiments. The determined properties are summarized in Table 4.2.

Table 4.2. Main characteristics of OPA batches BHE-24/1 and BLT-11/01.

Batch	**BHE-24/1**	**BLT-11/01**
Grain size	< 500 µm	< 200 µm
N_2-BET [a]	(41.3 ± 0.5) m^2/g	(38.8 ± 0.3) m^2/g
TOC [b]	(1.09 ± 0.06) wt.%	(0.96 ± 0.02) wt.%
TC [b]	(2.49 ± 0.02) wt.%	(1.87 ± 0.01) wt.%
CEC [c]	(10.26 ± 0.52) meq/100 g	(12.89 ± 0.14) meq/100 g
Main components / wt.% [d]		
SiO_2	39.04 ± 3.90	36.37 ± 3.64
Al_2O_3	17.91 ± 1.79	20.08 ± 2.01
Fe_2O_3	6.53 ± 0.65	6.04 ± 0.60
CaO	5.42 ± 0.11	3.16 ± 0.06
K_2O	3.47 ± 0.35	3.61 ± 0.36
MgO	2.32 ± 0.05	2.33 ± 0.05
U content [d]	(2.83 ± 0.28) ppm	(2.93 ± 0.29) ppm

[a] Determined by using a surface area and pore size analyzer (mod. Coulter SA 3100, Beckman Coulter, Fullerton, USA). [b] TOC … total organic carbon; TC … total carbon; determined by a multi N/C 2100 analyzer (Analytik Jena, Jena, Germany). [c] The cation exchange capacity (CEC) was determined by the compulsive exchange method (Sumner and Miller, 1996). [d] Determined by inductively coupled plasma-mass spectrometry (ICP-MS; mod. ELAN 9000, Perkin Elmer, Boston, USA; Error: ± 10%) and atomic absorption spectroscopy (AAS; mod. AAS-4100, Perkin Elmer; Error: ± 2%) after digestion of the OPA sample with HNO_3 (*p.a.*, Merck, Darmstadt, Germany; distilled by sub-boiling), HCl (*suprapur*, Merck) and HF (*suprapur*, Merck) in a microwave oven (mod. multiwave, Anton Paar, Perkin Elmer) (only compounds > 1 wt.% are shown).

The Fourier transform infrared (FTIR) spectra (FTIR spectrometer Spectrum 2000 GX, Perkin Elmer; KBr method) of the batches BHE-24/1 and BLT-11/01 are shown in Fig. 4.1a. The comparison of the spectra shows negligible differences between the batches. In Fig. 4.1b the IR spectra of some mineral components of OPA are compared to the IR spectrum of OPA. From all mineral spectra shown, spectral contributions can be found in the OPA spectrum.
The OPA batches were characterized additionally by X-ray diffraction (XRD). Powder XRD data were collected for both batches of OPA on a Bruker AXS D8 diffractometer (Bruker AXS GmbH, Karlsruhe, Germany) in θ-θ geometry with curved PG-secondary monochromator using CuKα radiation. The scan mode was 'locked-coupled' (Bragg-Brentano geometry). Data were collected from 7 to 70 °2θ using a step size of 0.05 °2θ and a step time of 21-54 s. The data were analyzed by phase evaluation using the EVA code (Bruker AXS).

The corresponding diffractograms and mineral patterns are shown in Fig. 4.2. Due to the mineralogical heterogeneity of OPA it was not possible to quantify the different mineral contributions by XRD. However, for the minerals shown in Fig. 4.2, XRD patterns were found in the diffractogram of OPA.

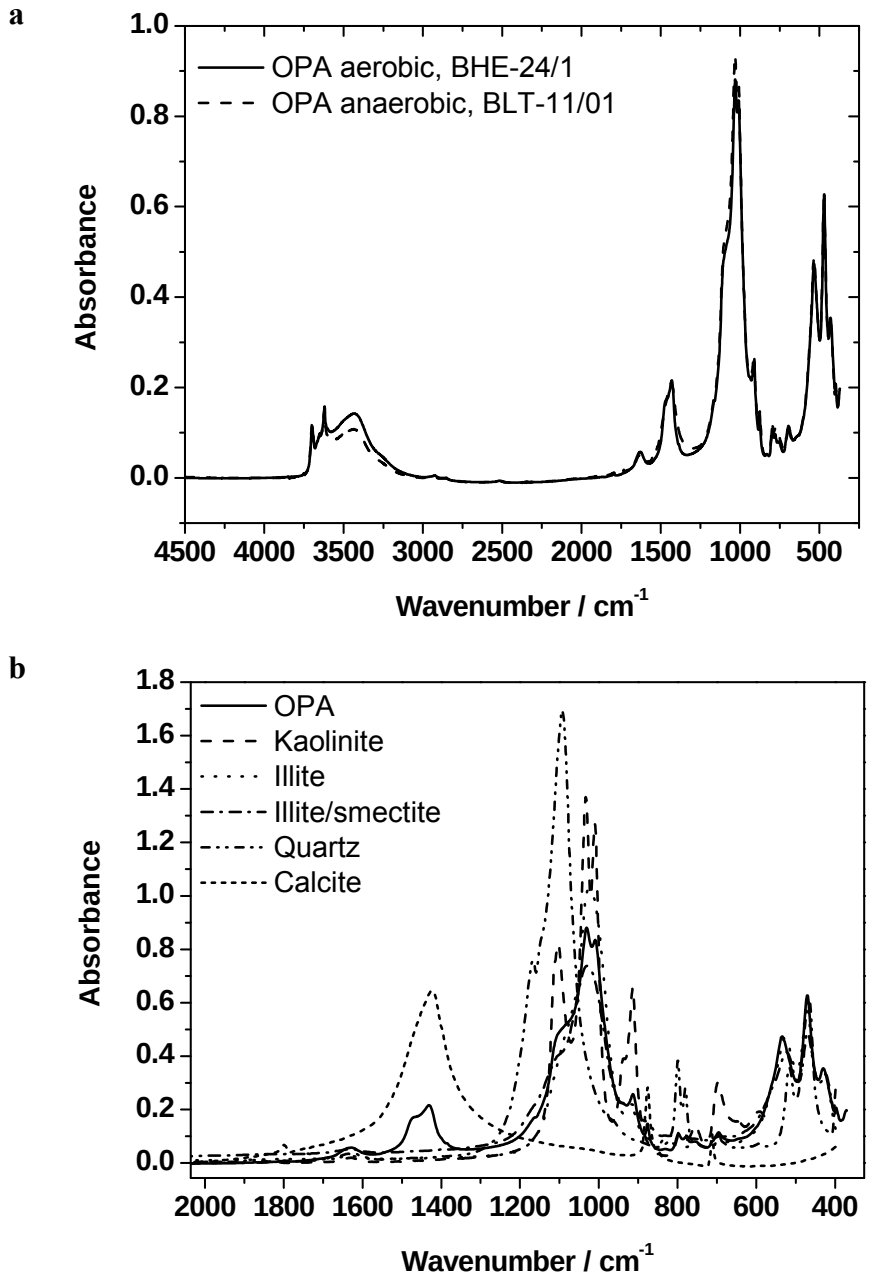

Fig. 4.1. (a) FTIR spectra of OPA batches. **(b)** FTIR spectra of some mineral components of OPA compared to FTIR spectra of OPA batch BHE-24/1.

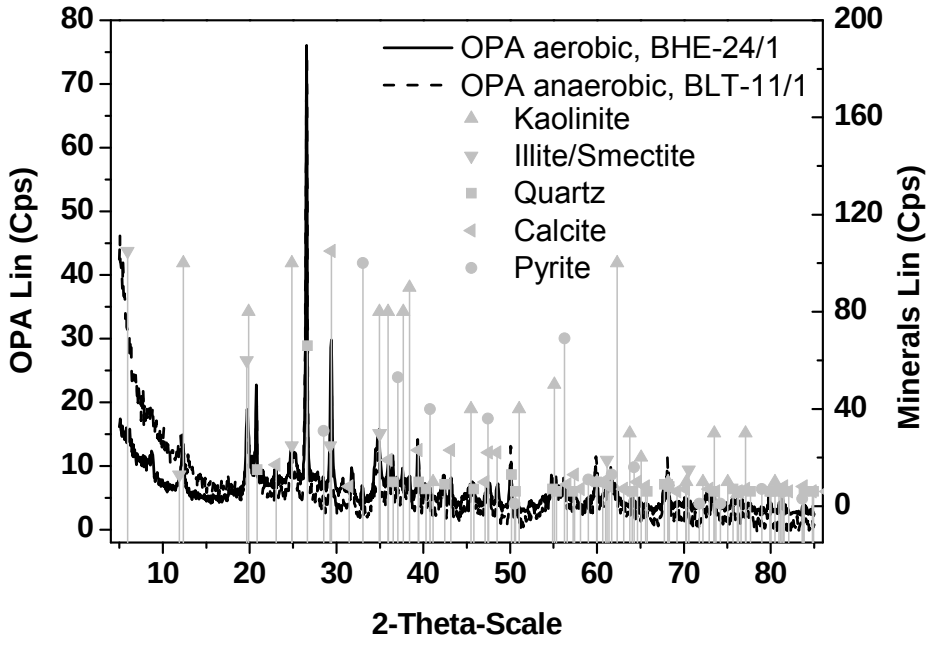

Fig. 4.2. X-ray diffractogram of the OPA batches BHE-24/1 and BLT-11/01 and patterns of different minerals contained in OPA.

The so-called OPA pore water was synthesized in this study according to the model of Pearson (1998) (pH 7.6; cf. Table 4.3) in Milli-Q water (18 MΩ; mod. Milli-RO/Milli-Q-System, Millipore, Schwalbach, Germany). For this composition the true ionic strength (I_t) of 0.36 M is calculated using the speciation code EQ3/6 (Wolery, 1992) (cf. Table 4.3).

Table 4.3. Composition of OPA pore water: modeled by Pearson (1998) (pore water$_{theor}$), prepared for the experiments (pore water$_{exp}$) and ions leached out from OPA during 7 d contact time with OPA pore water (Δleached$_{7d}$) (Δleached$_{7d}$ = difference between pore water$_{exp}$ and pore water$_{exp7d}$).

Element/Ion	Pore water$_{theor}$ / mol/L	Pore water$_{exp}$ / mol/L	Δleached$_{7d}$ / mol/L
Na [a]	2.4×10^{-1}	n.a. [e]	n.a. [e]
K [a]	1.6×10^{-3}	$(2.3 \pm 0.2)\times10^{-3}$	$-(0.1 \pm 0.5)\times10^{-3}$
Mg [b]	1.7×10^{-2}	$(1.6 \pm 0.03)\times10^{-2}$	$(0.03 \pm 0.06)\times10^{-2}$
Ca [b]	2.6×10^{-2}	$(2.5 \pm 0.05)\times10^{-2}$	$(0.2 \pm 0.1)\times10^{-2}$
Sr [a]	5.1×10^{-4}	$(4.9 \pm 0.5)\times10^{-4}$	$(0.1 \pm 1.0)\times10^{-4}$
Al [a]	-	b.d. [f]	$(1.6 \pm 0.2)\times10^{-7}$
Si [a]	-	b.d. [f]	$(7.7 \pm 0.8)\times10^{-5}$
U [a]	-	b.d. [f]	$(5.3 \pm 0.5)\times10^{-9}$
Cl^- [c]	3.0×10^{-1}	$(2.9 \pm 0.3)\times10^{-1}$	$-(0.06 \pm 0.57)\times10^{-1}$
SO_4^{2-} [c]	1.4×10^{-2}	$(1.4 \pm 0.04)\times10^{-2}$	$(0.11 \pm 0.09)\times10^{-2}$
CO_3^{2-}/HCO_3^- [d]	4.8×10^{-4}	$(4.0 \pm 0.1)\times10^{-4}$	$(3.4 \pm 0.3)\times10^{-4}$
I_t	0.36	0.37	-

[a] ICP-MS (Error: ± 10%).
[b] AAS (Error: ± 2%).
[c] IC (Error: ± 3-10%).
[d] TC – TOC (Error: ± 3%).
[e] n.a.: not analyzed.
[f] b.d.: below detection limit.

4.1.1 Leaching of Opalinus Clay with Opalinus Clay pore water

This experiment was carried out with batch BHE-24/1 after investigation of the U(VI) sorption onto OPA in OPA pore water in dependence on solid-to-liquid ratio (S/L) (section 4.4.2.1). Using the optimal S/L ratio, a leaching experiment was conducted in order to determine the ions released from the clay into the pore water in dependence on time.

4.1.1.1 Experimental

2 g OPA was weighed into a 500 mL polypropylene (PP) bottle. Subsequently, 500 mL of pore water were added. The pore water was prepared in a perfluoroalkoxy bottle, because glass bottles may release ions also present in the clay. The clay suspension was continuously shaken using an overhead shaker modified for the use of high volume bottles (mod. REAX 20, Heidolph Instruments, Schwabach, Germany). In the beginning of the experiment, samples were taken every day; after 8 d three times a week; after 34 d only once a week. After 90 d the experiment was stopped. The pH value was readjusted before each sampling. For sampling, the bottle was removed from the shaker and placed on a magnetic stirrer (mod. Big Squid, IKA, Staufen, Germany). Then, a well-mixed aliquot of the suspension of 10 mL was taken. The samples were centrifuged for phase separation (30 min, 4000 rpm; mod. Megafuge 1.0, Heraeus Sepatech, Osterode/Harz, Germany). After centrifugation, the supernatants were filtered (450 nm, polyethersulfone, vwr international, Darmstadt, Germany). Prior to filtering, the filters were rinsed with 1 mL sample solution. Filtrates were analyzed for K, Sr, Ba, Al, Si, Fe and U by ICP-MS, for Mg and Ca by AAS, and for F^-, Cl^-, SO_4^{2-} and PO_4^{3-} by ion chromatography (IC; mod. IC separation center 733, Metrohm, Herisau, Switzerland). The total inorganic carbon (TIC) content was measured using the multi N/C 2100 analyzer as difference of TC and TOC. During the investigations the concentrations of Fe, F^- and PO_4^{3-} were always below the detection limit of ICP-MS and IC.
After the leaching experiment, X-ray diffraction (XRD) experiments were performed to investigate a possible alteration of the clay mineral structure and formation of secondary mineral phases. For that, the solid was separated from the aqueous phase and lyophilized. Powder XRD data were collected for the leached out OPA.

4.1.1.2 Results and discussion

The leaching experiment showed that the concentrations of ions in the filtrates were in equilibrium after 7 d. Thus, this time was chosen as optimal pre-equilibration time for the

sorption experiments.

The initial ion composition of pore water in the experiment (pore $water_{exp}$) and the ions leached out during 7 d contact time of OPA with pore water ($\Delta leached_{7d}$) are shown in Table 4.3.

It can be seen that the leaching of the alkaline and earth alkaline metal ions (except for calcium) can be neglected since the experimental errors of the concentrations measured after 7 d are larger than the values themselves.

Obviously, aluminum and silicon ions are leached out due to dissolution processes of clay minerals and quartz in OPA. Sulfate and carbonate ions are also released. They originate from pyrite oxidation and different carbonate minerals in the clay. The increase of the calcium and carbonate concentration in solution indicates the dissolution of the calcite fraction of OPA.

On the basis of the composition of pore $water_{exp}$ and under consideration of the concentrations of the leached out ions calcium, aluminum, silicon, sulfate and carbonate an I_t of 0.34 M was calculated for the pore water used in our experiments.

After the leaching experiment, the remaining OPA was studied by XRD. Compared to the diffractogram of untreated OPA (cf. Fig. 4.2) additional patterns were detected in the resulting diffractogram of the leached out clay (not shown). These could be attributed to NaCl, which is the main salt component in pore water. Further changes in the diffractogram of the leached out OPA sample were not observed. Thus, it can be concluded, that the mineral structure of OPA is not changed due to contact with pore water. This verifies that pore water indeed is close to equilibrium with OPA.

4.1.2 Leaching of Opalinus Clay in dependence on pH

4.1.2.1 Experimental

Suspensions of OPA (batch BHE-24/1) in 0.1 M $NaClO_4$ were prepared as a function of pH to determine the amount of U(VI) and competing ions leached out of OPA.

The experiments were performed under ambient atmosphere ($pCO_2 = 10^{-3.5}$ atm) at room temperature. 40 mg OPA were weighed into 15 mL polypropylene (PP) centrifuge tubes (mod. Cellstar, Greiner Bio-One GmbH, Frickenhausen, Germany). Subsequently, 5 mL 0.1 M $NaClO_4$ were added and pH values were adjusted between pH 3 and 10. For pre-equilibration, the samples were continuously shaken on a horizontal shaker (mod. Promax 2020, Heidolph Instruments, Schwabach, Germany) and the pH values were periodically checked and readjusted. After one week of pH adjustment (4-5 times), the volume was filled

up to 10 mL with 0.1 M $NaClO_4$, thus, an S/L of 4 g/L was reached. After that, only small amounts of $HClO_4$ and NaOH had to be added for pH readjustment until the pH values were stable (usually after three weeks). Thus, the effect of pH adjustment on the S/L ratio was negligible.

At the end, the final pH values of the samples were determined and the samples were centrifuged and the supernatants were filtered as described in section 4.1.1.1.

The filtrates of the blank suspensions were analyzed for Na, K, Sr, Al, Si, P, Fe, and U by ICP-MS, for Mg and Ca by atomic absorption spectroscopy (AAS) (mod. AAS-4100, Perkin Elmer), and for F^-, Cl^- and SO_4^{2-} by ion chromatography (IC; mod. IC separation center 733, Metrohm, Herisau, Switzerland). The total inorganic carbon content was measured as difference of the total carbon and the total organic carbon determined using the multi N/C 2100 analyzer. During the investigations the concentration of P was always below the detection limit of ICP-MS. Additionally, the filtrates of the blank suspensions were investigated for colloids and for the size of the colloidal particles with a BI-90 photon correlation spectroscope (Brookhaven Instruments, USA). A detailed description of the instruments and the procedure is given in (Dreissig et al., 2011).

X-ray diffraction measurements

X-ray diffraction (XRD) experiments were performed to investigate a possible alteration of the clay mineral structure and formation of secondary mineral phases due to change of the pH value. 2 g OPA were weighed into three 500 mL PP bottles each. Subsequently, 500 mL 0.1 M $NaClO_4$ were added in each bottle to reach an S/L ratio of 4 g/L. The pH values were adjusted to pH 4, 7 and 10, respectively. The suspensions were continuously shaken using an overhead shaker modified for the use of high volume bottles (mod. REAX 20, Heidolph Instruments). The pH values were periodically checked and readjusted. After 90 d the experiment was stopped. Each solid was separated from the aqueous phase and lyophilized. Powder XRD data were collected for the leached out OPA.

Mössbauer spectroscopy

The OPA samples used for XRD measurements were also studied by Mössbauer spectroscopy to clarify the oxidation state of the iron mineral phases in OPA. ^{57}Fe Mössbauer spectra were recorded at room temperature in transmission mode using standard instrumental configuration by WissEl (Starnberg, Germany). The ^{57}Co in the rhodium matrix was used as Mössbauer source. A quantitative analysis of the spectra was made using the NORMOS program package of R.A. Brand (Brand, 1987).

Zeta potential measurements

Due to the high carbonate content of OPA, a determination of its point of zero charge (pzc) by potentiometric titration was not feasible. To get information about the clay charge, zeta potential measurements of OPA suspensions were performed with laser Doppler velocimetry using a Zetasizer Nano ZS (Malvern Instruments, Malvern, U.K.) with disposable capillary cells. Suspensions of OPA in 0.1 M $NaClO_4$ (S/L = 0.1 g/L) were prepared in the pH range from pH 2.5 to 7.5 as described in section 4.5.1. The zeta potential measurements were repeated tenfold. The temperature was maintained at 25 ± 0.1°C. Agglomerated colloids were re-suspended as flocks by ultrasound before measurement.

4.1.2.2 Characterization of the solid

The zeta potential of OPA suspensions decreased with increasing pH from pH 2.5 to 7.5. In this pH range, it remained always negative, which implies that the charge of the OPA particles is negative throughout the studied pH range.

Exemplary for the studied pH range, OPA samples, that were leached at pH 4, 7 and 10 for 90 d, were studied by XRD. Compared to the diffractogram of untreated OPA (Fig. 4.2), additional patterns were detected in the resulting diffractograms (not shown). These were attributed to the background electrolyte $NaClO_4$. As expected for pH 4 and 7, the calcite pattern in the respective diffractograms of the leached out samples did not appear due to acid addition. Further changes in the diffractograms were not observed. Secondary mineral phases could not be detected.

The samples used for XRD were investigated also by Mössbauer spectroscopy. The ratios of Fe(II)/Fe(III) in untreated aerobic OPA and pH-equilibrated OPA samples are shown in Table 4.4. The OPA is stored under aerobic conditions. Thus, about 45% of Fe occur as Fe(III). Due to contact with water a further oxidation takes place. This effect can be observed for the whole pH range studied. Thus, it can be assumed, that during the pH-dependent sorption experiments about 50% of iron is present as Fe(II) in the OPA samples.

Table 4.4. Results of Mössbauer spectroscopy.

Sample	Fe(II) / %	Fe(III) / %
Untreated OPA	55.1 ± 2.0	44.9 ± 1.2
pH 4	47.5 ± 2.8	52.5 ± 2.0
pH 7	49.5 ± 2.1	50.5 ± 1.5
pH 10	48.2 ± 4.4	51.8 ± 3.2

4.1.2.3 Characterization of the solution

Filtrates of OPA suspensions with pH values between pH 3 and 10 were analyzed for clay leached out ions. The filtrates were checked also for the presence of colloids by photon correlation spectroscopy. In all samples, colloids were not detected.

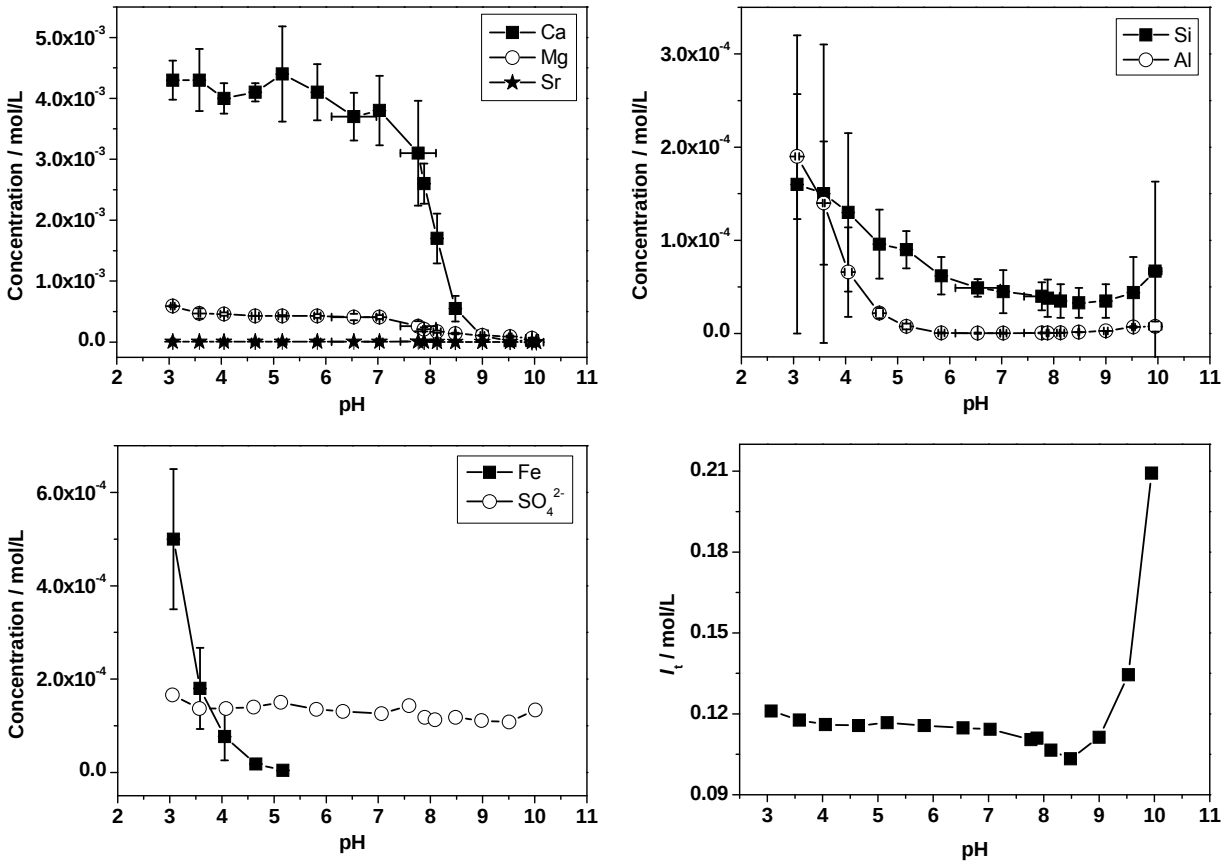

Fig. 4.3. Concentrations of Ca, Mg, Sr, Si, Al, Fe and SO_4^{2-} in the filtrates of OPA suspensions with 0.1 M $NaClO_4$ (S/L = 4 g/L) and the resulting true ionic strength (I_t) under consideration of the competing ions as a function of pH.

In Fig. 4.3, the concentrations of OPA leached out ions are shown for Ca, Mg, Sr, Si, Al, Fe and SO_4^{2-} as a function of pH. The comparison of the leached out alkaline earth elements shows that at pH 3 the calcium concentration is about seven times higher than the magnesium concentration. Strontium is only present in trace concentrations. The influence of pH on the clay mineral and quartz fractions of OPA is illustrated by the aluminum and silicon concentrations in solution. Only at pH $\leq$ 5, iron is measured in solution. Its contribution originates from the pyrite, siderite and chlorite fractions of OPA, which are dissolved under these conditions. Due to oxidation of pyrite, sulfate is formed (Pearson et al., 2003). The observed behavior of minerals dissolution is in agreement with their geochemistry.

The pH-dependent concentrations of competing ions in solution lead to a pH-dependent ionic strength (cf. Fig. 4.3). The resulting true ionic strength (I_t) was calculated under consideration of the composition of the background electrolyte including the competing ions K, Mg, Ca, Sr, Al, Si, Fe, F^-, Cl^-, SO_4^{2-} and CO_3^{2-} using the speciation code EQ3/6 (Wolery, 1992). In the pH range from pH 3 to 9, I_t amounts to 0.11 M in average. Above pH 9, I_t increases to 0.21 M at pH 10, which is due to carbonate dissolution. Under natural conditions the S/L ratio of clay rock and water is much larger resulting in a higher ionic strength in the background electrolyte, the so-called pore water. For OPA the composition of its pore water was modeled by Pearson (Pearson, 1998). Its I_t amounts to 0.36 M at pH 7.6 (Joseph et al., 2011). That means, under environmentally relevant conditions the ionic strength is two to three times larger than those observed in these experiments.

4.2 Speciation of U(VI) in dependence on background electrolyte

The U(VI) speciation was calculated using the speciation code EQ3/6 (Wolery, 1992) and the thermodynamic data for U(VI) compiled in (Guillaumont et al., 2003), including data for the $Ca_2UO_2(CO_3)_3(aq)$ complex (Bernhard et al., 2001). In the presence of HA, the U(VI) speciation was calculated using a modified EQ3/6 code (Sachs et al., 2004) with integrated metal ion charge neutralization model (CNM; (Kim and Czerwinski, 1996)) for description of the U(VI) humate complexation. The calculations were performed using literature data for the binary complex $UO_2HA(II)$ (Montavon et al., 2000; Pompe et al., 2000a, 2000b), the ternary complex $UO_2(OH)HA(I)$ (Sachs et al., 2007a) and the carbonato humate complex $UO_2(CO_3)_2HA(II)^{4-}$ (Steudtner et al., 2011a, 2011b).

For speciation calculations the pH-dependence of the HA loading capacity (LC) (Kim and Czerwinski, 1996) must be known. LC depends on the cation which is complexed. Due to the fact that in this study several competing ions are present in solution which can be complexed by HA an average pH-dependent LC equation was used for speciation calculations. Literature data show, that various divalent cations (e.g., calcium, strontium, lead, copper, cadmium, zinc) exhibit a similar complexation with HA (Paulenová et al., 2000; Mansel et al., 2003; Beck et al., 2004). In addition, the LC values determined for U(VI) HA complexation were considered (Pompe et al., 1998, 2000b; Montavon et al., 2000; Sachs et al., 2007a). The pH-dependence of LC was obtained by linear regression (Eq. (4.1)) and used for speciation calculations:

$$LC = 0.1633 \cdot pH - 0.4134 \quad (4.1)$$

In Fig. 4.4, the speciation of U(VI) (1×10^{-6} M) in dependence on the background electrolyte (0.1 M $NaClO_4$, 0.39 M NaCl, OPA pore water) is presented in the absence and presence of 50 mg/L HA, respectively.

Due to the fact that most of the sorption experiments were performed at pH 7.6, the pH of the OPA pore water, the first part of the following discussion is focused on pH 7.6.

In 0.1 M $NaClO_4$ (Fig. 4.4a,b), the U(VI) speciation is dominated by $(UO_2)_2CO_3(OH)_3^-$ (87%). In the presence of HA, the carbonato humate complex $UO_2(CO_3)_2HA(II)^{4-}$ determines the U(VI) speciation to almost 100%. If 0.39 M NaCl is used as background electrolyte (Fig. 4.4c,d), the U(VI) speciation changes to $UO_2(CO_3)_3^{4-}$ (59%), $(UO_2)_2CO_3(OH)_3^-$ (26%) and $UO_2(CO_3)_2^{2-}$ (13%). In the presence of HA, the U(VI) speciation is still dominated by $UO_2(CO_3)_2HA(II)^{4-}$.

Figures 4.4e,f show the speciation of U(VI) in the absence and presence of HA (50 mg/L) in pore water as a function of pH. It should be noted that the OPA pore water composition is only valid for pH 7.6. As the concentrations of all ions are a function of pH, Figs. 4.4e,f gives an exact picture only for pH 7.6. The changing carbonate concentrations and the dissolution of calcite as a function of pH, however, have been considered.

In pore water at pH 7.6, the U(VI) speciation is dominated by $Ca_2UO_2(CO_3)_3(aq)$ (Bernhard et al., 2001) (Fig. 4.4e), indicating a significant influence of calcium and carbonate ions present due to dissolution of calcite. Further charged alkaline earth carbonato complexes with U(VI) are reported in the literature, such as $CaUO_2(CO_3)_3^{2-}$, $SrUO_2(CO_3)_3^{2-}$ and $MgUO_2(CO_3)_3^{2-}$ (Dong and Brooks, 2006). Their presence was considered here, too, but was modeled to be negligible at pH 7.6 and thus, not considered in further discussions. The U(VI) speciation in the presence of HA is shown in Fig. 4.4f. Also in the presence of 50 mg HA/L the $Ca_2UO_2(CO_3)_3(aq)$ complex is the dominating species at pH 7.6. That means the presence of HA has no effect on the speciation of U(VI) in pore water.

0.1 M $NaClO_4$

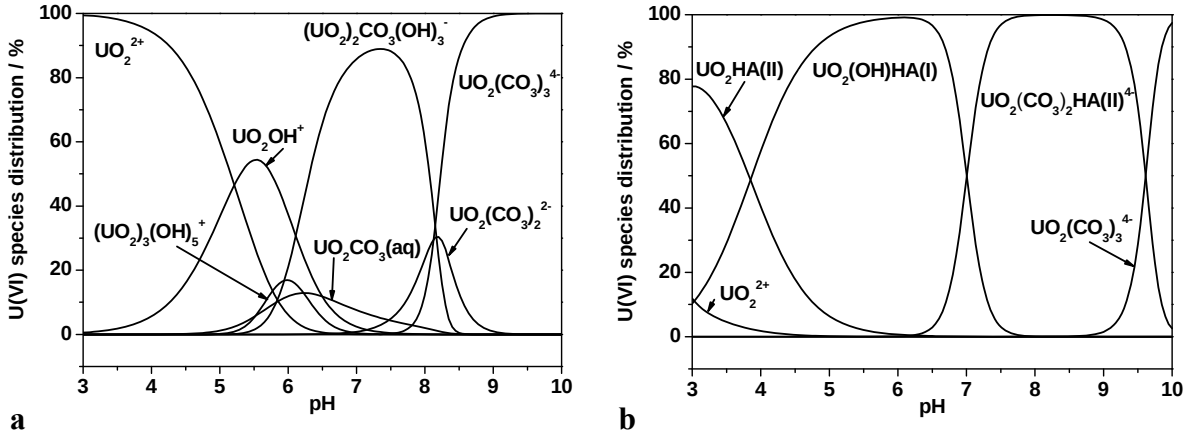

0.39 M NaCl

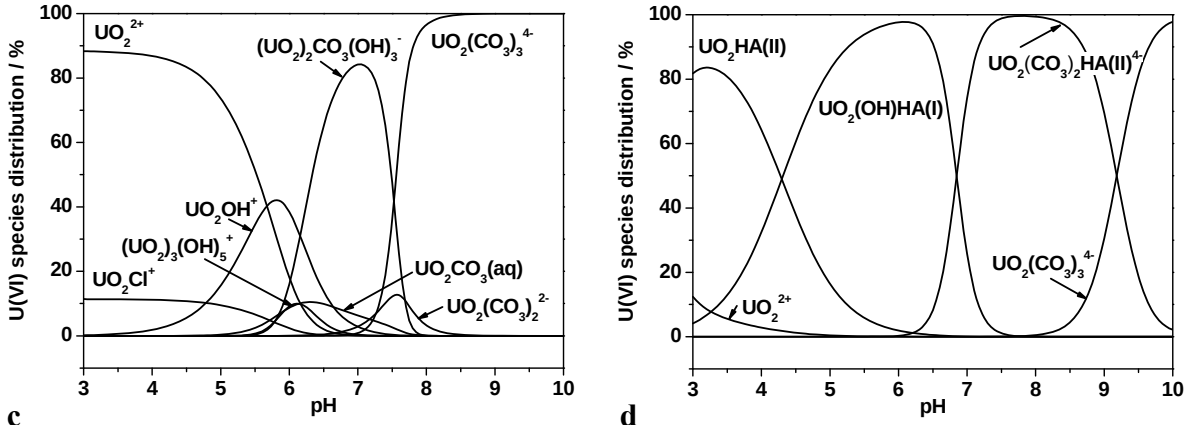

OPA pore water

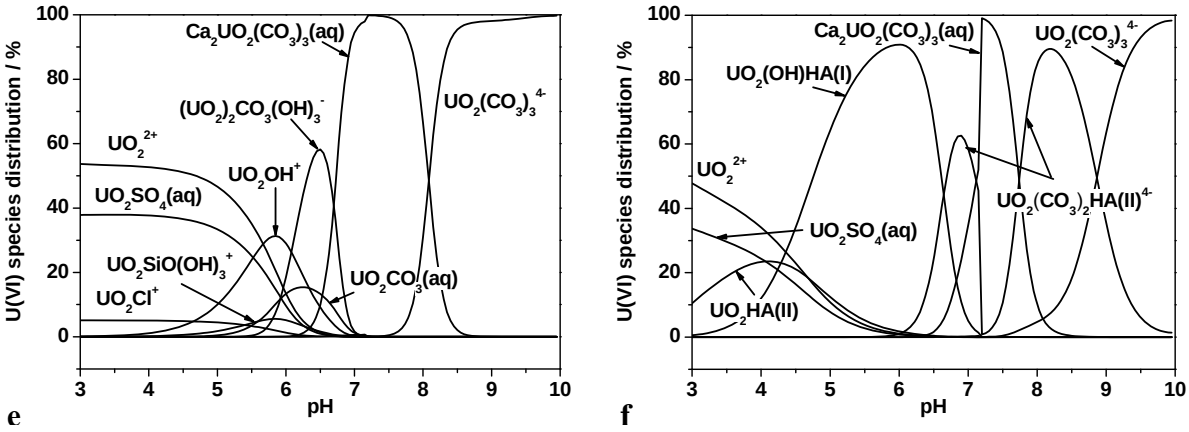

Fig. 4.4. Speciation of U(VI) in 0.1 M $NaClO_4$ (**a, b**), 0.39 M NaCl (**c, d**) and OPA pore water (**e, f**) in the absence (**a, c, e**) and presence (**b, d, f**) of HA ([U(VI)] = 1×10^{-6} M; [HA] = 50 mg/L; $pCO_2 = 10^{-3.5}$ atm). Only species > 5% are shown.

Because of the large effect of calcium on the U(VI) speciation, its influence on the HA speciation was also studied. The results from the speciation modeling show, that at pH 7.6 the

calcium humate complex, CaHA(II), clearly dominates the HA speciation with about 69% (not shown). It can be concluded that HA binding sites are nearly saturated with calcium ions in pore water. Due to the presence of the neutral $Ca_2UO_2(CO_3)_3(aq)$ complex in solution an interaction of U(VI) with HA can be excluded. That means that the HA speciation in OPA pore water is not affected by the presence of U(VI).

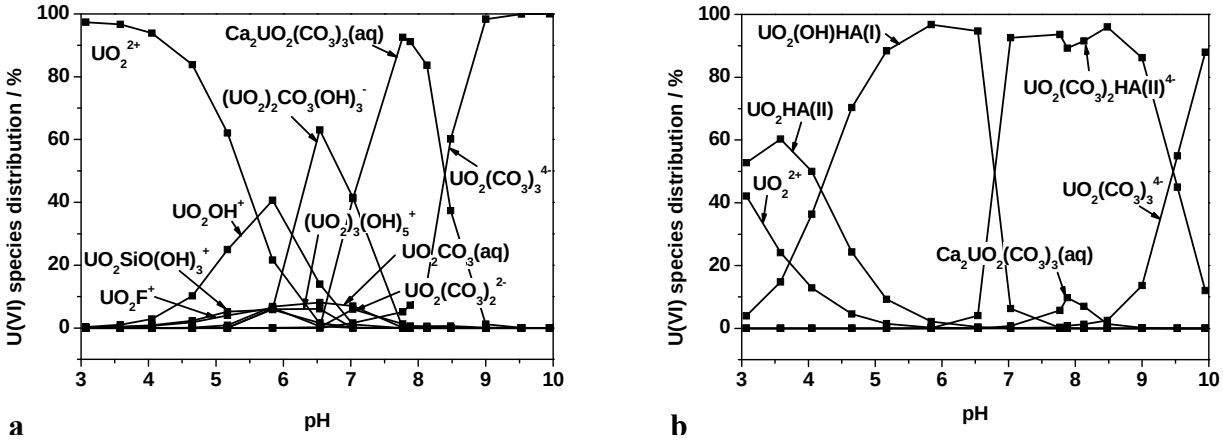

Fig. 4.5. Speciation of U(VI) in 0.1 M $NaClO_4$ in the (**a**) absence and (**b**) presence of 50 mg/L HA under consideration of the ions leached out from OPA ([U(VI)] = 1×10^{-6} M; [HA] = 50 mg/L; $pCO_2 = 10^{-3.5}$ atm). Only species > 5% are shown.

In connection with the OPA leaching experiments in dependence on pH discussed in section 4.1.2, in Fig. 4.5, the U(VI) speciation in the absence and presence of HA is shown as a function of pH. Since the concentration of ions leached out from OPA was determined at specific pH values (cf. section 4.1.2.3), the U(VI) speciation was calculated only for these pH values (shown as points in Fig. 4.5). The lines were drawn for visual reasons. In the absence of HA at pH > 6, the uranyl carbonato species $(UO_2)_2CO_3(OH)_3^-$, $Ca_2UO_2(CO_3)_3(aq)$ and $UO_2(CO_3)_3^{4-}$ are dominant due to the presence of carbonate in solution. The presence of $Ca_2UO_2(CO_3)_3(aq)$ demonstrates the large influence of the competing ion calcium on the U(VI) speciation. Further charged alkaline earth carbonato complexes with U(VI) are reported in the literature, such as $CaUO_2(CO_3)_3^{2-}$, $SrUO_2(CO_3)_3^{2-}$ and $MgUO_2(CO_3)_3^{2-}$ (Dong and Brooks, 2006), that theoretically can be present in the investigated sample solutions. However, they are modeled to be negligible in the investigated pH range and thus, not considered in further discussions.

The presence of HA affects the U(VI) speciation significantly (Fig. 4.5b). At low pH values (~ pH 3), $UO_2HA(II)$ dominates the speciation. Uranyl hydroxo humate, $UO_2(OH)HA(I)$, is the prevailing species in solution in the pH range from pH 4.5 to 7. Due to the presence of carbonate in solution at pH > 6, the uranyl carbonato humate complex $UO_2(CO_3)_2HA(II)^{4-}$ is

formed. $UO_2(CO_3)_2HA(II)^{4-}$ prevents significantly the formation of $Ca_2UO_2(CO_3)_3(aq)$ which is formed only in a very small amount in the pH range from pH 7 to 9.

The HA speciation, depicted in Fig. 4.6, shows that in the whole pH range the U(VI) humate complexes formed play only a subordinate role in comparison to the humate complexes formed with the OPA leached out calcium. CaHA(II) dominates the HA speciation in the pH range from pH 3 to about 8.5.

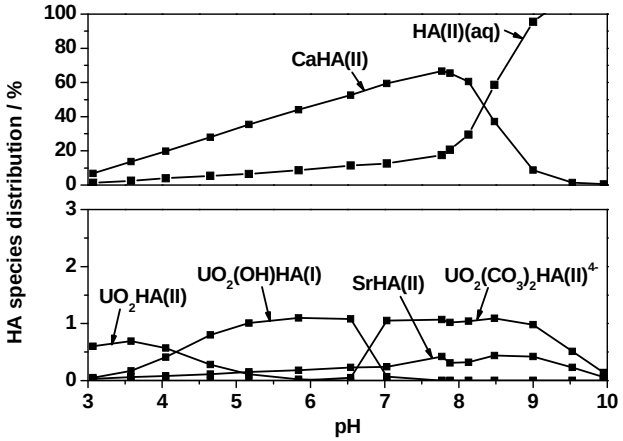

Fig. 4.6. Speciation of HA in 0.1 M $NaClO_4$ in the presence of U(VI) under consideration of the ions leached out from OPA ([U(VI)] = 1×10^{-6} M; [HA] = 50 mg/L; $pCO_2 = 10^{-3.5}$ atm).

Certain amounts of magnesium, aluminum and iron are also contained in solution, however, complexation data for humate complexes with these ions based on CNM are not available in the literature. Few studies determined conditional stability constants for such complexes (Pandey et al., 2000; Tipping et al., 2002; Lippold et al., 2005). However, for speciation calculations, pH- and ionic strength-independent complex formation constants and respective pH-dependent LC values are required. Especially for iron and aluminum different hydrolyzed species can be expected in solution in dependence on pH. Thus, different humate complexes can be expected analog to U(VI). Although there are only few complexation data available, it is known, that the interaction of aluminum with HA is stronger than that of calcium or magnesium (Beck et al., 2004), however, much weaker than that of iron (Lippold et al., 2007). Iron is a strongly competing ion concerning the complexation of HA with UO_2^{2+} (Teterin et al., 2001). Tochiyama et al. (2004) demonstrated that Fe(III) forms stronger complexes with HA than Fe(II). The oxidation state of the dissolved iron in the investigated system is not known. However, several redox processes can take place. On one hand, atmospheric oxygen can oxidize the mineralogically bound Fe(II) in OPA. On the other hand, HA has reducing properties (Reiller, 2005; Schmeide and Bernhard, 2009; Sachs and Bernhard, 2011a) and potentially could reduce Fe(III) present in solution. However, since the experiments were

performed under aerobic conditions, it is assumed, that Fe(III) is the dominating oxidation state in solution.

At low pH values, HA precipitates to a certain extent due to protonation of the HA carboxylic groups. In the presence of metal ions this effect is increased due to additional screening of the HA negative charge by these ions. Thus, one can expect that at pH 3, where increased concentrations of aluminum and iron are present in solution, no aquatic but rather solid complexes of HA with aluminum and iron are formed.

Based on this discussion a sequence of the present competing ions and U(VI) concerning their interaction strength with HA can be assumed as follows: Fe(III) > Al(III) ≥ U(VI) > Sr(II) > Ca(II) > Mg(II). However, since the calcium concentration in solution is about two orders of magnitude higher than the concentrations of the other ions (cf. Fig. 4.3) the HA speciation will still be dominated by CaHA(II) over a wide pH range, also after addition of the missing complexation data of various magnesium, aluminum and iron humate complexes to the EQ3/6 data base. The higher complexation constants of the Fe(III), Al(III), U(VI) and Sr(II) HA complexes can not compensate their low concentrations as shown by SrHA(II) and the various U(VI) humate complexes (cf. Fig. 4.6).

4.3 The system U(VI) / humic acid / kaolinite in dependence on background electrolyte

In order to determine the influence of the applied background electrolyte on the U(VI) and HA sorption onto kaolinite, batch sorption experiments were carried out using 0.1 M $NaClO_4$, 0.39 M NaCl and OPA pore water. The U(VI) sorption was investigated in the absence and presence of HA and the HA sorption was examined in the absence and presence of U(VI). The results were interpreted using the U(VI) speciation calculations shown in section 4.2.

4.3.1 Experimental

A ^{233}U(VI) stock solution was used for all experiments. For that, a solution of $^{233}UO_2(NO_3)_2$ (Eckert & Ziegler, Valencia, CA, USA) was dried up. After adding the threefold molar quantity of 0.01 M $NaHCO_3$ (*p.a.*, Merck, Darmstadt, Germany) to form $^{233}UO_2(CO_3)_3^{4-}$ as precursor, a surplus of 0.1 M HCl (*p.a.*, Merck) was added and $^{233}UO_2Cl_2$ was formed. The specific activity of the ^{233}U(VI) stock solution, determined with liquid scintillation counting (LSC; mod. TriCarb 3100 TR, Perkin Elmer, Freiburg, Germany) using Ultima Gold (Perkin Elmer) as scintillation cocktail, amounts to 11.93 kBq/mL (1.44×10^{-4} M $^{233}UO_2Cl_2$).

For the studies with HA, synthetic HA type M42 was applied both as ^{14}C-labeled synthetic HA (batch M180A, 23.08 MBq/g) and non-labeled HA (batch M145) (Pompe et al., 1998; Sachs et al., 2004). HA type M42 represents a HA like melanoidin from xylose and glutamic acid. It shows an elemental composition and functional group content (proton exchange capacity: (3.34 ± 0.18) meq/g (^{14}C-M42) and (3.51 ± 0.07) meq/g (M42)) comparable to those of most natural HA. Consequently, its sorption and metal ion complexation behavior is also comparable to that of natural HA (e.g. (Pompe et al., 1998; Schmeide et al., 2003, 2006; Křepelová et al., 2006)). A HA stock solution of 5 g/L was prepared by mixing 5 mg of ^{14}C-M42 with 45 mg M42, adding 1880 µL of 0.1 M NaOH and filling up the volume to 10 mL with Milli-Q water (18 MΩ; mod. Milli-RO/Milli-Q-System, Millipore, Schwalbach, Germany).

Solutions of 0.1 M $NaClO_4$ and 0.39 M NaCl were prepared by dissolution of $NaClO_4 \cdot H_2O$ (*p.a.*, Merck) or NaCl (*p.a.*, Merck), respectively, in Milli-Q water. A solution of OPA pore water was prepared as described in section 4.1.

For pH adjustment, diluted $HClO_4$ (*p.a.*, Merck), HCl and NaOH (*p.a.*, Roth, Karlsruhe, Germany) solutions were used. For studies with $NaClO_4$ and NaCl, a calculated amount of 1 M $NaHCO_3$ (*p.a.*, Merck) was added to accelerate equilibration with atmospheric CO_2. The pH values were measured using a laboratory pH meter (mod. inoLab pH 720, WTW, Weilheim, Germany) with SenTix® Mic pH microelectrodes (WTW), calibrated using standard buffers (WTW) at pH 7 and 9.

Batch sorption experiments were performed under ambient atmosphere ($pCO_2 = 10^{-3.5}$ atm) at room temperature. 40 mg kaolinite (KGa-1b, described in (Křepelová et al., 2006; Sachs et al., 2007b)) were weighed into 15 mL polypropylene (PP) centrifuge tubes (mod. Cellstar, Greiner Bio-One GmbH, Frickenhausen, Germany). Subsequently, 10 mL of the background electrolyte (0.1 M $NaClO_4$, 0.39 M NaCl, OPA pore water) were added and the pH value was adjusted to pH 7.6. Thus, an S/L ratio of 4 g/L was used. All sorption samples were prepared in triplicate. For pre-equilibration, the samples were continuously shaken on a horizontal shaker (mod. Promax 2020, Heidolph Instruments, Schwabach, Germany) and the pH values were periodically checked and readjusted for 13 d.

After pre-equilibration, 70 µL of a ^{233}U(VI) stock solution were added to the kaolinite suspensions to obtain a final ^{233}U(VI) concentration of 1×10^{-6} M. For the investigation of the U(VI) sorption onto kaolinite in the presence of HA, additionally 20 or 100 µL HA stock solution were added subsequently. The final concentration of HA in solution amounted to 10 or 50 mg/L. After U(VI) and HA addition, the pH values were readjusted immediately. For

equilibration, the samples were shaken on a horizontal shaker for 3 d, whereby the pH was readjusted each day. After 3 d, the final pH values of the samples were determined and the samples were centrifuged and the supernatants were filtered as described in section 4.1.1.1. For comparison, additional kaolinite samples with HA in the absence of $^{233}U(VI)$ were prepared. The filtrates were analyzed simultaneously for the final U(VI) and HA concentration by LSC. For LSC, 1 mL of the filtrate was mixed with 15 mL Ultima Gold (Perkin Elmer) as scintillation cocktail.

In addition, blank suspensions of kaolinite in the three different background electrolytes were prepared and processed under the same conditions to determine the amount of U(VI) leached out of kaolinite.

Finally, the U(VI) or HA sorption onto vial walls was determined. For this, 7 mL 1 M HNO_3 (U(VI) sorption) or 1 M NaOH (HA sorption) were added to the emptied vials and the vials were shaken for 3 d. The solutions were analyzed by LSC for U(VI) and HA, respectively.

The amount of U/HA adsorbed on the mineral surface was calculated as the difference between the initial U(VI)/HA concentration and U(VI)/HA remaining in solution after the sorption experiment. The values were corrected by the wall sorption and the U(VI) concentration in the blank samples.

4.3.2 Results and discussion

In Table 4.5, the results of the U(VI) sorption experiments with kaolinite are shown.

Table 4.5. U(VI) sorbed onto kaolinite in dependence on background electrolyte (S/L = 4 g/L, pH 7.6).

Background electrolyte	**0.01 M $NaClO_4$** [a]	**0.1 M $NaClO_4$**	**0.39 M NaCl**	**0.36 M OPA pore water**
[U(VI)] = 1×10^{-6} M	~ 98%	(88.4 ± 1.1)%	(85.1 ± 1.5)%	(42.4 ± 4.2)%
[U(VI)] = 1×10^{-6} M + *[HA] = 10 mg/L*	~ 90%	(87.2 ± 1.7)%	(85.4 ± 2.2)%	(36.0 ± 1.9)%
[U(VI)] = 1×10^{-6} M + *[HA] = 50 mg/L*	~ 65%	(38.8 ± 4.6)%	(53.1 ± 1.4)%	(30.7 ± 2.8)%

[a] At pH 7.5 (Křepelová et al., 2006).

With increasing ionic strength of the inert background electrolyte the U(VI) sorption onto kaolinite decreases only slightly. This effect was diminished (10 mg HA/L) and even inverted (50 mg HA/L) in the presence of HA. This decrease of U(VI) sorption in the absence of HA is

due to the rising presence of $UO_2(CO_3)_3^{4-}$ in U(VI) speciation at an ionic strength of 0.39 M at pH 7.6. This U(VI) species sorbs only weakly onto kaolinite compared to $(UO_2)_2CO_3(OH)_3^-$ dominating the U(VI) speciation at ionic strength of 0.1 M. In addition, the samples of the 0.39 M experiments showed an end pH of 7.5, where the U(VI) speciation is composed of $UO_2(CO_3)_3^{4-}$ (36%), $(UO_2)_2CO_3(OH)_3^-$ (48%) and $UO_2(CO_3)_2^{2-}$ (12%). Thus, the U(VI) sorption decreases only slightly. The U(VI) speciation in the presence of 50 mg HA/L does not give an explanation for the increase of U(VI) sorption with increasing ionic strength. In both systems $UO_2(CO_3)_2HA(II)^{4-}$ is the dominating species at pH 7.6. This U(VI) species sorbs to some extent onto kaolinite. With increasing ionic strength changes in the macromolecular configuration of HA occur. More and more negative charges of the HA molecules are screened by the ions in solution. Thus, HA folds itself to a coil. In this configuration more HA can sorb onto the clay surface compared to the more open HA form at low ionic strength.

If the complex background electrolyte OPA pore water is used in the sorption experiments, the amount of sorbed U(VI) decreases further. This is due to the formation of the neutral aquatic $Ca_2UO_2(CO_3)_3$ complex, which seems to sorb only weakly onto the clay possibly due to its neutral character.

The presence of 10 mg HA/L has in all investigated systems no significant effect on U(VI) sorption. However, at higher HA concentrations of 50 mg HA/L the U(VI) sorption decreases significantly in all investigated systems. This is due to the formation of the U(VI) humate complex, $UO_2(CO_3)_2HA(II)^{4-}$, which leads to the mobilization of U(VI).

Table 4.6. HA sorbed onto kaolinite in dependence on background electrolyte (S/L = 4 g/L, pH 7.6).

Background electrolyte	**0.01 M $NaClO_4$** [a]	**0.1 M $NaClO_4$**	**0.39 M NaCl**	**0.36 M OPA pore water**
[HA] = 10 mg/L	~ 23%	(72.1 ± 4.2)%	(74.0 ± 5.7)%	(68.9 ± 5.4)%
[HA] = 50 mg/L	~ 10%	(17.2 ± 1.6)%	(28.3 ± 1.5)%	(33.8 ± 1.5)%
[HA] = 10 mg/L + *[U(VI)] = 1×10^{-6} M*	~ 50%	(72.4 ± 3.5)%	(74.3 ± 6.0)%	(74.5 ± 4.8)%
[HA] = 50 mg/L + *[U(VI)] = 1×10^{-6} M*	-	(19.7 ± 1.2)%	(30.6 ± 1.5)%	(37.6 ± 1.4)%

[a] At pH 7.5 (Křepelová et al., 2006).

The HA sorption onto kaolinite in the absence and presence of U(VI) is given in Table 4.6. The increase of the ionic strength from 0.01 M to 0.1 M leads to an increase in HA sorption. As discussed, with increasing ionic strength more ions are present in solution which screen

the negatively charged functional groups of the HA molecules. Thus, less repulsing effects from negatively charged clay surface appear and HA sorption onto the clay mineral increases. However, an additional increase of the ionic strength to 0.39 M has no significant effect on HA sorption. Also the change to the complex background electrolyte, OPA pore water, has a negligible effect on HA sorption.
In all investigated systems the percentage of HA sorption decreases with increasing HA concentration. However, this effect is reduced with increasing ionic strength.
Unless for 0.01 M $NaClO_4$, in all other investigated systems U(VI) does not have an influence on HA sorption at both investigated HA concentrations.

4.4 The system U(VI) / humic acid / Opalinus Clay / Opalinus Clay pore water

In the present study, the U(VI) sorption onto OPA in the absence and presence of HA was investigated by means of batch sorption experiments. The ternary system U(VI) / HA / OPA is investigated using synthetic OPA pore water (Pearson, 1998) as background electrolyte. Due to the fact that the influence of competing ions, originating from the pore water, on this system is studied, it should be rather described as a quaternary system. The pore water consists of ions originating from mineral leaching processes such as calcium, strontium, sulfate and carbonate. These ions can control the speciation of U(VI) and HA by forming soluble or insoluble species or occupying important binding sites. In this study the discussion of the pore water effects on the speciation (cf. section 4.2) is coupled with sorption and spectroscopic experiments to verify the speciation results. The outcome of this study is published in (Joseph et al., 2011).

4.4.1 Experimental

In this study, OPA (batch BHE-24/1) and HA (M42, batch M180A) were used for the experiments as described in the sections 4.1 and 4.3.1, respectively, with the exception that HA was solved in OPA pore water. OPA pore water was applied as background electrolyte in all experiments (cf. section 4.1). In all experiments the pH was controlled and, if necessary, adjusted to pH 7.6 ± 0.05 using diluted HCl and NaOH. Due to the small amounts of added HCl and NaOH an effect on the S/L ratio was negligible. The pH value was measured using a laboratory pH meter (mod. inoLab pH 720, WTW, Weilheim, Germany) with SenTix® Mic pH microelectrodes (WTW), calibrated using standard buffers (WTW) at pH 7 and 9.

A U(VI) stock solution (5×10^{-4} M $^{238}UO_2(ClO_4)_2$ in 0.005 M $HClO_4$) was used for all experiments. In addition, ^{233}U was used as tracer. For that, a solution of $^{233}UO_2(NO_3)_2$ was applied, which was transformed into a $^{233}UO_2(ClO_4)_2$ solution by drying up and adding the threefold molar quantity of 0.01 M $NaHCO_3$ to form $^{233}UO_2(CO_3)_3^{4-}$ as precursor. After that, a surplus of 0.1 M $HClO_4$ was added and $^{233}UO_2(ClO_4)_2$ was formed. The specific activity of the ^{233}U stock solution was determined with LSC using Ultima Gold (Perkin Elmer) as scintillation cocktail. It amounts to 8.4 kBq/mL ([^{233}U] = 1.02×10^{-4} M).

At first, sorption experiments with the binary systems U(VI) / OPA and HA / OPA were performed. U(VI) sorption studies onto OPA were carried out to find the optimal solid-to-liquid ratio (S/L ratio) for the experiments, to avoid experimental conditions, where the U(VI) sorption is extremely high or low. After that, kinetic sorption studies with U(VI) or HA and OPA were performed to evaluate the time required to obtain sorption equilibrium. Distribution coefficients, K_d, for the sorption of U(VI) and HA onto OPA in pore water were determined by investigating the sorption isotherms for U(VI) and HA. Finally, the system U(VI) / HA / OPA was investigated. The experiments are discussed with increasing complexity in the order U(VI) or HA / OPA / pore water and U(VI) / HA / OPA / pore water. The experimental conditions of all experiments carried out are compiled in Table 4.7. The studies were performed under ambient atmosphere ($pCO_2 = 10^{-3.5}$ atm) at room temperature. With the exception of the system U(VI) / HA / OPA, which was investigated both under aerobic and anaerobic conditions.

Table 4.7. Experimental conditions of experiments.

Experiment	Solute	[U(VI)] / mol/L	[HA] / mg/L	S/L / g/L
S/L ratio dependence	U(VI)	1×10^{-6}	-	0.5 - 300
Kinetic sorption studies	U(VI) or HA	1×10^{-6}	10	60
U(VI) sorption isotherm	U(VI)	1×10^{-8} – 1×10^{-4}	-	60
		1×10^{-8} – 5×10^{-7}	-	4
HA sorption isotherm	HA	-	10 - 320	60
U(VI) and HA sorption	U(VI) and HA	1×10^{-6}	10, 50	60

4.4.1.1 Sorption experiments

According to the S/L ratio (cf. Table 4.7), a respective amount of clay was weighed into 15 mL PP centrifuge tubes (mod. Cellstar, Greiner Bio-One GmbH, Frickenhausen, Germany). Subsequently, 10 mL pore water were added and the pH value was adjusted. For pre-equilibration, the samples were continuously shaken on a horizontal shaker (mod. Promax 2020, Heidolph Instruments) for 7 d and the pH values were periodically readjusted.

After pre-equilibration, aliquots of a U(VI) or HA stock solution were added to the suspensions to obtain the U(VI) and HA concentrations compiled in Table 4.7. The pH values were readjusted immediately. The samples were shaken on the horizontal shaker to equilibrate for 3 d (U(VI) sorption) or 1 d (HA sorption). After that, the final pH values of the samples were determined. The samples were centrifuged and the supernatants were filtered as described in section 4.1.1.1. The filtrates were analyzed for the final U(VI) and HA concentration by ICP-MS and LSC, respectively. For LSC, 1 mL of the filtrate was mixed with 15 mL Ultima Gold. In addition, blank suspensions of OPA in pore water were prepared and processed under the same conditions to determine the amount of U(VI) leached out of OPA.

Finally, the U(VI) or HA sorption onto vial walls was investigated. 7 mL 1 M HNO_3 (U(VI) sorption) or 1 M NaOH (HA sorption) were added and the vials were shaken for 3 d. The solutions were analyzed by ICP-MS or LSC for U(VI) and HA, respectively.

The amount of U/HA adsorbed on the mineral surface was calculated as the difference between the initial U(VI)/HA concentration and U(VI)/HA remaining in solution after the sorption experiment. The values were corrected by the wall sorption and the U(VI) concentration in blanks.

Every sorption experiment was carried out as described in this section. Any deviations from this procedure are explained in the respective sections.

S/L ratio dependence

Due to the fact that these experiments were carried out before the leaching experiment (cf. section 4.1.1), a pre-equilibration and contact time of 3 d each was used according to previous U(VI) sorption studies performed with kaolinite in $NaClO_4$ (Křepelová et al., 2006). These experiments were performed in duplicate.

Kinetic sorption experiments

For this, 12 g OPA were weighed into 250 mL bottles and 200 mL pore water were added. Aliquots of a U(VI) or HA stock solution were added and the suspensions were stirred with a magnetic stirrer. After different contact times aliquots of the suspensions were taken.

U(VI) and HA sorption isotherms

For the U(VI) sorption isotherm ^{233}U was used. The U(VI) sorption isotherm was measured as a function of the U(VI) concentration and of the S/L ratio whereas the HA sorption isotherm

was only measured as a function of HA concentration. The ^{233}U(VI) and HA concentration in the filtrates was determined by LSC. All experiments were performed in duplicate.

Influence of HA on the U(VI) sorption

After pre-equilibration, HA was added instantly after addition of ^{233}U(VI). For comparison, additional OPA samples with ^{233}U(VI) in the absence of HA and with HA in the absence of ^{233}U(VI) were prepared. The further handling of the samples was analog to section 4.4.1.1 except that the filtrates were analyzed simultaneously for the final U(VI) and HA concentration by LSC. All sorption experiments were performed in triplicate.

Because of the presence of Fe(II) minerals in OPA, the filtrates were analyzed with respect to a possible reduction of U(VI) to U(IV). The redox speciation of U after the sorption experiments was determined by solvent extraction using thenoyltrifluoroacetone (TTA; p.a., Fluka/Sigma-Aldrich, Steinheim, Germany) according to Bertrand and Choppin (1982). For TTA extractions, 2 mL of the filtrates were acidified to pH 0.5 using degassed HCl (37%). After that, 2 mL of freshly prepared 0.5 M TTA solution in degassed xylene (p.a., Fluka) were added and the samples were shaken vigorously for 10 min. The samples were then centrifuged for phase separation (10 min, 4000 rpm). Under these conditions, U(IV) species are extracted by TTA into the organic phase whereas U(VI) remains in the aqueous phase. The resulting U(VI) concentrations in the aqueous phases were analyzed by LSC.

4.4.1.2 TRLFS measurements

To identify the U(VI) species in the pore water in the absence and presence of HA, TRLFS measurements were performed under cryogenic conditions at 153 K. TRLFS measurements at room temperature are not suitable, since the U(VI) concentration is too low. In addition, as reported by Bernhard et al. (2001) and Wang et al. (2004) the uranyl carbonato species ($(UO_2)_2(OH)_3CO_3^-$, $UO_2CO_3(aq)$, $UO_2(CO_3)_2^{2-}$, $UO_2(CO_3)_3^{4-}$), possibly present in solution, show no luminescence properties at room temperature.

Since pore water contains a large amount of chloride, which acts as strong luminescence quencher, special pore water was prepared for this experiment substituting all chloride by perchlorate. Speciation calculations confirmed that these small changes of the background electrolyte do not affect the speciation of U(VI) in solution at pH 7.6. Applying this, sorption experiments were performed analog to those described in 4.4.1.1 in the section *Influence of HA on the U(VI) sorption*. The filtrates after sorption experiments were studied in comparison to U(VI) added pore water samples by means of TRLFS.

For the measurements, aliquots of pore water and filtrates were filled into plastic cuvettes (mod. BI-SCP, Brookhaven Instruments, Holtsville, NY, USA), placed immediately in a freezer at 255 K and stored for 1 d. For TRLFS measurements, the frozen samples were transferred as ice cubes from the plastic cuvettes into a specifically designed sample holder. The sample holder has one hole to insert the ice cube and windows for laser irradiation. After transfer, the samples were cooled to 153 K via a cryogenic cooling system (mod. TG-KKK, KGW-Isotherm, Karlsruhe, Germany).

TRLFS laser pulses at 410 nm with an average pulse energy of 4 mJ (Nd:YAG-MOPO laser system, mod. GCR 230 (20 Hz), Spectra Physics, Mountain View, USA) were used for excitation of the U(VI) luminescence. The emitted luminescence light was detected in a right angle setup by a Jobin Yvon 270M spectrograph (Jobin Yvon GmbH, Munich, Germany). The resulting spectra were measured in time-resolved mode using an ICCD camera (512 pixel; mod. Spectrum One, Horiba-Jobin Yvon). The time difference between the trigger of the laser system and the start of the camera was adjusted by a delay generator DG 540 (Stanford Research Instruments, Sunnyvale, USA). The spectra were recorded in the wavelength range from 454 to 604 nm by accumulating 20 to 100 laser pulses using a gate time of the camera of 500 µs. Delay times varied from 50 ns to 4 ms after application of the laser pulse in 10 µs increments.

4.4.2 Results and discussion

4.4.2.1 Influence of S/L ratio on the U(VI) sorption

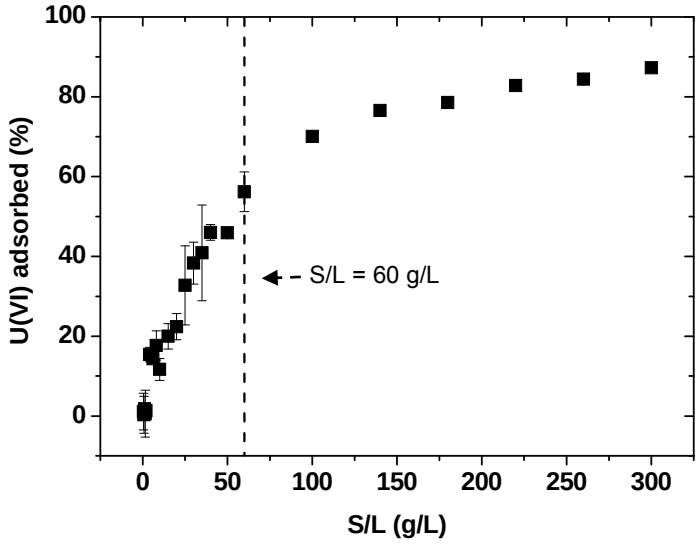

Fig. 4.7. U(VI) adsorbed onto OPA as a function of S/L ratio ([U(VI)] = 1×10^{-6} M; OPA pore water).

The U(VI) sorption onto OPA as a function of the S/L ratio is shown in Fig. 4.7. An S/L ratio of 60 g/L was chosen for the following sorption studies. Under these conditions, about 50% U(VI) is adsorbed onto OPA, an adequate amount for interpretation of the sorption results.

4.4.2.2 Kinetic of the U(VI) and humic acid sorption onto Opalinus Clay

The U(VI) and HA sorption onto OPA as a function of time is shown in Fig. 4.8. It becomes evident that HA reaches sorption equilibrium very fast (within 1 h) with an average amount of adsorbed HA of (91.2 ± 0.1)%. Thus, 1 d was considered to be sufficient to achieve the sorption equilibrium between HA and OPA during the sorption experiments. For U(VI) a much slower sorption kinetic was observed. The U(VI) sorption equilibrium is reached within 24 h with an average sorption of (55.0 ± 0.2)%. After that, the amount of sorbed U(VI) remains roughly stable for the investigated time of 247 h. Based on these results, an equilibration time of 3 d was chosen for the sorption experiments with U(VI).

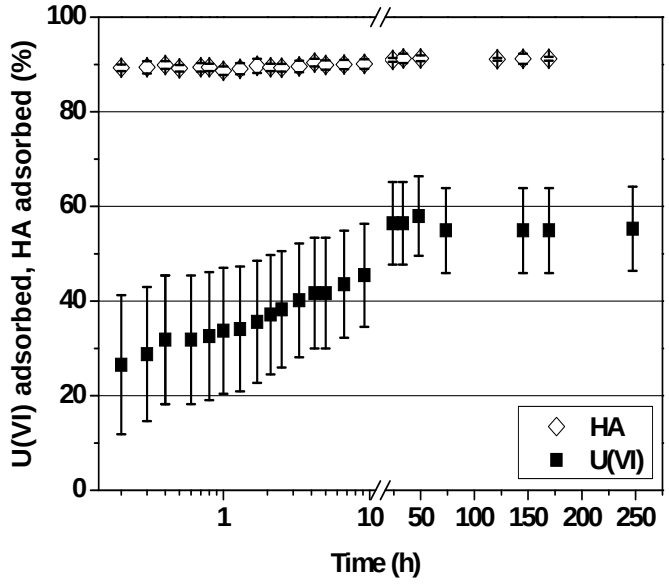

Fig. 4.8. U(VI) and HA sorbed onto OPA as a function of time ([U(VI)] = 1×10^{-6} M; [HA] = 10 mg/L; S/L = 60 g/L; OPA pore water).

4.4.2.3 Determination of K_d values for U(VI) and humic acid

The U(VI) and HA sorption results obtained by varying the U(VI) or HA concentration at constant S/L ratio are depicted in Fig. 4.9 and 4.10. The data were fitted using the Freundlich isotherm (Freundlich, 1906). The Freundlich isotherm is described by Eq. (4.2):

$$a_{eq} = c_{eq}^{n_F} \cdot k_F \qquad (4.2)$$

where a_{eq} (mg/g or Bq/g) is the amount of U(VI) or HA adsorbed on the solid phase, c_{eq} (mg/L or Bq/L) is the equilibrium concentration of U(VI) or HA in solution, k_F (m^3/kg) and n_F are the Freundlich coefficients.

The distribution coefficient K_d (m^3/kg) is defined as follows:

$$K_d = \frac{a_{eq}}{c_{eq}} \tag{4.3}$$

The K_d values for the U(VI) and HA sorption onto OPA were calculated using the logarithmic form of Eq. (4.2). Setting $n_F = 1$, k_F is equal to K_d.

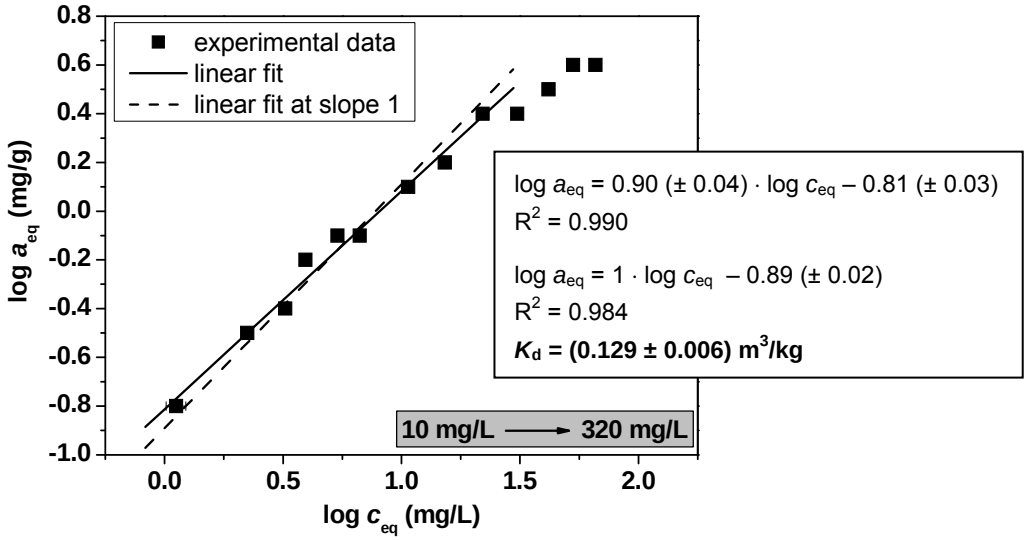

Fig. 4.9. Freundlich isotherm of the HA sorption onto OPA with varying HA concentration ([HA] = 10 – 320 mg/L; S/L = 60 g/L; OPA pore water); a_{eq}: amount of HA sorbed onto OPA, c_{eq}: equilibrium concentration of HA in solution, K_d: distribution coefficient.

The Freundlich sorption isotherm for the HA sorption onto OPA in pore water is shown in Fig. 4.9. With initial HA concentrations between 10 and 160 mg/L the amount of adsorbed HA increases linearly. At higher initial HA concentrations (> 160 mg/L) the slope of the adsorbed amount of HA slightly decreases indicating the achievement of a saturation of binding sites for HA sorption. Since the Freundlich isotherm definition excludes the saturation range, the K_d value of adsorbed HA onto OPA was determined for the range 10 - 160 mg HA/L. The K_d value amounts to (0.129 ± 0.006) m^3/kg.

In pore water, calcium humate is the dominant HA species in solution (cf. section 4.2). Previously, the influence of calcium ions on the HA sorption onto various clay minerals, such as kaolinite (Saada et al., 2003) and montmorillonite (Sutton and Sposito, 2006; Majzik and Tombacz, 2007), was investigated. An increased HA sorption was observed, when calcium

ions were present in solution (Saada et al., 2003). Sutton and Sposito (2006) simulated the HA sorption onto Ca-montmorillonite. They observed differences in the sorption behavior when Ca-saturated HA was used instead of pure HA. The protonated HA existing under acidic conditions interacted mainly with the clay mineral by hydrogen bonds. The Ca-saturated HA preferred to adsorb via cation bridges. But also a few water bridges and indirect hydrogen bonds mediated by water molecules were formed. For the present study, because of the heterogeneity of OPA, it can not be estimated which mineral phase of OPA acts as the main adsorbent for CaHA(II). However, it can be assumed, that also cation bridges originating mainly from calcium may play an important role in the sorption process.

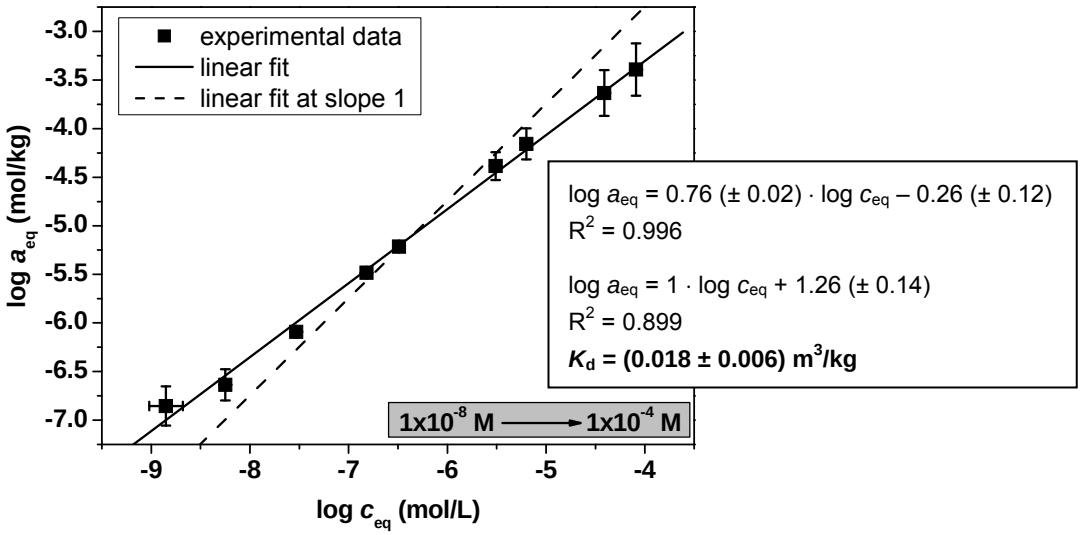

Fig. 4.10. Freundlich isotherm of the U(VI) sorption onto OPA with varying U(VI) concentration ([U(VI)] = 1×10^{-8} – 1×10^{-4} M; S/L = 60 g/L; OPA pore water); a_{eq}: amount of U(VI) sorbed onto OPA, c_{eq}: equilibrium concentration of U(VI) in solution, K_d: distribution coefficient.

In Fig. 4.10 the sorption isotherm for the U(VI) sorption onto OPA is presented. Using the Freundlich equation and a fixed slope of 1, a K_d value of (0.018 ± 0.006) m^3/kg was determined. Experiments with an S/L ratio of 4 g/L were also performed (not shown). There, a K_d value of (0.065 ± 0.025) m^3/kg was determined using U(VI) concentrations of 1×10^{-8} - 5×10^{-7} M. Amayri et al. (2008) determined for the U(VI) sorption onto OPA a K_d value of (0.03 ± 0.01) m^3/kg using an S/L ratio of 15 g/L and U(VI) concentrations of 1×10^{-8} - 1×10^{-4} M. They determined a Freundlich coefficient of $n_F = 1.21$, pointing to a non-linear sorption. For the U(VI) sorption onto OPA presented in this study, also a non-linear sorption behavior was observed, but in contrast to Amayri et al. (2008), n_F values of 0.76 (S/L = 60 g/L) and 0.64 (S/L = 4 g/L) were determined. Thus, two different interaction behaviors for the U(VI) sorption onto OPA were observed, which can be attributed to the

chosen U(VI) concentrations and S/L ratios during the experiments, which is discussed in detail next.

To extrapolate from laboratory experiments to real field conditions, it is necessary to assume that the K_d values are independent of S/L ratios. Comparing the results presented here and in the study of Amayri et al. (2008), it is obvious, that the determined K_d values depend on the S/L ratio used in the experiments. Phillippi et al. (2007) investigated the phenomenon of K_d-S/L ratio dependence in detail by modeling the sorption in the system U(VI) / carbonate / Fe(III)-coated sand. They observed that the U(VI) sorption in the absence of carbonate and also the carbonate sorption in the absence of U(VI) were independent of the S/L ratio. In the ternary system, however, a dependence on the S/L ratio was observed. The described effect was also observed by Zheng et al. (2003), who investigated the U(VI) sorption onto two soils containing different amounts of calcium carbonate. With increasing U(VI) concentration the U(VI) sorption decreased. They concluded, that this behavior was an artifact due to calcite dissolution. They proposed that high S/L ratios should be used for determining K_d values in calcareous soils. Then, the complete calcite dissolution can be avoided and the calcite saturation of the solution is maintained. To verify this assumption for our results, an additional Freundlich sorption isotherm was calculated using the data of the U(VI) sorption onto OPA as a function of S/L ratio (cf. Fig. 4.7). The results are depicted as K_d vs. S/L ratio in Fig. 4.11.

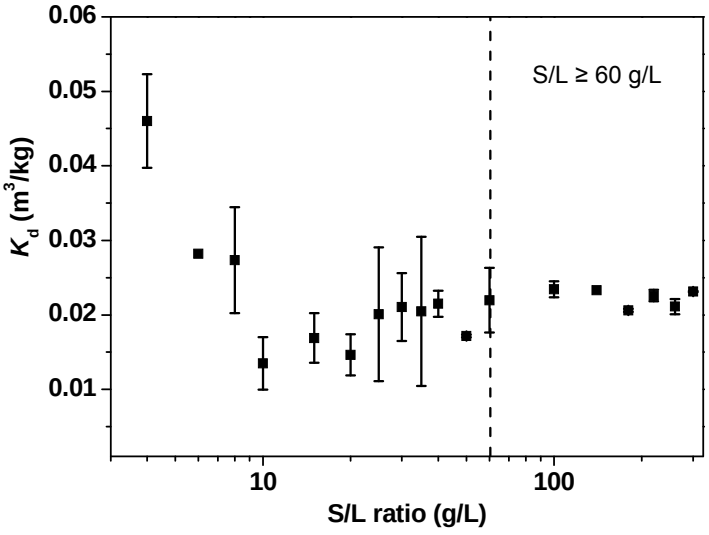

Fig. 4.11. Distribution coefficient (K_d) of the U(VI) sorption onto OPA as a function of S/L ratio ([U(VI)] = 1×10^{-6} M; S/L = 4 – 300 g/L; OPA pore water).

From the results given in Fig. 4.11 it can be concluded that for an initial U(VI) concentration of 1×10^{-6} M, an S/L ratio-independent K_d can only be obtained for S/L ratios ≥ 60 g/L. For

these S/L ratios the respective Freundlich isotherm shows the highest linearity of all discussed isotherms in this study (n_F = 0.997; not shown). The resulting K_d value amounts to (0.0222 ± 0.0004) m^3/kg. Thus, this K_d value is representative for the investigated system U(VI) / OPA / pore water. Since this K_d value is independent of S/L for S/L ≥ 60 g/L, it can be used to predict the sorption behavior of U(VI) onto OPA, which has relevance for performance assessment of OPA as a host rock for a nuclear waste repository.

The obtained K_d value of (0.0222 ± 0.0004) m^3/kg indicates a weak sorption affinity of U(VI) toward OPA, obviously due to the predominant formation of the $Ca_2UO_2(CO_3)_3$(aq) complex in solution.

Wu et al. (2009) determined a K_d value of (0.025 ± 0.005) m^3/kg for Np(V) sorption onto OPA by batch sorption experiments. This is very close to the respective U(VI) value determined in the present work, implying similar sorption affinities for U(VI) and Np(V) toward OPA. This is in contrast to results obtained for U(VI) and Np(V) sorption onto pure clay minerals, e.g. kaolinite (Křepelová et al., 2006; Schmeide and Bernhard, 2010), where at pH 7.5 98% of U(VI), but only 24.5% of Np(V) are sorbed. This difference can be attributed to the absence of $Ca_2UO_2(CO_3)_3$(aq) in those systems. Only little is known about the interaction of this complex with other minerals. Fox et al. (2006) investigated the U(VI) sorption onto ferrihydrite and quartz in the presence of different calcium concentrations in solution. Under conditions where the $Ca_2UO_2(CO_3)_3$(aq) species predominates the U(VI) speciation, a decreasing U(VI) sorption onto both minerals was observed with increasing calcium concentration. Meleshyn et al. (2009) studied the influence of this complex on the U(VI) sorption onto Ca- and Na-bentonites using $NaNO_3$ or $Ca(NO_3)_2$ as background electrolytes. Under near-neutral pH conditions, $Ca_2UO_2(CO_3)_3$(aq) dominates the U(VI) speciation in $Ca(NO_3)_2$, whereas $(UO_2)_2CO_3(OH)_3^-$ is the predominant species in $NaNO_3$. In $Ca(NO_3)_2$ a lower U(VI) sorption was observed than in $NaNO_3$. Using $NaNO_3$ as background electrolyte, the U(VI) sorption onto Ca-bentonite was lower compared to the U(VI) sorption onto Na-bentonite. This was also attributed to the formation of $Ca_2UO_2(CO_3)_3$(aq) due to leaching of calcium ions.

The low U(VI) sorption affinity toward OPA can not exclusively be attributed to the formed $Ca_2UO_2(CO_3)_3$(aq) complex. Bradbury and Baeyens (Personal communication, 2010) investigated U(VI) sorption onto Na-illite as principal sorbing mineral phase in OPA rock ((23 ± 2) wt.%). The experimental data were described by a two site protolysis non-electrostatic surface complexation and cation exchange sorption model. The modeling results were used to predict sorption isotherms measured onto OPA, whereby Bradbury and Baeyens

(Personal communication, 2010) observed an overestimation of the U(VI) sorption isotherm. After addition of the complexation constant of the so-called "non-sorbing U(VI) species" $Ca_2UO_2(CO_3)_3(aq)$ to the model, the resulting model underestimated the experimental data. It was concluded that illite is not a suitable model to predict the sorption behavior of U(VI) onto OPA. Other U(VI) species-sorbing mineral phases have to be present in OPA. Hartmann et al. (2008) studied the U(VI) sorption onto OPA from Benken, Switzerland, in 0.1 M $NaClO_4$ by batch and spectroscopic experiments as a function of pH. A significant decrease of the U(VI) sorption at pH 6.5-9.0 was observed. To reproduce the experimental data, model calculations were performed. They demonstrated that calculated and experimental data show a divergence, which was reduced when $Ca_2UO_2(CO_3)_3(aq)$ was included as non-sorbing species in calculations. They concluded that this complex prevents U(VI) sorption onto OPA significantly. But finally, they ascertained still a difference between calculations and experiments and assumed that $Ca_2UO_2(CO_3)_3(aq)$ adsorbs to some extent to the minerals surface. This assumption is confirmed in the present study. The U(VI) sorption onto the clay mineral kaolinite in pore water (S/L = 4 g/L) was studied under identical experimental conditions such as described in this section (cf. section 4.3 and (Joseph et al., 2009)). The results showed that the specifically sorbed amount of U(VI) toward kaolinite is higher ((2.2 ± 0.2) $\mu g/m^2$) than onto OPA ((0.045 ± 0.003) $\mu g/m^2$). Based on these results, it can be concluded, that also kaolinite as a main fraction in OPA ((15-33) wt.%) is not a sufficient model for description of the available binding sites. Zheng et al. (2003) investigated the U(VI) sorption in natural geologic settings, in detail onto two soils (pH 5 and pH 8) containing different concentrations of calcium carbonate. They showed that at high calcium carbonate concentrations (pH 8) the U(VI) sorption onto the soil was lower, which was attributed to the increased formation of $Ca_2UO_2(CO_3)_3(aq)$. They modeled their results using two different surface complexation models, a ferrihydrite model and a ferrihydrite and clay model. With the first model the sorption data at pH 8 were fitted very well, supporting ferrihydrite as main adsorbent fraction in the soil. With the second model nearly identical results were obtained. Zheng et al. (2003) concluded that under these conditions U(VI) sorption onto clay minerals is relatively weak compared to U(VI) sorption onto ferrihydrite. OPA contains about 2-6 wt.% iron containing mineral phases, namely pyrite and siderite. Whether these phases are the main adsorbent phases for $Ca_2UO_2(CO_3)_3(aq)$ in OPA is unknown up to now.

4.4.2.4 Influence of humic acid on the U(VI) sorption onto Opalinus Clay

OPA contains about 1 wt.% organic carbon (cf. Table 4.1). It is known that only a small portion of the TOC (about 0.15 wt.%) consists of humic material (Pearson et al., 2003), that means a fraction of 1.5×10^{-3} wt.% of OPA. In the present experiments, a HA concentration of 50 mg HA/L in maximum is used. Under consideration that HA type M42 contains (56.1 ± 0.3)% carbon (Sachs et al., 2004), at an S/L ratio of 60 g clay/L a TOC of 0.05 wt.% results. That means the experiments are performed in 30-fold excess. The results of the U(VI) sorption onto OPA in the absence and presence of HA are summarized in Table 4.8.

Table 4.8. U(VI) and HA sorption onto OPA under ambient atmosphere ($pCO_2 = 10^{-3.5}$ atm) or inert gas conditions (N_2-box) (S/L = 60 g/L; OPA pore water).

	U(VI) adsorbed / µg/m²		**HA adsorbed / µg/m²**	
	$pCO_2 = 10^{-3.5}$ atm	**N_2-box**	**$pCO_2 = 10^{-3.5}$ atm**	**N_2-box**
[U(VI)] = 1×10^{-6} M	0.045 ± 0.003	0.046 ± 0.002	-	-
[U(VI)] = 1×10^{-6} M + [HA] = 10 mg/L	0.044 ± 0.003	0.047 ± 0.001	3.5 ± 0.2	3.9 ± 0.1
[U(VI)] = 1×10^{-6} M + [HA] = 50 mg/L	0.045 ± 0.002	0.049 ± 0.002	17.6 ± 0.6	19.5 ± 0.4
[HA] = 10 mg/L	-	-	3.5 ± 0.3	3.9 ± 0.1
[HA] = 50 mg/L	-	-	17.6 ± 0.5	19.3 ± 0.4

Table 4.8 shows, that under ambient conditions the U(VI) sorption is not influenced by HA. These results are in agreement with the U(VI) speciation results, where the presence of HA has no effect on the U(VI) speciation at pH 7.6 (cf. Fig. 4.4). In contrast to this, Křepelová et al. (2006) showed that the presence of HA decreased the U(VI) sorption onto kaolinite at pH 7.5 in 0.1 M $NaClO_4$. This effect was increased with increasing HA concentration and was attributed to the formation of dissolved U(VI) humate complexes. However, in the presence of calcium ions the formation of U(VI) humate complexes is inhibited, as verified by the present data.

Table 4.8 presents the HA sorption onto OPA. With increasing HA concentration the adsorbed amount of HA onto OPA increases. At both HA concentrations used, no influence of U(VI) on the HA sorption can be observed. This corresponds to the HA speciation results and can be attributed to to the neutral character of the $Ca_2UO_2(CO_3)_3(aq)$ complex. Kornilovich et al. (2000) and Křepelová et al. (2008) proposed for the sorption of metal ions onto clay

minerals in the presence of humic acid, that the metal ion can be located between the solid phase and the humic acid. In the quaternary system U(VI) / HA / OPA / pore water studied here it is assumed that the place of the metal ion is occupied by calcium, but not by U(VI). U(VI) and HA do not affect each other in the sorption process.
Finally, it was tested by means of solvent extraction, whether the added U(VI) is reduced to U(IV) in the systems U(VI) / OPA / pore water or U(VI) / HA / OPA / pore water. U(IV) could not be detected in the extracts. Thus, a reduction of U(VI) by OPA or by HA can be excluded under the studied conditions.

4.4.2.5 Influence of CO_2

In addition to the sorption experiments performed under ambient conditions, the U(VI) sorption onto OPA was investigated under inert gas atmosphere. The results are also shown in Table 4.8. Due to the fact that in both experiments different OPA batches were used, the respective BET values of the OPA batches were incorporated in the data analysis. Thus, the sorbed U(VI) and HA amounts are presented in $\mu g/m^2$ OPA.
Because OPA pore water was used as background electrolyte, the U(VI) and HA speciation is independent of the surrounding atmosphere. Under inert gas conditions the same U(VI) and HA speciations are present in solution like under ambient conditions. That means, the $Ca_2UO_2(CO_3)_3(aq)$ complex still dominates the U(VI) speciation and CaHA(II) is still the determining species of the HA speciation. As expected, the amounts of sorbed U(VI) and HA onto OPA obtained under inert gas conditions agree well with the results obtained under ambient atmosphere. Small differences can be attributed to the different OPA batches applied in the respective sorption experiments.
The conclusion is, that CO_2 from the surrounding gas atmosphere has no significant influence on the U(VI) and HA sorption in the OPA / OPA pore water system.
The reduction of U(VI) to U(IV) by the systems OPA / OPA pore water and HA / OPA / OPA pore water was investigated by solvent extraction. U(IV) was not detected in the extracts. However, a potential formation of an insoluble U(IV) species on the clay surface can not be completely excluded. For this, the surface has to be investigated closer, for example, by extended X-ray absorption fine structure (EXAFS) spectroscopy.

4.4.2.6 Investigation of the U(VI) speciation by TRLFS under cryogenic conditions

To identify the U(VI) species present in solution, TRLFS measurements were performed at 153 K. The results are shown in Table 4.9.

Table 4.9. Luminescence properties of the measured U(VI) species (λ_{ex} = 410 nm).

Sample	Main luminescence emission bands / nm
Pore water (chloride free)	
[U(VI)] = 1×10^{-6} M	485.0, 501.6, 522.8, 545.4, 571.3
Filtered supernatant after sorption	
[U(VI)] = 1×10^{-6} M	485.1, 502.1, 523.2, 545.2, 571.1
[U(VI)] = 1×10^{-6} M + [HA] = 10 mg/L	485.4, 501.9, 522.9, 545.6, 571.9
[U(VI)] = 1×10^{-6} M + [HA] = 50 mg/L	485.8, 502.6, 523.9, 546.6, 569.5

[a] Error: ± 0.3 nm.

The main luminescence emission bands of the U(VI) species present in chloride free pore water and in the filtrates of the respective sorption samples in the absence and presence of HA are very similar. This indicates that the same U(VI) species is present in all solutions. Except for the first emission band, the measured peak positions are almost identical to those published by Wang et al. (2004) and Bernhard and Geipel (2007) for $Ca_2UO_2(CO_3)_3(aq)$. At low temperatures as shown in (Bernhard and Geipel, 2007), the main luminescence emission bands of $UO_2(CO_3)_3^{4-}$ are shifted to lower wavelengths in average by about 3.5 nm compared to the $Ca_2UO_2(CO_3)_3(aq)$. For measurements at cryogenic temperatures, Wang et al. (2004) showed the main luminescence emission bands of different uranyl carbonato species. These bands differ from the corresponding bands of the free uranyl ion by a blueshift of several nanometers (average values: $Ca_2UO_2(CO_3)_3(aq)$: 15 nm; $UO_2CO_3(aq)$: 19 nm; $UO_2(CO_3)_3^{4-}$: 19 nm; $UO_2(CO_3)_2^{2-}$: 21 nm; $(UO_2)_2(OH)_3CO_3^{-}$: 23 nm). The shift of the luminescence emission bands compared to the free uranyl ion (not shown) measured in the present study in average amounts to 15 nm and can be assigned to the blueshift obtained for $Ca_2UO_2(CO_3)_3(aq)$. Thus, the presence of other uranyl carbonato species can be excluded since then the shift has to be at least ≥ 4 nm higher than the measured shift.

For $Ca_2UO_2(CO_3)_3(aq)$ a luminescence lifetime of about 1 ms is reported (Wang et al., 2004; Bernhard and Geipel, 2007). The lifetimes of the U(VI) species in pore water and in the filtrates of the sorption samples in the absence and presence of HA approximate also 1 ms, which additionally indicates the occurrence of $Ca_2UO_2(CO_3)_3(aq)$. That means the calculated U(VI) speciation given in section 4.2 is confirmed by TRLFS measurements.

In conclusion, U(VI) sorption onto OPA in synthetic OPA pore water as background electrolyte was studied by batch sorption experiments. It was demonstrated that U(VI)

sorption onto OPA is very weak. A K_d value of (0.0222 ± 0.0004) m^3/kg was determined, which was shown to be independent of S/L ratios ≥ 60 g/L. Thus, this K_d value can be used to predict U(VI) sorption at real field conditions. The K_d value determined for U(VI) is close to that obtained for the Np(V) sorption onto OPA ((0.025 ± 0.005) m^3/kg; (Wu et al., 2009)). This points out that both actinides have nearly the same sorption affinity toward OPA in the OPA / pore water system.

Due to dissolution of calcite in OPA, calcium ions are present in the pore water and form the aquatic $Ca_2UO_2(CO_3)_3$ complex with U(VI). This complex predominates U(VI) speciation under pore water conditions. HA was added to the system to investigate the influence of organic matter on the U(VI) sorption onto OPA. $Ca_2UO_2(CO_3)_3(aq)$ predominates also the U(VI) species distribution in the presence of HA. Consequently, the U(VI) sorption onto OPA is not influenced by HA. The dominant presence of the $Ca_2UO_2(CO_3)_3(aq)$ complex in solution in the absence and presence of HA was verified by TRLFS measurements.

With regard to the sorption capability of complex clay formations, it is not sufficient to investigate the sorption and retention properties of pure clay minerals such as kaolinite or illite toward actinides. As shown for the U(VI) sorption onto OPA from Mont Terri, Switzerland, calcite is one of the most important mineral phases in this heterogeneous multicomponent system, since it determines the pore water composition, which in turn affects the U(VI) speciation and therefore, also the U(VI) sorption. That means not only the complexity of the natural clay formation but also the resulting pore water chemistry is of great importance for performance assessment studies.

The speciation of HA in this system is also influenced by the presence of dissolved calcium ions. The cations saturate the binding sites of HA almost completely.

Concerning a nuclear waste repository, where OPA is intended to be used as geological barrier, the following can be concluded. If U(VI) as part of the nuclear waste is released into clay formation in a worst case scenario, it will be complexed by Ca^{2+} and CO_3^{2-} ions leached out from OPA, whereby $Ca_2UO_2(CO_3)_3(aq)$ is formed. Due to the weak sorption affinity of this complex toward OPA, this can contribute to an enhanced mobility of U(VI) in the host rock. Organic matter such as HA shows no significant influence on the U(VI) sorption behavior.

Further studies were performed to approach further real field conditions by studying the diffusion of U(VI) in intact OPA rock cores (cf. section 5).

4.5 The system U(VI) / humic acid / Opalinus Clay / 0.1 M $NaClO_4$

In this section, the U(VI) sorption onto OPA in the absence and presence of HA was investigated by means of batch sorption experiments to study the influence of pH and competing ions on the ternary system U(VI) / HA / OPA. To identify the competing ions in solution, leaching studies were performed and the results were integrated in U(VI) and HA speciation calculations to assess their influence on speciation. The outcome of these studies will be published in (Joseph et al., 2012a, in preparation).

4.5.1 Experimental

A U(VI) stock solution (5×10^{-4} M $UO_2(ClO_4)_2$ in 0.005 M $HClO_4$) was used for all experiments.

For the studies with HA, synthetic HA type M42 was applied both as ^{14}C-labeled synthetic HA (batch R2/06A, 8.9 ± 0.6 MBq/g) and non-labeled HA (batch M145) (Pompe et al., 1998; Sachs et al., 2004). HA type M42 represents a HA like melanoidin from xylose and glutamic acid. It elemental composition and functional group content (proton exchange capacity: (3.61 ± 0.30) meq/g (^{14}C-M42) and (3.51 ± 0.07) meq/g (M42)) is comparable to those of most natural HA. Thus, its sorption and metal ion complexation behavior is also comparable to that of natural HA (e.g. (Pompe et al., 1998; Křepelová et al., 2006; Schmeide et al., 2006)). A HA stock solution of 5 g/L was prepared by mixing 16 mg of ^{14}C-M42 with 34 mg M42, adding 1940 µL of 0.1 M NaOH and filling up the volume to 10 mL with Milli-Q water.

A solution of 0.1 M $NaClO_4$ was prepared by dissolution of $NaClO_4{\cdot}H_2O$ in Milli-Q water.

For pH adjustment diluted $HClO_4$ and NaOH solutions were used. For studies at pH values > 7, a calculated amount of 1 M $NaHCO_3$ was added to accelerate equilibration with atmospheric CO_2. The pH values were measured using a laboratory pH meter with SenTix® Mic pH microelectrodes, calibrated using standard buffers at pH 1, 4, 7 and 9.

Batch sorption experiments were performed under ambient atmosphere ($pCO_2 = 10^{-3.5}$ atm) at room temperature. The samples were prepared as described in section 4.1.2.1.

After pre-equilibration, 20 µL of a U(VI) stock solution were added to the OPA suspensions to obtain a final U(VI) concentration of 1×10^{-6} M. For the investigation of the U(VI) sorption onto OPA in the presence of HA, additionally 100 µL HA stock solution were added 1 h before addition of U(VI) for saturation of HA with clay leached out competing ions. The final concentration of HA in solution amounted to 50 mg/L. After U(VI) and HA addition, the pH values were readjusted immediately. For equilibration, the samples were shaken on a

horizontal shaker for 3 d, whereby the pH was readjusted each day. After 3 d, the final pH values of the samples were determined and the samples were centrifuged and the supernatants were filtrated as described in 4.1.1.1. The filtrates were analyzed for the final U(VI) and HA concentration by ICP-MS and LSC, respectively. For LSC, 1 mL of the filtrate was mixed with 15 mL Ultima Gold as scintillation cocktail. Prior to the measurements of the U(VI) concentrations in the samples containing HA, HA was removed by digestion in a microwave oven (mod. Multiwave, Anton Paar, Graz, Austria) with HNO_3 (*p.a.*, Merck; distilled by sub-boiling) in order to avoid any disturbing effects of HA during ICP-MS measurements.

In addition, blank solutions of U(VI) and HA in 0.1 M $NaClO_4$ without clay were prepared as a function of pH to determine the amount of precipitated HA. These samples were processed under the same conditions.

Finally, the U(VI) or HA sorption onto vial walls was determined. For this, 7 mL 1 M HNO_3 (U(VI)) or 1 M NaOH (HA) were added to the emptied vials and the vials were shaken for 3 d. The solutions were analyzed by ICP-MS and LSC for U(VI) and HA, respectively.

The amount of U/HA adsorbed on the mineral surface was calculated as the difference between the initial U(VI)/HA concentration and U(VI)/HA remaining in solution after the sorption experiment. The values were corrected by the wall sorption and the U(VI) concentration in the blank samples (cf. section 4.1.2.1).

4.5.2 Results and discussion

4.5.2.1 U(VI) sorption in the absence of humic acid

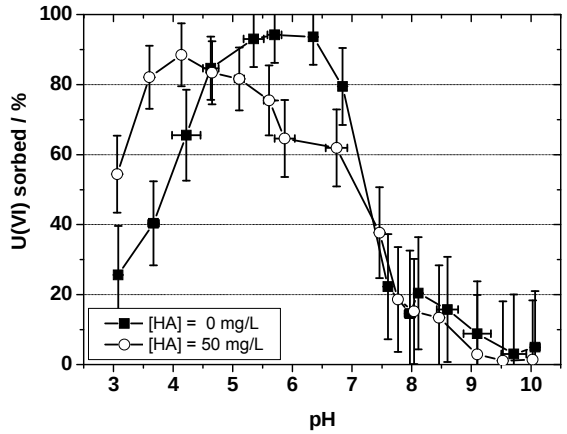

Fig. 4.12. U(VI) sorption onto OPA in the absence and presence of HA as a function of pH ([U(VI)] = 1×10^{-6} M; [HA] = 0 or 50 mg/L; $I = I_t$ (cf. Fig. 4.3); $pCO_2 = 10^{-3.5}$ atm). Uncertainties were calculated following the law of error propagation.

The U(VI) sorption onto OPA as a function of pH is shown in Fig. 4.12. In the absence of HA, the U(VI) sorption increases from about 20% at pH 3 to about 95% at pH 5.5. The comparison with the respective U(VI) speciation in Fig. 4.5a shows, that the strongest U(VI) sorption occurs when UO_2OH^+ and $(UO_2)_2CO_3(OH)_3^-$ are the dominating U(VI) species in solution. Above pH 7, a strong decrease of the U(VI) sorption is observed. This is due to formation of $Ca_2UO_2(CO_3)_3(aq)$, which is known to sorb only weakly onto OPA (Joseph et al., 2011). In the pH range from pH 7.5 to 10, the U(VI) sorption decreases further to about 5% at pH 10. Here, the weakly sorbing $UO_2(CO_3)_3^{4-}$ complex becomes the dominant species in solution.

Compared to the U(VI) sorption onto kaolinite (Křepelová et al., 2006), the U(VI) sorption curve is shifted to lower pH values in case of OPA, which points to the fact that OPA has a lower pzc than kaolinite. For the basal aluminol sites of kaolinite (KGa-1) pzc values between 3.9-6.0 (e.g., Brady et al., 1996; Redden et al., 1998) are reported. Thus, it can be concluded, that pzc of OPA has to be smaller than 6.0 at least. That means, at pH values > 8.5, where the surface of OPA is predominantly negatively charged, the weak sorption of $UO_2(CO_3)_3^{4-}$ can be interpreted by electrostatic repulsion effects. However, in the pH range, where the neutral $Ca_2UO_2(CO_3)_3(aq)$ complex is the dominant species in solution, a low but compared with $UO_2(CO_3)_3^{4-}$ higher U(VI) sorption can be observed. One reason can be that the neutral complex is less electrostatically repulsed than the negatively charged species, since the calcium ion possibly screens the negatively charged surface by charge neutralization.

4.5.2.2 U(VI) sorption in the presence of humic acid

The presence of HA influences the U(VI) sorption onto OPA significantly (Fig. 4.12). Between pH 3 and 4.5, the U(VI) sorption is increased in comparison to the U(VI) sorption in the absence of HA. This is due to precipitation of HA, which is caused by charge neutralization of their carboxylic groups by protons as well as by cations present in solution due to clay leaching or even by U(VI) added to the solution. Furthermore, a subsequent U(VI) sorption onto precipitated HA could be also possible. Both processes lead to an overestimation of the U(VI) sorption onto OPA. However, it can be concluded that HA, sorbed onto OPA or precipitated, offers additional binding sites for U(VI). Such influence of HA was already described in the literature for the U(VI) sorption on kaolinite (Křepelová et al., 2006; Sachs and Bernhard, 2008), cypris clay (Beneš et al., 1998), phyllite (Schmeide et al., 2000) and bentonite (Ren et al., 2010).

Between pH 4.5 and 7.5, the U(VI) sorption is decreased in comparison to the U(VI) sorption in the HA free system. This is due to the formation of the aquatic $UO_2(OH)HA(I)$ complex. Thus, the presence of HA leads to a mobilization of U(VI) in the near-neutral pH range which was also observed for kaolinite (Křepelová et al., 2006; Sachs and Bernhard, 2008).

In the pH range from pH 7.5 to 8, HA seems to have no effect on the U(VI) sorption onto OPA. This can be attributed to the presence of $Ca_2UO_2(CO_3)_3(aq)$ in solution and to the saturation of HA binding sites with calcium as already shown by Joseph et al. (2011) for the system U(VI) / HA / OPA / OPA pore water (pH 7.6, $I_t = 0.34$) where the U(VI) sorption onto OPA was also not influenced by HA. The present study shows that also at a lower ionic strength an influence of HA on the U(VI) sorption can not be observed. However, at lower pH values, where an even higher concentration of calcium is present in solution, HA interacts with U(VI) (cf. Fig. 4.5). That means, the absence of a HA interaction with U(VI) in the pH range from 7.5 to 8 can be exclusively ascribed to the presence of the neutral $Ca_2UO_2(CO_3)_3(aq)$ complex in solution and not to the saturation of HA binding sites by calcium or other competing ions.

At pH values > 8, no difference in U(VI) sorption can be observed compared to the U(VI) sorption in the absence of HA. This is in contrast to the U(VI) sorption on kaolinite (Sachs and Bernhard, 2008), cypris clay (Beneš et al., 1998) and phyllite (Schmeide et al., 2000), where an additional mobilization of U(VI) was observed. However, it is in agreement with the observations made for the U(VI) sorption onto muscovite (Schmeide et al., 2000).

4.5.2.3 Humic acid sorption in the presence of U(VI)

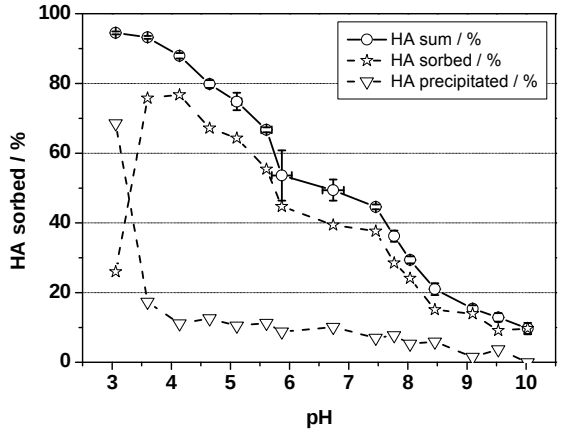

Fig. 4.13. HA sorption onto OPA in the presence of U(VI) as a function of pH ([HA] = 50 mg/L; [U(VI)] = 1×10^{-6} M; $I = I_t$ (cf. Fig. 4.3); $pCO_2 = 10^{-3.5}$ atm). Uncertainties were calculated following the law of error propagation.

To support the discussion in section 4.5.2.2, the HA sorption onto OPA in the presence of U(VI) was investigated. The results are shown in Fig. 4.13. The amount of precipitated HA was determined by pH-dependent HA+U(VI) blank solutions. The amount of HA sorbed was calculated as the difference of HA sum and HA precipitated.

Due to deprotonation of HA functional groups with increasing pH, HA becomes more negatively charged. Furthermore, the OPA surface charge is more negative with increasing pH. Thus, due to electrostatic repulsion effects, the HA sorption decreases with pH. Such sorption behavior is typical for HA and was already described for several systems (Schmeide et al., 2000; Křepelová et al., 2006; Sachs and Bernhard, 2008; Niu et al., 2009). The high amount of sorbed HA of nearly 95% at pH 3 points rather to a precipitation than a sorption, because the carboxylic groups of the HA are protonated as well as complexed by several metal ions present in solution. As shown by Fig. 4. both HA sorption and precipitation occurs.

The HA sorption onto OPA in 0.1 M $NaClO_4$ as a function of pH was already investigated by Lippold and Lippmann-Pipke (2009) and compared to the HA sorption onto illite and montmorillonite (S/L = 5 g/L, [HA] = 5 mg/L, pH 3-6). They observed the lowest sorption for OPA, which was explained with the presence of non-argillaceous constituents in OPA. Here, a tenfold higher HA concentration was used. However, the huge influence of non-argillaceous OPA constituents could be confirmed. As shown in section 4.1.2, calcium from the calcite mineral fraction is dissolved and complexed by HA. CaHA(II) dominates over a wide pH range the HA speciation.

In conclusion, U(VI) sorption onto OPA in 0.1 M $NaClO_4$ as background electrolyte was studied by batch sorption experiments as a function of pH and in the absence and presence of HA under consideration of the OPA leached out ions. The study showed, that the U(VI) speciation is affected by the dissolved competing ions. Predominantly calcium ions, which are formed by calcite dissolution, influence the U(VI) speciation between pH 7 and 8.5. The $Ca_2UO_2(CO_3)_3(aq)$ complex predominates the U(VI) speciation in solution. With appearance of this complex, which sorbs only in a low amount onto OPA (Joseph et al., 2011), the U(VI) sorption decreases strongly between pH 7 and 7.5.

The presence of HA influences the U(VI) sorption significantly. In the acidic pH range, an increase of the U(VI) sorption is observed. Under near-neutral conditions the U(VI) sorption is decreased due to mobilization of U(VI) by HA. At pH > 7, the negatively charged $UO_2(CO_3)_2HA(II)^{4-}$ complex determines the U(VI) speciation. This complex competes with the $Ca_2UO_2(CO_3)_3(aq)$ complex.

The competing ions leached out from OPA influence also the HA speciation. Over a wide pH range, the CaHA(II) complex is the dominating HA species in solution.

Concerning the application of OPA as host rock for a nuclear waste repository it can be concluded, that not the clay minerals but the calcite fraction plays the most important role due to its huge influence on U(VI) and HA speciation. Due to the formation of $Ca_2UO_2(CO_3)_3(aq)$, U(VI) is mobilized and due to the high salt content in solution, HA forms complexes with several ions which decreases its ability to complex actinides. OPA has the strongest retardation effect on U(VI) in the pH range 5-7. To approach natural conditions, the observations made at pH > 7 are interesting. Here, the biggest part of U(VI) (≥ 80%) is mobile and HA has no significant influence on the U(VI) / OPA interaction. That means, if U(VI) is released into the near field of a nuclear waste repository it is not stopped by the clay. However, further investigations concerning the migration behavior of U(VI) through OPA are needed. Also concerning the interaction of U(VI) with OPA there are still open questions. Especially the U(VI) species sorbed on OPA at pH 7.5 have to be determined closer. It is to clarify if U(VI) sorbs as a ternary uranyl carbonate surface species and onto which mineral fraction of OPA U(VI) is sorbed primarily.

4.6 Influence of low molecular weight organic acids on U(VI) sorption onto Opalinus Clay at 25°C

In natural clay, organic matter is strongly associated with mineral constituents. Besides humic substances, such as fulvic and humic acids, also low molecular weight organic acids, such as acetate, lactate, propionate and formate, can be released from the clay under certain conditions. This was shown by extraction experiments (Claret et al., 2003; Glaus et al., 2005; Courdouan et al., 2007, 2008). Thus, we studied the influence of formate, lactate, acetate, propionate, tartrate and citrate on the sorption of U(VI) onto OPA (Schmeide et al., 2012b, in preparation).

Applying a similar experimental procedure as described in section 4.4, the U(VI) sorption onto OPA (BHE-24/1) was studied under the following conditions: $[^{233}U(VI)] = 1\times10^{-6}$ M, [ligand] = 0 to 1×10^{-2} M, S/L = 60 g/L, OPA pore water, $pCO_2 = 10^{-3.5}$ atm, T = 25°C. The OPA suspensions were pre-equilibrated for 7 d. After that, aliquots of U(VI) and ligand stock solutions were added simultaneously. The sorption time was 7 d. The samples were analyzed by LSC.

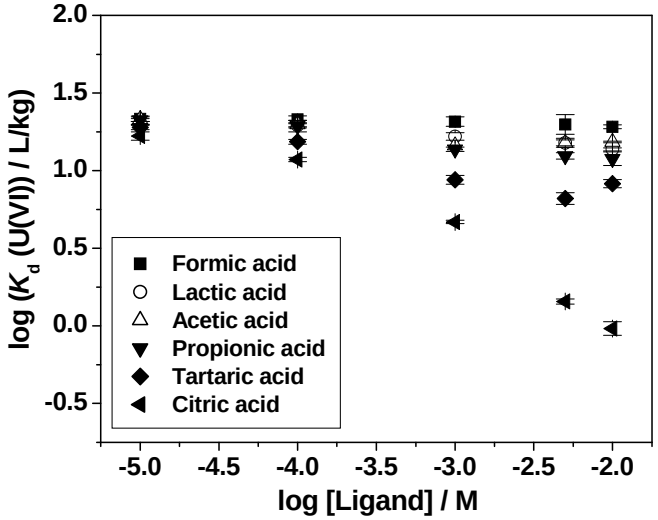

Fig. 4.14. Influence of low molecular weight organic acids on the U(VI) sorption onto OPA at 25°C.

Figure 4.14 shows the influence of the various model ligands on the U(VI) sorption onto OPA. The results show that the low U(VI) sorption onto OPA in the absence of ligands (K_d = (0.0222 ± 0.0004) m^3/kg, Joseph et al., 2011) further decreases with increasing concentration of low molecular weight organic acids (1×10^{-5} to 1×10^{-2} M) due to complex formation in aqueous solution. The mobilizing effect of the organic ligands on U(VI) increases in the following sequence: formate < lactate ≈ acetate ≤ propionate < tartrate < citrate (cf. Fig. 4.14). For instance, in the presence of citrate (1×10^{-2} M), which has been identified as important ligand in radioactive waste problems, the K_d value for U(VI) amounts to only (0.0011 ± 0.0003) m^3/kg. The influence of the organic ligands on the U(VI) sorption onto OPA correlates with the stability of the respective U(VI) complexes. In contrast, humic acid (≤ 50 mg/L) does not change U(VI) sorption (cf. Joseph et al., 2011). Also in the presence of the low molecular weight organic acids, a reduction of U(VI) to U(IV) was not detected.

4.7 Influence of temperature on U(VI) sorption onto Opalinus Clay in the absence and presence of clay organics

Since elevated temperatures are expected for the disposal of high-level nuclear waste in clay formations, the influence of temperature on the U(VI) sorption onto OPA was studied in the temperature range from 10 to 60°C both in the absence of ligands and in the presence of lactic acid or citric acid (Schmeide et al., 2012b, in preparation).

Applying a similar experimental procedure as described in section 4.4, the U(VI) sorption onto OPA (BHE-24/1) was studied under the following conditions: [^{233}U(VI)] = 1×10^{-6} M,

[lactic or citric acid] = 0 to 1×10^{-2} M, S/L = 60 g/L, OPA pore water, $pCO_2 = 10^{-3.5}$ atm, T = 10 - 60°C. The OPA suspensions were pre-equilibrated for 7 d. After that, aliquots of U(VI) and ligand stock solutions were added simultaneously. The sorption time was 7 d. The samples were analyzed by LSC.

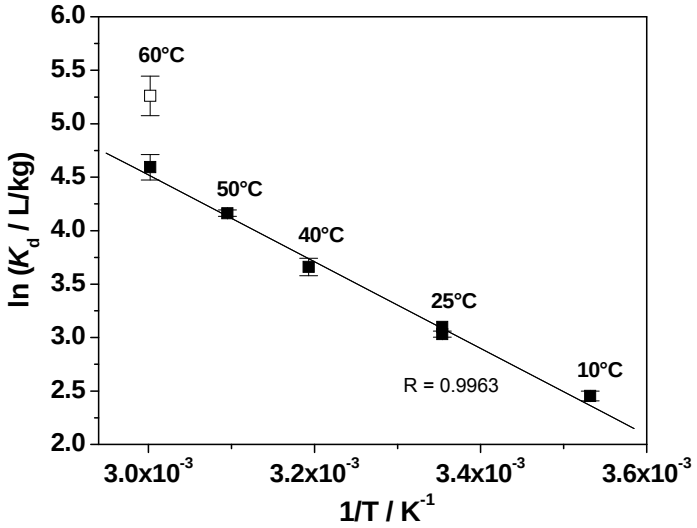

Fig. 4.15. Influence of temperature on the U(VI) sorption onto OPA in the absence of ligands.

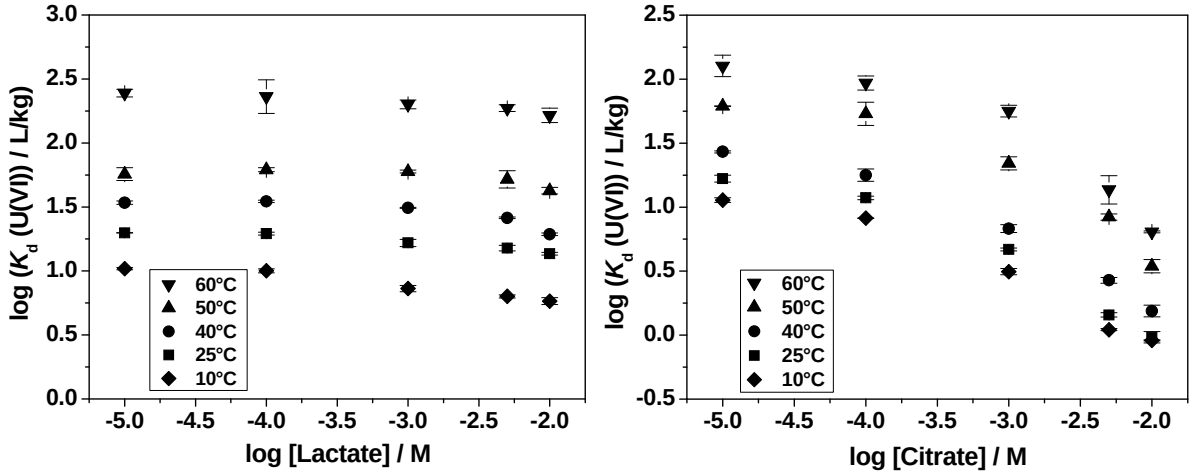

Fig. 4.16. Influence of temperature on the U(VI) sorption onto OPA in the presence of lactic acid and citric acid.

Figure 4.15 shows that the U(VI) sorption increases with increasing temperature in the absence of organic ligands (up to one order of magnitude in the temperature range 10-60°C). For U(VI), an apparent endothermic sorption enthalpy was determined with 34 ± 1 kJ/mol. The entropy amounts to ΔS = 139 ± 3 J·mol^{-1}·K^{-1}. An increased sorption with increasing temperature was also observed for the sorption of Ni^{2+} and Ln^{3+} onto montmorillonite (Tertre et al., 2005) as well as for the sorption of Eu^{3+} and NpO_2^+ onto OPA (Schott et al., 2012;

Fröhlich et al., 2012, submitted). Furthermore, an increased interaction of U(VI) with OPA at 60°C was also detected by diffusion experiments (cf. section 5.4.4).

Figure 4.16 shows that the stronger U(VI) sorption onto OPA with increasing temperature is maintained also in the presence of lactate and citrate, when present in the concentration range from 1×10^{-5} to 1×10^{-2} M.

For interpretation of the sorption results, the U(VI) speciation in aqueous solution has to be known. The temperature-dependent studies of the U(VI) complexation with lactate (pH 3.0, T = 7 - 65°C) or citrate (pH 1-10, T = 10 - 60°C) (cf. section 2.4 and (Steudtner et al., 2011c)) have shown that the complex formation constants increase with increasing temperature (about one order of magnitude in the studied temperature range). The complex formation between U(VI) and lactate as well as citrate was found to be endothermic and entropy-driven. The U(VI) citrate complexes are stronger than the U(VI) lactate complexes. Consequently, citric acid has to be taken into account for safety assessment for nuclear waste repositories.

Also in the presence of HA, the U(VI) sorption onto OPA increases (not shown), however, as was observed at 25°C, HA (50 mg/L) does not change U(VI) sorption up to 50°C.

5 Diffusion of U(VI) and humic acid in Opalinus Clay

For safety assessment, a profound knowledge of the migration behavior of radionuclides in natural clay formations such as OPA, which is governed by molecular diffusion processes, is required, also at elevated temperatures. So far, the diffusion studies in the case of OPA are mainly focused on experiments at room temperature with tracers such as tritiated water (HTO), $^{36}Cl^-$, $^{125}I^-$ (Van Loon et al., 2003) or $^{134}Cs^+$ (Jakob et al., 2009). However, only few studies are known, which are focusing on the diffusion properties of actinides in OPA. For instance, Wu et al. (2009) investigated the diffusion and sorption of Np(V) in/onto OPA and Bauer et al. (2006) the Pu diffusion in OPA. Actinides diffusion studies in natural clays at elevated temperatures can not be found in the literature. The first diffusion studies at elevated temperatures focused on conservative tracers and mainly on simple clay minerals. For instance, González-Sánchez et al. (2008) investigated the HTO diffusion through compacted clay minerals, namely illite, montmorillonite, and kaolinite, at different temperatures and ionic strengths. Natural clay was investigated at higher temperatures by Van Loon et al. (2005), who determined the activation energies of the self-diffusion of HTO, $^{22}Na^+$ and $^{36}Cl^-$ in OPA.

As discussed in section 4, HA are able to influence the migration behavior of metal ions. This was shown for the diffusion of U(VI) in quartz sand (Mibus et al., 2007b) and in compacted kaolinite (Sachs et al., 2007b) and for the diffusion of Eu(III) in sedimentary rock (Seida et al., 2010).

In the present work, the diffusion of HTO, ^{233}U(VI) and ^{14}C-labeled HA in OPA is studied at 25 and 60°C under anaerobic conditions using OPA core samples. From HTO diffusion experiments, values for the transport porosity (ε) of the respective clay samples are determined. The U(VI) diffusion is investigated in the absence and presence of HA. The speciation of U(VI) at elevated temperatures is unknown so far.

The obtained parameters contribute to the thermodynamic database used for modeling of geochemical migration processes of actinide ions through argillaceous rocks discussed as possible host rocks for a nuclear waste repository.

The outcome of this study will be published in (Joseph et al., 2012b, in preparation).

5.1 Experimental

Pristine OPA samples from the Mont Terri Rock Laboratory in Switzerland were used for diffusion experiments. The bore cores were taken by the Federal Institute for Geosciences and

Natural Resources (BGR) using air as drilling medium (Bossart and Thury, 2008). The bore core BLT-14 was taken at a depth of 0.25-0.5 m. The preparation of the OPA bore core samples (thickness: 11 mm, diameter: 25.5 mm) was performed at the Karlsruher Institut für Technologie, Institut für Nukleare Entsorgung (KIT-INE). The sample BLT-14 can be assigned to the sandy fraction of OPA. Table 5.1 presents the mineralogy of OPA sandy facies determined by Pearson et al. (2003).

Table 5.1. Mineralogy of OPA sandy facies (average of four samples). (Pearson et al., 2003).

Mineral	**wt.%**
Clay minerals	45-70
• Illite	15-35
• Illite/smectite ML	5-20
• Chlorite	4.4-15
• Kaolinite	13-35
Quartz	16-32
Calcite	7-17
Siderite	1.1-3
Albite	0.8-2.2
K-feldspar	2.5-5
Dolomite/ankerite	0.3-2
Pyrite	0.7-3.2
Organic carbon	0.2-0.5

According to Pearson (1998) synthetic OPA pore water (pH 7.6; cf. Table 4.3) was prepared in Milli-Q water and used as background electrolyte in all diffusion experiments. To avoid bacterial growth during the experiment, 1×10^{-3} mol/L NaN_3 (*purified*, Merck, Darmstadt, Germany) was added to the pore water.

A $^{233}U(VI)$ stock solution was used for all experiments and prepared as described in section 4.3.1. The specific activity of the $^{233}U(VI)$ stock solution determined with LSC using Ultima Gold as scintillation cocktail amounts to 15.2 kBq/mL (1.8×10^{-4} M $^{233}UO_2Cl_2$).

For the studies with HA, a synthetic ^{14}C-labeled HA type M42 was applied (batch M180A, 23.08 MBq/g, proton exchange capacity: 3.34 ± 0.18 meq/g) (Pompe et al., 1998; Sachs et al., 2004). A HA stock solution of 5 g/L was prepared by dissolving 50 mg of ^{14}C-M42 with 1890 µL of 0.1 M NaOH and filling up the volume to 10 mL with pore water.

The details of the diffusion cells applied in the experiments were described by Van Loon et al. (2003). Four identical diffusion cells were used for the experiments; two cells were conditioned at 25°C and two cells at 60°C, respectively. Each OPA bore core sample was placed in the cells between two stainless steel filter plates (316L, pore diameter: 0.01 mm,

thickness: 1.55 mm, porosity: 0.3, density: 5000 kg/m^3; MOTT industrial division, Farmington, USA).

The confining pressure on each sample was 5 MPa. The experimental set-up used for the diffusion experiments at 25°C was described previously (Van Loon et al., 2003). The experiments were performed under anaerobic conditions (N_2, 0% CO_2). Each diffusion cell was coupled with a peristaltic pump (mod. Ecoline, Ismatec, IDEX Health & Science, Glattbrugg, Switzerland) and a source and receiving reservoir filled with 200 mL and 20 mL synthetic OPA pore water, respectively. The solutions were circulating through the end plates of the cells in order to saturate the samples. The saturation time amounted to three weeks. Subsequently, the solutions were replaced by fresh ones, whereby the source reservoir contained the tracer and thereby tracer diffusion was started.

For the diffusion experiments at 60°C, the experimental set-up was changed slightly (Fig. 5.1). The diffusion cells were placed in a temperature controlled laboratory sand-bath (mod. ST-72, Harry Gestigkeit GmbH, Düsseldorf, Germany) and the reservoirs were stirred and heated on top of a magnetic stirrer with integrated heating function (mod. MR 3002, Heidolph, Schwabach, Germany).

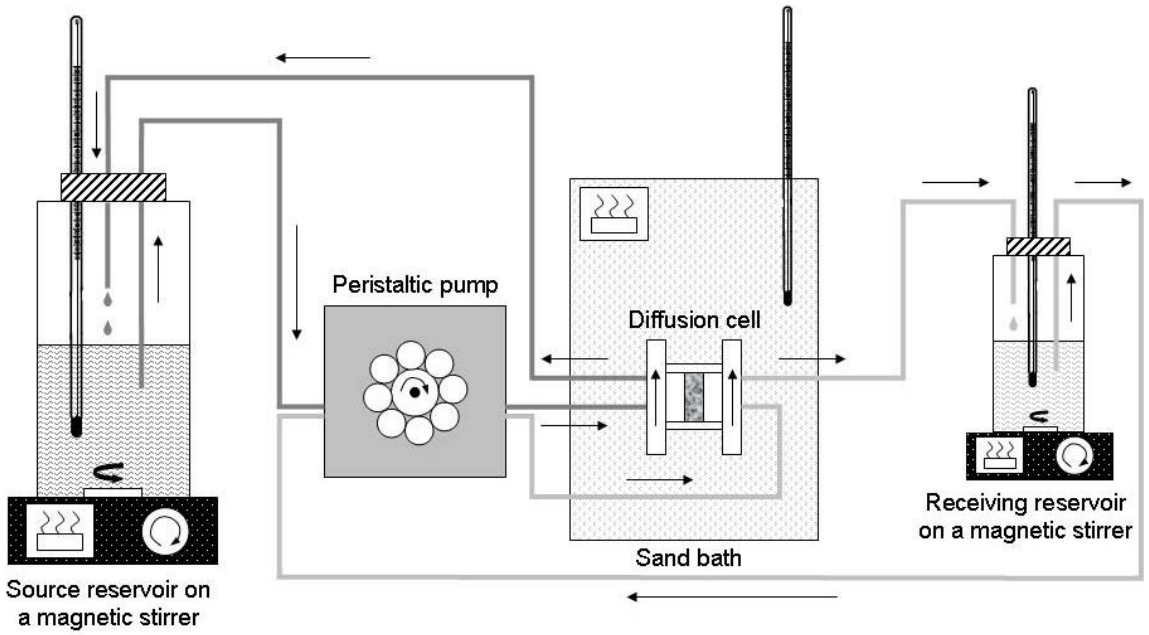

Fig. 5.1. Experimental set-up for the diffusion experiment at 60°C (based on Van Loon et al., 2003).

At first, with all four diffusion cells – two cells at 25°C, two cells at 60°C – HTO through- and out-diffusion experiments were performed as described by Van Loon et al. (2003) in order to determine values for the porosity (ε) of the clay samples ($[HTO]_0$ = 1000 Bq/mL). After that, the ^{233}U(VI) in-diffusion in the absence and presence of ^{14}C-HA was studied.

Using two diffusion cells, the $^{233}U(VI)$ diffusion at 25°C (cell 1) and 60°C (cell 3) was investigated. The simultaneous diffusion of $^{233}U(VI)$ and ^{14}C-HA was studied (cell 2 (25°C) and cell 4 (60°C)) under exclusion of light to minimize possible light-induced HA degradation processes ([$^{233}U(VI)$] = 1×10^{-6} mol/L, [^{14}C-HA] = 10 mg/L). During the duration of the experiment the pH in the concentration reservoirs was not readjusted.

After three months, the diffusion experiments were stopped and the clay samples were removed from the cells. Using the abrasive peeling technique (Van Loon and Eikenberg, 2005), U(VI) and HA diffusion profiles were determined. The peeled layers were extracted for $^{233}U(VI)$ content by 1 M HNO_3 (Roth, Karlsruhe, Germany) and for ^{14}C-HA content by 1 M NaOH (Merck, Darmstadt, Germany). The tracer concentrations in the extracts were determined by LSC.

The solutions of the source reservoirs tracered with $^{233}U(VI)$ and ^{14}C-HA were analyzed for Na, K, Sr, Ba, Al, Si, P, Mn, Fe and U by ICP-MS, for Mg and Ca by AAS, and for SO_4^{2-} and Cl^- by IC. The total inorganic carbon content was measured using the multi N/C 2100 analyzer as difference of the total carbon and the total organic carbon. During the diffusion experiments the concentrations of Fe and P were always below the detection limit of ICP-MS.

The pH value and the redox potential (BlueLine 31 Rx redox electrode; Schott, Mainz, Germany) of the source reservoir solutions for the $^{233}U(VI)$ and ^{14}C-HA diffusion experiments were measured only at the end of the experiment to decrease the impact of impurities and the loss of CO_2 into the surrounding N_2 atmosphere during the experiment.

Because of the presence of Fe(II) minerals in OPA, the solutions in the source reservoirs were analyzed with respect to a possible reduction of U(VI) to U(IV) by solvent extraction using thenoyltrifluoroacetone according to Bertrand and Choppin (1982) (cf. section 4.4.1.1).

Furthermore, the size distribution of $^{233}U(VI)$ and ^{14}C-HA in the solutions of the source and receiving reservoirs was determined by ultrafiltration at the start and end of diffusion experiments. Ultrafiltration centrifugal devices with molecular weight cutoffs of 1 to 1000 kD (Microsep™, Pall Corporation, Port Washington, NY, USA) were applied.

5.2 Data processing

For the migration of the used radionuclides through the OPA bore core samples molecular diffusion was assumed. The theoretical background of such a diffusion process has been described previously (Van Loon et al., 2003; Van Loon and Soler, 2004). For determination of the diffusion parameters a one-dimensional model composed of source reservoir, filter, OPA bore core sample, filter and receiving reservoir was applied as described in (Jakob et al.,

2009). The OPA sample and the filters were considered as homogeneous with a single value for the transport porosity.

The diffusive flux J [mol/(m^2·s)] of a solute is given by Fick's first law:

$$J = -D_e \cdot \frac{\partial C}{\partial x}, \tag{5.1}$$

where the effective diffusion coefficient D_e [m^2/s] is multiplied by minus concentration gradient. C [mol/m^3] means the tracer concentration in the mobile phase and x [m] denotes the spatial coordinate. The change of concentration with time, t [s], is expressed by Fick's second law:

$$\frac{\partial C}{\partial t} = D_a \cdot \frac{\partial^2 C}{\partial x^2}. \tag{5.2}$$

D_a [m^2/s] represents the apparent diffusion coefficient. In the evaluation of the experiments, the concentration values were decay corrected.

Both diffusion coefficients are linked by the rock capacity factor α [-] according to:

$$D_a = \frac{D_e}{\alpha}. \tag{5.3}$$

The rock capacity factor α is defined as:

$$\alpha = \varepsilon + \rho \cdot K_d \tag{5.4}$$

where ε [-] is the diffusion-accessible porosity, ρ [kg/m^3] the dry bulk density and K_d [m^3/kg] the sorption distribution coefficient. For non-sorbing tracers such as HTO with K_d = 0 it is assumed, that α is equal to ε. The parameter D_e represents a measure for the solute flux through the clay. D_a accounts additionally for the tracer interaction with the clay.

For HTO, D_e and α were determined by modeling the through-diffusion flux of HTO taking into account the time history of the HTO concentration in the receiving reservoir. For ^{233}U(VI) and ^{14}C-HA, the values for the diffusion parameters (D_e, α, ε, K_d) were determined by fitting the experimental tracer distribution profiles in the clay.

All experimental results were evaluated using the commercial software COMSOL Multiphysics 3.5a (2008).

5.3 Filter diffusion parameters

For fitting the clay diffusion parameters, the diffusion characteristics of the adjacent stainless steel filter plates for HTO, U(VI) and HA have to be included in the model, because they can

influence the retardation and migration of the tracer. In case of HTO, the filter K_d value was assumed to be 0. The corresponding filter D_e value, D_f, was taken from (Glaus et al., 2008) and amounts to 2.3×10^{-10} m^2/s at 25°C.

The temperature dependence of molecular diffusion can be described by the Arrhenius equation (Eisenberg and Kauzmann, 1969). With a known D_e value at a defined temperature (T_1), D_e at temperature T_2 can be calculated as follows:

$$D_e^{T_2} = D_e^{T_1} \cdot e^{\frac{E_a}{R}\left(\frac{1}{T_1}-\frac{1}{T_2}\right)} \tag{5.5}$$

where E_a is the activation energy [kJ/mol] and R is the gas constant, 8.3144621 J/mol/K. Using the E_a value of bulk water (E_a = 18 kJ/mol) (Van Loon and Soler, 2004), D_f of HTO at 60°C was determined to be 4.93×10^{-10} m^2/s.

In contradiction to HTO, for ^{233}U(VI) and ^{14}C-HA an interaction of the tracers with the filters can be assumed. The respective filter K_d values were obtained by sorption (25°C) and extraction experiments (60°C). For the sorption experiments, fresh filter plates were contacted with solutions of 1×10^{-6} mol/L ^{233}U(VI) or 10 mg/L ^{14}C-HA in OPA pore water. After 2, 5 and 7 d, aliquots of the sample solutions were analyzed by LSC. The sorption of ^{233}U(VI) and ^{14}C-HA onto the filter plates was in equilibrium almost after 2 d. K_d values were determined with 7×10^{-5} m^3/kg and 1×10^{-4} m^3/kg for ^{233}U(VI) and ^{14}C-HA, respectively. At 60°C, a sorption equilibrium of ^{233}U(VI) and ^{14}C-HA onto fresh filter plates was not reached within 28 d. Thus, after finishing the clay diffusion experiment, ^{233}U(VI) and ^{14}C-HA were extracted from the filter plates used in diffusion cells 3 and 4 with 1 M HNO_3 and 2 M NaOH, respectively. After 5 d shaking, the extracts were analyzed by LSC. The resulting K_d values amount to $K_d(^{233}\text{U(VI)}) = 5\times10^{-3}$ m^3/kg and $K_d(^{14}\text{C-HA}) = 3.4\times10^{-3}$ m^3/kg.

Values for D_f of U(VI) and HA were taken from literature. If the diffusion coefficient of a certain species in bulk water, D_w [m^2/s], is known, D_f can be estimated by $D_f = D_w/10$ (Glaus et al., 2008). At 25°C, D_f of $Ca_2UO_2(CO_3)_3$(aq), the dominating U(VI) species in OPA pore water (Joseph et al., 2011), was assumed to be 4.6×10^{-11} m^2/s based on the corresponding D_w from (Kerisit and Liu, 2010). During fitting routine this value had to be decreased slightly to 3.5×10^{-11} m^2/s. For D_w of HA at 25°C different values were published depending on origin and molecular size of HA (Morris et al., 1999; Mibus et al., 2007a). In this study, published D_w values for calcium humate complexes (Nebbioso and Piccolo, 2009) were applied and D_f was averaged to 1.3×10^{-11} m^2/s. Using Eq. (5.5), the applied D_f values at 60°C were $D_f(\text{U(VI)}) = 7.65\times10^{-11}$ m^2/s and $D_f(\text{HA}) = 2.84\times10^{-11}$ m^2/s.

5.4 Results and discussion

5.4.1 HTO diffusion in Opalinus Clay in dependence on temperature

The results obtained for HTO diffusion through OPA are summarized in Table 5.2. For both temperatures, 25 and 60°C, the values are in good agreement with literature data given by Van Loon and Soler (2004) for shaly facies OPA samples. The small differences observed can be explained by the sandy facies OPA samples applied in the current experiments. The ε values obtained by HTO diffusion experiments were incorporated in the ^{233}U(VI) and ^{14}C-HA diffusion model.

Table 5.2. Diffusion parameters of HTO in OPA determined by through-diffusion experiments at 25 and 60°C.

	25°C		**60°C**	
	Cell 1	**Cell 2**	**Cell 3**	**Cell 4**
C_0 [Bq/mL]	999 ± 8	1027 ± 4	1021 ± 4	1022 ± 11
V_0 [$\times 10^{-6}$ m^3][a]	201.62	202.48	200.57	201.22
D_e [$\times 10^{-11}$ m^2/s]	1.60 ± 0.09	1.31 ± 0.09	3.93 ± 0.07	4.10 ± 0.10
ε [–]	0.24 ± 0.02	0.20 ± 0.02	0.23 ± 0.07	0.26 ± 0.06
C_0 [Bq/mL][b]	1217 ± 83		~ 1200 ± 90	
D_e [$\times 10^{-11}$ m^2/s][b]	1.21 ± 0.08		3.67 ± 0.22 / 3.93 ± 0.24	
ε [–][a]	0.09 ± 0.02		0.12 ± 0.01 / 0.19 ± 0.02	

[a] Initial volume of the source reservoir.

[b] Values from Van Loon and Soler (2004) measured at 23°C (5 MPa) and at 65°C (3 MPa).

5.4.2 Aqueous U(VI) and humic acid speciation

To interpret the diffusion results, information about the aqueous U(VI) and HA species present in solution is needed. In section 4.2 is shown, that the $Ca_2UO_2(CO_3)_3$(aq) complex dominates the U(VI) speciation in OPA pore water at room temperature to nearly 100%. The presence of HA has no influence on this speciation. At the beginning of the diffusion experiment (25°C), the same U(VI) species predominates in solutions of the source reservoirs. The diffusion experiments were carried out for three months. After that, the U(VI) speciation was recalculated on the basis of the ion concentrations of Na, K, Sr, Al, Si, Ca, Mg, Ba, Mn, Cl^-, SO_4^{2-}, and CO_3^{2-}, the concentrations of ^{233}U(VI) and ^{14}C-HA, the pH and the redox potential (E_h) in the source reservoir solutions. The results are summarized in Table 5.3.

Table 5.3. Characterization of the source reservoir solutions at 25 and 60°C at the end of the ^{233}U(VI) and ^{14}C-HA diffusion experiments as well as U(VI) speciation in the reservoirs calculated for these conditions.

	25°C		60°C	
	Cell 1	**Cell 2**	**Cell 3**	**Cell 4**
$C(^{233}U(VI))$ [mol/L]	1.05×10^{-6}	9.30×10^{-7}	5.96×10^{-7}	5.00×10^{-7}
$C(^{14}C\text{-HA})$ [mg/L]	-	8.9	-	7.0
pH	8.75	8.60	7.92	7.66
E_h [mV]	300	240	140	30
T [°C]	23.3	23.3	61.5	59.2
U(VI) speciation (aqueous species accounting for 99% or more)				
- $Ca_2UO_2(CO_3)_3(aq)$	98.88%	98.14%	n.k.	n.k.
- $UO_2(CO_3)_3^{4-}$	0.84%	0.86%	n.k.	n.k.
- $UO_2(CO_3)_2HA(II)^{4-}$	-	0.71%	-	n.k.

n.k. … not known

At 25°C, at the end of the diffusion experiments, in all reservoir solutions the $Ca_2UO_2(CO_3)_3(aq)$ is still the dominating species, also in the presence of HA as shown for cell 2.

At 60°C, the present U(VI) species in OPA pore water are not known. Experiments still have to be performed to investigate the system closer.

The oxidation state of uranium in the source reservoir solutions was investigated by solvent extraction. No U(IV) was detectable in the reservoir solutions at 25°C and at 60°C.

In Fig. 5.2, the particle size distributions of ^{14}C-HA colloids in the presence of ^{233}U(VI) in the source reservoir solutions of cells 2 and 4 at start and at end of the experiments are shown.

At 25°C, before the diffusion experiment was started, the HA colloids present in source reservoir solution showed a wide size distribution, whereby HA colloids > 100 kD were clearly predominating. Furthermore, Fig. 5.2a shows, that no interaction occurred between ^{14}C-HA and ^{233}U(VI). In contrast to HA, ^{233}U(VI) passed all particle size filters without any significant hindrance. Thus, it was present in the filtrates to almost 100% related to the ^{233}U(VI) concentration of the unfiltered solution. Within three months (Fig. 5.2b), HA degradation processes occurred to some extent. The fraction of HA colloids < 100 kD was slightly increased. However, still no significant interaction between ^{14}C-HA and ^{233}U(VI) was observable even after 87 days.

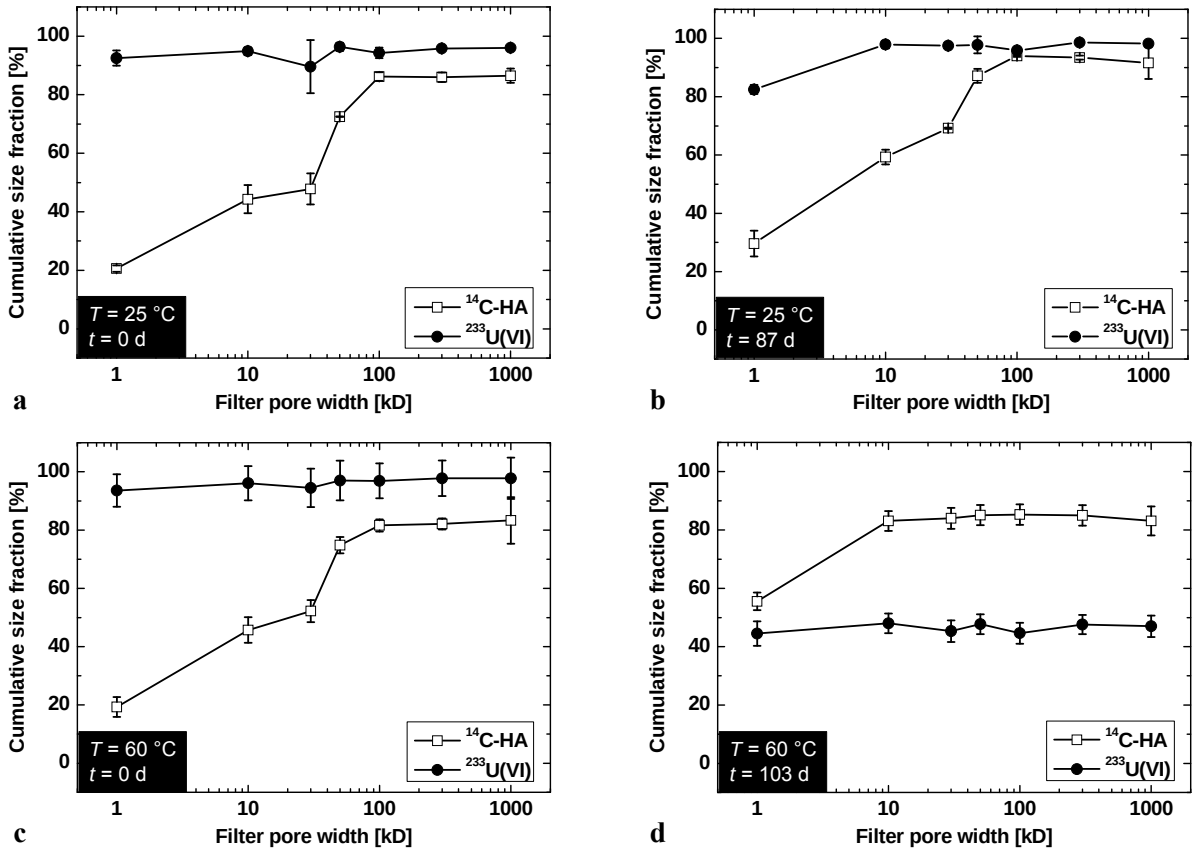

Fig. 5.2. Particle size distribution of ^{14}C-HA colloids in the presence of ^{233}U(VI) in the solutions of the source reservoirs at 25°C (cell 2; a + b) and 60°C (cell 4; c + d) at the beginning (a + c) and end (b + d) of the diffusion experiments.

At 60°C, the particle size distribution of ^{14}C-HA and ^{233}U(VI) at the beginning of the experiment (Fig. 5.2c) was similar to that at 25°C (Fig. 5.2a). However, the particle size distribution obtained after three months shows that the HA degradation at 60°C is stronger than that at 25°C, since the fractions of HA colloids < 100 kD are increased (Fig. 5.2d). An interaction between ^{14}C-HA and ^{233}U(VI), which would be depicted by a similar particle size distribution, can not clearly be detected. However, at 60°C, about 50% of ^{233}U(VI) was found to be retained on the various particle size filters (Fig. 5.2d). These U(VI) particles must have a size > 1000 kD. These results are an indication toward a change of the U(VI) speciation at 60°C. Presumably, U(VI) forms colloids in OPA pore water at 60°C. These are not able to pass the applied particle size filters. Otherwise, with a fraction of about 50% also aqueous U(VI) species were present in solution, which passed the filters.

Also the receiving reservoir solutions of cell 2 and cell 4 were analyzed regularly for their particle size distribution. No ^{233}U(VI) was detectable in these reservoirs. However, at the end of the diffusion experiment at 25°C diffused HA colloids (< 1 kD) were detected in the receiving reservoir of cell 2. At 60°C, already after one week, the solution in the receiving

reservoir of cell 4 turned yellow, which is an indication of the presence of HA. About 25 d after starting the diffusion experiment, small HA colloids (< 1 kD) could clearly be detected in the receiving reservoir solution. A further characterization of the diffused molecules was not performed due to their very low concentration. However, since the color of the solution changed, it can be excluded, that the detected diffused ^{14}C is CO_3^{2-}, which is a potential degradation product of HA. A filtration effect of the clay was observed also by Sachs et al. (2007b) for the HA diffusion through compacted kaolinite.

5.4.3 Diffusion of U(VI) and humic acid in Opalinus Clay at 25°C

The experiments were conducted for three months. Within this time span no $^{233}U(VI)$ could be detected in the receiving reservoirs of cell 1 and 2. However, as discussed in section 5.4.2, diffused HA colloids were found.

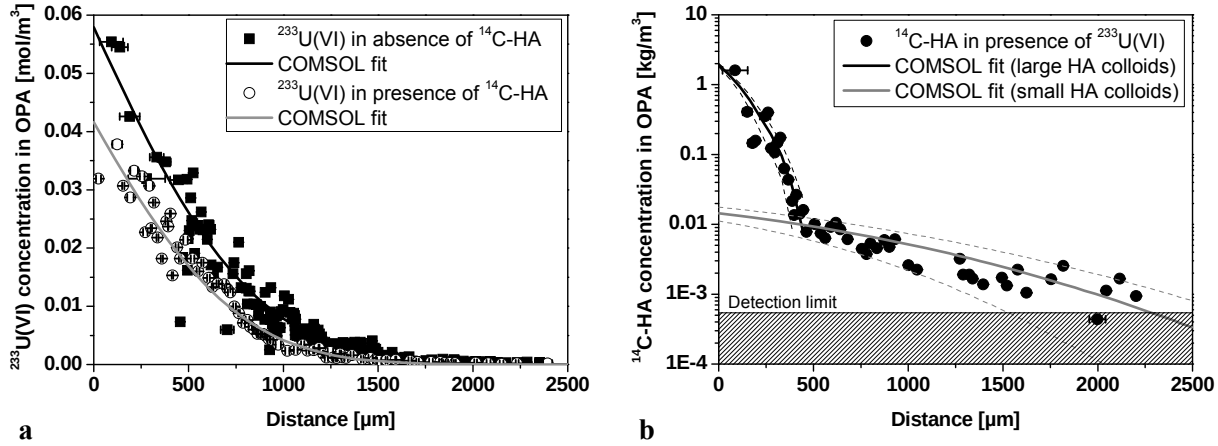

Fig. 5.3. Concentration profiles of $^{233}U(VI)$ in the absence (filled symbols) and presence (open symbols) of ^{14}C-HA (**a**) and of ^{14}C-HA in the presence of $^{233}U(VI)$ (**b**) in OPA at 25°C.

In Fig. 5.3a the $^{233}U(VI)$ diffusion profiles determined in the absence and presence of HA are shown. The comparison of the two data sets leads to the conclusion that in the presence of HA $^{233}U(VI)$ penetrates less the clay than in the absence of HA. Such a reduced metal ion diffusion in the presence of HA was already described by Seida et al. (2010) for the Eu(III) diffusion in sedimentary rock and by Mibus and Sachs (2006) for the U(VI) diffusion in compacted kaolinite.

Based on the $^{233}U(VI)$ distribution profiles in the samples both transport parameters, D_e and K_d, can be adjusted individually. Their values are summarized in Table 5.4. The K_d value for U(VI) determined by the present diffusion studies agrees well with the K_d value determined previously by means of sorption experiments using crushed OPA material (cf. section 4, Joseph et al., 2011). In contrast, Wu et al. (2009) determined for the Np(V) / OPA system a

larger K_d value by means of diffusion experiments (K_d = 0.1 ± 0.01 m^3/kg) than by batch sorption measurements (K_d = 0.025 ± 0.005 m^3/kg). The authors concluded that during the diffusion experiment Np(V) was partially reduced to Np(IV). Since in the present study the K_d values determined for the U(VI) / OPA system by batch sorption and diffusion experiments are comparable, a reduction of U(VI) to U(IV) can be excluded. This was also verified by solvent extraction experiments (cf. section 5.4.2).

Table 5.4. Compilation of further data of the experiments and of the best-fit parameter values. The data are based on the ^{233}U(VI) and ^{14}C-HA diffusion profiles and concentration data in the source and receiving reservoir at 25°C.

	U(VI) in the absence of HA (cell 1)	**U(VI) in the presence of HA (cell 2)**		
	^{233}U(VI)	**^{233}U(VI)**	**HA**	
			large colloids	**small colloids**
C_0(^{233}U(VI)) [mol/L]	1.07×10^{-6}	9.98×10^{-7}		
C_0(^{14}C-HA) [mg/L]	-		10.1	3[a]
V_0 [$\times10^{-6}$ m^3]	202.18		167.71	
t [d]	89		87	
ρ [kg/m^3]	2424		2392	
ε [–][b]	0.24 ± 0.02		0.20 ± 0.02	
α [–]	61 ± 7	48 ± 7	309 ± 45	5 ± 1.2
D_e [$\times10^{-12}$ m^2/s]	1.9 ± 0.4	1.2 ± 0.3	0.65 ± 0.25	0.4 ± 0.25
D_a [$\times10^{-14}$ m^2/s]	3.1 ± 0.3	2.5 ± 0.3	0.21 ± 0.05	8 ± 3
K_d [m^3/kg]	0.025 ± 0.003	0.020 ± 0.003	0.129 ± 0.018	0.002 ± 0.0005
K_d [m^3/kg][c]	0.0222 ± 0.0004		0.129 ± 0.006	

[a] Based on C_0 and the fact, that about 30% of HA colloids are < 1 kD (cf. Fig. 5.2b).

[b] Determined by HTO through-diffusion.

[c] Determined by sorption experiments (cf. section 4, Joseph et al., 2011).

In comparison to Np(V) (Wu et al., 2009), the K_d of U(VI) determined by diffusion is one order of magnitude smaller, which implicates a weaker interaction of U(VI) with OPA compared to that of Np(V) – or of Np(IV) after reduction – with OPA. This is in contrast to the findings of Křepelová et al. (2006) and Schmeide and Bernhard (2010), who investigated the U(VI) and Np(V) sorption onto kaolinite, respectively. At pH 8, the K_d value of U(VI) was about one order of magnitude higher than the K_d of Np(V) (C_0(An) = 1×10^{-5} M, I = 0.01 M $NaClO_4$, pCO_2 = $10^{-3.5}$ atm). The reason for these results was the absence of non-argillaceous components in the investigated system. In the present study, these components

determine the U(VI) speciation (calcite) and Np oxidation state (pyrite) and lead to the reverse result.

The D_e value for the Np(V) diffusion in OPA amounts to $(6.9 \pm 1.1)\times10^{-12}$ m^2/s (Wu et al., 2009). The D_e of U(VI) shown in Table 5.4 is smaller. That means, if the same concentration gradient in diffusion experiments with Np(V) and U(VI) is applied, U(VI) would diffuse with a smaller flux through OPA than Np(V). However, the comparison of the D_a values, where the interaction of the actinides with OPA is considered additionally, shows, that the Np(V) diffusion in OPA is with a value of $D_a = (2.8 \pm 0.4)\times10^{-14}$ m^2/s in the same range as that for U(VI). This leads to the conclusion, that the migration of both actinides through OPA is similar.

A comparison of the K_d as well as D_e values determined for U(VI) in the absence and presence of HA shows that the diffusion of U(VI) might be slightly hindered in the presence of HA molecules. However, based on the experimental uncertainties, it is concluded that HA does not have a significant effect on U(VI) diffusion through compacted water-saturated OPA. The system U(VI) / HA / OPA was also investigated by means of batch sorption experiments (cf. section 4.4, Joseph et al., 2011). There, also no influence of HA on the U(VI) interaction with OPA was observed. This result is confirmed by the diffusion experiments with intact OPA bore core samples.

In Fig. 5.3b, the diffusion profile measured for HA in OPA at 25°C is shown. The profile is indicative for the presence of two size fractions of HA colloids, which are assigned to 1) a high molecular size HA colloid fraction (large HA colloids) and 2) a low molecular size HA colloid fraction (small HA colloids). Within three months, the larger colloids diffused only about 500 µm into the OPA bore core due to restriction in the available pore space and due to strong sorption onto the OPA surface. However, the smaller HA colloid fraction showed a weaker sorption affinity toward OPA and diffused through the entire OPA sample and therefore, could be detected in the receiving reservoir. For both HA size fractions, the values for the diffusion parameters are presented in Table 5.4.

In comparison to the HA diffusion through compacted kaolinite ($D_a = 2.2\times10^{-12}$ m^2/s, pH 7, $\rho = 1670$ kg/m^3; (Sachs et al., 2007b)), the HA diffusion through OPA is much slower, which is due to the higher bulk dry density of OPA providing less pore space for diffusion. Joseph et al. (2011) determined the K_d value of HA with OPA by batch sorption experiments (cf. section 4.4.2.3 and Table 5.4). This result is in very good agreement with the K_d value fitted for the large HA colloid fraction in the present diffusion experiment.

5.4.4 Diffusion of U(VI) and humic acid in Opalinus Clay at 60°C

Similar to the experiments at 25°C, also at 60°C no ^{233}U(VI) (cell 3 and 4), however, diffused small HA colloids (cell 4) were detected in the receiving reservoirs.

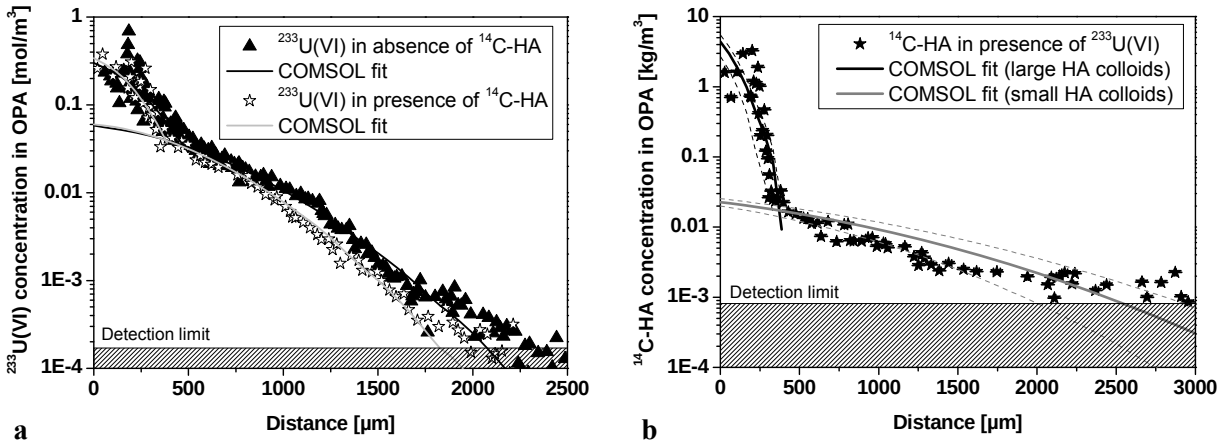

Fig. 5.4. Concentration profiles of ^{233}U(VI) in the absence (filled symbols) and presence (open symbols) of ^{14}C-HA (**a**) and of ^{14}C-HA in the presence of ^{233}U(VI) (**b**) in OPA at 60°C.

Fitting the ^{233}U(VI) diffusion profiles, it became obvious that at least two different U(VI) species are involved in the diffusion process (Fig. 5.4a). Taking into account the particle size distribution, these two species were attributed to a diffusing colloidal and aqueous U(VI) species, respectively. The colloidal U(VI) species was restricted in its migration and diffused only about 500 µm into the OPA sample. The aqueous U(VI) species was more mobile (about sixfold D_a of the colloidal species; cf. Table 5.5) and could be detected at a diffusion distance of about 2.5 mm.

In comparison to the ^{233}U(VI) diffusion at 25°C, the interaction of ^{233}U(VI) with OPA is stronger at 60°C for both U(VI) species. The fitted K_d value for the colloidal U(VI) species is one order of magnitude larger than that at 25°C. Several studies investigated the interaction of metal ions with mineral surfaces in dependence on temperature. For instance, an increased sorption at elevated temperatures was observed for Ni^{2+} and Ln^{3+} onto montmorillonite (Tertre et al., 2005) and for Eu^{3+} onto OPA (Schott et al., 2012, accepted). In the case of actinides, Fröhlich et al. (2012, submitted) described such a behavior for the Np(V) sorption onto OPA and Schmeide et al. (2012b, in preparation) for the U(VI) sorption onto OPA (cf. section 4.7).

Table 5.5. Compilation of further data of the experiments and of the best-fit parameter values. The data are based on the ^{233}U(VI) and ^{14}C-HA diffusion profiles and concentration data in the source and receiving reservoir at 60°C.

	U(VI) in the absence of HA (cell 3)		U(VI) in the presence of HA (cell 4)			
	^{233}U(VI)		^{233}U(VI)		HA	
	colloidal	aqueous	colloidal	aqueous	large colloids	small colloids
C_0(^{233}U(VI)) [mol/L]	1.00×10^{-6}		9.94×10^{-7}			
C_0(^{14}C-HA) [mg/L]	-				9.91	5.95[a]
V_0 [$\times10^{-6}$ m^3]	202.02		221.67			
t [d]	102		103			
ρ [kg/m^3]	2421		2404			
ε [–]	0.23 ± 0.07[b]		0.26 ± 0.06[b]			
α [–]	605 ± 122	109 ± 12	722 ± 120	120 ± 12	962 ± 481	3.9 ± 0.5
D_e [$\times10^{-12}$ m^2/s]	3 ± 1	3 ± 0.5	2.2 ± 0.8	2.5 ± 0.5	1.2 ± 0.8	0.35 ± 0.15
D_a [$\times10^{-14}$ m^2/s]	0.50 ± 0.07	2.8 ± 0.2	0.30 ± 0.07	2.1 ± 0.2	0.12 ± 0.02	9 ± 2
K_d [m^3/kg]	0.25 ± 0.05	0.045 ± 0.005	0.3 ± 0.05	0.05 ± 0.005	0.4 ± 0.2	0.0015 ± 0.0002

[a] Based on C_0 and the fact, that about 60% of HA colloids are < 1 kD (cf. Fig. 5.2d).

[b] Determined by HTO through-diffusion.

With increasing temperature also D_e increases. Using Eq. (5.5), concerning the U(VI) diffusion in OPA for the activation energy E_a a value of about 10 kJ/mol was estimated. Such a value seems low when compared to an E_a value for HTO of 21.1 ± 1.6 kJ/mol, for Na^+ of 21.0 ± 3.5 kJ/mol and for Cl^- of 19.4 ± 1.5 kJ/mol (Van Loon et al., 2005). This result shows that the migration of U(VI) in OPA is less influenced by temperature than the diffusion of HTO, Na^+ or Cl^-. However, the calculated activation energy is based on two temperatures and therefore only a preliminary result. More temperature-dependent measurements have to be performed to verify this value. In the future, the knowledge of the verified E_a for U(VI) in OPA would enable the calculation of D_e values at other temperatures.

The D_a values for the U(VI) diffusion in OPA at 25°C and 60°C (aqueous U(VI) species) are, considering their uncertainties, almost equal to each other. This leads to the conclusion, that the migration of U(VI) through OPA is similar at both investigated temperatures. The breakthrough of U(VI) through OPA at 25°C and at 60°C will be nearly at the same time. Based on the averaged values of the diffusion parameters at 25°C and 60°C modeling calculations were performed. In Fig. 5.5, the calculated concentration of ^{233}U(VI) in the receiving reservoir as a function of time is presented. The results show, that at 25°C and 60°C and using 11 mm thick OPA samples about 9 and 14.5 years, respectively, would be needed

for U(VI) breakthrough.

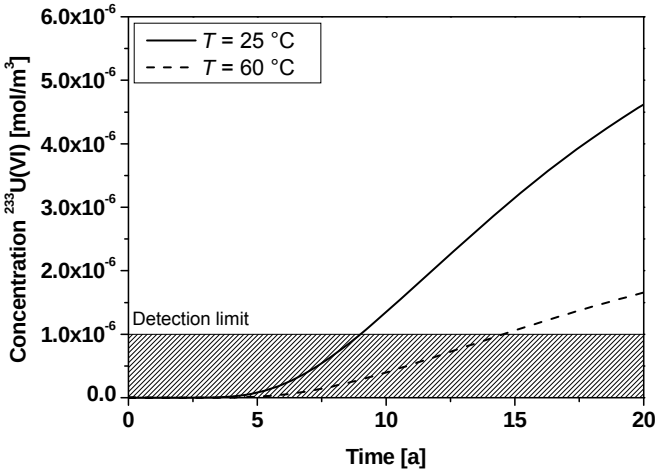

Fig. 5.5. Calculated ^{233}U(VI) concentration in the receiving reservoir as a function of time for a temperature of 25°C and 60°C, respectively.

In Fig. 5.4a, the ^{233}U(VI) diffusion profiles at 60°C in the absence and presence of HA are shown. The differences between both profiles are smaller compared to the analog profiles obtained at 25°C. This points to the fact that also at 60°C, HA has a negligible effect on the ^{233}U(VI) diffusion through OPA. Indeed, the corresponding diffusion parameter values support such a conclusion (Table 5.5).

The comparison of the U(VI) diffusion parameters in the absence and presence of HA of both U(VI) species shows, that their K_d values are slightly increased and their D_e values are slightly decreased in the presence of HA. However, within experimental uncertainties, no significant influence of HA on U(VI) diffusion at 60°C can be observed. That means, independent of temperature, HA has no significant influence on U(VI) migration through OPA. It should be mentioned, that small diffusing HA colloids have only a very minor potential for complexing and transporting U(VI).

In Fig. 5.4b, the HA diffusion through OPA at 60°C is presented. The profile is very similar to that depicted in Fig. 5.3b and shows again the presence of at least two diffusing HA size fractions. In contrast to the profile at 25°C, at 60°C the data of the large HA colloid fraction scatter over a much wider range close to the OPA boundary downstream making the fitting procedure more difficult. Presumably, this scatter results from the HA degradation process (cf. Fig. 5.2), which is taking place during the diffusion experiment and is increased at elevated temperature. The different present and formed HA degradation species show different sorption and diffusion properties resulting in a more complex HA diffusion profile in OPA. However, in this case, the interpretation of the HA profile was limited to two HA size fractions only.

However, the obtained K_d values indicate a little stronger interaction of the large HA colloid fraction with OPA at 60°C than at 25°C. For the small HA colloid fraction such an influence of temperature on K_d was not detected. Due to large uncertainties, also no effect of temperature on D_e for both HA fractions could be detected. However, the earlier detection of HA in the receiving reservoir at 60°C in comparison to the experimental findings at 25°C points to a higher D_e value for HA diffusion (small HA colloids) at 60°C.

In conclusion, diffusion experiments with $^{233}U(VI)$ in pristine samples of consolidated OPA were carried out under anaerobic conditions. The influence of both HA and elevated temperature on the $^{233}U(VI)$ diffusion was investigated.

Speciation calculations showed, that $Ca_2UO_2(CO_3)_3(aq)$ is the dominating U(VI) species in the source reservoir solution and thus, the main diffusing U(VI) species at 25°C during the whole diffusion experiment. At 60°C, particle size distribution measurements pointed to the presence of at least one colloidal and one aqueous U(VI) species in solution. For HA, a wide particle size distribution was measured, whereby a degradation process occurred which became stronger at higher temperature.

By fitting the diffusion profiles best-fit parameter values for K_d and D_e were determined. At 25°C, K_d values were obtained for U(VI) ($K_d = 0.025 \pm 0.003$ m^3/kg) and HA (large HA colloids; $K_d = 0.129 \pm 0.018$ m^3/kg) which are in good agreement with K_d values from batch sorption experiments using crushed OPA material (cf. section 4.4.2.3, Joseph et al., 2011).

In agreement with the speciation studies, at 60°C diffusion profiles of two U(VI) species were observed, which were attributed to a colloidal and an aqueous U(VI) species. The colloidal U(VI) species showed a stronger interaction with OPA. Hence, this species diffused only about 500 µm in OPA. Compared to the colloidal U(VI) species, the aqueous U(VI) species showed a weaker interaction with OPA and it penetrated deeper into the clay. However, compared to U(VI) at 25°C, both U(VI) species showed higher K_d and D_e values. Based on D_e at 25°C and 60°C, for an activation energy E_a a preliminary value of about 10 kJ/mol was determined for diffusion of U(VI) in OPA. In addition, almost equivalent D_a values were determined for the U(VI) diffusion at 25°C and 60°C (aqueous U(VI) species) through OPA. The breakthrough of U(VI) through OPA would thus be independent of temperature and occurs nearly at the same time.

All diffusion experiments showed, that the effect of HA on $^{233}U(VI)$ diffusion is negligible and independent of temperature.

The diffusion results for HA at 25°C and 60°C showed that two distinct HA size fractions – a large- and a small-sized colloid fraction – were diffusing through the OPA samples. Within

three months the high molecular size HA colloids diffused only about 500 µm into the clay, whereas the low molecular size HA colloids diffused through the entire OPA samples and were consequently detected in the receiving reservoir. These findings demonstrate the filtration effect of the compacted clay. For the large HA colloid fraction an increased K_d value was determined at 60°C compared to that at 25°C.

Regarding the suitability of OPA as host rock for a future nuclear waste repository, it can be concluded, that OPA has indeed a good retardation potential for U(VI). In this study, it could be shown, that the U(VI) diffusion behavior through OPA is comparable to that of the Np(V)/Np(IV) system. Calculations for 25°C and 60°C at a sample thickness of 11 mm show that it would need about 9 and 14.5 years, respectively, for U(VI) breakthrough. Thereby, humic substances being ubiquitous in soils and sediments and which show good complexation abilities for cations, have only a minor influence on U(VI) migration through OPA even at elevated temperatures.

6 Summary and outlook

The objective of this project was the study of basic interaction processes in the systems actinide - clay organics - aquifer and actinide - natural clay - clay organics - aquifer. Thus, the studies performed can be divided into complexation, redox, sorption and diffusion studies.

The complexation of Am(III), U(IV) and U(VI) with a variety of ligands in aqueous systems was studied by means of various spectroscopic techniques, such as UV-Vis absorption spectroscopy, attenuated total reflection Fourier-transform infrared (ATR FT-IR) spectroscopy as well as time-resolved laser-induced fluorescence spectroscopy (TRLFS). The TRLFS measurements were performed both in the temperature range between 7 and 65°C and at cryogenic temperature (-120°C, cryo-TRLFS). Furthermore, TRLFS with femtosecond laser pulses (fs-TRLFS) was applied.

One objective of the complexation studies was the identification of further humic acid functional groups that contribute to the actinide complexation beside the oxygen containing functional groups that are generally acknowledged as the main complexing sites of humic substances. For this, simple organic model ligands that can occur as humic acid building blocks (e.g., anthranilic, nicotinic, picolinic, phenylphosphonic, benzenesulfonic and 4-hydroxybenzenesulfonic acid as well as phthalic acid for comparison) were applied to study

the influence of nitrogen, phosphorus and sulfur containing functional groups on the complexation of actinides in different oxidation states (Am(III) and U(VI)). The complexation of Am(III) with anthranilic, nicotinic, picolinic and phthalic acid in aqueous solution was studied for the first time. The results show that Am(III) is mainly coordinated via carboxylic groups, however, probably stabilized by nitrogen groups. The studies of the U(VI) complexation with the nitrogen and sulfur containing ligands show that the U(VI) complexation is dominated by carboxylic groups. The complexation strength of aromatic phosphonate groups toward U(VI) is comparable or even higher than that of carboxylic groups. Thus, the phosphorus containing functional groups may contribute to the U(VI) complexation by humic acid, however, due to the low phosphorus concentration in humic acid also this functionality plays only a subordinate role compared to carboxylic groups. The humate complexation of Am(III) should be more influenced by nitrogen containing functional groups than that of U(VI).

These model investigations on actinide complexation by various functional groups were extended by studying the role of sulfur functionalities of humic acid for the U(VI) complexation applying synthetic humic acid model substances with varying sulfur contents (0 to 6.9 wt.%). These were synthesized based on the melanoidin concept. The results have shown that sulfur functionalities can be involved in U(VI) humate complexation, however, at environmentally relevant sulfur concentrations in humic acid (0-2 wt.%), reduced sulfur functionalities play only a subordinate role for the U(VI) complexation compared to carboxylic groups.

A further objective of the complexation studies was the determination of complex formation constants not known so far or their validation by complementary spectroscopic methods to improve the thermodynamic database. Thus, the U(IV) complexation with citric, succinic, mandelic and glycolic acid was studied at room temperature. Especially the interaction between U(IV) and citric acid was found to be very strong ($\log \beta_{101} = 13.5 \pm 0.2$ and $\log \beta_{102} = 25.1 \pm 0.2$). However, also the other ligands are able to increase the solubility and thus, the mobility of U(IV) in aquatic systems due to complex formation. The U(VI) complexation with lactic acid was studied in the temperature range 7 to 65°C. Thermodynamic parameters of the U(VI) lactate system were determined by absorption and fluorescence spectroscopy. The complex stability constants of the U(VI) lactate complexes (UO_2Lac^+, $UO_2(Lac)_2$) were found to increase with increasing temperature. The complexation of U(VI) with lactate is endothermic (ΔH pos.) and entropy-driven (ΔS pos.). In contrast, the

complex stability constants determined for the U(VI) humate complexation at 20 and 40°C are comparable, however, decrease at 60°C.

For the first time, luminescence emission properties and complex formation constants were determined for aqueous U(VI) citrate and oxalate species in the acidic pH range by cryo-TRLFS (-120°C). The stability constants determined for these species at cryogenic temperature are in good agreement with those determined by TRLFS measurements at room temperature and moreover, validate the existing data base. Generally, the U(VI) citrate and oxalate complexes are stronger than the U(VI) lactate complexes. Thus, their influence on the U(VI) migration should be stronger than that of lactate.

For the first time, the U(VI) complexation by humic acid was studied in the presence of carbonate applying cryo-TRLFS and ATR FT-IR spectroscopy. The formation of a ternary U(VI) carbonato humate complex of the type $UO_2(CO_3)_2HA(II)^{4-}$ was detected. The complex formation constant was determined with $\log \beta_{0.1\ M} = 24.57 \pm 0.17$. Speciation calculations for the alkaline pH range show that at humic acid concentrations > 2 mg/L, the U(VI) speciation changes from predominantly $UO_2(CO_3)_3^{4-}$ to predominantly $UO_2(CO_3)_2HA(II)^{4-}$. It can be concluded that under environmentally relevant conditions in the presence of humic acid the formation of the ternary U(VI) carbonato humate complex can significantly influence the U(VI) speciation.

The role of humic acid sulfur functionalities for the Np(V) reduction in aqueous solution was studied applying synthetic humic acid model substances with varying sulfur contents (0 to 6.9 wt.%). The results have shown that in addition to quinone-like moieties and non-quinoid phenols that dominate the redox behavior of humic substances, sulfur functional groups act as further redox-active sites in humic substances toward Np. However, in nature the extent of the contribution of sulfur functional groups to the overall redox capacity of humic substances is expected to be less pronounced since the content of sulfur functionalities in natural humic substances is low compared to other redox-active functional units. Moreover, the ratio of reduced to total sulfur functional groups is lower in most natural humic substances.

The sorption and diffusion studies within this project focused on the natural clay ‘Opalinus Clay’ from the Mont Terri underground laboratory, Switzerland. The U(VI) sorption onto crushed Opalinus Clay was investigated in the absence and presence of humic acid or low

molecular weight organic acids, in dependence on temperature. Thereby, Opalinus Clay pore water was used as background electrolyte. The results show that the U(VI) sorption onto Opalinus Clay is low and not influenced by humic acid (≤ 50 mg/L). This can be attributed to the dissolution of calcite, a mineral constituent of the clay. The resulting calcium ions in the pore water influence both the U(VI) speciation and the speciation of humic acid. Thus, the U(VI) speciation in pore water is dominated by the neutral $Ca_2UO_2(CO_3)_3(aq)$ complex both in the absence and presence of humic acid. The humic acid speciation is predominated by the CaHA(II) complex. Distribution coefficients, K_d, for the sorption of U(VI) and humic acid onto Opalinus Clay were determined with (0.0222 ± 0.0004) m^3/kg and (0.129 ± 0.006) m^3/kg, respectively. These values were confirmed by diffusion experiments using compacted Opalinus Clay.

In contrast to humic acid, low molecular weight organic acids ($\geq 1\times10^{-5}$ M) are able to decrease U(VI) sorption due to complex formation in solution. The mobilizing effect of the organic ligands on U(VI) increases in the following sequence: formate < lactate ≈ acetate ≤ propionate < tartrate < citrate. The influence of the organic ligands on the U(VI) sorption onto Opalinus Clay correlates with the stability of the respective U(VI) complexes.

In the absence of organic ligands, the U(VI) sorption onto Opalinus Clay increases with increasing temperature. For U(VI), an apparent endothermic sorption enthalpy was determined with 34 ± 1 kJ/mol. The stronger U(VI) sorption onto Opalinus Clay with increasing temperature is maintained also in the presence of lactate and citrate, when present in the concentration range from 1×10^{-5} to 1×10^{-2} M.

The studies of the U(VI) sorption onto Opalinus Clay performed in Opalinus Clay pore water as well as the pH-dependent studies in 0.1 M $NaClO_4$ lead to a better process understanding. Furthermore, the obtained sorption results contribute to the thermodynamic sorption database used for modeling the geochemical interaction processes of actinide ions and potential host rocks for nuclear waste repositories.

The U(VI) diffusion in compacted Opalinus Clay was studied in the absence and presence of humic acid at 25 and 60°C under anaerobic conditions using synthetic Opalinus Clay pore water. The objective was to determine U(VI) migration in Opalinus Clay as well as the influence of humic acid and temperature on U(VI) migration. The diffusion and distribution coefficients (D_e and K_d) determined for U(VI) and humic acid at 25 and 60°C show that humic acid has no significant influence on the U(VI) diffusion. The diffusion profiles obtained for humic acid in Opalinus Clay at 25 and 60°C show the contributions of at least

two different humic acid particle size fractions (< 1 kD and 10-100 kD). The smaller humic acid fraction diffused through the whole Opalinus Clay samples at both temperatures within three months whereas the larger humic acid fraction diffused only about 500 µm into the clay. This shows a filtration effect of the compacted clay and also the different sorption affinity of the humic acid size fractions toward Opalinus Clay. At 60°C, the diffusion profiles of two U(VI) species were observed, which were attributed to a colloidal and an aquatic U(VI) species. The colloidal U(VI) species and the large humic acid colloid fraction showed a stronger interaction with the clay at 60°C. In addition, the D_e value of the aquatic U(VI) species increased with increasing temperature. Altogether, predictions of the U(VI) diffusion show that an increase of the temperature to 60°C does not accelerate the migration of U(VI) through Opalinus Clay. With regard to uranium-containing waste, it can be concluded that Opalinus Clay is suitable as host rock for a future nuclear waste repository since Opalinus Clay has a good retardation potential for U(VI).

The U(VI) sorption and especially the U(VI) diffusion experiments contribute to a more realistic description of the migration behavior of U(VI) in the natural clay rock Opalinus Clay since the obtained parameters can be used for modeling the actinide migration through argillaceous rocks in the absence and presence of clay organics in the temperature range up to 60°C. This leads to an improved risk assessment for potential nuclear waste repositories.

Building on the complexation, sorption and diffusion studies performed so far, future studies should focus on the geochemical behavior of radionuclides and especially actinides in solutions with higher ionic strength as relevant for potential nuclear waste repositories in clay formations in the north of Germany as well as in salt rock. Thus, the complexation of actinides with relevant clay organics has to be studied at higher salinities and partly at higher temperatures. Furthermore, actinide sorption and diffusion on/in natural clay rock (Opalinus Clay) and clay minerals (e.g., illite, montmorillonite) have to be investigated in the absence and presence of clay organics at higher salinities and exemplarily also at higher temperatures. With regard to sorption and migration, beside quantitative parameters also the speciation of the formed surface complexes has to be determined by means of spectroscopic methods. In addition, the influence of higher salinities on the retention capacity of potential container corrosion products (secondary iron (hydro)oxides such as magnetite or green rust) for actinides has to be quantified.

7 References

Acker, M. (2003) Zeitaufgelöste laserinduzierte Fluoreszenzspektroskopie mit ultrakurzen Anregungspulsen und ihre Anwendung zur Untersuchung der Fluoreszenzeigenschaften von gelösten Huminstoffen, Protocatechusäure und deren U(VI)komplexen, PhD Thesis, TU Dresden, Dresden.

Aeschbacher, M., Vergari, D., Schwarzenbach, R.P. and Sander, M. (2011) Electrochemical analysis of proton and electron transfer equilibria of the reducible moieties in humic acids. Environ. Sci. Technol. **45**, 8385-8394.

Alcock, N.W., Kemp, T.J., Roe, S.M. and Leciejewicz, J. (1996a) The roles of N- and O-coordination in the crystal and molecular structures of uranyl complexes with anthranilic and pyrazinic acids. Inorg. Chim. Acta **248**, 241-246.

Alcock, N.W., Errington, W., Kemp, T.J. and Leciejewicz, J. (1996b) Diaquadioxobis(pyridine-3-carboxylato)-uranium(VI). Acta Cryst. C **52**, 615-617.

Amayri, S., Buda, R.A., Fröhlich, D., Heinrich, J., Klimach, T., Kratz, J.V., Reich, T., Trautmann, N. and Wunderlich, T. (2008) Sorption of actinides (Th, U, Np, Pu, Am) on Opalinus Clay in synthetic porewater. NRC 7, Budapest, Hungary.

Artinger, R., Rabung, T., Kim, J.I., Sachs, S., Schmeide, K., Heise, K.H., Bernhard, G. and Nitsche, H. (2002) Humic colloid-borne migration of uranium in sand columns. J. Contam. Hydrol. **58**, 1-12.

Bargar, J.R., Reitmeyer, R., Lenhart, J.J. and Davis, J.A. (2000) Characterization of U(VI)-carbonato ternary complexes on hematite: EXAFS and electrophoretic mobility measurements. Geochim. Cosmochim. Acta **64**, 2737-2749.

Bauer, A., Fiehn, B., Marquardt, C.M., Klein, M., Römer, J., Schäfer, T., Görtzen, A. and Kienzler, B. (2006) Results on the Pu Diffusion in the Opalinus Clay. 6th EC FP - FUNMIG IP, Stockholm, Schweden.

Beck, H.P., Wagner, H., Gottfreund, T. and Zeitz, M. (2004) Investigations of the behaviour of the heavy elements Cu, Zn, Cd, and Pb in the ternary system metal - humic acid - sand. In: Wissenschaftliche Berichte, FZK-6999, C.M. Marquardt (Ed.), Forschungszentrum Karlsruhe, Karlsruhe, pp. 155-156.

Beneš, P., Kratzer, K., Vlčková, Š. and Šebestová, E. (1998) Adsorption of uranium on clay and the effect of humic substances. Radiochim. Acta **82**, 367-373.

Bernhard, G., Geipel, G., Reich, T., Brendler, V., Amayri, S. and Nitsche, H. (2001) Uranyl(VI) carbonate complex formation: Validation of the $Ca_2UO_2(CO_3)_3$(aq.) species. Radiochim. Acta **89**, 511-518.

Bernhard, G. and Geipel, G. (2007) Bestimmung der Bindungsform des Urans in Mineralwässern. Vom Wasser **105**, 7-10.

Bertrand, P.A. and Choppin, G.R. (1982) Separation of actinides in different oxidation-states by solvent-extraction. Radiochim. Acta **31**, 135-137.

Billard, I., Ansoborlo, E., Apperson, K., Arpigny, S., Azenha, M.E., Birch, D., Bros, P., Burrows, H.D., Choppin, G., Couston, L., Dubois, V., Fanghänel, T., Geipel, G., Hubert, S., Kim, J.I., Kimura, T., Klenze, R., Kronenberg, A., Kumke, M., Lagarde, G., Lamarque, G., Lis, S., Madic, C., Meinrath, G., Moulin, C., Nagaishi, R., Parker, D., Plancque, G., Scherbaum, F., Simoni, E., Sinkov, S. and Viallesoubranne, C. (2003) Aqueous solutions of uranium(VI) as studied by time-resolved emission spectroscopy: A round-robin test. Appl. Spectrosc. **57**, 1027-1038.

Binstead, R.A., Zuberbühler, A.D. and Jung, B. (2005) SPECFIT - Global Analysis System. Version 3.0.37, Spectrum Software Associates, Marlborough.

Bonin, L., Den Auwer, Ch., Ansoborlo, E., Cote, G. and Moisy, P. (2007) Study of Np speciation in citrate medium. Radiochim. Acta **95**, 371-379.

Bonin, L., Cote, G. and Moisy, Ph. (2008) Speciation of An(IV) (Pu, Np, U and Th) in citrate media. Radiochim. Acta **96**, 145-152.

Bossart, P. and Thury, M. (2008) Mont Terri Rock Laboratory. Project, Programme 1996 to 2007 and Results. Reports of the Swiss Geological Survey No. 3, Swiss Geological Survey.

Bradbury, M.H. and Baeyens, B. (2006) Modelling sorption data for the actinides Am(III), Np(V) and Pa(V) on montmorillonite. Radiochim. Acta **94**, 619-625.

Brady, P.V., Cygan, R.T. and Nagy, K.L. (1996) Molecular controls on kaolinite surface charge. J. Colloid Interface Sci. **183**, 356-364.

Brand, R.A. (1987) Improving the validity of hyperfine fields distributions from magnetic-alloys. 1. Unpolarized source Nucl. Instrum. Methods Phys. Res., Sect. B **28**, 398-416.

Brasser, T., Droste, J., Müller-Lyda, I., Neles, J.M., Sailer, M., Schmidt, G. and Steinhoff, M. (2008) Endlagerung wärmeentwickelnder radioaktiver Abfälle in Deutschland. GRS - 247, Öko-Institut and Gesellschaft für Anlagen- und Reaktorsicherheit (GRS).

Bräse, S., Bülle, J. and Hüttermann, A. (2007) Organische und bioorganische Chemie. Das Basiswissen für Master- und Diplomprüfungen, Wiley-VCH, Weinheim.

Budantseva, N.A., Andreev, G.B., Fedoseev, A.M., Antipin, M.Y. and Krupa, J.-C. (2006) Interaction of neptunium(V) with picolinic, nicotinic and isonicotinic acids. Radiochim. Acta **94**, 69-74.

Cerfontain, H., Koeberg-Telder, A. and Kruk, C. (1975) Solutes in Sulfuric-Acid. 7. Ionization of benzenesulfonic acid; determination of pK_{BH} by ^{13}C NMR. Tetrahedron Lett. **42**, 3639-3642.

Choppin, G.R. (1992) The role of natural organics in radionuclide migration in natural aquifer systems. Radiochim. Acta **58**, 113-120.

Choppin, G.R. (2006) Actinide speciation in aquatic systems. Marine Chem. **99**, 83-92.

Claret, F., Schäfer, T., Bauer, A. and Buckau, G. (2003) Generation of humic and fulvic acid from Callovo-Oxfordian Clay under high alkaline conditions. Sci. Total Environ. **317**, 189-200.

COMSOL (2008) Multiphysics 3.5a. Finite-element software package. http://www.comsol.com.

Cory, R.M. and McKnight, D.M. (2005) Fluorescence spectroscopy reveals ubiquitous presence of oxidized and reduced quinones in dissolved organic matter. Environ. Sci. Technol. **39**, 8142-8149.

Courdouan, A., Christl, I., Meylan, S., Wersin, P. and Kretzschmar, R. (2007) Characterization of dissolved organic matter in anoxic rock extracts and in situ pore water of the Opalinus Clay. Appl. Geochem. **22**, 2926-2939.

Courdouan, A., Christl, I., Rabung, T., Wersin, P. and Kretzschmar, R. (2008) Proton and trivalent metal cation binding by dissolved organic matter in the Opalinus Clay and the Callovo-Oxfordian formation. Environ. Sci. Technol. **42**, 5985-5991.

Croué, J.P., Benedetti, M.F., Violleau, D. and Leenheer, J.A. (2003) Characterization and copper binding of humic and nonhumic organic matter isolated from the south platte river: Evidence for the presence of nitrogenous binding site. Environ. Sci. Technol. **37**, 328-336.

Czerwinski, K.R., Buckau, G., Scherbaum, F. and Kim, J.I. (1994) Complexation of the uranyl ion with aquatic humic acid. Radiochim. Acta **65**, 111-119.

Dean, J.A. (1999). Lange's handbook of chemistry. McGraw-Hill, Inc., New York.

Denecke, M.A., Pompe, S., Reich, T., Moll, H., Bubner, M., Heise, K.H., Nicolai, R. and Nitsche, H. (1997) Measurements of the structural parameters for the interaction of uranium(VI) with natural and synthetic humic acids using EXAFS. Radiochim. Acta **79**, 151-159.

Denecke, M.A., Panak, P.J., Burdet, F., Weigl, M., Geist, A., Klenze, R., Mazzanti, M. and Gompper K. (2007) A comparative spectroscopic study of U(III)/Am(III) and Ln(III) complexed with N-donor ligands. C. R. Chimie **10**, 872-882.

Dierckx, A., Maes, A. and Vancluysen, J. (1994) Mixed complex-formation of Eu^{3+} with humic acid and a competing ligand. Radiochim. Acta **66**, 149-156.

Dodge, C.J. and Francis, A.J. (1997) Biotransformation of binary and ternary citric acid complexes of iron and uranium. Environ. Sci. Technol. **31**, 3062-3067.

Dong, H.T., Du, H.B., Wickramasinghe, S.R. and Qian, X.H. (2009) The Effects of Chemical Substitution and Polymerization on the pK_a Values of Sulfonic Acids. J. Phys. Chem. B **113**, 14094-14101.

Dong, W.M. and Brooks, S.C. (2006) Determination of the formation constants of ternary complexes of uranyl and carbonate with alkaline earth metals (Mg^{2+}, Ca^{2+}, Sr^{2+}, and Ba^{2+}) using anion exchange method. Environ. Sci. Technol. **40**, 4689-4695.

Dreissig, I., Weiss, S., Hennig, C., Bernhard, G. and Zänker, H. (2011) Formation of uranium(IV)-silica colloids at near-neutral pH. Geochim. Cosmochim. Acta **75**, 352-367.

Durbin, P.W., Kullgren, B., Xu, J. and Raymond, K.N. (1998) Development of decorporation agents for the actinides. Rad. Protec. Dos. **79**, 433-443.

Eisenberg, D. and Kauzmann, W. (1969). The structure and properties of water. Oxford University Press, Ely House, London.

Felmy, A.R., Cho, H., Dixon, D.A., Xia, Y., Hess, N.J. and Wang, Z. (2006) The aqueous complexation of thorium with citrate under neutral to basic conditions. Radiochim. Acta **94**, 205-212.

Fimmen, R.L., Cory, R.M., Chin, Y.-P., Trouts, T.D. and McKnight, D.M. (2007) Probing the oxidation-reduction properties of terrestrially and microbially derived dissolved organic matter. Geochim. Cosmochim. Acta **71**, 3003-3015.

Fox, P.M., Davis, J.A. and Zachara, J.M. (2006) The effect of calcium on aqueous uranium(VI) speciation and adsorption to ferrihydrite and quartz. Geochim. Cosmochim. Acta **70**, 1379-1387.

Freundlich, H. (1906) Concerning adsorption in solutions. Z. Phys. Chem. Stoechiom. Verwandtschafts. **57**, 385-470.

Fröhlich, D.R., Amayri, S., Drebert, J. and Reich, T. (2012, submitted) Influence of temperature and background electrolyte on the sorption of neptunium(V) on Opalinus Clay. Appl. Clay Sci.

Gaffney, J.S., Marley, N.A. and Clark, S.B. (1996) Humic and fulvic acids - Isolation, structure and environmental role, American Chemical Society.

Gampp, H., Maeder, M., Meyer, C.J. and Zuberbühler, A.D. (1985) Calculation of equilibrium-constants from multiwavelength spectroscopic data. 2. SPECFIT - 2 user-friendly programs in basic and standard fortran-77. Talanta **32**, 257-264.

Geipel, G., Acker, M., Vulpius, D., Bernhard, G., Nitsche, H. and Fanghänel, Th. (2004) An ultrafast time-resolved fluorescence spectroscopy system for metal ion complexation studies with organic ligands. Spectrochim. Acta Part A **60**, 417-424.

Glaus, M.A., Hummel, W. and van Loon, L.R. (1995) Stability of mixed-ligand complexes of metal-ions with humic substances and low-molecular-weight ligands. Environ. Sci. Technol. **29**, 2150-2153.

Glaus, M.A., Baeyens, B., Lauber, M., Rabung, T. and Van Loon, L.R. (2005) Influence of water-extractable organic matter from Opalinus Clay on the sorption and speciation of Ni(II), Eu(III) and Th(IV). Appl. Geochem. **20**, 443-451.

Glaus, M.A., Rossé, R., Van Loon, L.R. and Yaroshchuk, A.E. (2008) Tracer diffusion in sintered stainless steel filters: measurement of effective diffusion coefficients and implications for diffusion studies with compacted clays. Clay Clay Min. **56**, 677-685.

Glorius, M., Moll, H. and Bernhard, G. (2007) Complexation of uranium(VI) with aromatic acids in aqueous solution – a comparison of hydroxamic acids and benzoic acid. Radiochim. Acta **95**, 151-157.

Glorius, M., Moll, H., Geipel, G. and Bernhard, G. (2008) Complexation of uranium(VI) with aromatic acids such as hydroxamic and benzoic acid investigated by TRLFS. J. Radioanal. Nucl. Chem. **277**, 371-377.

González-Sánchez, F., Van Loon, L.R., Gimmi, T., Jakob, A., Glaus, M.A. and Diamond, L.W. (2008) Self-diffusion of water and its dependence on temperature and ionic strength in highly compacted montmorillonite, illite and kaolinite. Appl. Geochem. **23**, 3840-3851.

Guillaumont, D. (2006) Actinide(III) and lanthanide(III) complexes with nitrogen ligands: Counterions and ligand substitutent effects on the metal-ligand bond. Theochem - J. Molec. Struct. **771**, 105-110.

Guillaumont, R., Fanghänel, Th., Fuger, J., Grenthe, I., Neck, V., Palmer, D.A. and Rand, M.H. (2003) Update on the Chemical Thermodynamics of Uranium, Neptunium, Plutonium, Americium and Technetium. Chemical Thermodynamics Vol. 5. (OECD Nuclear Energy Agency, ed.) Elsevier, Amsterdam.

Günther, A., Geipel, G. and Bernhard, G. (2007) Complex formation of uranium(VI) with the amino acids L-glycine and L-cysteine: A fluorescence emission and UV-Vis absorption study. Polyhedron **26**, 59-65.

Günther, A., Steudtner, R., Schmeide, K. and Bernhard, G. (2011) Luminescence properties of uranium(VI) citrate and uranium(VI) oxalate species and their application in the determination of complex formation constants. Radiochim. Acta **99**, 535-541.

Hartmann, E., Geckeis, H., Rabung, T., Lützenkirchen, J. and Fanghänel, T. (2008) Sorption of radionuclides onto natural clay rocks. Radiochim. Acta **96**, 699-707.

He, Z., Ohno, T., Cade-Menum, B.J., Erich, M.S. and Honeycutt, C.W. (2006) Spectral and chemical characterization of phosphates associated with humic substances. Soil Sci. Soc. Am. J. **70**, 1741-1751.

Heitzmann, M., Bravard, F., Gateau, C., Boubals, N., Berthon, C., Pécaut, J., Charbonnel, M.-C. and Delangle, P. (2009) Comparison of two tetrapodal N,O ligands: Impact of the softness of the heterocyclic N-donors pyridine and pyrazine on the selectivity for Am(III) over Eu(III). Inorg. Chem. **48**, 246-256.

Helburn, R.S. and MacCarthy, P. (1994) Determination of some redox properties of humic acid by alkaline ferricyanide titration. Anal. Chim. Acta **295**, 263-272.

Hesterberg, D., Chou, J.W., Hutchison, K.J. and Sayers, D.E. (2001) Bonding of Hg(II) to reduced organic sulfur in humic acid as affected by S/Hg ratio. Environ. Sci. Technol. **35**, 2741-2745.

Hummel, W., Anderegg, G., Rao, L., Puigdomènech, I. and Tochiyama, O. (2005) Chemical Thermodynamics of Compounds and Complexes of U, Np, Pu, Am, Tc, Se, Ni and Zr with Selected Organic Ligands. Chemical Thermodynamics Vol. 9. (OECD Nuclear Energy Agency, ed.) Elsevier, Amsterdam.

Hutchison, K.J., Hesterberg, D. and Chou, J.W. (2001) Stability of reduced organic sulfur in humic acid as affected by aeration and pH. Soil Sci. Soc. Am. J. **65**, 704-709.

Jain, A., Yadav, K., Mohopatra, M., Godbole, S.V. and Tomar, B.S. (2009) Spectroscopic investigation on europium complexation with humic acid and its model compounds. Spectrochim. Acta Part A **72**, 1122-1126.

Jakob, A., Pfingsten, W. and Van Loon, L. (2009) Effects of sorption competition on caesium diffusion through compacted argillaceous rock. Geochim. Cosmochim. Acta **73**, 2441-2456.

Johnson, L.H., Niemeyer, M., Klubertanz, G., Siegel, P. and Gribi, P. (2002) Calculations of the temperature evolution of a repository for spent fuel, vitrified high-level waste and intermediate level waste in Opalinus Clay. Technical Report 01-04, Nagra, Wettingen.

Jolivet, J.P., Thomas, Y., Taravel, B. and Lorenzelli, V. (1980) Vibrational study of coordinated CO_3^{2-} ions. J. Mol. Struct. **60**, 93-98.

Joseph, C., Raditzky, B., Schmeide, K., Geipel, G. and Bernhard, G. (2008) Complexation of Uranium by Sulfur and Nitrogen Containing Model Ligands in Aqueous Solution. In: Uranium Mining and Hydrogeology, B. J. Merkel and A. Hasche-Berger (Eds.), Springer, Berlin, pp. 539-548.

Joseph, C., Schmeide, K., Sachs, S. and Bernhard, G. (2009) Uranium(VI) and humic acid sorption onto kaolinite and Opalinus Clay. Annual Report 2008, FZD-511, Forschungszentrum Dresden-Rossendorf, Institute of Radiochemistry, 47.

Joseph, C., Schmeide, K., Sachs, S., Brendler, V., Geipel, G. and Bernhard, G. (2011) Sorption of uranium(VI) onto Opalinus Clay in the absence and presence of humic acid in Opalinus Clay pore water. Chem. Geol. **284**, 240-250.

Joseph, C., Schmeide, K., Sachs, S., Stockmann, M., Brendler, V. and Bernhard, G. (2012a, in preparation) Sorption of U(VI) onto Opalinus Clay: Effects of pH and humic acid. Appl. Clay Sci.

Joseph, C., Van Loon, L.R., Jakob, A., Schmeide, K., Sachs, S. and Bernhard, G. (2012b, in preparation) Diffusion of U(VI) in Opalinus Clay: Influence of temperature and humic acid. Geochim. Cosmochim. Acta.

Kerisit, S. and Liu, C.X. (2010) Molecular simulation of the diffusion of uranyl carbonate species in aqueous solution. Geochim. Cosmochim. Acta **74**, 4937-4952.

Kim, J.I. (1986) Chemical behaviour of transuranic elements in natural aquatic systems, Handbook on the Physics and Chemistry of the Actinides, Elsevier.

Kim, J.I. and Czerwinski, K.R. (1996) Complexation of metal ions with humic acid: Metal ion charge neutralization model. Radiochim. Acta **73**, 5-10.

Kim, J.I. (2006) Significance of actinide chemistry for the long-term safety of waste disposal. Nucl. Eng. Technol. **38**, 459-482.

Koban, A. and Bernhard, G. (2007) Uranium(VI) complexes with phospholipid model compounds – a laser spectroscopic study. J. Inorg. Biochem. **101**, 750-757.

Kolokassidou, C., Pashalidis, I., Costa, C.N., Efstathiou, A.M. and Buckau, G. (2007). Thermal stability of solid and aqueous solutions of humic acid. Thermochim. Acta **454**, 78-83.

Kornilovich, B., Pshinko, G., Spasenova, L. and Kovalchuk, I. (2000) Influence of humic substances on the sorption interactions between lanthanide and actinide ions and clay minerals. Adsorpt. Sci. Technol. **18**, 873-880.

Kowal-Fouchard, A., Drot, R., Simoni, E. and Ehrhardt, J.J. (2004) Use of spectroscopic techniques for uranium(VI)/montmorillonite interaction modeling. Environ. Sci. Technol. **38**, 1399-1407.

Křepelová, A., Sachs, S. and Bernhard, G. (2006) Uranium(VI) sorption onto kaolinite in the presence and absence of humic acid. Radiochim. Acta **94**, 825-833.

Křepelová, A., Reich, T., Sachs, S., Drebert, J. and Bernhard, G. (2008) Structural characterization of U(VI) surface complexes on kaolinite in the presence of humic acid using EXAFS spectroscopy. J. Colloid Interface Sci. **319**, 40-47.

Kurková, M., Klika, Z., Kliková, C. and Havel, J. (2004) Humic acids from oxidized coals. I. Elemental composition, titration curves, heavy metals in HA samples, nuclear magnetic resonance spectra of HAs and infrared spectroscopy. Chemosphere **54**, 1237-1245.

Kwak, E.-J. and Lim, S.-I. (2004) The effect of sugar, amino acid, metal ion, and NaCl on model Maillard reaction under pH control. Amino Acids **27**, 85-90.

Lefevre, G., Kneppers, J. and Fedoroff, M. (2008) Sorption of uranyl ions on titanium oxide studied by ATR-IR spectroscopy. J. Colloid Interface Sci. **327**, 15-20.

Lindberg, B.J., Hamrin, K., Johansson, G., Gelius, U., Fahlmann, A., Nordling, C. and Siegbahn, K. (1970) Molecular spectroscopy by means of ESCA. II. Sulfur compounds. Correlation of electron binding with structure. Phys. Scripta **1**, 286-298.

Lippold, H., Mansel, A. and Kupsch, H. (2005) Influence of trivalent electrolytes on the humic colloid-borne transport of contaminant metals: competition and flocculation effects. J. Contam. Hydrol. **76**, 337-352.

Lippold, H., Evans, N.D.M., Warwick, P. and Kupsch, H. (2007) Competitive effect of iron(III) on metal complexation by humic substances: Characterisation of ageing processes. Chemosphere **67**, 1050-1056.

Lippold, H. and Lippmann-Pipke, J. (2009) Effect of humic matter on metal adsorption onto clay materials: Testing the linear additive model. J. Contam. Hydrol. **109**, 40-48.

Lovley, D.R., Coates, J.D., Blunt-Harries, E.L., Phillips, E.J.P. and Woodward, J.C. (1996) Humic substances as electron acceptors for microbial respiration. Nature **382**, 445-448.

Mahmoud, M.R., Ibrahim, S.A., Hassan, A.M.A. and Ahmed, I.T. (1996) Ternary complexes of N-(2-acetamido)iminodiacetic acid and some aromatic acids. Isolation and stability constants in solution. Transition Met. Chem. **21**, 1-4.

Majzik, A. and Tombacz, E. (2007) Interaction between humic acid and montmorillonite in the presence of calcium ions I. Interfacial and aqueous phase equilibria: Adsorption and complexation. Org. Geochem. **38**, 1319-1329.

Makarov, M.I. (1997) Phosphorus compounds of soil humic acids. Eurasian Soil Sci. **30**, 395-402.

Makarov, M.I. (2005) Phosphorus-containing components of soil organic matter: P-31 NMR spectroscopic study (a review). Eurasian Soil Sci. **38**, 153-164.

Mansel, A., Crustewitz, C. and Kupsch, H. (2003) Geochemische Untersuchungen zur Retention von reaktiven Kohlenstoffverbindungen für toxische Schwermetalle. Abschlussbericht, Universität Leipzig, Institut für Interdisziplinäre Isotopenforschung.

Marquardt, C., Herrmann, G. and Trautmann, N. (1996) Complexation of neptunium(V) with humic acids at very low metal concentrations. Radiochim. Acta **73**, 119-125.

Martell, A.E., Smith, R.M. and Motekaitis, R.J. (1998) NIST Critically Selected Stability Constants of Metal Complexes Database, Version 5.0.

Martell, A.E., Smith, R.M. and Motekaitis, R.J. (2003) NIST Critically Selected Stability Constants of Metal Complexes Database, Version 7.0.

McCarthy, J.F., Czerwinski, K.R., Sanford, W.E., Jardine, P.M. and Marsh, J.D. (1998) Mobilization of transuranic radionuclides from disposal trenches by natural organic matter. J. Contam. Hydrol. **30**, 49-77.

Meleshyn, A., Azeroual, M., Reeck, T., Houben, G., Riebe, B. and Bunnenberg, C. (2009) Influence of (Calcium-)Uranyl-Carbonate Complexation on U(VI) Sorption on Ca- and Na-Bentonites. Environ. Sci. Technol. **43**, 4896-4901.

Merkusheva, S.A., Kumok, V.N. and Skorik, N.A. (1970) Radiokhim. **12**, 175-178.

Mibus, J. and Sachs, S. (2006) Impact of humic colloids on uranium(VI) migration in clay. Annual Report 2005, FZR-443, Forschungszentrum Rossendorf, 60.

Mibus, J., Müller, C., Sachs, S. and Küchler, R. (2007a) Determination of diffusion coefficients of humic acid in bulk water. Annual Report 2006, FZD-459, Forschungszentrum Dresden-Rossendorf, 63.

Mibus, J., Sachs, S., Pfingsten, W., Nebelung, C. and Bernhard, G. (2007b) Migration of uranium(IV)/(VI)in the presence of humic acids in quartz sand: A laboratory column study. J. Contam. Hydrol. **89**, 199-217.

Moll, H., Geipel, G., Reich, T., Bernhard, G., Fanghänel, T. and Grenthe, I. (2003) Uranyl(VI) complexes with alpha-substituted carboxylic acids in aqueous solution. Radiochim. Acta **91**, 11-20.

Montavon, G., Mansel, A., Seibert, A., Keller, H., Kratz, J.V. and Trautmann, N. (2000) Complexation studies of UO_2^{2+} with humic acid at low metal ion concentrations by indirect speciation methods. Radiochim. Acta **88**, 17-24.

Morgenstern, M., Klenze, R. and Kim, J.I. (2000) The formation of mixed-hydroxo complexes of Cm(III) and Am(III) with humic acid in the neutral pH range. Radiochim. Acta **88**, 7-16.

Morris, K.F., Cutak, B.J., Dixon, A.M. and Larive, C.K. (1999) Analysis of diffusion coefficient distributions in humic and fulvic acids by means of diffusion ordered NMR spectroscopy. Anal. Chem. **71**, 5315-5321.

Moulin, V., Robouch, P., Vitorge, P. and Allard, B. (1987) Spectrophotometric study of the interaction between americium(III) and humic materials. Inorg. Chim. Acta **140**, 303-306.

Musso, H. (1967) Phenol coupling. In: Taylor, W.I., Battersby, A.R., editors. Oxidative coupling of phenols. New York, Marcel Dekker, p. 1-94.

Müller, K., Brendler, V. and Foerstendorf, H. (2008) Aqueous uranium(VI) hydrolysis species characterized by attenuated total reflection fourier-transform infrared spectroscopy. Inorg. Chem. **47**, 10127-10134.

Müller, K., Foerstendorf, H., Tsushima, S., Brendler, V. and Bernhard, G. (2009) Direct spectroscopic characterization of aqueous actinyl(VI) species: A comparative study of Np and U. J. Phys. Chem. A **113**, 6626-6632.

Müller, M., Acker, M., Taut, S. and Bernhard, G. (2010) Complex formation of trivalent americium with salicylic acid at very low concentrations. J. Radioanal. Nucl. Chem. **286**, 175-180.

Nebbioso, A. and Piccolo, A. (2009) Molecular rigidity and diffusivity of Al^{3+} and Ca^{2+} humates as revealed by NMR spectroscopy. Environ. Sci. Technol. **43**, 2417-2424.

Nebel, D. (1966) Spektralphotometrische Untersuchung des Gleichgewichtes Pu^{IV}-Citrat in wässriger Lösung. Z. Phys. Chem. **232**, 161-175.

Nebel, D. and Urban, G. (1966) Potentiometrische Untersuchungen zur Komplexbildung von Ce^{III}, Ce^{IV}, Th^{IV}, U^{IV} und Citrat in wässriger Lösung. Z. Phys. Chem. **233**, 73-84.

Neck, V. and Kim, J.I. (2001) Solubility and hydrolysis of tetravalent actinides. Radiochim. Acta **89**, 1-16.

Niu, Z.W., Fan, Q.H., Wang, W.H., Xu, J.Z., Chen, L. and Wu, W.S. (2009) Effect of pH, ionic strength and humic acid on the sorption of uranium(VI) to attapulgite. Appl. Radiat. Isot. **67**, 1582-1590.

Olivella, M.A., del Rio, J.C., Palacios, J., Vairavamurthy, M.A. and de las Heras, F.X.C. (2002) Characterization of humic acid from leonardite coal: an integrated study of Py-GC-MS, XPS and XANES techniques. J. Anal. Appl. Pyrol. **63**, 59-68.

Opel, K., Weiß, S., Hübener, S., Zänker, H. and Bernhard, G. (2007) Study of the solubility of amorphous and crystalline uranium dioxide by combined spectroscopic methods. Radiochim. Acta **95**, 143-149.

Panak, P., Klenze, R., Kim, J.I. and Wimmer, H. (1995) A study of intramolecular energy transfer in Cm(III) complexes with aromatic ligands by time-resolved laser fluorescence spectroscopy. J. Alloys Compd. **225**, 261-266.

Panak, P., Klenze, R. and Kim, J.I. (1996) A study of ternary complexes of Cm(III) with humic acid and hydroxide or carbonate in neutral pH range by time-resolved laser fluorescence spectroscopy. Radiochim. Acta **74**, 141-146.

Pandey, A.K., Pandey, S.D. and Misra, V. (2000) Stability constants of metal-humic acid complexes and its role in environmental detoxification. Ecotoxicol. Environ. Safety **47**, 195-200.

Park, Y.J., Lee, B.H., Kim, W.H. and Do, Y. (1999) Investigation of Coordinational Properties of Europium(III) Complexes with Picolinic Acid Using Eu(III) Excitation Spectroscopy. J. Colloid Interface Sci. **209**, 268-270.

Pashalidis, I. and Buckau, G. (2007) U(VI) mono-hydroxo humate complexation. J. Radioanal. Nucl. Chem. **273**, 315-322.

Paulenová, A., Rajec, P., Žemberyová, M., Sasköiová, G. and Višacký, V. (2000) Strontium and calcium complexation by humic acid. J. Radioanal. Nucl. Chem. **246**, 623-628.

Pearson, F.J. (1998) Opalinus Clay experimental water: A1Type, Version 980318. PSI Internal report TM-44-98-07, Paul Scherrer Institut.

Pearson, F.J., Arcos, D., Bath, A., Boisson, J.Y., Fernández, A.M., Gäbler, H.E., Gaucher, E., Gautschi, A., Griffault, L., Hernán, P. and Waber, H.N. (2003) Mont Terri Project - Geochemistry of Water in the Opalinus Clay Formation at the Mont Terri Rock Laboratory. Reports of the Federal Office for Water and Geology, Geology Series No. 5, Federal Office for Water and Geology.

Pearson, G.R. (1963) Hard and soft acids and bases. J. Am. Chem. Soc. **85**, 3533-3539.

Phillippi, J.M., Loganathan, V.A., McIndoe, M.J., Barnett, M.O., Clement, T.P. and Roden, E.E. (2007) Theoretical solid/solution ratio effects on adsorption and transport: Uranium(VI) and carbonate. Soil Sci. Soc. Am. J. **71**, 329-335.

Pompe, S., Bubner, M., Denecke, M.A., Reich, T., Brachmann, A., Geipel, G., Nicolai, R., Heise, K.H. and Nitsche, H. (1996) A comparison of natural humic acids with synthetic humic acid model substances: characterization and interaction with uranium(VI). Radiochim. Acta **74**, 135-140.

Pompe, S., Brachmann, A., Bubner, M., Geipel, G., Heise, K.H., Bernhard, G. and Nitsche, H. (1998) Determination and comparison of uranyl complexation constants with natural and model humic acids. Radiochim. Acta **82**, 89-95.

Pompe, S., Bubner, M., Schmeide, K., Heise, K.H., Bernhard, G. and Nitsche, H. (2000a) Influence of humic acids on the migration behavior of radioactive and non-radioactive substances under conditions close to nature. Synthesis, radiometric determination of functional groups, complexation. Wissenschaftlich-Technische Berichte, FZR-290, Forschungszentrum Rossendorf.

Pompe, S., Schmeide, K., Bubner, M., Geipel, G., Heise, K.H., Bernhard, G. and Nitsche, H. (2000b) Investigation of humic acid complexation behavior with uranyl ions using modified synthetic and natural humic acids. Radiochim. Acta **88**, 553-558.

Prietzel, J., Thieme, J., Salomé, M. and Knicker, H. (2007) Sulfur K-edge XANES spectroscopy reveals differences in sulfur speciation of bulk soils, humic acid, fulvic acid, and particle size separates. Soil Biol. Biochem. **39**, 877-890.

Quiles, F. and Burneau, A. (2000) Infrared and Raman spectra of uranyl(VI) oxo-hydroxo complexes in acid aqueous solutions: a chemometric study. Vib. Spectrosc. **23**, 231-241.

Raditzky, B., Schmeide, K., Sachs, S., Geipel G. and Bernhard, G. (2010) Interaction of uranium(VI) with nitrogen containing model ligands studied by laser-induced fluorescence spectroscopy. Polyhedron **29**, 620-626.

Raghavan, A. and Santappa, M. (1970) Complexes of uranyl ion with some amino and mercapto acids. Curr. Sci. **13**, 302-303.

Raghavan, A. and Santappa, M. (1973) Complexes of uranyl ion with amino and mercapto acids. J. Inorg. Nucl. Chem. **35**, 3363-3365.

Rajan, K.S. and Martell, A.E. (1965) Equilibrium studies of uranyl complexes. III. Interaction of uranyl ion with citric acid. Inorg. Chem. **4**, 462-469.

Rao, L.F., Jiang, J., Zanonato, P.L., Di Bernardo, P., Bismondo, A. and Garnov, A.Y. (2002) Complexation of uranium(VI) with malonate at variable temperatures. Radiochim. Acta **90**, 581-588.

Rao, L.F. (2007) Thermodynamics of actinide complexation in solution at elevated temperatures: Application of variable-temperature titration calorimetry. Chem. Soc. Rev. **36**, 881-892.

Ratasuk, N. and Nanny, M.A. (2007) Characterization and quantification of reversible redox sites in humic substances. Environ. Sci. Technol. **41**, 7844-7850.

Raymond, D.P., Duffield, J.R. and Williams, D.R. (1987) Complexation of plutonium and thorium in aqueous environments. Inorg. Chim. Acta **140**, 309-313.

Redden, G.D., Jinhe, L. and Leckie, J. (1998) Adsorption of U(VI) and Citric Acid on Goethite, Gibbsite, and Kaolinite. Comparing Results for Binary and Ternary Systems. In: Adsorption of Metals by Geomedia. Variables, Mechanisms and Model ApplicationsAcademic Press, San Diego, pp. 291.

Reiller, P. (2005) Prognosticating the humic complexation for redox sensitive actinides through analogy, using the charge neutralisation model. Radiochim. Acta **93**, 43-55.

Ren, X.M., Wang, S.W., Yang, S.T. and Li, J.X. (2010) Influence of contact time, pH, soil humic/fulvic acids, ionic strength and temperature on sorption of U(VI) onto MX-80 bentonite. J. Radioanal. Nucl. Chem. **283**, 253-259.

Rocha, J.C., Sargentini, E., Zara, L.F., Rosa, A.H., Santos, A. and Burba, P. (2003) Reduction of mercury(II) by tropical river humic substances (Rio Negro) - Part II. Influence of structural features (molecular size, aromaticity, phenolic groups, organically bound sulfur). Talanta **61**, 699-707.

Ryan, D.K. and Weber, J.H. (1982) Fluorescence quenching titration for determination of complexing capacities and stability constants of fulvic acid. Anal. Chem. **54**, 986-990.

Saada, A., Gaboriau, H., Cornu, S., Bardot, F., Villieras, F. and Croue, J.P. (2003) Adsorption of humic acid onto a kaolinitic clay studied by high-resolution argon adsorption volumetry. Clay Miner. **38**, 433-443.

Sachs, S., Schmeide, K., Brendler, V., Křepelová, A., Mibus, J., Geipel, G., Heise, K.H. and Bernhard, G. (2004) Investigation of the Complexation and the Migration of Actinides and Non-radioactive Substances with Humic Acids under Geogenic Conditions: Complexation of Humic Acids with Actinides in the Oxidation State IV Th, U, Np. Wissenschaftlich-Technische Berichte, FZR-399, Forschungszentrum Rossendorf.

Sachs, S. and Bernhard, G. (2005) NIR spectroscopic study of the complexation of neptunium(V) with humic acids: Influence of phenolic OH groups on the complex formation. Radiochim. Acta **93**, 141-145.

Sachs, S., Schmeide, K., Reich, T., Brendler, V., Heise, K.H. and Bernhard, G. (2005) EXAFS study on the neptunium(V) complexation by various humic acids under neutral pH conditions. Radiochim. Acta **93**, 17-25.

Sachs, S., Brendler, V. and Geipel, G. (2007a) Uranium(VI) complexation by humic acid under neutral pH conditions studied by laser-induced fluorescence spectroscopy. Radiochim. Acta **95**, 103-110.

Sachs, S., Křepelová, A., Schmeide, K., Koban, A., Günther, A., Mibus, J., Brendler, V., Geipel, G. and Bernhard, G. (2007b) Joint Project: Migration of actinides in the system clay, humic substance, aquifer - Migration behavior of actinides (uranium, neptunium) in clays:

Characterization and quantification of the influence of humic substances. Wissenschaftlich-Technische Berichte, FZD-460, Forschungszentrum Dresden-Rossendorf.

Sachs, S. and Bernhard, G. (2008) Sorption of U(VI) onto an artificial humic substance-kaolinite-associate. Chemosphere **72**, 1441-1447.

Sachs, S., Reich, T. and Bernhard, G. (2010) Study of the role of sulfur functionalities in humic acids for uranium(VI) complexation. Radiochim. Acta **98**, 467-477.

Sachs, S. and Bernhard, G. (2011a) Humic acid model substances with pronounced redox functionality for the study of environmentally relevant interaction processes of metal ions in the presence of humic acid. Geoderma **162**, 132-140.

Sachs, S. and Bernhard, G. (2011b) Influence of humic acids on the actinide migration in the environment: suitable humic acid model substances and their application in studies with uranium-a review. J. Radioanal. Nucl. Chem. **290**, 17-29.

Samadfam, M., Niitsu, Y., Sato, S. and Ohashi, H. (1996) Complexation thermodynamics of Sr(II) and humic acid. Radiochim. Acta **73**, 211-216.

Schmeide, K., Pompe, S., Bubner, M., Heise, K.H., Bernhard, G. and Nitsche, H. (2000) Uranium(VI) sorption onto phyllite and selected minerals in the presence of humic acid. Radiochim. Acta **88**, 723-728.

Schmeide, K., Sachs, S., Bubner, M., Reich, T., Heise, K.H. and Bernhard, G. (2003) Interaction of uranium(VI) with various modified and unmodified natural and synthetic humic substances studied by EXAFS and FTIR spectroscopy. Inorg. Chim. Acta **351**, 133-140.

Schmeide, K., Reich, T., Sachs, S., Brendler, V., Heise, K.H. and Bernhard, G. (2005) Neptunium(IV) complexation by humic substances studied by X-ray absorption fine structure spectroscopy. Radiochim. Acta **93**, 187-196.

Schmeide, K., Reich, T., Sachs, S. and Bernhard, G. (2006) Plutonium(III) complexation by humic substances studied by X-ray absorption fine structure spectroscopy. Inorg. Chim. Acta **359**, 237-242.

Schmeide, K. and Bernhard, G. (2008) Spectroscopic study of the uranium(IV) complexation by organic model ligands in aqueous solution. In: Uranium, Mining and Hydrogeology (B.J. Merkel, A. Hasche-Berger, eds.), Springer Verlag, Berlin Heidelberg, 591-598.

Schmeide, K. and Bernhard, G. (2009) Redox stability of neptunium(V) and neptunium(IV) in the presence of humic substances of varying functionality. Radiochim. Acta **97**, 603-611.

Schmeide, K. and Bernhard, G. (2010) Sorption of Np(V) and Np(IV) onto kaolinite: Effects of pH, ionic strength, carbonate and humic acid. Appl. Geochem. **25**, 1238-1247.

Schmeide, K., Sachs, S. and Bernhard, G. (2012a, in press) Np(V) reduction by humic acid: Contribution of reduced sulfur functionalities to the redox behavior of humic acid. Sci. Total Environ., DOI: 10.1016/j.scitotenv.2011.12.052.

Schmeide, K., Joseph, C. and Bernhard, G. (2012b, in preparation) Influence of organic ligands and temperature on U(VI) sorption onto Opalinus Clay.

Schott, J., Acker, M., Barkleit, A., Brendler, V., Taut, S. and Bernhard, G. (2012, in press) The influence of temperature and small organic ligands on the sorption of Eu(III) on Opalinus Clay. Radiochim. Acta, DOI: 10.1524/ract.2012.1921.

Schulten, H.R. and Schnitzer, M. (1998) The chemistry of soil organic nitrogen: a rewiev. Biol. Fertil. Soil **26**, 1-15.

Scott, D.T., McKnight, D.M., Blunt-Harris, E.L., Koselar, S.E. and Lovley, D.R. (1998) Quinone moieties act as electron acceptors in the reduction of humic substances by humics-reducing microorganisms. Environ. Sci. Technol. **32**, 2984-2989.

Seida, Y., Terashima, M., Tachi, Y., Iijima, K., Nakazawa, T., Yamada, M. and Yui, M. (2010) Sorption and diffusion of Eu in sedimentary rock in the presence of humic substance. Radiochim. Acta **98**, 703-709.

Sevostyanova, E.P. (1983) Stability of Np(IV), Np(V), and Np(VI) in citric acid solutions. Soviet Radiochem. **25**, 321-326.

Shanbhag, P.M. and Choppin, G.R. (1981) Binding of Uranyl by Humic-Acid. J. Inorg. Nucl. Chem. **43**, 3369-3372.

Silva, R.J. and Nitsche, H. (1995) Actinide environmental chemistry. Radiochim. Acta **70**, 377-396.

Skyllberg, U., Bloom, P.R., Qian, J., Lin, C.M. and Bleam, W.F. (2006) Complexation of mercury(II) in soil organic matter: EXAFS evidence for linear two-coordination with reduced sulfur groups. Environ. Sci. Technol. **40**, 4174-4180.

Solomon, D., Lehmann, J. and Martinez, C.E. (2003) Sulfur K-edge XANES spectroscopy as a tool for understanding sulfur dynamics in soil organic matter. Soil Sci. Soc. Am. J. **67**, 1721-1731.

Starý, J. and Balek, V. (1962) Untersuchung der Uran(VI)-Komplexe mit alpha-Hydroxysäuren durch Extraktionsmethode. Coll. Czech. Chem. Comm. **27**, 809-815.

Stern, O. and Volmer, M. (1919) The fading time of fluorescence. Physik. Zeitschr. **20**, 183-188.

Steudtner, R., Arnold, T., Geipel, G. and Bernhard, G. (2010) Fluorescence spectroscopic study on complexation of uranium(VI) by glucose - a comparison of room and low temperature measurements. J. Radioanal. Nucl. Chem. **284**, 421-429.

Steudtner, R., Sachs, S., Schmeide, K., Brendler, V. and Bernhard, G. (2011a) Ternary uranium(VI) carbonato humate complex studied by cryo-TRLFS. Radiochim. Acta **99**, 687-692.

Steudtner, R., Müller, K., Schmeide, K., Sachs, S. and Bernhard, G. (2011b) Binary and ternary uranium(VI) humate complexes studied by attenuated total reflection Fourier-transform infrared spectroscopy. Dalton Trans. **40**, 11920-11925.

Steudtner, R., Schmeide, K. and Bernhard, G. (2011c) Uranium(VI) complexation with lactate and citrate in dependence on temperature (7-65°C). Mineralog. Magazine **75**, 1940.

Steudtner, R., Schmeide, K. and Bernhard, G. (2012, in preparation) Complexation of U(VI) with lactate between 7 and 65°C. J. Alloys Comp.

Stevenson, F.J. (1982). Humus Chemistry. 1st ed., John Wiley and Sons, New York.

Stevenson, F.J, (1994) Humus Chemistry. Genesis, Composition, Reactions. 2nd ed., John Wiley and Sons, New York.

Sumner, M.E. and Miller, W.P. (1996) Cation exchange capacity and exchange coefficients. In: Methods of Soil Analysis. Part 3: Chemical Methods, D. L. Sparks, A. L. Page, P. A. Helmke, R. H. Loeppert, P. N. Soltanpour, M. A. Tabatabai, C. T. Johnston and M. E. Sumner (Eds.), Soil Science Society of America Inc., USA, pp. 1201.

Sutton, R. and Sposito, G. (2006) Molecular simulation of humic substance-Ca-montmorillonite complexes. Geochim. Cosmochim. Acta **70**, 3566-3581.

Suzuki, Y., Nankawa, T., Yoshida, T., Ozaki, T., Ohnuki, T., Francis, A.J., Tsushima, S., Enokida, Y. and Yamamoto, I. (2006) Reduction behavior of uranium in the presence of citric acid. Radiochim. Acta **94**, 579-583.

Szulczewski, M.D., Helmke, P.A. and Bleam, W. (2001) XANES spectroscopy studies of Cr(VI) reduction by thiols in organosulfur compounds and humic substances. Environ. Sci. Technol. **35**, 1134-1141.

Tertre, E., Berger, G., Castet, S., Loubet, M. and Giffaut, E. (2005) Experimental sorption of Ni^{2+}, Cs^{+} and Ln^{3+} onto a montmorillonite up to 150°C. Geochim. Cosmochim. Acta **69**, 4937-4948.

Teterin, Y.A., Nefedov, V.I., Nikitin, A.S., Teterin, A.Y., Ivanov, K.E., Maslakov, K.I., Utkin, I.O., Bubner, M., Reich, T., Pompe, S., Heise, K.H. and Nitsche, H. (2001) Interaction of UO_2^{2+} and Fe^{3+} ions with natural humic acid. Russ. J. Inorg. Chem. **46**, 886-891.

Thompson, H.A., Parks, G.A. and Jr. Brown, G.E. (1998) Structure and composition of uranium(VI) complexes at the kaolinite-water interface. In: Adsorption of metals by geomedia. Variables, mechanisms and model applications, E. A. Jenne (Ed.), Academic Press, San Diego, pp. 349-370.

Thuéry, P. (2007) Uranyl ion complexation by citric and citramalic acids in the presence of diamines. Inorg. Chem. **46**, 2307-2315.

Thuéry, P. (2008) Novel two-dimensional uranyl-organic assemblages in the citrate and D(-)-citramalate families. Cryst. Eng. Comm. **10**, 79-85.

Tipping, E., Rey-Castro, C., Bryan, S.E. and Hamilton-Taylor, J. (2002) Al(III) and Fe(III) binding by humic substances in freshwaters, and implications for trace metal speciation. Geochim. Cosmochim. Acta **66**, 3211-3224.

Tochiyama, O., Niibori, Y., Tanaka, K., Kubota, T., Yoshino, H., Kirishima, A. and Setiawan, B. (2004) Modeling of the complex formation of metal ions with humic acids. Radiochim. Acta **92**, 559-565.

Urban, N.R., Ernst, K. and Bernasconi, S. (1999) Addition of sulfur to organic matter during early diagenesis of lake sediments. Geochim. Cosmochim. Acta **63**, 837-853.

Vairavamurthy, M.A., Maletic, D., Wang, S., Manowitz, B., Eglinton, T. and Lyons, T. (1997) Characterization of sulfur-containing functional groups in sedimentary humic substances by X-ray absorption near-edge structure spectroscopy. Energ. Fuel **11**, 546-553.

Vairavamurthy, A. and Wang, S. (2002) Organic nitrogen in geomacromolecules: Insights on speciation and transformation with K-edge XANES spectroscopy. Environ. Sci. Technol. **36**, 3050-3056.

Van Loon, L.R., Soler, J.M. and Bradbury, M.H. (2003) Diffusion of HTO, $^{36}Cl^-$ and $^{125}I^-$ in Opalinus Clay samples from Mont Terri - Effect of confining pressure. J. Contam. Hydrol. **61**, 73-83.

Van Loon, L.R. and Soler, J.M. (2004) Diffusion of HTO, $^{36}Cl^-$, $^{125}I^-$, and $^{22}Na^+$ in Opalinus Clay: Effect of Confining Pressure, Sample Orientation, Sample Depth and Temperature. PSI-Bericht Nr. 04-03, Paul Scherrer Institut.

Van Loon, L.R. and Eikenberg, J. (2005) A high-resolution abrasive method for determining diffusion profiles of sorbing radionuclides in dense argillaceous rocks. Appl. Radiat. Isot. **63**, 11-21.

Van Loon, L.R., Muller, W. and Iijima, K. (2005) Activation energies of the self-diffusion of HTO, $^{22}Na^+$ and $^{36}Cl^-$ in a highly compacted argillaceous rock (Opalinus Clay). Appl. Geochem. **20**, 961-972.

Wang, Z.M., van de Burgt, L.J. and Choppin, G.R. (1999) Spectroscopic study of lanthanide(III) complexes with carboxylic acids. Inorg. Chim. Acta **293**, 167-177.

Wang, Z.M., Zachara, J.M., Yantasee, W., Gassman, P.L., Liu, C.X. and Joly, A.G. (2004) Cryogenic laser induced fluorescence characterization of U(VI) in Hanford vadose zone pore waters. Environ. Sci. Technol. **38**, 5591-5597.

Wang, Z., Zachara, J.M., Liu, C., Gassman, P.L., Felmy, A.R. and Clark, S.B. (2008) A cryogenic fluorescence spectroscopic study of uranyl carbonate, phosphate and oxyhydroxide minerals. Radiochim. Acta **96**, 591-598.

Warwick, P., Hall, A., Zhu, J., Dimmock, P.W., Robbins, R., Carlsen, L. and Lassen, P. (1997) Effect of temperature on the nickel humic acid equilibrium reaction. Chemosphere **35**, 2471-2477.

Wimmer, C., Arnold, T. and Großmann, K. (2009) Untersuchungen zur Fluoreszenz von Lactat bei Raumtemperatur und tiefen Temperaturen. CIT **81**, 501-504.

Wolery, T.J. (1992). EQ3/6, A Software Package for the Geochemical Modeling of Aqueous Systems, UCRL-MA-110662 Part I, Lawrence Livermore National Laboratory.

Wu, T., Amayri, S., Drebert, J., Van Loon, L.R. and Reich, T. (2009) Neptunium(V) sorption and diffusion in Opalinus Clay. Environ. Sci. Technol. **43**, 6567-6571.

Xia, K., Bleam, W. and Helmke, P.A. (1997) Studies of the nature of binding sites of first row transition elements bound to aquatic and soil humic substances using X-ray absorption spectroscopy. Geochim. Cosmochim. Acta **61**, 2223-2235.

Xia, K., Weesner, F., Bleam, W.F., Bloom, P.R., Skyllberg, U.L. and Helmke, P.A. (1998) XANES studies of oxidation states of sulfur in aquatic and soil humic substances. Soil Sci. Soc. Am. J. **62**, 1240-1246.

Xia, K., Skyllberg, U.L., Bleam, W.F., Bloom, P.R., Nater, E.A. and Helmke, P.A. (1999) X-ray absorption spectroscopic evidence for the complexation of Hg(II) by reduced sulfur in soil humic substances. Environ. Sci. Technol. **33**, 257-261.

Yule, L. (1991) A comparison of the binding of plutonium and iron to transferrin and citrate. Thesis, University of Wales.

Zeh, P., Czerwinski, K.R. and Kim, J.I. (1997) Speciation of uranium in Gorleben groundwaters. Radiochim. Acta **76**, 37-44.

Zheng, Z.P., Tokunaga, T.K. and Wan, J.M. (2003) Influence of calcium carbonate on U(VI) sorption to soils. Environ. Sci. Technol. **37**, 5603-5608.

8 Acknowledgements

The authors would like to thank S. Heller and J. Seibt for HA synthesis, characterization and sample preparation as well as S. Gürtler, A. Ritter, Ch. Müller, J. Seibt and A. Schliephake for their help in performing the experiments.

Furthermore, we thank H. Görner for elemental analyses, U. Schaefer, A. Ritter and C. Eckardt for ICP-MS analyses, ion chromatography and BET determination, C. Nebelung for the help during LSC measurements, S. Weiß for zeta potential and photon correlation spectroscopic measurements, A. Scholz for XRD measurements and Dr. H. Reuther for Mössbauer spectroscopy.

We also thank Dr. K. Müller and K. Heim for FTIR and ATR FTIR measurements and for their help in spectra interpretation, Dr. G. Geipel for support during TRLFS measurements and for discussion of laser spectroscopic results, M. Eilzer for technical support during TRLFS measurements as well as Dr. V. Brendler for speciation calculations and helpful discussions and Dr. A. Barkleit for helpful discussions concerning f-element spectroscopy.

We thank Prof. Dr. T. Reich and J. Drebert (Johannes Gutenberg-Universität Mainz, Institut für Kernchemie) for XPS measurements and data evaluation.

Dr. L.R. Van Loon and Dr. A. Jakob (Paul Scherrer Institut, Laboratory for Waste Management) is especially thanked for their immense support concerning diffusion experiments and COMSOL modeling.

Furthermore, we thank the Bundesanstalt für Geowissenschaften und Rohstoffe (BGR) and the Karlsruher Institut für Technologie, Institut für Nukleare Entsorgung (KIT-INE) (especially C.M. Marquardt) for providing and preparing ground and homogenized OPA as well as intact OPA bore core samples.

The authors are grateful for providing of ^{243}Am from the transplutonium element production facilities at Oak Ridge National Laboratory within a collaboration between the Forschungszentrum Dresden-Rossendorf and Prof. Nitsche from the Lawrence Berkeley National Laboratory, supported by the U.S. Department of Energy, Office of Basic Energy Sciences.

Finally, we would like to thank all other colleagues who contributed to the success of the project.